STRUCTURAL PERFORMANCE OF ROUNDED DOVETAIL CONNECTIONS

by

Thomas Tannert

A THESIS SUBMITTED IN PARTIAL FULFILLMENT OF THE REQUIREMENTS FOR THE DEGREE OF

DOCTOR OF PHILOSOPHY

in

The Faculty of Graduate Studies

(Forestry)

THE UNIVERSITY OF BRITISH COLUMBIA

(Vancouver)

April 2008

Abstract

The structural performance of Rounded Dovetail Connections (RDC) has been studied experimentally and numerically to provide information needed for connection structural design.

RDC are mainly used to transfer vertical shear forces, but test results show that they can carry considerable load in tension and bending. Geometric parameters, such as dovetail flange angle and dovetail height are shown to significantly effect affect the structural performance of RDC. Results show that it is impractical to determine a set of empirical equations to describe the structural performance of RDC based on basic wood material properties. RDC manufactured and tested with low and constant moisture content outperformed those evaluated under other climatic conditions, and test results demonstrate that RDC should be produced at low machine speed and with minimal a gap between the connecting members. RDC in laminated strand lumber have higher capacity and fail under larger deformations compared to RDC in western hemlock.

A three-dimensional finite element method model is presented and validated with experimental tests. Good agreement is achieved between the load deformation response predicted by the model and the experimentally observed load deformation response. Therefore the model is deemed suitable for estimating the stresses needed to develop failure criteria. A failure criterion for the analysis of RDC is presented taking into account size effect in the strength of wood. Based on the experimental and numerical studies, a design equation for RDC is presented that provides the engineering community with a new design tool. Finally, self tapping screws as reinforcement have been studied and are shown to significantly improve the structural performance of RDC under vertical shear loading.

Table of contents

List of tables

List of figures

Acknowledgements

I owe particular gratitude to my family, who has supported me throughout my years of education. I offer my thanks to the faculty, staff and colleagues at the Faculty of Forestry of The University of British Columbia and my friends at the UBC Graduate Student Society, who have inspired and supported me during the years working on my PhD. Special thanks are owed to:

- Dr. Frank Lam – for providing the research topic and the necessary funding,
- Dr Helmut Prion and Dr. David Barrett – for their general guidance,
- Robert Myronuk and George Lee – for their advise on setting up the experimental tests,
- Dr. Tony Kozak and Dr. Valerie LeMay – for their advise on statistical analyses,
- Dr. Ricardo Foschi and Dr. Ireneusz Beitka – for their advice on scientific aspects,
- Dr. Dave Cohen – for providing data on the marketing of western hemlock,
- Dr. Richard Schmidt – for serving as external examiner,
- Jianzhong Gu, Jung-Pyo Hong, Minghao Li and Xiabin Song – for their help with developing the numerical model for the research,
- Hiba Anastas – for her help with the experimental tests and proofreading manuscripts,
- Technicians in Wood Mechanics Lab – for their help with the experimental tests.

Co-authorship statement

Chapter 2 was co-authored by Dr. Helmut Prion and Dr. Frank Lam. Thomas Tannert was responsible for designing the research programme, performing the research, analyzing the results and preparing the manuscript. Dr. Helmut Prion and Dr. Frank Lam offered advice during the design of the research and the interpretation of the results.

Chapters 3, 4, 6, 7, 8, 9 and 10 were co-authored by Dr. Frank Lam. Thomas Tannert was responsible for designing the research programme, performing the research, analyzing the results and preparing the manuscript. Dr. Frank Lam offered advice during the design of the research and the interpretation of the results.

Chapter 5 was co-authored by Hiba Anastas, Dr. David Barrett and Dr. Frank Lam. Hiba Anastas was responsible for designing the research programme and performing the research. Thomas Tannert helped conducting the experiments and preparing the manuscript and was responsible for analyzing the results. Dr. David Barrett and Dr. Frank Lam offered advice during the design of the research and the interpretation of the results.

Chapter 1: Introduction

1.1. Background

Connections are arguably one of the most important parts of any timber structure. They transfer forces between components, anchor the superstructure to the foundation, and maintain integrity of the system in the event of overloading. Most collapses that occur during extreme load events are attributable to inadequate or inappropriate connections, and serviceability and durability of structures can also be governed by connections (Snow et al. 2006).

Wood connections can be categorized as engineering, glued and carpentry wood-to-wood connections. For centuries, buildings all over the world have been constructed using large timbers joined together using various types of carpentry wood-to-wood connections. Different cultures derived distinct methodologies, but all of these buildings using primarily wooden joints are considered timber frames. An array of carpentry connection details in traditional American, European and Japanese timber-framing are known to be suitable for various applications (Sobon 2001; Graubner 1990; Zwerger 1997).

Until the mid-20th century, wood-to-wood connections commonly used in construction were designed and manufactured based on the experience of wood-workers. High labour costs, high degree of required workmanship, assembly difficulties and inefficient use due to over dimensioning made these connections too expensive and heavy timber structures became less competitive. With the ease of producing dimensional lumber, light-frame construction became more common and replaced timber framing as the mainstay of low-rise wooden buildings.

More recently, important developments in wood processing machines have created the possibility of producing more cost effective carpentry wood-to-wood connections (Bamford 2003; Bobacz 2002). Use of advanced computer numerical controlled (CNC) milling machinery greatly reduces the requirement of skilled labour to produce these connections. Since CNC technology is associated with precise cut quality at a competitive cost and connections are often controlling the cost of timber structures, there are potentially large savings in wood-to-wood connections when compared to the costs of off the shelf steel fasteners.

The acceptance of carpentry connections by the North American structural engineering and architectural community is affected by a lack of design values and provisions in building codes and a lack of faith in construction techniques that require high levels of manual labour and skill (Bamford 2003; Snow et al. 2006). Furthermore there is a perception that over-sizing of timbers is necessary and the seismic resistance in wood-to-wood connections is of major concern. Although trends in timber design and construction include the innovative use of wood as a building material coupled with a desire for efficient construction and fabrication methods, there is little perceived impact of CNC technology on timber design. Nevertheless, a revival of interest in timber frame building in the United States occurred during the 1970s and since that time, the timber framing industry has grown to keep up with demand for timber frame houses, barns, churches, and other structures (O'Connell and Smith 1999) and carpentry connections are being used in a growing number of timber buildings (Schmidt and Scholl 2000).

Different geometric configurations of the carpentry connections have been used, primarily governed by practical considerations such as carpenters skills and available tools. The development in CNC wood-processing machinery has changed these constraints and almost any desired geometry is possible. The Rounded Dovetail Connection (RDC) is a relatively new

concept based on the dovetail, but specifically adapted to be processed automated with a CNC-timber processor. The use of RDC in timber construction has significantly increased in Europe, with the most common application being the connection of joist to a beam or a beam to a girder. RDC are named after the rounded shape in the longitudinal direction of the joist, similar to a dovetail (Figure 1-1).

Figure 1-1: Rounded Dovetail Connection

1.2. Motivation

Use of the Rounded Dovetail Connection is increasing although there is a lack of research regarding its structural performance. There is a need and demand for guidance in designing such connections in wood construction throughout North America. The motivation for this research is to provide appropriate information, so that existing design codes can be expanded and updated to reflect the acceptance and use of this modern connection concept.

1.3. Objectives

The general objective of the research is to experimentally and numerically study the structural performance of Rounded Dovetail Connections. The specific objectives are:

- Evaluate the effect of loading, geometric, manufacturing and material parameters as well as reinforcements on the structural performance of RDC
- Develop an appropriate Finite Element Method model for RDC
- Develop a failure criterion for RDC that takes into account size effect
- Propose a design guideline for RDC based on the preceding studies

1.4. Organization of thesis

The thesis is presented in manuscript based format. The remainder of Chapter 1 gives a literature review and provides the information to develop sufficient understanding of the field of study of the thesis. Chapters 2 to 10 elaborate on the objectives, and Chapter 11 contains a discussion relating the manuscript chapters to each other and proposes new ideas related to the field of study.

1.5. Literature review

1.5.1. Connections in wood

Previous studies Rounded Dovetail Connections

A number of experimental studies provided valuable insight into the structural performance of Rounded Dovetail Connections (RDC). Kreuzinger and Spengler (1999) tested 18 specimens produced from solid wood. It was shown that the load-carrying capacity of the connection depends crucially on the load carrying mechanism between main and joist. They differentiated between three cases: I) properly matching geometry with no friction in the contact area, II) properly matching geometry with friction in the contact area, and III) manufacturing of a gap at the bottom of the dovetail. They concluded that if an originally properly matched connection shrunk and no frictional forces were transferred, RDC behaved similar to conventional mortise and tenon joints. The perpendicular to grain tensile stresses were crucial for the connection capacity and friction must be guaranteed if the connection is to be used for higher loads. An optimization is to be aimed at the relation of dovetail height to beam member height.

Barthel et al. (1999) numerically simulated the tests conducted by Kreuzinger and Spengler (1999). They examined different failure mechanisms: I) shear in the tenon, II) compression perpendicular in the range of the fillet, III) crushing of the tenon due to compression perpendicular, IV) tension perpendicular in the secondary beam, and V) fracture of the main beam due to tension perpendicular. Wood was modelled assuming orthotropic material properties. The deformations and stresses resulting from initially applied forces that close existing connection gaps were not considered in the model. The analysis showed that RDC capacity depended crucially on the load carrying mechanism between main beam and joist. When the geometry was properly matching and no friction occurred in the contact area, the load

was transferred over the flanks and deformations were small; concentrated vertical tension perpendicular to grain stress caused the connection to fail by horizontal cracking. When the geometry was properly matching but friction occurred, the load transferred over the flanks was large and the resulting force was transferred higher into the main beam; the tension perpendicular to grain stress was evenly distributed. Deformations were small and the connection capacity was higher. When a gap existed on the bottom of the dovetail between the connecting members, the loads were transferred even higher into the main beam and the tenon was squeezed horizontally. The vertical perpendicular tensile stresses were smallest but deformations were very large.

Blass and Saal (1999) described three test series with RDC. The first series consisted of specimens with properly matching joints. To evaluate manufacturing tolerances and changes of wood moisture a gap of 1.2 mm at the flanks was produced in the second series. The third series consisted of tightly fitting joints reinforced with self-tapping wood screws. Longitudinal splitting of the secondary beam due to combined transverse tensile and shear stresses caused joint failure. The reinforced specimens showed higher connections stiffness but similar capacity.

Hochstrate (2000) tested 77 RDC specimens from European softwood and glulam. He studied different joint geometries and support conditions and concluded that the tenon tapering in vertical direction transferred the load evenly over the connection height; it distributed friction forces, and reduced problematic tension stress concentrations that occurred in conventional notches or mortise and tenon joints. Depending on the support conditions, RDC also produced normal stresses on the face of the joist where the activated friction forces transferred part of the shear force in vertical direction. He concluded that RDC behave similarly to mortise and tenon joints if a properly matched connection shrunk and no frictional forces were transferred.

A preliminary study at The University of British Columbia (UBC)[1] tested RDC in glulam specimens that connected beams to rafters. It was concluded that RDC could be used in designs with long spans where deflection of the beam would usually be the limiting design factor. The connections appeared to have large reserve strength and cracked and deflected significantly before failing. It was suggested to design RDC based on the assumption that it was a truly pinned connection and limiting possible rotations of the joint to 0.5° and deflections of the beams to L/360.

The complex load transfer mechanism of RDC is governed by its specific geometric features that also permit the connection to resist longitudinal tension and moment loads in horizontal and vertical direction. The tension capacity is of interest when RDC are used in roof components. The companies Annen Holzbau and Holzbau Bucher AG conducted tension tests of beam to rafter joints at the Engineering School Freiburg[2]. Two series of specimens were tested; six specimens in bending with beams at both ends of the rafters and six traction tests, and average design strength values were determined.

Bobacz (2002) tested four series of RDC specimens to determine the influence of joint geometry on their capacities and then modelled the joints with a Finite Element Methos (FEM) programme. The material was assumed as linear elastic, the post-critical behaviour and the initial load slip behaviour were not modelled. Deviations between numerical and test results were

---

[1] Campbell, D., Forsyth, M., Miller, J., Parker R., Weber, D. 2001. Heavy Timber Dovetail Connections: Preliminary design approaches for engineers. Unpublished Report, The University of British Columbia.

[2] Zöllig, S. 2001. Anschluss Neben- an Hauptträger mit Schwalbenschwanzverbindung. Zug- und Scherversuche, Annen Holzbau AG, Holzbau Bucher AG. Personal communication.

explained by the initial slip where the connection did not behave in a linear elastic manner. The critical stress concentrations at the bottom of the dovetail were correctly identified.

Steiniger[3] (2004) conducted preliminary research on RDC comparing TimberStrand® Laminated Strand Lumber (LSL) and solid sawn, kiln-dried western hemlock. The joints were tested under pure shear load and the free end of the secondary beam was simply supported. LSL specimens presented higher average connection strength and did not fail in a brittle mode. Specimens with varying joint geometry (single, double and triple dovetail) were tested and the effect on failure mode and connection strength was studied. The modified RDC showed higher strength and less brittle failure modes than single RDC.

Dietsch (2005) used linear elastic FEM models to study the importance of geometry parameters. The study revealed that the flange angle had a substantial impact on the connection capacity with optimal stress conditions for angles below 15º. The dovetail angle was found to have little influence on the structural performance. An optimum height of the dovetail was found at 120 mm when the height of both beams was 200 mm. It was suggested that future studies of the RDC failure mechanism should include fracture mechanics and size effect considerations.

Garbin et al. (2006) presented experimental and numerical analyses on RDC. The joint geometry and the wood fibre configuration of the tenon were taken into account in order to characterize the connection. Different failure modes were observed depending on geometry and an empirical model was developed to describe the behaviour of RDC.

---

[3] Steiniger, M. 2004. Performance of CNC-processed wood-to-wood joinery with structural composite lumber and solid timber. PhD Thesis Proposal, Faculty of Forestry. The University of British Columbia Vancouver.

Design guidelines for Rounded Dovetail Connections

There are currently no design equations for RDC in building codes. Due to their similarity to notched beam support, the design criteria for notched beam may be a guide for designing RDC. Design formulas for end-notched beams estimate capacity (V) by reduction of the allowable beam shear stress according to Equation 1-1:

$$\frac{1.5 * V}{(b * h_e)} = f_S * k_V \qquad \text{Equation 1-1}$$

where b is the beam width, h_e the notch height, f_S the shear strength of the wood and k_V a reduction factor which reflects the influence of the stress concentration due to the notch. Early design formulas for end-notched beams are not known to have any theoretical basis and the reduction factor k_V was equal to the ratio of h_e to h, where h the beam height.

Gustafsson (1988) studied the strength of wooden beams with a rectangular end-notch on the tension side and concluded that notch failure developed at the tip of a notch and that this failure could be analysed theoretically using linear elastic fracture mechanics. The distance from the support to the notch tip was found to be of significant importance for notch strength and a closed-form equation based on fracture mechanics considerations was presented. This equation in modified form is now given in many design codes such as EC5 to calculate the capacity of end notched beam supports. For supports with 90° notches, the factor k_V can be calculated according to Equation 1-2:

$$k_V = \frac{k_n}{\sqrt{h} * \left[\sqrt{\left(\frac{h_e}{h} - \left(\frac{h_e}{h} \right)^2 \right)} + 0.8 * \frac{x}{h} * \sqrt{\frac{h}{h_e} - \left(\frac{h_e}{h} \right)^2} \right]} \qquad \text{Equation 1-2}$$

where x is the distance between notch edge and midpoint of support force. Following conditions apply: $k_V \le 1,\ h_e \le h,\ x/h \le 0.5$. The factor k_n is material dependent and is equal to 5 for solid timber and 6.5 for glulam.

Holzner (2000) studied the load carrying mechanism of RDC with a framework modeling approach and concluded that the design equation for notched beam supports could be applied in a modified form to take into account the different load carrying mechanism of RDC. Hochstrate (2000) presented a diagram of the RDC mortise member load capacity as a function of its geometry.

A design procedure and criterion for RDC was proposed by Werner (2002). He examined load-deformation curves and recommended limiting the expected slip of the connection to 1.5 mm. Since RDC could fail either by breaking of joist or main beam, the two members were designed separately, see Equation 1-3. The design criterion for the joist was based on an effective tenon area A_{ef}, and the admissible shear stress of the material f_S. The criterion for the main beam was an empirically based formula. It estimated the design capacity based on the expected location of the crack that develops on the mortise base before the main beams fails.

$$F_{adm(Joist)} = \frac{2}{3} * A_{ef} * f_S$$

$$F_{adm(Main\ beam)} = 0.09 * \left(h_M - h_1 + \frac{b_1}{2} \right) \quad (h_M, h_1, b_1 \text{ in mm, F in kN}) \qquad \text{Equation 1-3}$$

The connection stiffness C can be estimated with Equation 1-4:

$$C = 0.7 * \min \begin{cases} F_{adm(Main\ beam)} \\ F_{adm(Joist)} \end{cases} \quad (F \text{ in kN, C in kN/mm}) \qquad \text{Equation 1-4}$$

Werner (2002) further made following design recommendations:

- limit tenon height to less than half the secondary beam height,
- maintain minimum width of the main beam of t + 50 mm,
- maintain minimum main beam width of t + 100 mm for RDC on both sides of the beam,
- limit tenon length to 25 - 30 mm
- limit mortise length to t + 3 mm,
- consider reduced section of the main beam in its member design,
- guarantee precise manufacturing (recommended tolerance of 0.2 mm),
- cut and process only dry timber,
- maintain minimum 600 mm distance between two joints connecting to one main beam,
- and maintain minimum 500 mm end distance between RDC and main beam end.

Studies on wood-to-wood connections

Most research on wood-to-wood connections has been conducted in the last two decades. Schelling and Hinkes (1985) studied the performance of mortise and tenon joints examining different geometries and the influence of moisture content. Heimeshoff and Köhler (1989) evaluated design rules related to traditional carpenter joints and studied their behaviour. Reyer and Schmidt (1989) developed design procedures for longitudinal connections (straight sheet, diagonal sheet, scarf joints, dovetail). Kessel and Augustin (1990) studied the tensile load capacity for mortise and tenon joints and proposed appropriate design values. Görlacher and Kromer (1993) developed a design approach for joints to resist tension loads.

Notable research in the United States on timber frames was conducted by Brungraber (1985) with two test programs combined with computer analyses of joinery-connected structures. Brungraber modelled the behaviour of mortise and tenon connections applying a linear, plane-frame program which included a spring model. Sandberg et al. (2000) studied traditional mortise and tenon joints and concluded that joint behaviour is primarily linear. Church and Tew (1995) investigated pegged joints and found the dowel bearing strength to be relatively insensitive to dowel diameter, dowel-hole clearance and species grain orientation. Burnett et al. (2003) investigated the influence of end distance on the behaviour of wood-dowel joints and indicated that the 1997 National Design Specifications for wood constructions should be revised.

The most extensive research on wood-to-wood connections was carried out at the University of Wyoming with a series of studies on mortise and tenon joints. Schmidt and MacKay (1997) modified the European Yield Model failure mode equations to predict strength of connections with wooden dowels including peg shear failure and mortise splitting as additional failure modes specific to these connections. Schmidt and Daniels (1999) determined dowel bearing, peg bending, and peg shear strength and developed detailing requirements, such as end and edge distances, to ensure a ductile peg failure. Schmidt and Scholl (2000) showed that draw-boring increased joint stiffness but did not alter the joint yield capacity. They also explored seasoning and load-duration effects on full-sized joints and suggested modifications to the detailing requirements. Miller and Schmidt (2004) quantified the shear capacity of wooden pegs in mortise and tenon joints by both physical testing of full-scale specimens and modeling their macroscopic behaviour by using numerical simulations. The work culminated with the proposal of new specifications for timber frame constructions (Schmidt 2006).

Mihailescu (2001) used FEM analysis to predict the performance of different mortise and tenon joints studying the influence of joint geometry, grain and growth ring orientation, and position and area of bond in joints. Mihailescu modelled different joints with linear orthotropic material properties and studied problems connected with the approximation of the geometry, the type of elements used, and the boundary conditions. Schober (1999) presented numerical simulations of the semi–rigid behaviour of step joints in traditional roofs under monotonic loading. Drdacky et al. (2000) investigated historic carpentry joints and described their behaviour by a FEM approach. Chang et al. (2004) studied the rotational stiffness of timber joints, proposed an equation to estimate the initial rotational stiffness and demonstrated that friction between tenon and mortise played an important role in the rotational behaviour.

Most research on wood-to-wood connections focused on individual joint behaviour within the elastic range. Seo et al. (1999) presented static and cyclic lateral load tests on full-scale models of two types of the wooden frames with beam-column tenon joints. The tests showed a significant nonlinearity and inelasticity in the load-displacement curve. Parisi and Piazza (2000) studied the mechanics of traditional and reinforced step joints under monotonic and cyclic loading. Erikson and Schmidt (2002) conducted research on single- and multiple-story bents subjected to lateral load and showed that in order to accurately model the frame displacement, the joint characteristics must be included in the model.

Studies on bolted timber connections

More research has been done on the modelling of bolted connections. Patton-Mallory et al. (1997) developed a tri-linear stress-strain material model for wood to predict connection behaviour. Moses (2000) used 3D FEM models to predict load-displacement behaviour, ultimate

strength and mode of failure for bolted joints in structural solid wood and composite lumber. An anisotropic plasticity constitutive model was used with the Weibull weakest link strength criterion for brittle materials. Kharouf et al. (2003) developed an elastic-plastic model for bolted wood connections loaded in both tension and compression. Chen et al. (2003) proposed a FEM model for un-reinforced and reinforced dowel-type timber joints to investigate the mechanical performance and a stress-interaction based failure criterion to predict joint strength. Guan and Rodd (2003) studied contact problems in timber joints and showed that these affected the convergence, the deformation, and the failure mode of the joints.

Effect of manufacturing on connection performance

The structural performance of timber joints is affected by the manufacturing quality and the moisture content (MC) of the timber members amongst other factors such as wood species and the existence of defects in the wood. Wood-to-wood connections rely on interlocking of their form to provide stiffness and strength; therefore it is essential to have accurately cut components (Erman 2002). Wood shrinks and swells if exposed to moisture fluctuations below the fibre saturation point. Shrinkage becomes important when the MC of the timber at the time of manufacturing differs significantly from the MC of the timber under service conditions; e.g. structures constructed with green timbers that dry while in service may experience the loosening of originally tight joinery over time.

Moisture gradients have been shown to affect the capacity of curved glue-laminated beams. The capacity of beams in a moistening phase is almost halved compared to the mean value of seasoned specimens and beams subjected to climate change display larger variability in capacity than seasoned specimens (Jönsson 2005). Although timber structures are exposed to

various climatic conditions, in most cases the strength and stiffness properties of connections are evaluated from results of test specimens conditioned to a standard condition (Nakajima 2000). The performance of the joints of these structures should be properly evaluated according to the conditions in which they are used.

Manufacturing tolerances can significantly impact the performance of connections. Therefore, reducing the variations in geometry and improving the quality of workmanship directly affects connection performance. Reducing the variability in the manufacturing process, CNC-processing technology provides repetitive, identical, very accurate and precise joint geometry. The individual set-up and the service condition of the processing machine and tooling, however, may affect the cut-quality and geometry, hence, the connection performance.

Timber connections in engineered wood products

Engineered wood products have been successfully adopted in the construction industry. Parallel Strand Lumber, Laminated Veneer Lumber, thick Oriented Strand Board, and Laminated Strand Lumber (LSL) are the most important engineered wood products. Together with glued-laminated beams and I-joists, these products have been substituted for traditional solid sawn timber components such as beams, headers, columns, and chord members, and are starting to be used in applications typically dominated by steel or concrete. In the future, with the reduced availability of large-size solid sawn structural members, engineered wood products will play an even more important role as structural materials. The mechanical and physical properties of these products depend on the interacting relationships between the quality of the resource and the manufacturing process, and are in general more uniform compared with solid sawn material; hence, higher allowable properties are available in engineering design (Lam 2001).

TimberStrand® Laminated Strand Lumber (LSL) is highly uniform and dense, and compared to other wood products, LSL has a high shear strength to bending strength ratio and low variability in properties. Such characteristics can lead to improved connection efficiency. High-grade structural composite lumber products in combination with CNC-technology present an opportunity for applying innovative connection methods in timber construction. Some studies that addressed this issue focused on bolted connections (Moses 2000), timber rivets (Hampson 2003) and INDUO connectors (Steiniger 2003). It was found that the performance of LSL in connections was superior to other wood composites and enabled less severe requirements for spacing and end distances. Unfortunately these favourable characteristics of LSL are neither fully understood nor applied. As a result, LSL is mostly used in residential construction as headers and beams products. In such applications, designers rely on basic specifications on connection strength properties for common mechanical fasteners provided by the manufacturers. More efficient connection methods and increased knowledge on timber joinery are needed to allow expanded general use of structural composite lumber products in timber construction.

The performance of TimberStrand® LSL in beams with RDC under shear loading was examined in preliminary tests at UBC[4]. The LSL specimens presented 50% higher connection strength compared to western hemlock (*Tsuga heterophylla*) and showed less brittle failure justifying further research.

[4] Steiniger, M. 2004. Performance of CNC-processed wood-to-wood joinery with structural composite lumber and solid timber. PhD Thesis Proposal, Faculty of Forestry. The University of British Columbia Vancouver.

Connection reinforcements with self-tapping screws

The use of screws in heavy timber construction did not become popular until recently due to the limitations on the strength and available lengths of screws and code provisions that assumed that screws had no (or limited) withdrawal resistance. Modern self-tapping screws with continuous threads have diameters up to 12 mm and lengths up to 600 mm, and they are hardened to produce a high yield moment, tensile and torsion strength. The cutting thread and surface coating are designed to avoid the need for pre-drilling thereby guaranteeing easy assembly. The continuous thread provides a mechanical connection along the embedded length, which makes them efficient for reinforcing timber prone to splitting. Self-tapping screws with continuous threads present an alternative to the traditional reinforcement methods and provide new possibilities as reinforcements for numerous applications in timber structures.

Since the tensile and compressive strength of timber perpendicular to the grain is much lower than the respective strength values parallel to the grain, timber structures should be detailed minimizing stresses perpendicular to the grain (Blass and Bejtka 2004). Examples of structural details where tension perpendicular to the grain stresses occur are end notched beam supports, connections with load components perpendicular to the member axis as well as beams with holes. Beam supports are an example for a structural detail with compressive stresses perpendicular to the grain (Bejtka and Blass 2006) where self-tapping screws provide an opportunity to increase capacity and stiffness. Self-tapping screws can increase the capacity of connection perpendicular to grain and produce a more ductile failure mode compared to non-reinforced members. To avoid bending of screws and to increase connection stiffness, they can be placed at an angle to the interface between the connected members (Blass and Bejtka 2001).

1.5.2. Material model for wood

The key to successful connection modeling is finding an appropriate mathematical description of the material behaviour. A study of constitutive models for orthotropic materials is necessary to identify the approach that provides a feasible level of accuracy and is possible to implement into a commercial FEM programme. Often, individual phenomena of the material behaviour of wood are studied without concern for their interaction with others. Eberhardsteiner (2002) listed the following parameters that should be taken into account: I) biological parameters such as the tree species; II) physical parameters like density, temperature, air humidity, moisture content; III) mechanical parameters defining the anisotropic failure surface; and IV) structural parameters on the local and the global level.

Linear elastic material model

Timber is a natural, anisotropic (cylindrically isotropic) and inhomogeneous material. Although wood structure is very complex, in material models it often is assumed to be homogeneous and defect free, ignoring natural imperfections such as knots and distortions in the alignment of grain. For samples cut far from the tree centre and small in size in relation to the distance to the pith, the growth ring curvature can be ignored and properties are regarded as orthotropic with three orthogonal planes of material symmetry: longitudinal (L), radial (R), and tangential (T). The linear elastic orthotropic constitutive equations that relate stresses (σ_i and σ_{ij}) to strains (ε_i and γ_{ij}) can be written in matrix form according to Equation 1-5.

$$\begin{Bmatrix} \varepsilon_L \\ \varepsilon_R \\ \varepsilon_T \\ \gamma_{RT} \\ \gamma_{LT} \\ \gamma_{LR} \end{Bmatrix} = \begin{bmatrix} \frac{1}{E_L} & \frac{-\nu_{RL}}{E_R} & \frac{-\nu_{TL}}{E_T} & 0 & 0 & 0 \\ \frac{-\nu_{LR}}{E_L} & \frac{1}{E_R} & \frac{-\nu_{TR}}{E_T} & 0 & 0 & 0 \\ \frac{-\nu_{LT}}{E_L} & \frac{-\nu_{RT}}{E_R} & \frac{1}{E_T} & 0 & 0 & 0 \\ 0 & 0 & 0 & \frac{1}{2G_{LR}} & 0 & 0 \\ 0 & 0 & 0 & 0 & \frac{1}{2G_{RT}} & 0 \\ 0 & 0 & 0 & 0 & 0 & \frac{1}{2G_{TL}} \end{bmatrix} * \begin{Bmatrix} \sigma_L \\ \sigma_R \\ \sigma_T \\ \sigma_{RT} \\ \sigma_{LT} \\ \sigma_{LR} \end{Bmatrix} \qquad \text{Equation 1-5}$$

where E_L, E_T, E_R are the Young's or elastic moduli in directions L, T, R; G_{LT}, G_{TR}, G_{RL} are the shear moduli for planes L–T, T–R, R–L; and ν_{ij} are the Poisson's ratios (i;j = L, T, R) - the ratios of strains in the i direction resulting from an applied stress in the j direction. The resulting nine independent parameters can be determined by testing. While the number of available tests gives certainty about the longitudinal elastic modulus, less certainty exists about the transverse moduli and shear moduli, and very little research has been carried out determining the Poisson's ratios. Values given in the Wood Handbook (Green et al. 1999) have to be used with caution. In addition to having different values for tension and compression stresses, each value may be non-linearly dependent on strain and also dependent on the specimen size as indicated by Madsen (1992).

Orthotropic elasticity is generally the most plausible material model for wood, but owing to the complexity of the solutions, wherever possible 2D approximations are made to reduce the number of constitutive equations and simplify solutions of 3D problems (Dinwoodie 2000). For bigger specimens with more equal section dimensions, the assumption of orthotropy has to be questioned and for simplicity in modeling, transverse isotropy assuming identical properties in the radial and tangential directions is often used (Bodig and Jayne 1982). The

transverse isotropic assumption works well as long as linear elastic behaviour is sustained (Mihailescu 2001). The combined direction is referred to as perpendicular to grain (⊥) while the longitudinal is referred to as parallel to grain (II), see Equation 1-6:

$$\begin{Bmatrix} \varepsilon_{II} \\ \varepsilon_{\perp,1} \\ \varepsilon_{\perp,2} \\ \gamma_{\perp\perp} \\ \gamma_{II\perp,1} \\ \gamma_{II\perp,2} \end{Bmatrix} = \begin{bmatrix} \frac{1}{E_{II}} & \frac{-\nu_{\perp II}}{E_{\perp}} & \frac{-\nu_{\perp II}}{E_{\perp}} & 0 & 0 & 0 \\ \frac{-\nu_{II\perp}}{E_{II}} & \frac{1}{E_{\perp}} & \frac{-\nu_{\perp\perp}}{E_{\perp}} & 0 & 0 & 0 \\ \frac{-\nu_{II\perp}}{E_{II}} & \frac{-\nu_{\perp\perp}}{E_{\perp}} & \frac{1}{E_{\perp}} & 0 & 0 & 0 \\ 0 & 0 & 0 & \frac{1}{2G_{\perp\perp}} & 0 & 0 \\ 0 & 0 & 0 & 0 & \frac{1}{2G_{II\perp}} & 0 \\ 0 & 0 & 0 & 0 & 0 & \frac{1}{2G_{II\perp}} \end{bmatrix} * \begin{Bmatrix} \sigma_{II} \\ \sigma_{\perp,1} \\ \sigma_{\perp,2} \\ \sigma_{\perp\perp} \\ \sigma_{II\perp,1} \\ \sigma_{II\perp,2} \end{Bmatrix} \qquad \text{Equation 1-6}$$

where $E_{II}, E_{\perp}$ are the Young's moduli in directions parallel and perpendicular to grain; G is the shear modulus; and $\nu_{i,j}$ is the Poisson's ratio. Both, orthotropic and transverse isotropic models are simplifications of the real material (Figure 1-2).

Figure 1-2: Simplifications of wood material orientation

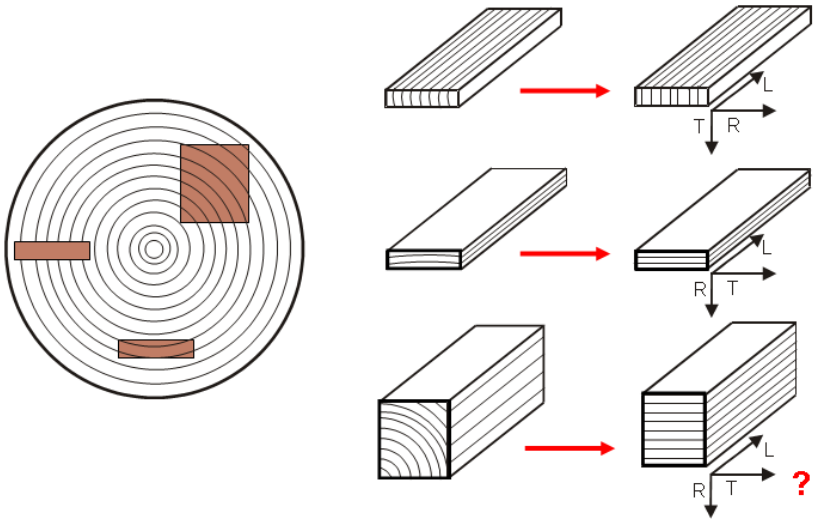

Plasticity

Plasticity theory allows a set of constitutive equations for a multi-axial stress state to be derived from uni-axial stress–strain test data based on 3 basic properties: I) a yield criterion; II) a flow rule, and III) a hardening rule. The yield criterion determines the stress-level where non-linear behaviour starts. It is the yield stress in the case of a uni-axial loading. For multi-axial stresses the interactions between the individual components of the stress tensor have to be considered when defining material failure. Kharouf et al. (2003) performed uni-axial compressive tests with large deformation on different wood species and described the nonlinear behaviour within the framework of plasticity. A fundamental difficulty in an incremental plasticity model for representing the constitutive relations for anisotropic materials is the need to select a unique stress strain relation when none truly exists. Schmidt et al. (1993) proposed an invariant based model that does not require defining an effective stress-effective strain relation.

Uni-axial and multi-axial behaviour of wood

Poulsen et al. (1997) studied the uni-axial compression behaviour of wood. The process was shown to consist of three stages: incipient kinking, transient kinking and steady state kinking. Incipient kinking occurred shortly before peak stress and initiated from the areas of high local fibre misalignment where fibres sheared and buckled plastically. During transient kinking, the regions grew and eventually formed a macroscopic kink band across the specimen, wherein the fibres were rotated and axially compressed, causing the stress to drop. During steady-state kinking, the band broadened under constant stress and the fibres within the band underwent no further deformation. The fibres outside the band were rotated and axially compressed as the kink band edges propagated. Adalian and Morlier (2001) determined characteristic values for wood compressive behaviour in the three material directions and approximated the stress/strain curve

for each material direction. Grosse and Rautenstrauch (2004) studied load-carrying reserves of timber-concrete connections in the post-critical range and divided the longitudinal compression strength-degradation into five stages, splitting the incipient kinking into a two parts (below and above proportional limit) and adding a hardening phase.

In tension and shear, wood behaves essentially linear elastic and failure is marked by a brittle fracture with crack formation. A small process zone forms with the damage not spreading outside the crack line. In tension loading perpendicular to the grain, the longitudinal crack propagation is predefined by the fibre direction. The crack surface of a longitudinal tension fracture is very fibrous; only little energy is dissipated and it is very difficult to enforce stable crack propagation; even in a displacement-controlled test (Grosse and Rautenstrauch 2004). Shear represents a condition in which the principal stress trajectories are at an angle of approximately 45 degree to the treated plane and shear failure is very similar to tension failure.

The constitutive behaviour of wood under multi-axial stress states has been considered only rarely and relatively little is known about failure behaviour under multiple stress conditions. Spengler (1986) investigated loading zones of beams subjected to shear stress under superposed lateral compression. Hemmer (1986) used cylindrical pipes subjected to tension, torque, internal pressure, and combinations of it. Eberhardsteiner (2002) measured the stress-strain behaviour of clear spruce wood under multi-axial loading and identified pre-failure behaviour and the failure location. By using a clear wood cruciform specimen in combination with an optical measurement system it was possible to cover the whole set of distinguishable stress states for an orthotropic material under plane stress. Three major observations were made: I) the failure strongly depended on angle between material directions and applied load, II) the behaviour of the

specimens was reproducible for similar testing parameters, and III) the deformation of the specimens in the domain of interest was homogeneous.

Wood failure on different scales

The modes of failure of a timber connection vary depending on material type and strengths as well as geometry of the member and connection. Eberhardsteiner (2002) identified four basic failure modes of spruce: I) brittle tensile failure in fibre direction - this mode had a cascading crack pattern, showed a large variation of strength and could only be found for small grain angles; II) brittle tensile failure perpendicular to grain - a distinct straight crack developed parallel to grain; this mode could be found for all grain angles; III) compressive failure perpendicular to grain - a behaviour similar to saturation type hardening as known from metal plasticity that did not cause strength degradation; and IV) compressive failure in fibre direction - damaged cell bands developed and strength degradation is followed by a strength plateau. Brittle modes should be avoided in connection design since they could result in sudden, catastrophic failure.

Wood properties are influenced by material features over a large range of length scales: from the macroscopic growth features (shakes and checks are starting points for crack growth and knots that represent locations of stress concentration at which cracks can extend), all the way down to the molecular level (Smith et al. 2003). Microscale heterogeneity is manifested through cell overlap, pits and pores, and earlywood-latewood transitions. At the fibre scale, perpendicular to grain tensile fracture may develop through the cell walls or along cell walls. At the growth ring scale, the commonly observed failure modes perpendicular to grain are tension and shear failure in the early wood, and tangential tensile failure. In larger pieces with varying growth ring

angle or when the crack plane orientation is governed by an initial crack, the fracture plane may develop at an angle to the orientation of the growth rings (Gustafsson 2003). Natural variations and defects in a tree caused a big difference between the properties of small clear wood specimens and the properties of structural timber. In bending, for instance, clear wood and commercial timber show different failure initiation. In clear wood, the formation of wrinkles in the compression zone governs; and in timber, failure often initiates from tension perpendicular to grain stresses close to knots (Madsen 2000).

There are many issues that present challenges for the development of material models. Kucera and Bariska (1982) showed that there are fracture patterns characteristic of wood in general and other patterns characteristic of the wood species. Smith et al. (2003) postulated that models for wood should be able to accommodate the following materials issues: I) multi-scale effects: the range of material length scales affecting fracture properties (traditional modeling is problematic because the detail required to capture small scale phenomena quickly makes the modeling of a large scale structure untractable); II) geometry dependencies: the relationship between the microstructure of the material and the fracture process zone affecting both measurements of material properties and prediction of structural capacity; and III) species issues: the considerably different fracture processes amongst different species and the variation within species. Frühmann (2002) showed that the consideration of wood, on a macroscopic scale, as a homogeneous, cylindrically-orthotropic material was insufficient, since structural characteristics such as density and growth ring orientation strongly affected the fracture behaviour.

Failure criteria for wood

Special attention has to be directed towards finding an appropriate failure criterion for timber if it is of interest to predict the strength of structural components. Failure criteria are analytical expressions that use basic strength properties to predict failure: whether a certain state of stress will produce plastic deformation in a ductile material or fracture in a brittle material. Every material has certain strength, expressed in terms of stress or strain. When loaded beyond the strength level, the material fractures or fails to carry the load. Failure criteria can be used to characterize the failure and a failure theory is the theory behind the failure criterion.

Failure theories are empirical rules developed from the physical material behaviour that provide a good fit to experimental data. A number of failure criteria applicable to composite materials and wood have been developed, amongst them: Hankinson (1921), Norris (1962) Tsai and Azzi (1965), Hoffmann (1967), Tsai and Wu (1971), Ashkenazi and Ganov (1972), Hashin (1980), Tan (1990), and Tan and Cheng (1993). A detailed overview on these criteria is given in Appendix A. More in depth studies are given by Narayanaswami and Adelman (1977), Edlund (1982), Nahas (1986), Tsai (1984), Rowland (1985), Echabi et al. (1996), Tsai and Kuraishi (2000), París (2001), Aicher and Klöck (2001), and Kasal and Leichti (2005).

Application of failure criteria to wood

Leichti et al. (1989) applied the Tsai-Wu criterion coupled with FEM analyses to predict the failure modes, location of failure and capacity of wood-composite I-beams. Zhang and Tsai (1989) showed that both Tsai-Wu and Norris criteria could predict the crack growth direction in orthotropic materials. Hasebe and Usuki (1989) modified the Tsai-Wu criterion and derived a criterion for plane stress conditions, where the stress perpendicular to the grain was neglected.

Van der Put and Leijten (1999) discussed a modified Hankinson criterion and a method to safely use uni-axial tests to assess properties. He concluded that the tensor polynomial failure criterion could be regarded as a polynomial expansion of the real failure criterion. Leichti and Cheng (1999) studied the biaxial characteristics of plywood using the Tsai–Wu criterion and predicted the strength in the tension-compression and compression–tension quadrants of the stress space. Clouston (1995) investigated multi-axial failure criterion for LVL treating strength parameters as random variables and incorporating size effects. A comparison between established orthotropic failure theories was done and the Tsai-Wu theory was shown to best predict the values of the off-axis data. Wood failure in uni-axial tensile stress states was studied by Galicki and Czech (2005) and the Ashkenazi, Hankinson and Tsai–Wu criteria were shown to correctly describe strength.

Most failure criteria like Tsai-Wu are based on curve fitting considerations and not on physical reasoning. Hashin (1980) pointed out that failure in the Tsai-Wu criterion under biaxial tensile stress depends on the values of the compressive failure stresses which is physically unacceptable. The Tsai-Wu theory does not include material-specific failure mechanisms nor the resulting strength-degradation in the post-critical range in dependence of type and direction of loading.

According to the theory of plasticity, there are two possibilities to describe the change of the yield surface. It can be expanded in size (isotropic hardening) or translated in space (kinematic hardening). Mackenzie-Helnwein et al. (2003) proposed a multi-surface plasticity model that permitted the identification of distinct micromechanical failure modes. Wood under biaxial loading in plane stress considering linear elastic orthotropic behaviour, failure locations in the stress space and hardening type plasticity in the pre-failure domain were studied. Wood

that contained a compressive radial component of stress was subjected to biaxial loading exhibited linear elastic-hardening type plastic behaviour instead of nonlinear elastic behaviour.

Grosse and Rautenstrauch (2004) developed a material model based on maximum-stress criteria and included interactions between transverse tension, longitudinal and rolling shear in the LT- and LR-plane respectively and a third interaction between longitudinal shear strength in LR-plane with transverse compression. Different failure mechanisms were taken into account by separate yield criteria and the strength degradations related to the mode and direction of loading were characterised independently of each other. The interaction between yield criteria was taken into account using multi-surface plasticity and the strength-reduction as result of shear or tension failure was described as dependent of fracture-energy dissipated during crack formation.

Weibull theory

Relating the strength of a material to the weakest link in the structure of the material is one aspect to the engineering approach to strength and fracture of wood. Three approaches to explain size effect on the strength of wood were developed: I) the probability of encountering a very weak point increases in a large volume of a material where more weak points exist; II) the higher stiffness in the radial direction in the middle of a lumber board creates a region of stress higher than the nominal mean stress; and III) defects such as drying cracks tend to be larger in large specimens, (Dinwoodie 2000).

The fact that strength decreases with an increase of stressed volume is usually explained on a stochastic basis, using Weibull theory, relying on the increased probability of encountering a strength-reducing flaw when the stressed volume of the material is increased. Weibull (1939) postulated that a critical flaw in the material dictates failure strength and that the measured

strength distribution of a material was determined by the probability that a critical flaw was present. Weibull theory allows estimating the influence of size of the stressed volume and the stress distribution over this volume on the strength of homogeneous, isotropic materials with brittle fracture behaviour. Although wood is neither homogeneous nor isotropic, Weibull theory has been successfully applied to wood. It assumes that elements of a member with reference volume V_r under a uniform tensile stress have a cumulative probability distribution given by Equation 1-7:

$$F = 1 - \exp\left[-\left(\frac{\sigma - \sigma_0}{m} \right)^k \right] \qquad \text{Equation 1-7}$$

where F is the cumulative probability of failure, σ is the material strength, m a scale parameter, k a shape parameter, and σ_0 the minimum strength of the 3-parameter Weibull distribution for this volume. Often, the strength threshold σ_0 is accepted as being equal to zero and the resulting formulation is called a 2-parameter Weibull distribution. All parameters can be estimated using experimental data and maximum likelihood procedures.

The cumulative failure probability of a volume V subjected to a non-uniform stress distribution $\sigma = \sigma(x, y, z)$ is given by Equation 1-8:

$$F = 1 - \exp\left[-\frac{1}{V} * \int_V \left(\frac{\sigma - \sigma_0}{m} \right)^k dV \right] \qquad \text{Equation 1-8}$$

An equivalent volume V_e subject to a uniform stress σ^* with the same probability of failure as the member subject to the non-uniform stress can be defined by Equation 1-9:

$$V_e \sigma^{*k} = \int_V \sigma_n^k dV \qquad \text{Equation 1-9}$$

For two members of volumes V_1 and V_2 subject to equal loading and with the same probability of failure, a comparison of the strengths of the volumes leads to Equation 1-10:

$$P_f\left(\sigma_{n1}^k\right) = P_f\left(\sigma_{n2}^k\right) \Rightarrow V_1 \cdot \left(\frac{\sigma_1}{m}\right)^k = V_2 \cdot \left(\frac{\sigma_2}{m}\right)^k \Rightarrow \frac{\sigma_1}{\sigma_2} = \left(\frac{V_2}{V_1}\right)^{1/k} \qquad \text{Equation 1-10}$$

Application of Weibull theory to wood

Weibull theory has been widely applied to characterize the magnitude of size effects on the brittle failure of timber. One of the first applications was the evaluation of bending strength. Bohannan (1966) showed that the strength of wood beams varied with beam depth and length. Barrett (1974) and Barrett et al. (1975) successfully applied Weibull theory to the determination of strength of Douglas fir (*Pseudotsuga menziesii*) in tension perpendicular to grain. The ultimate stresses at a given survival probability for pitched tapered beams, curved beams and nail connections were derived and the theoretical results were shown to be in good agreement with experimental data. Foschi and Barrett (1976) provided a volume size based strength model for Douglas fir beam failing in shear. Colling (1986) confirmed the size effect for shear and perpendicular to grain failure for other species and discussed the influence of stress distribution and size of stressed volume for beams and developed a design method. Larsen and Riberholt (1981) studied size effect for Scandinavian wood and concluded that a 2-parameter Weibull distribution with a shape parameter of k = 5 describes the strength variation.

Weibull's theory has also been successfully applied to describe failure of engineered wood products. Clouston (1995) incorporated size effects into a failure criterion for LVL treating

strength parameters as random variables. Fonselius (1997) studied experimentally the effect of size on bending strength for LVL and found member width to have no effect and the effect of length to be more severe than the effect of depth. Liu (1981) expanded the analysis of size effect on bending strength to include tapered wood beams under arbitrary loading conditions and proposed a new design procedure. Blass and Schmidt (1999) studied the tensile strength perpendicular to grain of glulam and the volume effect was described with a shape parameter k = 3.3 - similar to findings of Ranta-Maunus (1996). Dill-Langer et al. (2003) confirmed the size effect for tension parallel strength of clear wood and a significant dependency of the mean strength on the cross-sectional specimen size and fit the distribution of the strength values with a shape parameter k = 8. Gustafsson (2003) compiled test results from Gustafsson (1988), Larsen and Riberholt (1983) and Aicher et al. (1998) and obtained a logarithmic linear relation for tension perpendicular to grain strength: $f_{t,90}/f_0 = 1.5(V / V_0)^{-0.2}$ (f_0 = 1.0 MPa and V_0 = 1.0 dm^3).

Ranta-Maunus (1996) suggested an integration of the tension stress perpendicular to the grain in order to incorporate the non-uniform stress state introduced by the transverse anisotropy. The effective stress, or damage relevant Weibull stress, is calculated according to Equation 1-11:

$$\sigma_{t,90,Wei} = \left(\frac{1}{V} \int_V \sigma_{t,90}^k dV \right)^{1/k} \qquad \text{Equation 1-11}$$

where the Weibull stress $\sigma_{t,90,Wei}$, is the value of constant stress that gives the same probability of failure as the actual stress distribution. The underlying idea of damage relevant stresses is to weigh local stress peaks according to the Weibull theory. The non-uniform stress state was reported by Hanhijarvi and Ranta-Maunus (1996) and used by Aicher et al. (1998) with the modification that the integral over the volume was replaced with an integral along a line.

While most studies on the strength of timber confirmed the size effect, disagreement exists regarding the influence of specific member dimensions. Mistler (1998) suggested to replace volume by height in beam design as strength was found to vary more with specimen height than with specimen volume. While Madsen (1992) reported inconsistent width effects for bending and tension members, Johnson et al. (1989) reported similar width effect for tension and bending members. Barrett et al. (1995) developed a unified size-effect model to represent statistical size effects in visually graded lumber and concluded that size effect factors were not statistically different across grades species or strength levels in contrast to findings from Madsen and Buchanan (1986) who suggested that size effect was grade dependent.

Critique of the application of Weibull theory to wood

Progress has been made towards applications of size effect to a variety of loading conditions and materials, refinements of the statistical basis, and implementation of the theory's predictions to design standards (Smith et al. 2003). But despite the successful use of Weibull theory to wood, there are some fundamental questions towards its applicability. Bazant (1999) argues that the theory presumed that a given flaw size equated with a certain critical load, which was an appropriate assumption for purely brittle materials, but not for materials where stress redistribution could take place at a crack when toughening mechanisms were mobilised. Wood contains quite extensive damage of various types and from various causes, and there is no basis on which to presume that these flaws are homogenously dispersed in a truly statistic sense. There is not necessarily a relationship between the critical flaw sizes of clear specimens and the real flaws in wood, and since fracture is typically confined to planes of weakness along the grain, strength cannot be truly random throughout the volume (Boatright and Garrett 1980).

Aicher et al. (1993) investigated size effects of notched specimens and found that the test results could be better approximated by means of fracture mechanics than with Weibull theory. Blass and Schmidt (1999) postulated for tensile strength perpendicular to grain that the presence of macroscopic defects which led to failure governed by stable crack growth were more important than size effect. Pedersen et al. (2003) presented experiments on clear wood under tension perpendicular loading and showed that all specimens failed in the midsection radial plane, independent of specimen height. In consequence of this deterministic failure location, Pedersen et al. (2003) argued that strength did not depend on the strength distribution in the material outside the failure zone and the observed strength decrease with increased volume could not be explained by Weibull theory.

Using Weibull theory to analyse components with stress concentrations (e.g. drilled or notched members, mechanical connections), capacities can be under-predicted considerably (Smith et al. 2003). This is because predictions usually are made for one stress component at a time and only for states of stress expected to exhibit brittle-elastic characteristics (tension and shear). There is no allowance for softening of stress peaks as it often occurs under complex multi-axial stress states that accompany stress concentrations. Usually it is assumed that failure probability is an integration of probabilities for all increments of volume which is questionable for stress concentrations that are loci for major fracturing and constrain the location of the failure plane. This discrepancy can be particularly acute if the 2-parameter form of the Weibull theory is employed. Strategies that mitigate problems associated with application of statistical fracture theories include the use of models that recognise that materials do not have zero threshold strength and recognition that all regions of a member are not equally liable to be the site of fracture.

Nevertheless, recognition of size effects is important when using conventional strength-based failure criteria (Smith et al. 2003) as shown by Clouston et al. (1998) who implemented Weibull theory into the Tsai-Wu failure criterion to assess volume effects in LVL. By integrating these two approaches, size effects can be introduced into a stress based failure criterion.

Other approaches to describe wood failure

The conventional model in timber engineering for strength analysis is linear elasticity together with a stress-based failure criterion, assuming timber to be a continuous, homogeneous, transversely isotropic and brittle material with deterministic properties (Smith et al. 2003). Looking at perpendicular to grain failures, this approach often gives poor results and in consequence, many building codes do not state a tension perpendicular to grain strength. To consider size effect and the stochastic nature of material properties are steps towards more accurate modelling in relation to fracture perpendicular to grain. But it is important to recognise that traditional strength criteria often fail in regions with steep stress gradients, since they are incapable of representing stress redistribution, or variability in properties within and across growth rings (Smith et al. 2003).

Linear elastic fracture mechanics (LEFM) deals with the behaviour of cracks and their influence on structural members. The distinction between clear wood that is nominally free of defects and structural timber that has an assortment of defects is not necessary in a fracture mechanics context. Wood is full of cracks and as fracture mechanics explicitly deals with the relationship between a material's cracks and its strength, the application seems natural. However, much of fracture mechanics solutions were derived for homogeneous and isotropic materials; therefore, these have to be applied with caution to wood. LEFM analysis of wood works well in

situations where the stress intensity region adjacent to a stress raising feature is small in comparison with overall dimensions of the member (Smith et al. 2003).

Probabilistic fracture mechanics refers to models, where the stochastic nature of the material and the non-zero fracture toughness of timber are taken into account. Foschi et al. (1989) applied a combination of LEFM and stochastics to the shear force strength design of timber beams. The length of end cracks which are assumed to govern the beam shear strength is defined as a stochastic variable according to empirical observations. A reliability strength design method is proposed, in which both a fracture mechanics and a scatter size effect can be included.

Bazant and Pfeiffer (1987) proposed an approximate non-linear size effect model which was used by Aicher and Reinhardt (1993) to model single-edge notched wood specimens. The Finite Small Area Fracture Criterion (Masuda 1996) is based on the concept that fracture occurs when average strains in a finite small area satisfied a criterion, for example the Norris criterion. The criterion includes both concepts of fracture mechanics and ordinary stress criteria; it can explain size effects and can predict fracture loads with and without sharp cracks. A combination of fracture mechanics and probabilistic theory was outlined by Gustafsson and Serrano (1999).

Daudeville (1999) presents a damage mechanics (DM) model for the simulation of fracture in wood. DM is a phenomenological approach that has been developed for materials that do not exhibit plastic deformations, but also cannot be characterized by brittle rupture. The basic idea is that materials exhibit a decrease in stiffness due to the formation of microcracks, or more generically, damage. Applications of damage mechanics to wood have been sparse due to the difficulty in covering the wide range of length scales in a continuum framework.

1.5.3. Western hemlock

The research presented in this dissertation used primarily western hemlock (*Tsuga heterophylla*). Tsuga is from the Japanese Tsu-ga, the elements for "tree" and "mother," and heterophylla is Greek for "different leaves". Common names for western hemlock are Alaska pine, Pacific hemlock and west coast hemlock. Western hemlock occurs in the coast ranges from Sonoma County California to the Kenai Peninsula in Alaska, and inland along the slopes of the Cascade Range in Oregon and Washington and west of the Continental Divide in the northern Rocky Mountains. Outstanding examples can be found throughout the lowlands of Olympic National Park and at Pacific Rim National Park on Vancouver Island. Portions of the Washington and Oregon Coast Ranges are managed primarily for western hemlock production. In terms of biomass production, western hemlock forests are amongst the most productive forests in the world (USDA 2002).

Naturally grown 90-year-old western hemlock stands represent much of the emerging timber supply in the British Columbia (BC) coastal forest (Figure 1-3). Western hemlock usually grows between 30 m and 50 m tall and from 60 cm to 120 cm in trunk diameter. On best sites, old-growth trees can reach diameters greater than 200 cm and heights of 60 m; maximum height has been reported as 79 m (USDA 2002). Western hemlock has a long slender trunk often becoming fluted when large, a short, narrow crown and mostly down-sweeping branches and delicate feathery foliage.

Figure 1-3: Western hemlock exemplar (left) and range within BC (right), (Government of BC 2001)

Western hemlock is recognized as an all-purpose raw material. The wood is superior to that of other hemlocks for building purposes and it makes excellent pulp for paper production. It is the principal source of alpha cellulose fibre used in the manufacture of rayon, cellophane, and many plastics. Large cross section members suitable for heavy timber construction can be produced from these trees. Other uses are lumber for railway ties, mine timbers, and marine piling. The wood has an even grain and resists scraping, and is widely used for doors, windows, parts of staircases, ladders and other architectural millwork items (USDA 2002).

Information characterizing the commercial quality of western hemlock's physical properties was provided by Jozsa et al. (1998) who studied second-growth western hemlock properties including relative density, shrinkage, moisture content, proportions of heartwood-sapwood, content and distribution of compression wood, incidence and degree of spiral grain, and bending strength of small clear samples. Lam et al. (2001) and Barrett et al. (2001) studied the elastic material properties of western hemlock used in Japanese post and beam building.

Marketing challenges of western hemlock

Canada is steward to about 10% of the world's forests, with 309.8 million hectares of forest land. These forests are the backbone of an $82 billion forest industry that adds over $33 billion to the gross domestic product (GDP). In 2003, forest product exports reached almost $40 billion and contributed almost $30 billion to Canada's positive trade balance (NRCAN 2005).

BC is dependent upon natural resource industries as its engines of growth. In 2001, forest products accounted for 32% of exports with an estimated $20 billion and more than 270,000 British Columbians (14% of the total workforce) were employed by the forest industry. Forestry activity contributes approximately $17 billion to the province's GDP and generates approximately $4 billion in government revenues (Baxter et al. 2005). The BC forest industry is characterized by two distinct regions: the Coast and the Interior. These regions are separated by different species, product lines and marketplaces. The Coast industry is over 40% reliant upon the international market and focuses its product lines towards high-valued and specialized applications, with Japan being the coast's most critical market.

Western hemlock has traditionally been a prime export material for the Japanese market for post and beam houses. Since the 1920s, the quality of coastal BC hemlock has allowed the manufacture of distinct products for the Japanese housing market. In the 1960's, BC started shipping regularly to Japan and since the early 1980's these were shipped in metric dimensions and green state. There was a price premium due to the aesthetic values and BC coastal mill producers became price setters in an international market. The majority of lumber shipped to Japan by Coastal operators were building components used in traditional Post and Beam or "Zairai" buildings.

After the 1995 Kobe earthquake, the perception of timber changed and hemlock lost markets to kiln-dried and engineered timber products. Specifically, green hemlock became increasingly non-competitive. The Japanese lumber market saw a significant decline in the use of solid lumber and a parallel increase in the use of laminated lumber. From 1997 to 2004, the usage rate of imported lumber as post material by big builders (more than 200 houses per year) decreased from 14% to 1%. In any scale of builders, the usage rate of imported solid lumber decreased from over 80% to less than 30%, while the use of laminated lumber increased by the same rate ("Structural lumber" 2005). In April 1997, a consumption tax was introduced in Japan and triggered an economic recession with decreasing housing starts. Compared to the 1993 numbers, there was a drop of approximately 30 % until 1997 and since then housing starts have remained at the same low level.

Japanese customers purchased less solid wood and increased the utilization of European laminated post and beam components of traditional Japanese housing. Green and kiln dried solid hemlock continues to be used in ground sills, roof components and small structural applications, but faces stiff competition in retaining market share. The recession combined with the advent of increased lumber shipments from other countries, resulted in a significant loss of market share for BC hemlock. Imports to Japan dropped from more than 4.01 million cubic metres per year in 1996 to less than 2.60 Million cubic metres in 1998.

Although the economy recovered, a shift had occurred to BC producers' disadvantage. After the mid 90s, Japanese customers were no longer willing to pay a price premium for appearance grade BC wood products. Another setback came in 2000 when new building standards were introduced in Japan requiring a 10 year warranty. Shipments in 2003 fell below 1.89 million cubic metres per year. The total share of coastal BC softwood lumber in the

Japanese market declined from 35% in 1995 to 23% in 2003. By comparison, exports of kiln dried western hemlock doubled from 1998 to 2000, albeit from a very low base.

BC's forest industry can try to regain competitive advantage by either being the lowest cost producer of the commodity wood or by differentiating itself with specialty products. Cost minimization is not be a promising long term strategy for BC regional economic development; differentiation is a more effective way if it is clearly identified at every part of the value chain, from harvesting, processing, marketing, sales and post-sale service. Rather than trying to imitate European producers by producing engineered products, the coastal industry concentrated its efforts towards branding its products as Canada Tsuga. In partnership with both the Provincial and Federal governments, a marketing campaign promotes hemlock and provides technical information on strength and stability. Scientific studies investigated the physical and mechanical properties of western hemlock, improving drying methods, and establishing the E120 grade, a special quality of kiln dried hemlock graded according to Japanese standards (Edgington 2004). The freefall in market share was successfully stopped (CFPA 2004) and efforts were mounted to recapture market share in Japan and to increase market diversification in developing economies.

1.6. References

Adalian, C., and Morlier, P. (2001). A model for the behaviour of wood under dynamic multi-axial compression. Composites Science and Technology, 61, 403-408.

Aicher, S., and Klöck, W. (2001). Linear versus quadratic failure criteria for inplane loaded wood based panels. Otto-Graf Journal, 12, 187-200.

Aicher, S., and Reinhardt, H. W. (1993). Einfluss der Bauteilgrösse in der linearen und nichtlinearen (Holz-) Bruchmechanik, Influence of structure size in linear and nonlinear (wood) fracture mechanics (in German). Holz als Roh- und Werkstoff, 51(3), 215-220.

Aicher, S., Reinhardt, H. W., and Klöck, W. (1993). Nichtlineares Bruchmechanik-Maßstabsgesetz für Fichte bei Zugbeanspruchung senkrecht zur Faserrichtung (in German). Holz als Roh- und Werkstoff, 51(6), 385-394.

Aicher. S., Dill-Langer, G., and Ranta-Maunus, A. (1998). Duration of load effect in tension perpendicular to the grain of glulam in different climates. Holz als Roh- und Werkstoff, 56, 295-305.

Askhenazi, E. K., and Ganov, E. V. (1972). Anizotropia konstrukcionnych materialov - Anisotropy of Structural Materials (in Russian). Machinostroenie.

Azzi, V. D., and Tsai, S. W. (1965). Anisotropic strength of composites. Journal of Experimental Mechanics, 5(9), 283-288.

Bamford, S. (2003). The effects of advanced wood processing technologies on contemporary timber design. BSc graduating essay, The University of British Columbia, Vancouver, Canada.

Barrett, J. D, Foschi, R. O., and Fox, S. P. (1975). Perpendicular-to-grain strength of Douglas-fir. Canadian Journal of Civil Engineering, 2, 50-57.

Barrett, J. D. (1974). Effect of size on tension perpendicular-to-grain strength of Douglas-fir. Wood and Fiber, 6(2), 126-143.

Barrett, J. D., Lam, F. and Nakajima, S. (2001). Material strength properties for Canadian species used in Japanese post and beam construction. Proceedings, CIB-W18, Venice, Italy, 34-6-1.

Barrett, J. D., Lam, F., and Lau, W. (1995). Size effect in visually graded softwood structural lumber. Journal of Materials in Civil Engineering, 7(1), 19-30.

Barthel, R., Jagfeld, M., and Gengnagel, C. (1999). Analytische Untersuchungen einer maschinell abgebundenen Zapfenverbindung aus Konstruktionsvollholz zwischen Haupt- und Nebenträger mit Hilfe der FE- Methode (in German). Report, Technical University Munich, Germany.

Baxter, D., Berlin, R., and Ramlo, A. (2005). Regions & resources: The foundations of British Columbia's economic base. Report 62, Urban Futures Institute, Vancouver, Canada.

Bazant, Z. P. (1999). Size effect on structural strength: a review. Archive of Applied Mechanics, 69(9-10), 703-725.

Bazant, Z. P., and Pfeiffer, P. A. (1987). Determination of fracture energy from size effect and brittleness number. ACI Materials Journal, 84(6), 463-480.

Bejtka, I., and Blass, H. J. (2006). Self-tapping screws as reinforcements in beam supports. Proceedings, CIB-W18, Florence, Italy, 39-7-2.

Blass, H. J., and Bejtka, I. (2001). Screws with continuous threads in timber connections. Proceedings, RILEM Symposium on Joints in Timber Structures, Stuttgart, Germany, 193-201.

Blass, H. J., and Bejtka, I. (2004). Reinforcements perpendicular to the grain using self-tapping screws. Proceedings, 8th World Conference on Timber Engineering, Lahti, Finland, Vol.I, 233-238.

Blass, H. J., and Saal, H. (1999). Orientierende Tragfähigkeitsversuche an Haupt-Nebenträgeranschlüssen mit schwalbenschwanzähnlicher Zapfenverbinding sowie SFS-Holzschrauben (in German). Test report No. 996107, Universität Karlsruhe, Germany.

Blass, H. J., and Schmidt, M. (1999). Tensile strength perpendicular to grain of glued laminated timber. Proceedings, CIB-W18, Graz, Austria, 32-6-4.

Boatright, S. W. J., and Garrett, G. G. (1980). On the statistical approach to the fracture toughness variations with specimen size in wood. Engineering Fracture Mechanics, 13, 107-110.

Bobacz, D. (2002). In CNC-Technik gefertigte zimmermannsmäßige Verbindungsmittel - Untersuchung des Schwalbenschwanzzapfens (in German). Diploma thesis, Universität für Bodenkultur, Vienna, Austria.

Bodig, J., Jayne, B. (1982). Mechanics of wood and wood composites. Krieger Publishing Company, New York, USA.

Bohannan, B. (1966). Effect of size on bending strength of wood members. Research paper FPL 56, Forest Products Laboratory, Madison, USA.

Brungraber, R. L. (1985). Traditional timber joints: a modern analysis. Doctoral dissertation, Stanford University, Palo Alto, USA.

Burnett, D. T., Clouston, P., Damery, D. T., and Fisette, P. (2003). Structural properties of pegged timber connections as affected by end distance. Forest Products Journal, 53, 50-57.

CFPA. (2004). Coastal Clarion. Coastal Forest Products Association. <http://www.coastforest.org> (November, 2005).

Chang, W., Hsu, M., and Chen, C. (2004). Estimating Rotational Stiffness of Timber Joints by Using fractional factorial experiments combined with simulation. Proceedings, 8th World Conference on Timber Engineering, Lahti, Finland, Vol.II, 101-106.

Chen, C. J., Lee, T.L., and Jeng, D. S. (2003). Finite element modeling for the mechanical behavior of dowel-type timber joints. Computers and Structures, 81(30-31), 2731-2738.

Church, J. R., and Tew, B. W. (1997). Characterization of bearing strength factors in pegged connections. Journal of Structural Engineering, 123(3), 326-332.

Clouston, P. (1995). The Tsai-Wu strength theory for Douglas-Fir laminated veneer. MApplSc thesis, The University of British Columbia, Vancouver, Canada.

Clouston, P. Lam, F., and J. D. Barrett. (1998). Incorporating size effects in the Tsai-Wu strength theory for Douglas-fir laminated veneer. Wood Science and Technology, 32(3), 215-226.

Colling, F. (1986). Einfluss des Volumes und der Spannungsverteilung auf die Festigkeit eines Rechteckträgers, Influence of volume and stress distribution on the strength of a beam with rectangular cross section, (in German). Holz als Roh- und Werkstoff, 44(4), 121-125.

Daudeville, L. (1999). Fracture in Spruce: experiment and numerical analysis by linear and nonlinear fracture mechanics. Holz als Roh- und Werkstoff, 57, 425-432.

Dietsch, P. (2005). Development of a finite-element model for parameter studies of a dovetail connection. Diploma thesis, Technische Universität, Munich, Germany.

Dill-Langer, G., Cruz Hidalgo, R., Kun, F., Moreno, Y., Aicher, S. and Herrmann, H. J. (2003). Size dependency of tension strength in natural fiber composites. Physica A: Statistical Mechanics and its Applications, 325(3-4), 547-560.

Dinwoody, J. M. (2000). Timber, its nature and behaviour. Van Nostrand Reinholds Co, New York, USA.

Drdacky, M. F., Wald, F., and Mares, J. (2000). Modelling of real historic timber joints. In: Brebbia, C. A., and Jager, W. (eds.), Structural studies, repairs and maintenance of historical buildings. Wessex Institute of Technology, England.

Eberhardsteiner, J. (2002). Mechanisches Verhalten von Fichtenholz - Experimentelle Bestimmung der biaxialen Festigkeitseigenschaften. Springer-Verlag, Vienna, Austria.

Echabi, J., Trochu, F., and Gauvin, R. (1996). Review of failure criteria of fibrous composite materials. Polymer Composites, 17(6), 786-798.

Edgington, D. W. (2004). British Columbia's coastal forests, hemlock timber and the Japanese housing market. Canadian Journal of Regional Science, 27, 415-446.

Edlund, B. (1982). Bruchhypothesen für orthotropes Material (in German). In Ehlbeck, J., and Steck, G. (eds), Ingenieurholzbau in Forschung und Praxis, 17-22. Bruder-Verlag, Karlsruhe, Germany.

Erikson, R. J., and Schmidt, R. J. (2003). Behavior of Traditional Timber Frame Structures Subjected to Lateral Load. Research report, USDA NRI/CGP Contract No. 97-35103-5053, University of Wyoming, Laramie, USA.

Erman, E. (2002). Timber joint design: The geometric breakdown method. Building Research and Information, 30(6), 446-469.

Fonselius, M. (1997). Effect of size on the bending strength of laminated veneer lumber. Wood Science and Technology, 31(6), 399-413.

Foschi, R. O., and Barrett, J. D. (1976). Longitudinal shear strength of Douglas-fir. Canadian Journal of Civil Engineering, 3(2), 198-208.

Foschi, R. O., Folz, B. R., and Yao, F. Z. (1989). Reliability based design of wood structures. Structural research series, report No 34, The University of British Columbia, Vancouver, Canada.

Frühmann, K. (2002). Fracture of wood on different hierarchical levels. Doctoral dissertation, Technische Universität, Vienna, Austria.

Galicki, J., and Czech, M. (2005). Tensile strength of softwood in LR orthotropy plane. Mechanics of Materials, 37(6), 677–686.

Garbin, E., Valuzzi, M. R., and Modena, C. (2006). Characterization of a dovetail joint for timber roofs. Proceedings, 9th World Conference on Timber Engineering, Portland, USA, 2-1-4.

Görlacher, R., and Kromer, M. (1993). TTragfähigkeit von zugbeanspruchten Blattverbindungen in historischen Holzkonstruktionen, Load-carrying capacity of tension scarfs in historical timber constructions, (in German). Bauen mit Holz, 95(4), 290-297.

Government of BC. (2001). Tree book - learning to recognize trees of British Columbia. Government of British Columbia, Ministry of Forestry. <http://http://www.for.gov.bc.ca/hfd/library/documents/treebook> (November, 2004).

Graubner, W. (1990). Holzverbindungen: Gegenüberstellung japanischer und europäischer Lösungen (in German). Deutsche Verlags-Anstalt, Munich, Germany.

Green, D. W., Winandy, J. E., and Kretschmann, D. E. (1999). Mechanical properties of wood. In: Wood handbook - wood as an engineering material. Forest Products Laboratory, Madison, USA.

Grosse, M., and Rautenstrauch, K. (2004). Numerical modelling of timber and fasteners used in timber-concrete-composite constructions. Proceedings, CIB-W18, Edinburgh, Scotland, 37-7-16.

Guan, Z. W., and Rodd, P. D. (2000). A three-dimensional finite element model for locally reinforced timber joints made with hollow dowel fasteners. Canadian Journal of Civil Engineering, 27, 785-797.

Gustafsson, P. J. (2003). Fracture perpendicular to grain - structural applications. In: Thelanderson, S., and Larsen, H. J. (eds), Timber engineering. Wiley & Sons.

Gustafsson, P.J. (1988). A Study of Strength of Notched Beams. Proceedings, CIB-W18, Parksville, Canada, 21-10-1.

Gustafsson, P.J., and Serrano, E. (1999). Fracture mechanics in timber engineering – some methods and applications. Proceedings, RILEM Symposium on Timber Engineering, Stockholm, Sweden, 141-150.

Hampson, J. A. (2003). Moment resistant connections with timber rivets in wood product substrates. MApplSc thesis, The University of British Columbia, Vancouver, Canada.

Hanhijaervi, A., and Ranta-Maunus, A. (1996). Computational analysis of the effect of transverse anisotropy and annual ring pattern in cross-sections of curved glulam beams on the size effect of strengths. Proceedings, European Workshop on Application of Statistics and Probabilities in Wood Mechanics, Bordeaux, France, unpublished.

Hankinson, R. L. (1921). Investigation of crushing strength of spruce at varying angles of grain. Air service Information Circular, 3(259), US Air Service, Ohio, USA.

Hasebe, K., and Usuki, S. (1989). Application of orthotropic failure criterion to wood. Journal of Engineering Mechanics, 115(4), 867-872.

Hashin, Z. (1980). Failure criteria for unidirectional fiber composites. Journal of Applied Mechanics, 47, 329-334.

Heimeshoff, B., and Köhler, N. (1989). Untersuchung über das Tragverhalten von zimmermannsmäßigen Holzverbindungen (in German). Lehrstuhl für Baukonstruktionen und Holzbau, Forschungsbericht T2189, Fraunhofer IRB Verlag, Stuttgart, Germany.

Hemmer, K. (1984). Versagensarten des Holzes der Weisstanne unter mehrachsiger Beanspruchung (in German). Doctoral thesis, Universität Karlsruhe, Germany.

Hochstrate, M. (2000). Untersuchungen zum Tragverhalten von CNC gefertigten Schwalben-schwanzverbindungen (in German). Diplom thesis, FH Hildesheim, Germany.

Hoffman, O. (1967). The brittle strength of orthotropic materials. Journal of Composite Materials, 1(2), 200-207.

Holzner, H. (2000). Entwicklung eines Nachweisverfahrens zur Bemessung von speziellen Zapfenverbindungen (in German). Diplomar thesis, Technische Universität, Munich, Germany.

Johnson, L., Evans, J. W., and Green, D. W. (1989). Volume effect adjustments for the in-grade data. Proceedings 47363, In-grade testing of structural lumber, 56-67. Forest Products Research Society, Madison, USA.

Jönsson, J. (2005). Load carrying capacity of curved glulam beams reinforced with self-tapping screws. Holz als Roh- und Werkstoff, 63(5), 342-346.

Jozsa, L. A., Munro, B. D., and Gordon, J. R. (1998). Basic wood properties of second-growth Western Hemlock. Special Publication No. Sp-38, Forintek Canada Corp, Vancouver, Canada.

Kasal, B., and Leichti, R. J. (2005). State of the art in multi-axial phenomenological failure criteria for wood members. Progress in Structural Engineering and Materials, 7(1), 3-13.

Kessel, M. H., and Augustin, R. (1990). Untersuchungen über das Tragverhalten von Verbindungen mit Eichenholznägeln - Load behavior of connections with oak pegs, (in German). Bauen mit Holz, 04/90, 246-250.

Kharouf, N., McClure, G., and Smith, I. (2003). Elasto-plastic modeling of wood bolted connections. Computers and Structures, 81(8-11), 747-754.

Kreuzinger, H., and Spengler, R. (1999). Zum Tragverhalten von maschinell abgebundenen Zapfenverbindungen aus Konstruktionsvollholz zwischen Haupt- und Nebenträger (in German). Technical report LKI 7313, Technische Universität, Munich, Germany.

Kucera, L. J., and Bariska, M. (1982). On the fracture morphology in wood, Part 1. Wood Science and Technology, 16(4), 241-259.

Lam, F. (2001). Modern structural wood products. Progress in Structural Engineering and Materials, 3(3), 238-245.

Lam, F., Barrett, J.D., and Nakajima, S. (2001). Engineering properties of Hem-Fir used in Japanese post and beam housing. Forest Products Journal, 51(10), 79-87.

Larsen H. J., and Riberholt, H. (1981). Strength of glued laminated beams. Institute of Building Technology and Structural Engineering, Technical report 8110, Aalborg University Centre, Aalborg, Denmark.

Leichti, R. J., and Cheng, P. (1999). An initial assessment of plywood subjected to biaxial loads. Proceedings, Pacific Timber Engineering Conference, New Zealand Forest Research Institute Limited, Rotorua, New Zealand, Vol.III, 229–235.

Leichti, R. J., Corvallis, O. R., and Tang, R. C. (1989). Predicting the load capacity of wood composite I-beams using the tensor polynomial strength theory. Wood Science and Technology, 23(2), 109-121.

Liu, J. Y. (1981). Shear Strength of Tapered Wood Beams. Journal of the Structural Division, 107(5), 719-731.

Mackenzie-Helnwein, P., and Hanhijärvi, A. (2003). Computational analysis of quality reduction during drying of lumber due to irrecoverable deformation, II: algorithmic aspects and practical application. Journal of Engineering Mechanics, 129(9), 1006-1016.

Madsen, B. (1992). Behaviour of timber. Timber engineering Ltd., Vancouver, Canada.

Madsen, B. (2000). Behaviour of timber connections. Vancouver: Timber engineering Ltd., Vancouver, Canada.

Madsen, B., and Buchanan, A. H. (1986). Size effects in timber explained by a modified weakest link theory. Canadian Journal of Civil Engineering, 13(2), 218-232.

Masuda, M. (1996). Application of the finite small area fracture criteria to bending of beams with end sloped notches. Proceedings, International Wood Engineering Conference, New Orleans, USA, Vol.IV, 136-143.

Mihailescu, T. (2001). An investigation of the performance of mortise and tenon joints using the finite element method. Journal of the Institute of Wood Science, 15(5).

Miller, J. F., and Schmidt, R. J. (2004). Capacity of pegged mortise and tenon joinery. Research report for Timber Frame Business Council, University of Wyoming, Laramie, USA.

Mistler, H. (1998). Querzug-Bemessung von BSH-Trägern nach EC 5, Ein Vergleich mit Forschungsergebnissen, Design of glulam beams according to EC 5 with regard to perpendicular-to-grain tensile strength: a comparison with research results, (in German). Holz als Roh- und Werkstoff, 56(1), 51-59.

Moses, D. M. (2000). Constitutive and analytical models for structural composite lumber with applications to bolted connections. PhD thesis, The University of British Columbia, Vancouver, Canada.

Nahas, M. N. (1986). Survey of failure and post-failure theories of laminated fiber-reinforced composites. Journal of Composite Technology and Research, 8(4), 138–153.

Nakajima, S. (2000). The effect of the moisture contents on the strength and stiffness properties of nailed joints and shear walls. Proceedings, 6th World Conference on Timber Engineering, Whistler, Canada, 1-1-3.

Narayanaswami, N., and Adelman, H. M. (1977). Evaluation of the tensor polynomial and Hoffman strength theories for composite materials. Journal of Composite Materials, 11(4), 366-377.

Norris, C. B. (1962). Strength of orthotropic materials subjected to combined stresses. Report No.1816, Forest Products Laboratory, Madison, USA.

NRCAN. (2005). The State of Canada's Forests 2003-2004. Natural Resources Canada. Online: http://www.nrcan-rncan.gc.ca> (November, 2005).

O'Connell, T., and Smith, P. (1999). The North American timber frame housing industry. Forest Products Journal, 49(1), 36-42.

París, F. (2001). A study of failure criteria of fibrous composite materials. Report NASA/CR-2001-210661, George Washington University, Hampton, USA.

Parisi, M. A., and Piazza, M. (2000). Mechanics of plain and retrofitted traditional timber connections. Journal of Structural Engineering, 126(12), 1395-1403.

Patton-Mallory, M., Cramer, S. M., Smith, F. W., and Pellicane P. J. (1997). Nonlinear material models for analysis of bolted connections. Journal of Structural Engineering, 123(8), 1063-1070.

Pedersen, M. U., Clorius, C. O., Damkilde, L., and Hoffmeyer, P. (2003). A simple size effect model for tension perpendicular to the grain. Wood Science and Technology, 37(2), 125-140.

Poulsen, J. S., Moran, P. M., Shih, C. F., and Byskov, E. (1997). Kink band initiation and band broadening in clear wood under compressive loading. Mechanics of Materials, 25(1), 67-77.

Ranta-Maunus, A. (1996). The influence of changing state of stress caused by mechano-sorptive creep on the duration of load effect. Proceedings, International COST 508 Wood Mechanics Conference, Stuttgart, Germany, 187-201.

Reyer, R., and Schmidt, M. (1989). Zum Tragverhalten zimmermannsmäßiger Holzverbindungen (in German). Bauen mit Holz, 07/89, 493-499.

Rowlands, R. E. (1985). Strength (failure) theories and their experimental correlation. In: Sih, G. C., and Sudra, A. M. (eds.), Failure mechanics of composites. Elsevier Science Publications, Amsterdam, The Netherlands.

Sandberg, L. B., Bulleit, W. M., and Reid E. H. (2000). Strength and stiffness of Oak pegs in traditional timber-frame joints. Journal of Structural Engineering, 126(6), 717-723.

Schelling, W., and Hinkes, F.J. (1985). Tragverhalten von Zapfenverbindungen (in German). Forschungsbericht T1533, Fraunhofer IRB Verlag, Stuttgart, Germany.

Schmidt R. J. (2006). Specification for timber frame construction. Draft report, Timber Framers Guild, Becket, USA.

Schmidt, R. J., and Daniels, C. E. (1999). Design considerations for mortise and tenon connections. Research report, USDA NRI/CGP Contract No. 9702896, University of Wyoming, Laramie, USA.

Schmidt, R. J., and MacKay, R. B. (1997). Timber frame tension joinery. Research report for Timber Frame Business Council, University of Wyoming, Laramie, USA.

Schmidt, R. J., and Scholl, G. F. (2000). Load Duration and Seasoning Effects on Mortise and Tenon Joints. Research report, USDA NRI/CGP Contract No. 97-35103-5053, University of Wyoming.

Schmidt, R. J., Wang, D. Q., and Hansen, A. C. (1993). Plasticity theory for transversely isotropic materials. Journal of Engineering Mechanics, 119(4), 748-766.

Schober, K. U. (1999). Numerical Studies of Timber Joints. Proceedings, COST-C1, EUR 18854, Liege, Belgium, 507-516.

Seo, J. M., Choi, I. K., and Lee, J. R. (1999). Static and cyclic behavior of wooden frames with tenon joints under lateral load. Journal of Structural Engineering, 125(3), 344-349.

Smith, I., Landis, E., and Gong, M. (2003). Fracture and fatigue in wood. Wiley & Sons, Chichester, England.

Snow, M., Zheng Chen, A. A., and Chui, Y. H. (2006). North American practices for connections in wood construction. Progress in Structural Engineering and Materials, 8(2), 39–48.

Sobon, J. A. (2001). Historic American timber joinery: A graphic guide. Timber Framers Guild, Becket, USA.

Spengler, R. (1986). Festigkeitsverhalten von Brettelementen aus Fichte unter zweiachsiger Beanspruchung (in German). Project report 68098450340, Technische Universität, Munich, Germany.

Steiniger, M. (2003). Strength and performance of the INDUO-heavy-timber connector in combination with structural composite lumber and Douglas-fir. MSc thesis, The University of British Columbia, Vancouver, Canada.

Structural lumber for conventional wooden post and beam housing - Precut lumber and laminated lumber. (2005). Japan Lumber Journal, 46(17), 2-6.

Tan, S. C. (1990). A new approach of three-dimensional strength theory for anisotropic materials. International Journal of Fracture, 45(1), 35-50.

Tan, S. C., and Cheng, S. (1993). Failure criteria for fibrous anisotropic materials. Journal of Materials in Civil Engineering, 5(2), 198-211.

Tsai, S. W. (1984). A Survey of Macroscopic Failure Criteria for Composite Materials. Journal of Reinforced Plastics and Composites, 3(1), 40-62.

Tsai, S. W., and Kuraishi, A. (2000). Comparison of various failure criteria for orthotropic materials. Proceedings, International Conference on Wood and Wood Fiber Composites, Stuttgart, Germany, 573–584.

Tsai, S. W., and Wu, E. M. (1971). A general theory of strength for anisotropic materials. Journal of Composite Materials, 5(1), 58-80.

USDA. (2002). Tree List. U.S. Department of Agriculture. <http://www.fs.fed.us/database/feis/plants/tree/tsuhet/all.html> (November, 2005).

Van der Put, T. A. C. M., and Leijten, A. J. M. (1999). Evaluation of perpendicular to grain failure of beams caused by concentrated loads of joints. Proceedings, CIB-W18, Delft, Netherlands, Paper 33-7-7.

Weibull, W. (1939). A statistical theory of strength of materials. Proceedings of the Royal Swedish Institute, Research No.151, Stockholm, Sweden.

Werner, H. (2002). Queranschlüsse mit Schwalbenschwanz-Zapfenverbindungen, Vorschlag für die Bemessung (In German). Verband-High-Tech-Abbund im Zimmerhandwerk, Stuttgart, Germany.

Zhang, S. Y., and Tsai, L. W. (1989). Extending Tsai-Hill and Norris criteria to predict cracking direction in orthotropic materials. Journal of Fracture, 40(4), R101-R104.

Zwerger, K. (1997). Das Holz und seine Verbindungen - traditionelle Bautechniken in Europa und Japan (in German). Verlag Birkhäuser, Basel, Switzerland.

Chapter 2: Structural performance of Rounded Dovetail Connections under different loading conditions [5]

2.1. Introduction

Until the mid-20th century, carpentry wood-to-wood connections were commonly used in construction with their design and manufacturing aspects being based on the experience of skilled wood workers. An array of connection details in traditional American, European and Japanese timber-framing is known to be suitable for various applications (Sobon 2001; Graubner 1990; Zwerger 1997). High labour costs, a high degree of required workmanship, assembly difficulties and inefficient use due to over-dimensioning made these connections too expensive and reduced the competitiveness of timber as a construction material.

More recently, important developments in wood processing machines have created the possibility of producing more cost-effective carpentry wood-to-wood connections (Bamford 2003; Bobacz 2002). Use of advanced computer numerical controlled (CNC) milling machinery greatly reduces the requirement of skilled labour to produce wood-to-wood connections such that precision cut quality can be achieved at a competitive cost. As connections often control the cost of timber structures, there are potentially large savings in carpentry wood-to-wood connections when compared with that of off-the-shelf steel fasteners.

[5] A version of this chapter has been published. Tannert, T., Prion, H., and Lam, F. (2007). Performance of Rounded Dovetail Connections under different loading conditions. Canadian Journal of Civil Engineering. 34(12), 1600-1605.

The acceptance of carpentry connections in the North American structural engineering community is affected by a lack of design values and provisions in building codes. Nevertheless, timber framing has experienced a revival in the past two decades and carpentry connections are being used in a growing number of timber-framed buildings (Schmidt and Scholl 2000).

The wooden dovetail is a centuries old connection that has been used extensively throughout Europe and Asia. It was developed as a simple yet effective means to join orthogonal members when other more complicated connections were not feasible. The Rounded Dovetail Connection (RDC) is a relatively new concept specifically adapted to be manufactured using completely automated procedures with a CNC timber processor. The use of RDC in timber construction has significantly increased in Europe, with the most common applications being the connection of two beams (Figure 2-1). RDC are named after the rounded shape in the longitudinal direction of the joist similar to a dovetail (Figure 2-2).

Figure 2-1: Application of RDC in beam-to-joist connection

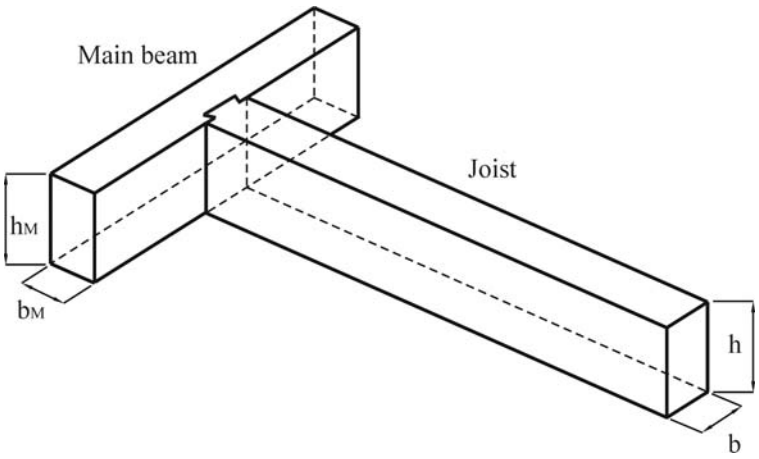

A number of experimental studies on the RDC provided valuable insight into the structural performance of this versatile connection (Kreuzinger and Spengler 1999; Hochstrate 2000; Bobacz 2002). The performance of RDC was found to be superior to end-notched lap joints. Two failure modes were observed: i) tension perpendicular to grain failure at the mortise base; or ii) tenon failure with splitting of the joist member.

A new design, the Double Rounded Dovetail Connection (DRDC) was developed at The University of British Columbia (UBC)[6]. Pilot research indicated that a less brittle failure mode may be achieved as the load is transferred over the bearing areas of the two staggered dovetails, dispersing the stress concentrations. Figure 2-2 compares RDC and DRDC. The complex load transfer mechanism of RDC is governed by its distinct geometric features (Figure 2-3) that also permit the connection to resist longitudinal tension and moment loads in bending along the strong and the weak axis of the joist.

Figure 2-2: Comparison between RDC (left) and DRDC (right)

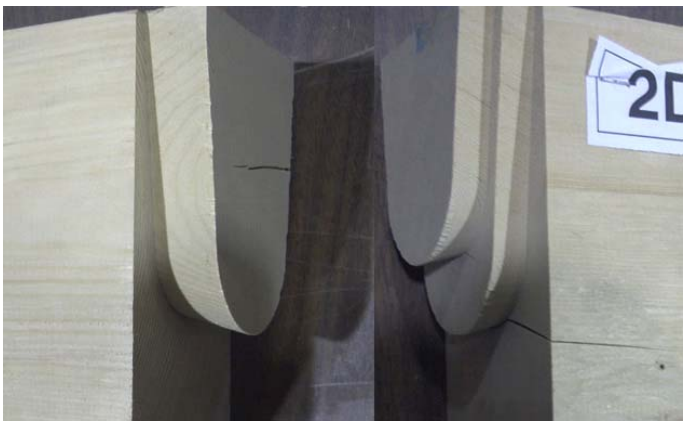

[6] Steiniger, M. 2004. Performance of CNC-processed wood-to-wood joinery with structural composite lumber and solid timber. PhD Thesis Proposal, Faculty of Forestry. The University of British Columbia Vancouver.

Figure 2-3: Geometric parameters of RDC (left) and DRDC (right)

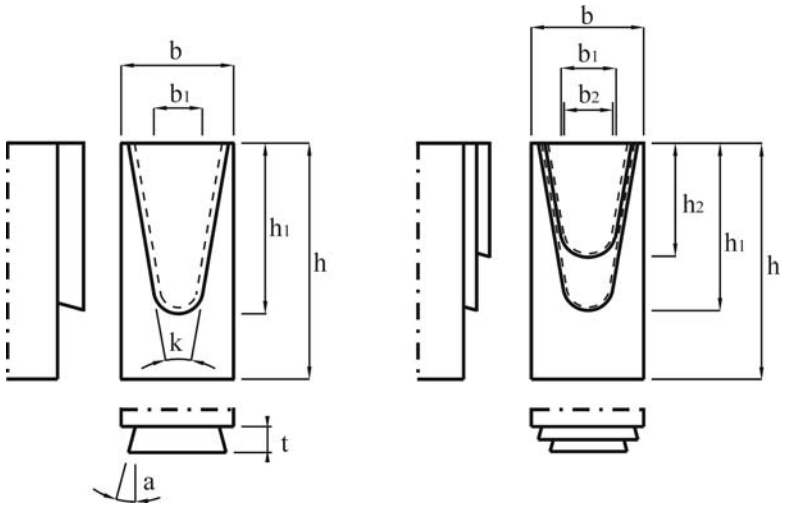

2.2. Objective

In order to comprehend the load carrying mechanism of RDC, experimental tests were conducted with the objective to study the capacity, stiffness, and failure modes of RDC under shear, tension, and bending moment loading (along both axes of the joist), and to compare the structural performance of the single and the double dovetail configurations.

2.3. Material

Kiln-dried western hemlock (*Tsuga heterophylla*) was used for the study. Naturally grown 90-year-old western hemlock stands represent much of the emerging timber supply in the British Columbia coastal forest and have traditionally been a prime export material for the Japanese post and beam construction market. Large cross section members suitable for timber construction can be produced from these trees. The moisture content (MC) and the apparent density (based on specimen as tested weight and volume) of each specimen were determined.

The average and standard deviation of MC were 15.1% and 1.8%, respectively, and the average and standard deviation of apparent density were 490 kg/m³ and 47 kg/m³, respectively.

The RDC was used to connect a joist to a main beam. The member dimensions, b, h, b_M and h_M (Figure 2-3) were chosen as 184 mm x 89 mm respectively in order to allow comparisons with previous studies with similar dimensions. The length of the main beam was chosen as 800 mm, the length of the joist was 1,200 mm for the shear test and 600 mm for the tension and bending tests. The dovetail geometry was chosen as: height h_1 = 109 mm, width b_1 = 50 mm, depth t = 28 mm, dovetail angle a = 15°, and flange angle k = 15°. For the DRDC, the dimensions of the second dovetail were: h_2 = 69 mm and width b_2 = 57.5 mm. A total of 43 specimens were tested: 11 each in shear and tension, and 21 in bending.

2.4. Methods

2.4.1. Shear tests:

The test specimens were mounted on a test apparatus by clamping the main beam with two 200 mm x 100 mm x 10 mm steel brackets to a steel frame (Figure 2-4a), thus preventing rotation about its long axis. The free end of the joist was simply supported on a 100 mm x 100 mm x 10 mm steel plate which rested on a damper with a spring stiffness of approximately 1 kN/mm, thus simulating a longer beam. The load was applied at a distance of 350 mm from the joint and distributed onto the joist with a steel plate with a diameter of 100 mm and 10 mm thickness. The load regime was displacement controlled. A prototype specimen was used to estimate the capacity and set the load application speed for the following tests to ensure that failure of the connection occurred after approximately six minutes, in accordance to EN-26891 (1991). The applied load from the actuator, the vertical and horizontal movement of the joint (as

the relative displacement between main beam and joist), and the deflection of the joist at the load application point were recorded with calibrated transducers.

Figure 2-4: Set-up of experimental tests in: a) shear, and b) tension; all dimensions in mm

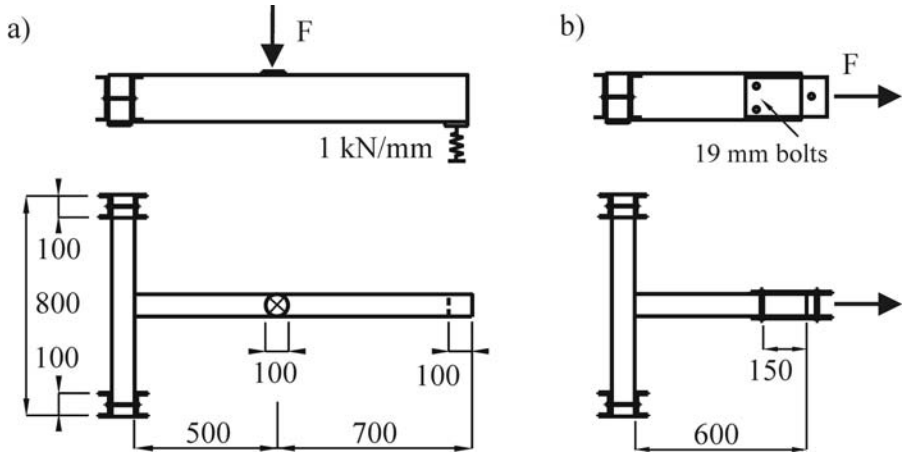

2.4.2. Tension tests

The specimens were mounted on a test apparatus by clamping the main beam to a steel frame (Figure 2-4b). The displacement-controlled load was applied at a distance of 150 mm from the free end of the joist using two 19 mm diameter steel bolts. A prototype specimen was used to estimate the capacity and set the load regime for the following tests to ensure that failure occurred after approximately six minutes. The applied load and the joint deformation in load direction (as the relative displacement between main beam and joist) were recorded.

2.4.3. Bending tests

The specimens were mounted on a test apparatus by clamping the main beam to a steel frame. One series of 10 specimens was subjected to bending along the strong axis of the joist, parallel to the dovetail (Figure 2-5a). A second series of 10 specimens was subjected to bending

along the weak axis of the joist, perpendicular to the dovetail (Figure 2-5b). The displacement-controlled load was applied at a distance of 500 mm from the free end of the joist using a 100 mm x 100 mm x 10 mm steel plate. A prototype specimen was used to estimate the capacity and set the speed for the following tests. The applied load and the absolute deflection of the joist at a distance of 500 mm from the connection were recorded. The rotation was calculated using the deflection values; the bending was calculated moment using the applied load. Photos of all configurations of the tests under different loading conditions are shown in Appendix B.

Figure 2-5: Set-up of experimental tests in: a) bending along the strong joist axis, and b) bending along the weak joist axis; all dimensions in mm

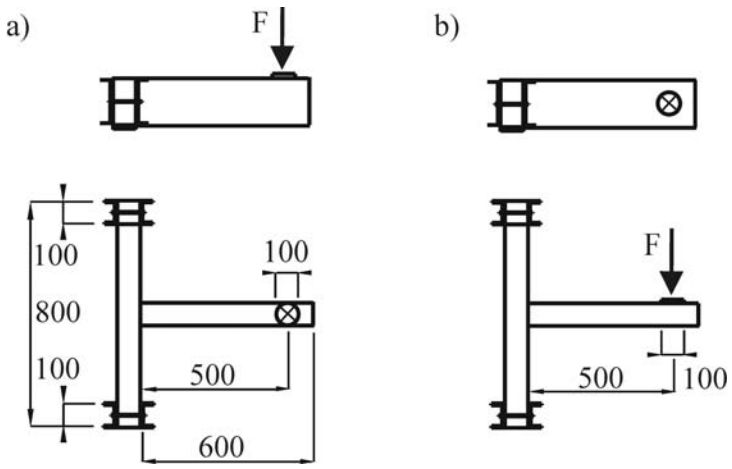

2.4.4. Deformation limits

The maximum forces (F_{ult}) and moments (M_{ult}) applied represent the connection capacities. It is important to consider a deformation limit of the joint in order to prevent unacceptable non-structural damages of the surrounding structure. In this study, a 3 mm limit for the relative vertical deformation between main beam and joist was used and the load at 3 mm deformation ($F_{@3mm}$) was determined. For specimens that failed before deforming 3 mm, the

peak force applied represents the load at 3 mm deformation. The moment at a rotation of 1° ($M_{@1^\circ}$) was used a deformation limit for bending.

2.4.5. Statistical analysis

The test results were evaluated using analysis of variance (ANOVA). ANOVA can be used for comparing means when there are more than two levels of a single factor and to determine whether observed differences in means are statistically significant. A p-value is calculated and compared to α, the significance level. If the p-value is smaller than α, then the null hypothesis of no differences between means is very unlikely, and is rejected. Detailed explanations can be found in textbooks such as Montgomery and Runger (2003).

2.5. Results

2.5.1. Shear tests

In the shear tests, RDC show a linear elastic behaviour until reaching a load that leads to crack development. At that point the load bearing capability drops abruptly, and following a load redistribution process, stable crack development is observed. The load further increases until brittle failure occurs at capacity. Figure 2-6 a and b show the load deformation curves for the individual test specimens. All results for the tests under different loading conditions are listed in Appendix C.

The average shear capacity and the average shear load at 3 mm deformation of RDC and DRDC specimens were almost identical. It was determined using ANOVA that capacity and load at 3 mm deformation of RDC and DRDC are not significantly different at a level $\alpha = 0.05$. The average maximum deformation (d_{max}) of the RDC specimens (4.3 mm) was 10% smaller than

that of the DRDC specimens (4.8 mm). Table 2-1 shows a summary of the results and the p-values from the ANOVA comparing RDC and DRDC in shear and tension tests.

Table 2-1: Summary of shear and tension test and ANOVA results

	Shear test				Tension test			
	$F_{ult,S}$ (kN)		$F_{@3mm,S}$ (kN)		$F_{ult,T}$ (kN)		$F_{@3mm,T}$ (kN)	
	RDC	DRDC	RDC	DRDC	RDC	DRDC	RDC	DRDC
Mean	14.42	14.09	9.15	8.99	8.27	6.11	6.55	5.28
StDev	5.15	3.39	1.32	2.73	0.62	1.31	1.14	0.88
p-value	0.91		0.90		0.01		0.07	

2.5.2. Tension tests

The structural performance of RDC and DRDC in tension showed higher variability among the specimens. The initial stiffness of the specimens varied considerably: some specimens showed linear behaviour until reaching capacity; other specimens showed linear behaviour only initially. All specimens were able to resist considerable tension load and sustained significant deformation before failure. Figure 2-6 c and d show the individual load deformation curves for each test specimen.

RDC exhibit 35% higher capacity compared to DRDC (8.3 kN versus 6.1 kN) and 24% higher load at 3 mm deformation (6.6 kN versus 5.3 kN). It was determined using ANOVA that the capacities are significantly different at a level $\alpha = 0.05$. The average d_{max} of RDC specimens was 41% larger than the average d_{max} of the DRDC specimens (5.4 mm versus 3.9 mm).

2.5.3. Bending tests

In the bending tests, RDC and DRDC showed some variability among the specimens. In all except two specimens, the bending moment dropped beyond approximately 2° of rotation and the maximum moment did not occur at the maximum deformation. All test specimens could undergo very large rotations (more than 15°) while maintaining some moment resistance. In bending along the strong axis of the joist, the RDC and DRDC specimens had similar capacities (0.71 kNm and 0.73 kNm) and identical strength at 1° rotation. The average bending moment along the weak axis of the joist of RDC was 47% higher than that of DRDC specimens (0.50 kNm versus 0.34 kNm). RDC also have 24% higher strength at 1° rotation than DRDC (0.26 kNm versus 0.21 kNm). It was determined using ANOVA that none of the differences are significantly different at a level $\alpha = 0.05$.

Table 2-2 summarizes the test results and the p-values from the ANOVA. Figure 2-6 e, f, g and h show the individual specimen moment deformation curves.

Table 2-2: Summary of bending test and ANOVA results

	bending along the strong axis				bending along the weak axis			
	M_{ult} (kNm)		$M_{@1°}$ (kNm)		M_{ult} (kNm)		$M_{@1°}$ (kNm)	
	RDC	DRDC	RDC	DRDC	RDC	DRDC	RDC	DRDC
Mean	0.71	0.73	0.35	0.35	0.50	0.34	0.26	0.21
StDev	0.14	0.05	0.13	0.10	0.24	0.15	0.07	0.11
p-value	0.76		0.99		0.20		0.38	

Figure 2-6: Load deformation response of: RDC and DRDC in shear, tension, bending along the strong joist axis (I), and bending along the weak joist axis (II)

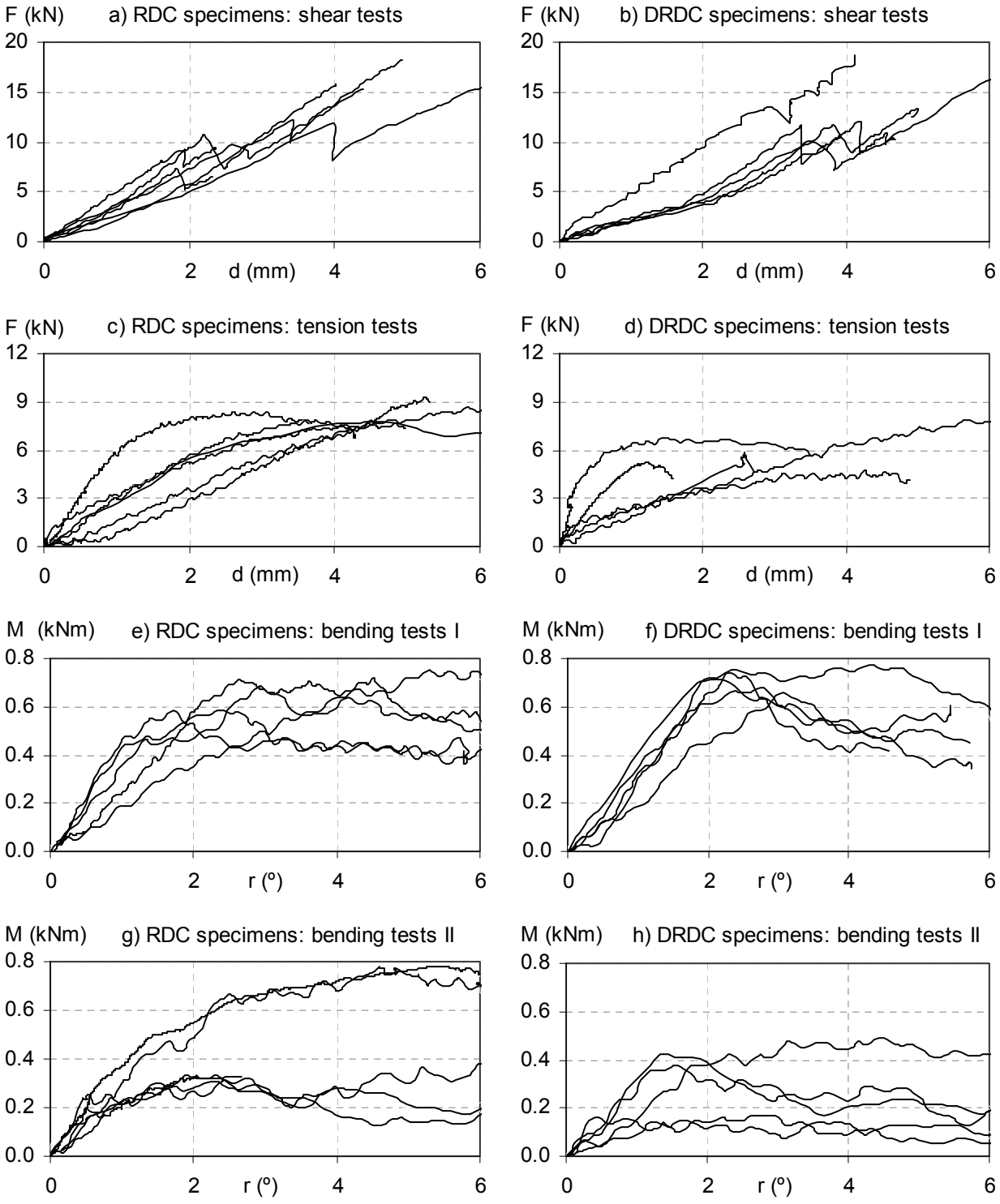

2.6. Discussion

The shear tests demonstrated that RDC show almost linear elastic behaviour until reaching a load that leads to crack development. The carried load of the connections increased even in a cracked state until reaching capacity. No statistically significant difference between RDC and DRDC in shear capacity and shear load at 3 mm deformation was found. Most DRDC specimens developed the first crack after reaching a deformation of 3 mm and the second crack at a higher load. Figure 2-7 illustrates the difference. RDC were stiffer and showed smaller maximum deformations than DRDC. The double dovetail shape makes this connection more susceptible to manufacturing inaccuracies and the load transfer is not continuously guaranteed over the whole bearing area.

Figure 2-7: Typical failure of RDC (left) and DRDC (right)

While RDC are primarily used as shear connection, they also have considerable tension capacity and moment resistance in bending along both axis of the joist. The structural performance, specifically the initial stiffness varied among specimens in tension tests. This can be explained by small differences in the accuracy of the connection fit that can cause different initial slip behaviour. RDC showed a statistically significant 35% higher tension capacity. The

suggested tension load at a deformation of 3 mm was 24% higher, but not statistically significant. In bending tests, it was shown that RDC provide moment resistance, although this resistance is rather small compared to the bending capacity of a beam with the given section. For the tested connections, the resistance in bending along the strong axis of the joist (parallel to the dovetail) being approximately 50% higher than the resistance in bending along the weak axis of the joist (perpendicular to the dovetail). Most of the test specimens showed no further increase in bending moment beyond 2° of rotation. At that point the bending capacity either levels off or decreases. Further results that were obtained indicate that the connection can undergo very large deformation without breaking and maintain some moment resistance. Differences between the single and the double dovetail configurations are statistically not significant.

2.7. Conclusions

The presented work reduces the existing knowledge gap regarding the structural performance of RDC under different loading conditions. It has demonstrated that this versatile connection, although designed and used as a shear connection has high tension capacity and considerable moment resistance in bending. Given the scope of the presented work, the authors cannot comment on whether RDC are appropriate to resist seismic loads under reverse loading conditions or whether the results can be extended to significantly larger dimensions. The observed capacities and the loads at the suggested deformation limit depend on the moisture content and moisture fluctuations of the timber used. The reduction in cross section in timber members caused by RDC needs to be considered in the structural design process. Additional work at UBC further studies this innovative connection to establish amongst other factors the influence of geometric parameters and manufacturing parameters on its structural performance.

2.8. References

Bamford, S. (2003). The effects of advanced wood processing technologies on contemporary timber design. BSc graduating essay, The University of British Columbia, Vancouver, Canada.

Bobacz, D. (2002). In CNC-Technik gefertigte zimmermannsmäßige Verbindungsmittel - Untersuchung des Schwalbenschwanzzapfens (in German). Diploma thesis, Universität für Bodenkultur, Vienna, Austria.

EN-26891. (1991). Timber structures, Joints made with mechanical fasteners, General principles for the determination of strength and deformation characteristics. DIN Deutsches Institut für Normung e.V., Beuth Verlag GmbH, Berlin, Germany.

Graubner, W. (1990). Holzverbindungen: Gegenüberstellung japanischer und europäischer Lösungen (in German). Deutsche Verlags-Anstalt, Munich, Germany.

Hochstrate, M. (2000). Untersuchungen zum Tragverhalten von CNC gefertigten Schwalben-schwanzverbindungen (in German). Diplom thesis, FH Hildesheim, Germany.

Kreuzinger, H., and Spengler, R. (1999). Zum Tragverhalten von maschinell abgebundenen Zapfenverbindungen aus Konstruktionsvollholz zwischen Haupt- und Nebenträger (in German). Technical report LKI 7313, Technische Universität, Munich, Germany.

Montgomery, D. C., and Runger, G. C. (2003). Applied statistics and probability for engineers. Wiley & Sons, New York, USA.

Schmidt, R. J., and Scholl, G. F. (2000). Load Duration and Seasoning Effects on Mortise and Tenon Joints. Research report, USDA NRI/CGP Contract No. 97-35103-5053, University of Wyoming, Laramie, USA.

Sobon, J. A. (2001). Historic American timber joinery: A graphic guide. Timber Framers Guild, Becket, USA.

Zwerger, K. (1997). Das Holz und seine Verbindungen - traditionelle Bautechniken in Europa und Japan (in German). Verlag Birkhäuser, Basel, Switzerland.

Chapter 3: Geometry parameters of Rounded Dovetail Connections [7]

3.1. Introduction

Until the mid-20th century, carpentry wood-to-wood connections were commonly used in construction with their design and manufacturing aspects based on the experience of skilled wood workers. High labour costs, high degree of required workmanship, assembly difficulties, and inefficient use due to over dimensioning made these connections too expensive. Recent developments in wood processing machines have created the possibility of producing these connections cost effectively. The Rounded Dovetail Connection (RDC), named after the rounded shape similar to a dovetail, is a relatively new concept specifically adapted to be produced with a CNC-timber processor.

The use of RDC in timber construction has significantly increased in Europe, with the most common application being the connection of two beams. Different configurations of the wooden dovetail have been extensively used throughout Europe and Asia, primarily governed by practical considerations such as carpenters skills and available tools. Modern CNC wood-processing machinery has changed these constraints and almost any desired geometry is possible. One shape of interest is the Double Rounded Dovetail Connection (DRDC) that was developed at The University of British Columbia (UBC). Preliminary tests on DRDC indicated that a less brittle failure mode may be achieved since the load is transferred over the bearing areas of the two staggered dovetails, dispersing the stress concentrations.

---

[7] A version of this chapter has been published. Tannert, T., and Lam, F. (2006). Geometry parameters of Rounded Dovetail Connections. Proceedings, 9th World Conference on Timber Engineering, Portland, USA, 3-13-4.

The complex load transfer mechanism of RDC and DRDC are governed by their geometric features (Figure 3-1). A number of experimental studies on RDC provided valuable insight into the structural performance of this versatile connection (Kreuzinger and Spengler 1999; Hochstrate 2000; Bobacz 2002). The performance of RDC was found to be superior to end-notched lap joints. Two failure modes were observed: 1) tension perpendicular to grain failure at the mortise base; or 2) tenon failure with splitting of the joist member.

Figure 3-1: Geometric parameters of RDC (left) and DRDC (right)

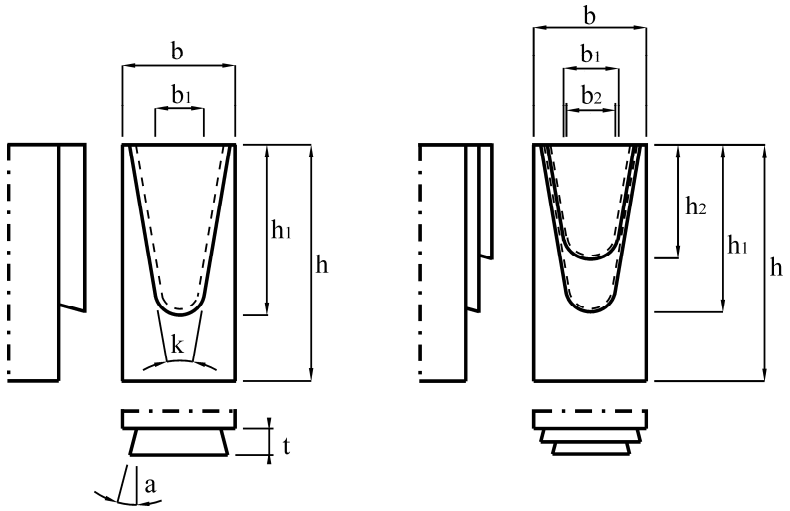

To examine possible improvements in connection efficiency, a sensitivity study based on finite element method analyses was conducted at UBC (Dietsch 2005). Three geometric parameters were studied: 1) the flange angle k; 2) the dovetail angle a; and 3) the dovetail height h_1. The study revealed that the flange angle and the dovetail height have substantial impact on the stress state in the connection while the dovetail angle has little influence. The distinct geometric features of RDC also permit the connection to resist longitudinal tension and moment loads in bending along the strong and the weak axis of the joist. Tannert et al. (2007) reported test results on the structural performance of RDC under these loading conditions. The connection

capacity and the loads at 3 mm deformation of single and double dovetail configurations in tension and bending tests were studied. The work demonstrated that RDC have also considerable tension and bending resistance, and that RDC have higher tension capacity, while not performing significantly different than DRDC under other loading conditions.

3.2. Objective

This work expands on previous studies exploring the influence of geometric parameters on the structural performance of RDC and DRDC in order to comprehend their load carrying mechanism. The objective was to study the influence of the dovetail height h_1 and the flange angle k on the connection capacity, load at 3 mm deformation and maximum deformation of RDC and DRDC under static shear loading.

3.3. Experimental design

Three different dovetail heights and three different flange angles were compared to control geometries for RDC and DRDC. The experimental layout for both studies (dovetail height and flange angle) was a two factor completely randomized design evaluated using analyses of variance (ANOVA). For the first analysis, one factor is the dovetail height with four levels (control and three variations) and the second factor is the dovetail configuration with two levels (single and double dovetail). For the second analysis, the factors are the flange angle (control and three variations) and the dovetail configuration (single and double dovetail).

To enable comparisons with previous studies, the dovetail geometry of the control geometry was chosen as: width b_1 = 50 mm, depth t = 28 mm, dovetail angle a = 15°, flange angle k = 15° and dovetail height h_1 = 119 mm, resulting in a connection back-cut BC

(difference between member height h and dovetail height h_1) of 65 mm. For the DRDC, the dovetail height and width of the second dovetail were h_2 = 79 mm and 57.5 mm, respectively. The three levels of back-cut for the dovetail height study were 75 mm, 55 mm and 45 mm. The test series were labelled as BC75, BC55 and BC45. The heights of the second dovetail of the double dovetail configuration were 115 mm, 95 mm and 85 mm. The three levels of the flange angle k were 20°, 10° and 5°. These test series were labelled as A20, A10 and A05.

3.4. Material

Kiln-dried western hemlock (*Tsuga heterophylla*) was used for the study. Naturally grown 90-year-old western hemlock stands represent much of the emerging timber supply in the British Columbia coastal forest and have traditionally been a prime export material for the Japanese post and beam construction market. Large cross section members suitable for timber construction can be produced from these trees. The moisture content (MC) and the apparent density (based on specimen as tested weight and volume) of each specimen were determined. The average and standard deviation of MC were 12.9% and 1.6%, respectively. The average apparent density was 496 kg/m³ with a standard deviation of 57 kg/m³. A total of 80 specimens were tested, 40 of them with single and 40 with double dovetail configuration, 10 specimens for each of the control series and five specimens for each of the factor levels.

The RDC was applied to connect a joist to a main beam. The member dimensions b and h were chosen as 89 mm x 184 mm, respectively. Since it was of interest to study the behaviour of the connection and not the bending strengths of the beams, vertical shear loading mode was chosen with beam and joist lengths of 600 mm and 800 mm, respectively. The BC75 series was produced from material with dimensions b and h of 84 mm and 178 mm, respectively.

3.5. Methods

Tests were performed similar to previous research on RDC so that the results can be compared. The test specimens were mounted on a test apparatus by supporting the main beam on two 100 mm x 100 mm x 10 mm steel plates, two other steel plates of 50 mm x 50 mm x 5 mm on the backside of the specimens prevented these from moving back (Figure 3-2). The main beam was not clamped, thus allowing minor rotation about its long axis, a situation that simulates the supporting condition in a real structure. The free end of the joist was simply supported on a 100 mm x 100 mm x 10 mm steel plate which rested on a damper with a spring stiffness of approximately 1 kN/mm, thus simulating an approximately 4 m long beam of the given section. The load was applied at a distance of 350 mm from the joint and distributed onto the joist with a steel plate with a diameter of 100 mm and 10 mm thickness. A photo of the set up for the shear tests is given in Appendix D.

Figure 3-2: Set up of shear tests; all dimensions in mm

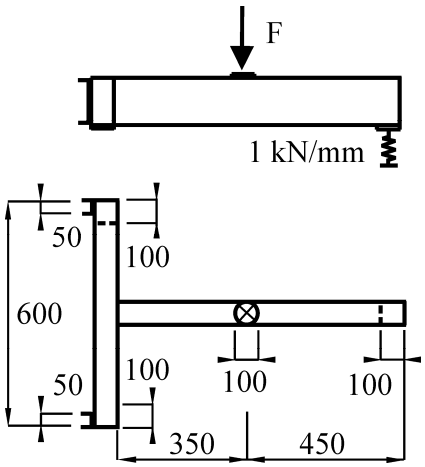

The applied load from the actuator, the force at the support of the free end of the joist, the vertical movement of the joint on both sides of the joint (as the relative displacements between main beam and joist), the horizontal movement of the joint, the deflection of the main beam, as well as the deflection of the joist at the load application point were recorded with calibrated transducers. The force transmitted by the connection was calculated as the difference between the applied load and the load recorded at the free end of the joist. The vertical joint deflection was calculated as the average between the vertical movements of the two joint sides. The load regime was load controlled. One prototype specimen was used to estimate the capacity and set the load application speed for the following tests to ensure that failure of the connection occurred after approximately six minutes, in accordance to EN-26891 (1991). The load was applied until a reading was shown, all the transducer readings were set to zero, and then the load was increased until ultimate failure with a constant rate of loading.

The maximum force applied (F_{ult}) represents the connection capacity. It is important to consider a deformation limit of the joint in order to prevent unacceptable non-structural damages of the surrounding structure. In this study, a 3 mm deformation limit was used and the load at 3 mm deformation ($F_{@3mm}$) of the connection under shear loading was determined. For specimens that failed before deforming 3 mm, the peak force represents the load at 3 mm deformation.

3.6. Results

RDC control specimens show little initial connection slack due to alignment issues. The load increases linearly until reaching deformations between 2 and 3 mm. At that point a load is reached that leads to crack development with a drop in the load deformation curve in some of the test specimens. A load redistribution process initiates and stable crack development is observed.

Further increases in load are associated with bigger increases in deformation until brittle failure occurs at capacity. RDC specimens show large variability in their capacity with 14 kN to 30 kN and fail after reaching deformations between 3 mm and 9 mm.

DRDC control specimens do not show any initial slack due to alignment behaviour. The load-deformation curve is almost tri-linear. The load increases at the beginning of the actuator movement and linear behaviour occurs until reaching a deformation of approximately 1 mm. Then the curve flattens until reaching a deformation of approximately 4 mm. After this point the connection tends to stiffen until reaching capacity. The DRDC specimens also show large variability in their capacity with values between 13 kN and 29 kN and fail after reaching deformations between 4 mm and 9 mm.

The RDC specimens with different dovetail height and flange angles show high variability among the specimens in terms of capacity, maximum deformation and initial stiffness. Some specimens show linear behaviour until reaching capacity; other specimens show linear behaviour only initially. Some specimens show significant initial alignment behaviour with the load increasing only after considerable deformations, in other specimens the load starts to increase at 0.5 mm deformation.

The DRDC specimens with different dovetail height and flange angles show less variability among the specimens and fail at larger deformations in contrast to the RDC specimens. Similar to the control specimens, the load-deformation curves are almost tri-linear. The load increases linearly until reaching a deformation of between 1 mm and 2 mm. Then the curve flattens until reaching a deformation of approximately 3 mm where it gets steeper again until failure.

The load deformation curves of the relative vertical deformation for all test specimens are shown in Figure 3-3. Table 3-1 gives a summary of the test result with the means and standard deviations of the tested variables. All test results are listed in Appendix E; complete load deformation curves are given in Appendix F.

Figure 3-3: Load deformation response of test specimens with varied geometric parameters

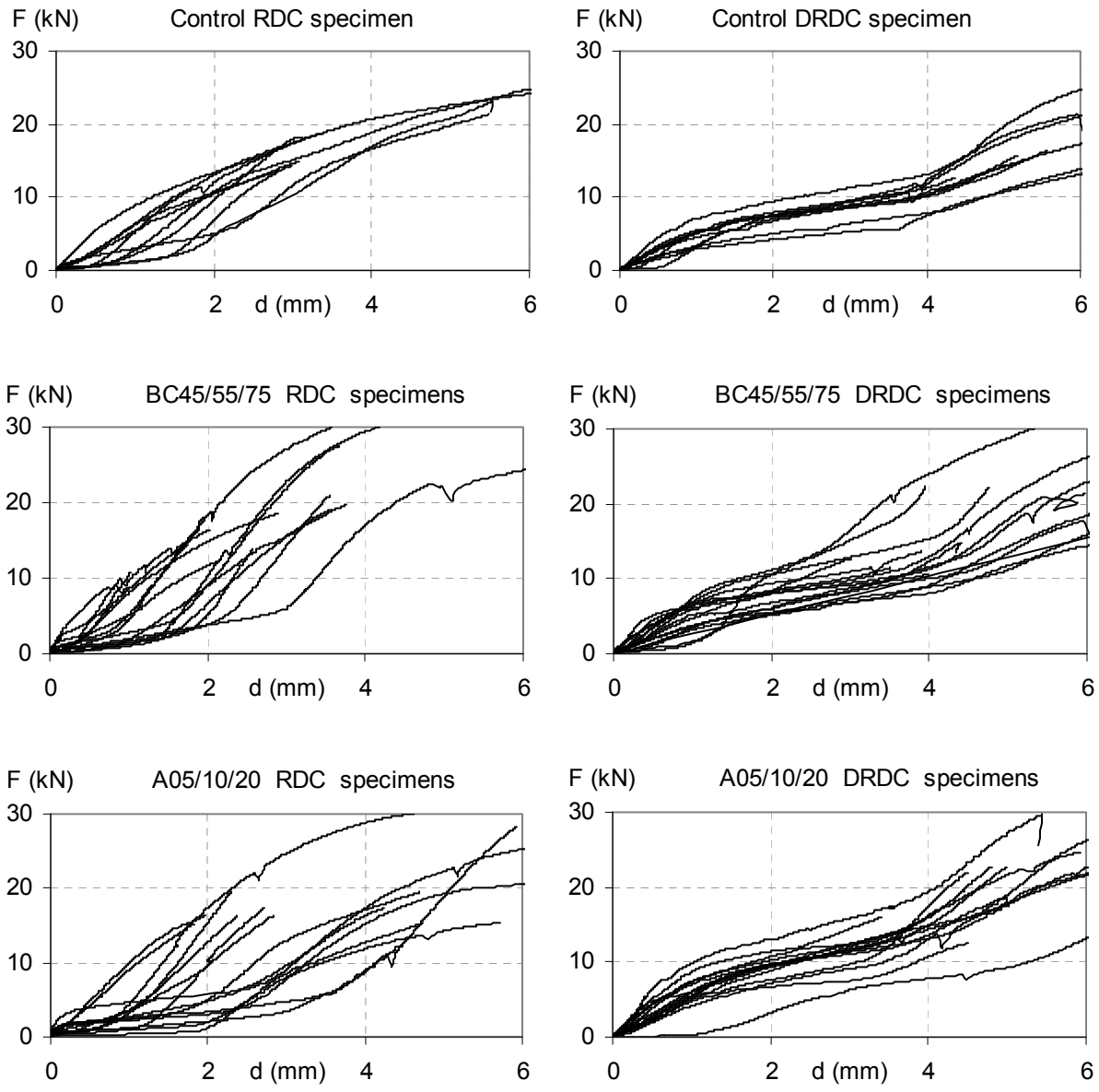

Table 3-1: Summary of shear test results with varied geometric parameters

Test series	F_{ult} (kN)		$F_{@3mm}$ (kN)		d_{max} (mm)	
	Mean	StDev	Mean	StDev	Mean	StDev
Contr.-RDC	19.9	5.6	14.9	2.7	4.6	2.3
Contr.-DRDC	20.0	5.5	8.6	1.7	6.6	1.5
BC75-RDC	12.5	2.9	12.5	2.9	1.8	0.7
BC75-DRDC	12.6	1.7	10.3	1.5	3.8	0.5
BC55-RDC	25.9	11.9	19.6	5.3	4.4	2.3
BC55-DRDC	23.9	6.0	10.8	3.1	5.9	1.7
BC45-RDC	22.8	4.5	15.1	5.9	4.1	2.0
BC45-DRDC	29.7	4.1	9.4	4.0	9.5	2.4
A20-RDC	16.3	0.8	16.3	0.8	2.4	0.4
A20-DRDC	21.2	6.3	12.0	1.7	4.9	1.9
A10-RDC	24.5	9.1	15.0	6.9	6.9	4.3
A10-DRDC	25.0	5.5	12.0	2.4	5.9	1.9
A05-RDC	19.0	6.1	6.6	2.4	5.5	1.1
A05-DRDC	21.4	6.3	9.7	2.7	7.5	2.9

3.7. Analysis

The capacity (F_{ult}), the load at 3 mm deformation ($F_{@3mm}$), and the maximum deformation (d_{max}) of the connection under shear load were recorded and statistically analysed using ANOVA. ANOVA can be used for comparing means when there are more than two levels of a single factor and to determine whether observed differences in means are statistically significant. A p-value is calculated and compared to α, the significance level. If the p-value is smaller than α, then the null hypothesis of no differences between means is very unlikely, and is rejected. Table 3-2 gives a summary of the ANOVA comparing the different dovetail heights and flange angles, as well as RDC and DRDC.

In the study of different dovetail heights, it was determined that the interaction between the factors dovetail height and dovetail configuration is not statistically significant for all response variables. Therefore the factors can be interpreted separately. Multiple comparison tests for the capacity (Bonferroni at $\alpha = 0.05$) showed that the BC75 specimens have a significantly lower capacity than all other dovetail heights, while there is no statistically significant difference between the RDC and DRDC configurations. Regarding the load at 3 mm deformation, RDC are stronger than DRDC, independently from the dovetail height. BC75 RDC specimens are weaker than BC55 RDC specimens. Both factors dovetail height and dovetail configuration are statistically significant for testing the maximum deformation. Multiple comparison tests showed that d_{max} of BC75 specimens are significantly larger than that of all other series and that DRDC show significantly larger maximum deformations for all dovetail heights.

In the study of flange angles, it was determined that the interaction between the factors dovetail height and dovetail configuration has no statistically significant effect on the capacity and maximum deformation. Capacities of A20 specimens are lower than those of A10 and A15 specimens; however, based on the number of specimens tested, this difference is not statistically significant. The maximum deformation of the A05 series is significantly larger than that of the A20 series and DRDC show significantly larger maximum deformations within the A05 and the A20 series. For the load at 3 mm deformation in the study of flange angles, it was determined that the interaction between flange angle and dovetail configuration and is statistically significant. Therefore the factors cannot be interpreted separately. A05 specimens are weaker than all other levels of flange angle. DRDC are stronger within the A05 series while weaker for all other flange angles.

The comparisons of average values, minima and maxima for the connection capacity, load at 3 mm deformation and maximum deformation are illustrated in Figure 3-4, Table 3-2 gives the ANOVA p-values from comparing the different dovetail heights and flange angles, as well as RDC to DRDC.

Figure 3-4: Test results with varied geometric parameters (bounds show extreme values)

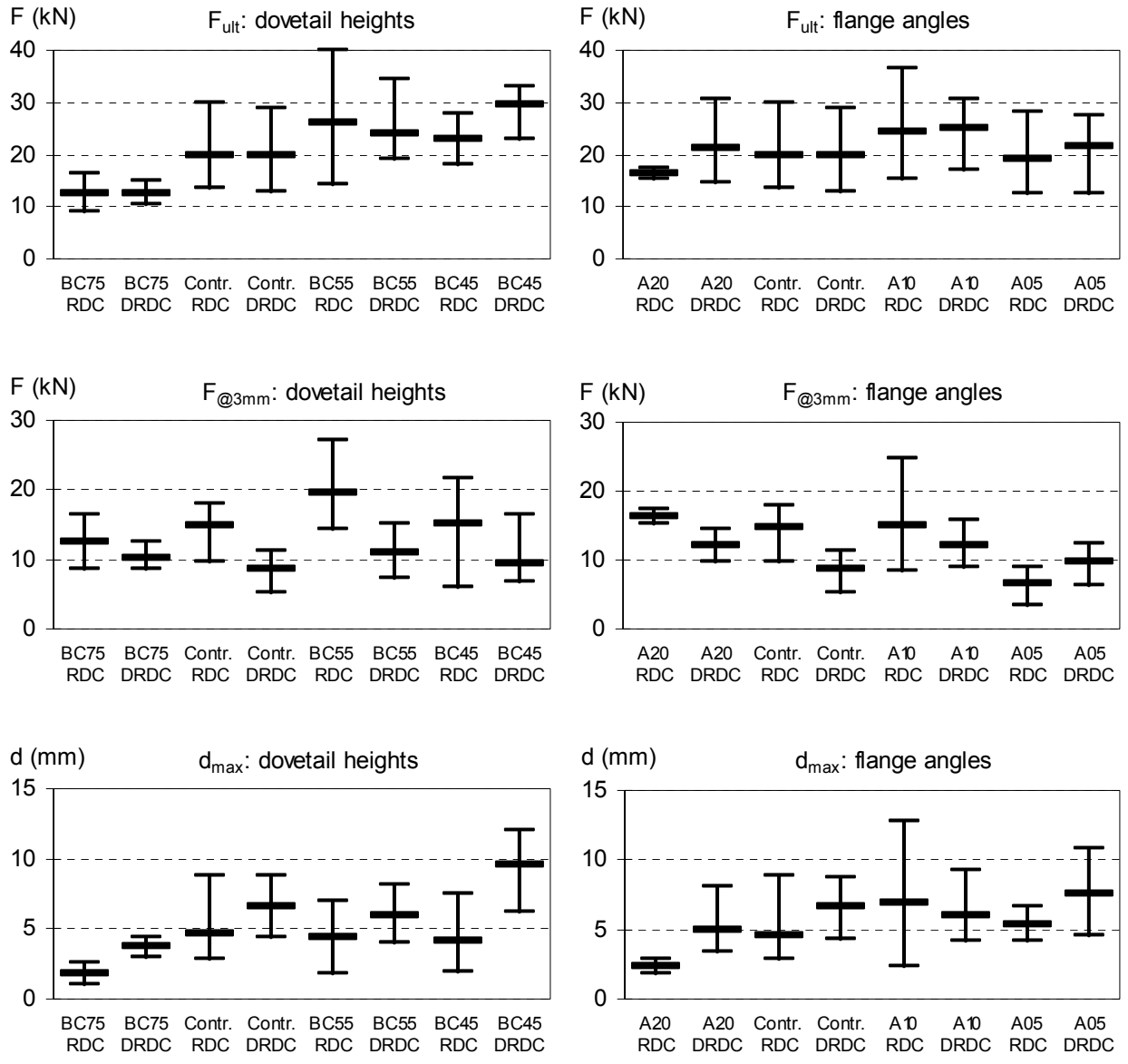

Table 3-2: ANOVA results of shear tests with varied geometric parameters

Tested variable	Study of dovetail heights			Study of flange angles		
	p-value Interaction	p-value Height	p-value Dovetail	p-value Interaction	p-value Angle	p-value Dovetail
F_{ult} (kN)	0.470	<0.001	0.362	0.752	0.125	0.267
$F_{@3mm}$ (kN)	0.198	0.047	<0.001	0.002	<0.001	0.005
d_{max} (mm)	0.071	<0.001	<0.001	0.280	0.020	0.039

Additional statistical analyses including a Multiple Analysis of Variance that confirms the findings of the ANOVA's are given in Appendix G. Other recorded measurements of the shear tests, including the relative horizontal joint deformation are given in Appendix H.

3.8. Discussion

RDC specimens perform somewhat linear throughout the load deformation curve until reaching a deformation that leads to crack development. RDC specimens show initial connection slack due to alignment issues resulting in variability of initial stiffness and loads at 3 mm deformation. Unlike previous studies (Kreuzinger and Spengler 1999; Hochstrate 2000), the presented study did not apply any preload to close initial connection gaps, a testing procedure that may reflect more realistically the condition in practice. In consequence, minor cutting inaccuracies led to the difference in initial alignment behaviour amongst the individual test specimens.

DRDC in contrast show less variability in capacity and maximum deformation. The specimens show little initial connection slack since the first dovetail has immediate connection contact. The load-deformation curve is almost tri-linear. The low stiffness of the middle part of

the curve can possibly be attributed to connection inaccuracies with the second dovetail not completely participating in the load bearing process.

In contrast to the previous tests at UBC (Tannert et al. 2007), DRDC specimens developed only one crack along the planes with high tension perpendicular to the grain stresses and failures of RDC and DRDC were very similar (Figure 3-5). The main difference is that in the previous study the main beam was clamped at the ends while in the presented study a simply supported condition was adopted allowing the main beam to rotate along its long axis.

Figure 3-5: Typical failure of RDC (left) and DRDC (right)

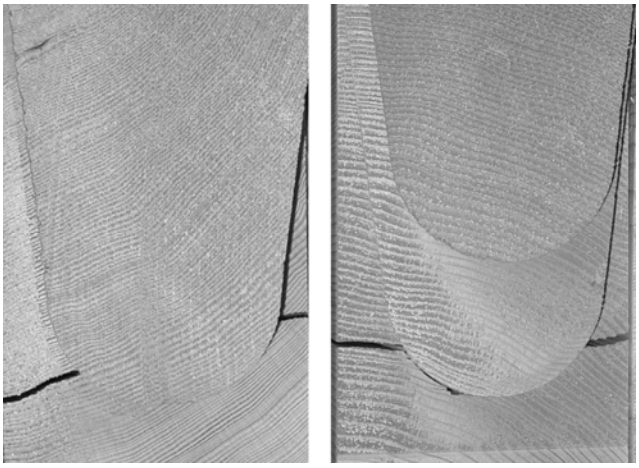

3.9. Conclusion

The presented work reduces the existing knowledge gap regarding the structural performance of RDC. The study showed that shear capacity and shear load at 3 mm deformation do not increase when using the double dovetail configuration. RDC were stiffer and showed smaller maximum deformations than DRDC. The double dovetail shape makes this connection

more susceptible to manufacturing inaccuracies and the load transfer is not continuously guaranteed over the whole bearing area. Based on the results from the presented work, the authors recommend producing RDC with flange angles between 10º and 15º and dovetail heights of approximately 2/3 the member height.

Given the scope of the presented work, the authors cannot comment on whether RDC are appropriate to resist seismic loads under reverse loading conditions or whether the results can be extended to significantly larger dimensions. The observed capacities and the loads at 3 mm deformation depend on the moisture content and moisture fluctuations of the used timber. The reduction in cross section in timber members caused by RDC needs to be considered in the structural design process. Additional work at UBC further studies this innovative connection to establish amongst other factors the influence of manufacturing parameters on its structural performance. The authors recommend to further study applications of RDC to establish amongst other factors the initial alignment behaviour causing the variability in loads at 3 mm deformation and how to avoid it.

3.10. References

Bobacz, D. (2002). In CNC-Technik gefertigte zimmermannsmäßige Verbindungsmittel - Untersuchung des Schwalbenschwanzzapfens (in German). Diploma thesis, Universität für Bodenkultur, Vienna, Austria.

Dietsch, P. (2005). Development of a finite-element model for parameter studies of a dovetail connection. Diploma thesis, Technische Universität, Munich, Germany.

EN-26891. (1991). Timber structures, Joints made with mechanical fasteners, General principles for the determination of strength and deformation characteristics. DIN Deutsches Institut für Normung e.V., Beuth Verlag GmbH, Berlin, Germany.

Hochstrate, M. (2000). Untersuchungen zum Tragverhalten von CNC gefertigten Schwalben-schwanzverbindungen (in German). Diplom thesis, FH Hildesheim, Germany.

Kreuzinger, H., and Spengler, R. (1999). Zum Tragverhalten von maschinell abgebundenen Zapfenverbindungen aus Konstruktionsvollholz zwischen Haupt- und Nebenträger (in German). Technical report LKI 7313, Technische Universität, Munich, Germany.

Chapter 4: Material influence on the structural performance of Rounded Dovetail Connections [8]

4.1. Introduction

Rounded Dovetail Connections (RDC) are a relatively new connection concept adapted to be processed with a CNC-timber processor. Previous work provided valuable insight into the structural performance of RDC and indicated that it depends on geometric parameters (Kreuzinger and Spengler 1999; Hochstrate 2000; Bobacz 2002; Tannert and Lam 2006).

4.2. Objective

This work studies the relationship between the material properties of the wood used and the structural performance of RDC.

4.3. RDC shear tests

Tannert and Lam (2006) studied the influence of the geometry on the capacity and failure mode of RDC and Double Rounded Dovetail Connections (DRDC) under static shear loading. Kiln-dried western hemlock (*Tsuga heterophylla*) was used for the study. The results for capacity (F_{ult}), load at 3 mm deformation ($F_{@3mm}$) and maximum deformation (d_{max}) are summarised in Table 4-1.

[8] A version of this chapter has been prepared for publication. Tannert, T., and Lam, F. (2007). Material influence on the structural performance of Rounded Dovetail Connections.

Table 4-1: Summary of shear test results with varied geometric parameters

Test series	F_{ult} (kN)		$F_{@3mm}$ (kN)		d_{max} (mm)	
	Mean	StDev	Mean	StDev	Mean	StDev
Contr.-RDC	19.9	5.6	14.9	2.7	4.6	2.3
Contr.-DRDC	20.0	5.5	8.6	1.7	6.6	1.5
BC75-RDC	12.5	2.9	12.5	2.9	1.8	0.7
BC75-DRDC	12.6	1.7	10.3	1.5	3.8	0.5
BC55-RDC	25.9	11.9	19.6	5.3	4.4	2.3
BC55-DRDC	23.9	6.0	10.8	3.1	5.9	1.7
BC45-RDC	22.8	4.5	15.1	5.9	4.1	2.0
BC45-DRDC	29.7	4.1	9.4	4.0	9.5	2.4
A20-RDC	16.3	0.8	16.3	0.8	2.4	0.4
A20-DRDC	21.2	6.3	12.0	1.7	4.9	1.9
A10-RDC	24.5	9.1	15.0	6.9	6.9	4.3
A10-DRDC	25.0	5.5	12.0	2.4	5.9	1.9
A05-RDC	19.0	6.1	6.6	2.4	5.5	1.1
A05-DRDC	21.4	6.3	9.7	2.7	7.5	2.9

4.3.1. Relation between wood properties and structural performance of RDC

Regression analysis can be used to make inferences of covariates on the response variables. Covariates are variables that can be measured but cannot be controlled in the experiments. In an analysis of covariance, the variation in the response variable that is associated with the covariate is removed from the error variance resulting in a more powerful test. The objectives of the regression analysis are to: (I) determine whether the covariates have a significant influence on the response variables and (II) formulate equations that describe the structural performance of RDC.

Six covariates were recorded for all test specimens: moisture contents (MC) and apparent densities (ρ) of joist and main beam, growth ring density (ω - number of growth rings within 50 mm) and the growth ring orientation (ϕ - angle with values between 0º for horizontal and 90º for vertical orientation) of each joist member. Growth ring density and growth ring orientation were roughly constant in the area close to the tenon. Knots and other strength determining defect were not encountered. The results are summarised in Table 4-2.

Table 4-2: Summary of material properties for test series

Test series	MC_{Joist} (%)		MC_{Main} (%)		ρ_{Joist} (kg/m^3)		ρ_{Main} (kg/m^3)		ϕ (º)		ω (No/50mm)	
	Mean	StDev	Mean	StDev	Mean	StDev	Mean	StDev	Mean	StDev	Mean	StDev
Contr.-RDC	12.3	1.5	12.9	1.2	498	39	474	32	64	22	46	14
Contr.-DRDC	11.7	0.4	13.7	1.5	441	27	512	44	53	30	41	12
BC75-RDC	12.4	1.6	13.2	1.5	420	40	420	38	52	31	23	3
BC75-DRDC	13.4	1.4	12.8	3.5	427	46	434	38	48	29	20	2
BC55-RDC	12.0	1.4	13.0	3.0	508	73	490	38	82	8	55	18
BC55-DRDC	12.2	0.4	12.9	1.8	504	49	532	43	77	10	47	9
BC45-RDC	12.6	0.8	14.5	1.4	530	35	489	43	73	10	59	17
BC45-DRDC	11.9	0.6	12.5	0.4	453	25	540	42	58	30	54	24
A20-RDC	11.8	0.3	13.7	1.2	506	22	544	77	81	8	37	14
A20-DRDC	12.2	0.4	12.4	0.8	522	37	524	43	75	16	36	12
A10-RDC	12.6	0.9	15.6	1.5	532	8)	550	70	51	45	40	3
A10-DRDC	12.9	0.7	13.6	1.0	528	17	532	39	76	7	42	5
A05-RDC	14.0	1.6	15.0	1.6	473	62	543	83	55	15	41	13
A05-DRDC	13.1	1.0	12.5	1.0	488	68	520	41	83	69	44	11

The study investigated the relation of the geometric parameters (h_1, k), dovetail type (DT converted into a dummy variable), material properties (MC, ρ, ϕ, ω) and the response

variables that describe the structural performance of the test specimens (F_{ult}, $F_{@3mm}$, d_{max}) in order to formulate a set of equations (Equation 4-1):

$$\hat{R}_i = \beta_{i0} + \beta_{i1} * DT + \beta_{i2} * h_1 + \beta_{i3} * k + \beta_{i4} * MC_J + \beta_{i5} * MC_M + \beta_{i6} * \rho_J + \beta_{i7} * \rho_M + \beta_{i8} * \phi + \beta_{i9} * \omega \quad \text{Equation 4-1}$$

where R_i are the response variables and β_i are the parameter estimates.

A regression model was run to determine the parameters estimates and their respective p-values as well as the overall R^2 of the regression (Table 4-3). The R^2 indicate how much of the variation in the response variable can be explained due to the variation in the variables and covariates. The response variables are not well described by the regressions and furthermore, most individual variables and covariates do not contribute significantly to the overall model.

Table 4-3: Complete regression model for RDC and DRDC

Variable	F_{ult}		$F_{@3mm}$		d_{max}	
	β_{1j}	p_{1j}	β_{2j}	p_{2j}	β_{3j}	p_{3j}
Intercept	15.33	0.28	-10.66	0.22	14.04	0.02
DT	3.01	0.02	-3.28	<.001	2.21	<.001
h_1	-0.25	0.01	0.06	0.30	-0.09	0.02
k	-0.25	0.15	0.35	<.001	-0.23	<.001
MC_J	-0.85	0.17	0.12	0.74	-0.33	0.19
MC_M	0.69	0.07	0.06	0.80	0.18	0.24
ρ_J	0.03	0.02	0.03	<.001	0.00	0.62
ρ_M	0.00	0.77	-0.01	0.47	0.00	0.68
ϕ	0.06	0.03	0.03	0.06	0.01	0.33
ω	0.08	0.13	0.05	0.11	0.01	0.70
R^2	0.47		0.53		0.39	

The non-significant variables were dropped one at a time, and a reduced regression model was run taking into consideration only those parameters that have a p-value smaller than 0.05 (meaning they are significant at $\alpha = 0.05$). The reduced models were analysed (Table 4-4). The numbers of parameters needed to describe the response variables were reduced, see Equation 4-2, but the overall R^2 of the regressions decreased. Using an F-test, it was determined that the slopes are not equal between test series. Therefore the covariates do not equally influence the response variables but the trend differs for different factor levels and in consequence, Equation 4-2 is no good predictor for the structural performance of RDC. The relation between basic wood material properties and structural performance of RDC is illustrated in Appendix I.

$$\hat{F}_{ult} = 16.06 + 2.34*DT - 0.32*h_1 + 0.04*\rho_J + 0.06*\phi$$

$$\hat{F}_{@3mm} = -5.22 - 3.45*DT + 0.33*k + 0.04*\rho_J \qquad \text{Equation 4-2}$$

$$\hat{d}_{max} = 11.70 + 2.10*DT - 0.11*h_1 - 0.20*k$$

Table 4-4: Reduced regression model for RDC and DRDC

Variable	F_{ult}		$F_{@3mm}$		d_{max}	
	β_{1j}	p_{1j}	β_{2j}	p_{2j}	β_{3j}	p_{3j}
Intercept	16.06	0.09	-5.22	0.21	11.70	0.00
DT	2.34	0.05	-3.45	0.00	2.10	0.00
h_1	-0.32	0.00			-0.11	0.00
k			0.33	0.00	-0.20	0.00
ρ_J	0.04	0.01	0.04	0.00		
ϕ	0.06	0.03				
R^2	0.39		0.48		0.35	

4.4. Small specimen tests

4.4.1. Materials and methods

Four small specimens were cut from each of the joist members used in the RDC shear tests. A total of 80 specimens each were tested for tension perpendicular to grain and shear parallel to grain strength according to ASTM-D143 (2002). It was assured that these specimens were cut from defect free wood away from the actual failures zones or damaged areas. The specimens were conditioned in a constant climate room to 12% moisture content and the apparent densities based on weight and volume were recorded. The average apparent density was 513 kg/m^3 with a standard deviation of 71 kg/m^3 for the tensions specimens. For the shear specimens the average apparent density was 510 kg/m^3 with a standard deviation of 68 kg/m^3.

4.4.2. Results

The specimen dimensions of the area at the failure location were measured, the peak loads were recorded and the strength values were calculated based on these values. The average tension perpendicular to grain strength was 2.96 N/mm^2 with a standard deviation of 0.80 N/mm^2. The average shear parallel to grain strength was 7.80 N/mm^2 with a standard deviation of 1.53 N/mm^2. These values agree with the in the literature reported values for western hemlock (Green et al. 1999). The detailed results for the small specimen tests are listed in Appendix J.

4.4.3. Relating small specimen test results to RDC shear test results

Plotting the small clear specimen strength values versus the RDC capacity (Figure 4-1 a and b), almost zero correlation was found, indicating that the variability of material strength within a joist member is so high that the strengths of the tested small specimens do not represent

the strength of the part of the large specimens that failed in the RDC. The low correlation of strength values for both shear parallel to grain and tension perpendicular to grain between the two small clear specimens cut from the same joist member supports this hypothesis (Figure 4-1 c and d). This finding is consistent with previous findings of little correlation between notch strength and tension perpendicular to grain strength (Gustafson 1988) and is important for future consideration towards developing a strength based failure criterion for RDC where the high variability of strength values and the influence of size effect have to be taken into account.

Figure 4-1: Correlations: a) RDC capacity vs. shear parallel strength, b) RDC capacity vs. tension perpendicular to grain strength, c) within specimens correlation of shear parallel to grain strength, and d) within specimens correlation of tension perpendicular to grain strength

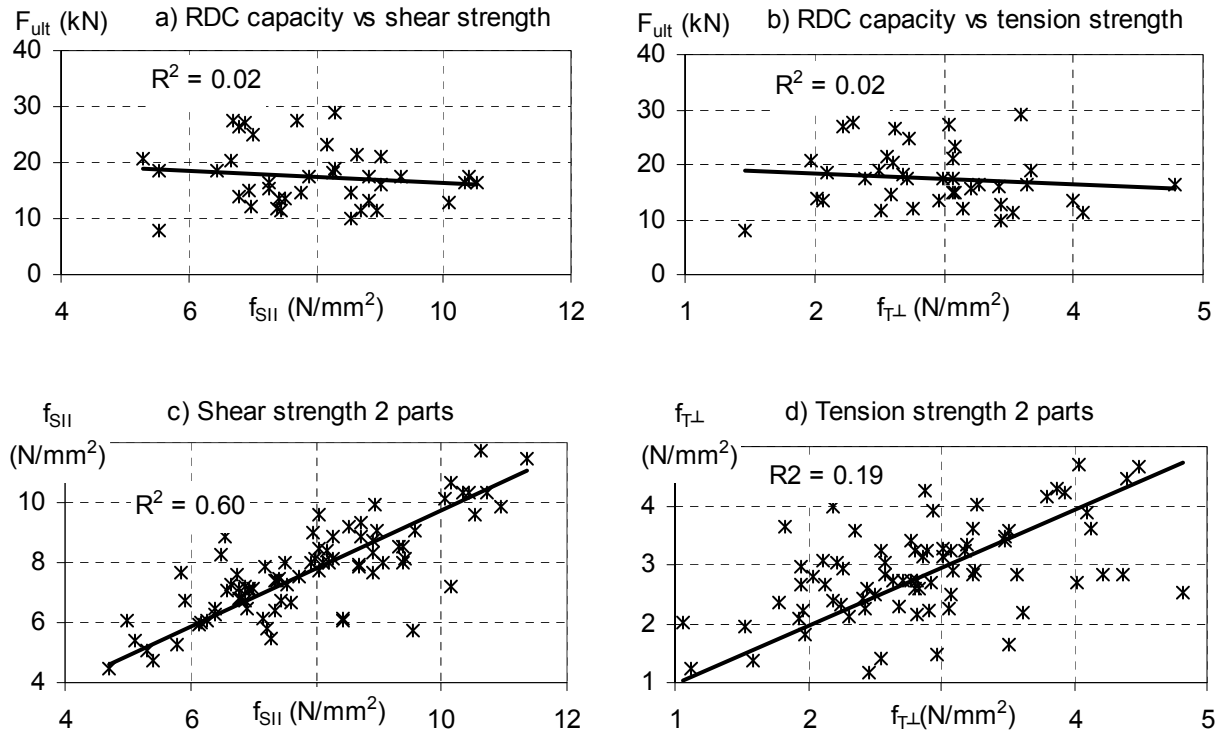

4.5. Discussion and conclusions

The structural performance of RDC in shear loading was related to the physical material properties of the wood used to produce the connected members. A regression analysis indicated that the geometric parameters and the variation within the covariates account for less than 50% of the variation of the response variables. Some covariates have significant influence on the structural response variables, namely joist density and growth ring orientation, but it was shown that the influence of these covariates is not consistent across the different test series. Therefore it is impractical to formulate a set of empirical equations that describe the performance of RDC.

Small specimen tests according to ASTM-D143 (2002) were carried out to determine the shear parallel to grain and tension perpendicular to grain strengths. No correlation was found between these strength values and the RDC capacity. The strength of the tested small clear specimens cannot be used directly to predict the strength of the connection. The low correlations between strength values for the two specimens from the same timber member support this hypothesis. This finding is consistent with previous findings of little correlation between notch strength and tension perpendicular to grain strength (Gustafson 1988) and is important for future consideration towards developing a strength based failure criterion for RDC where the high variability of strength values and the influence of size effect have to be taken into account.

The physical material properties of the wood used to produce the connected members do not dictate the structural performance of RDC. Given the scope of the presented work, the authors cannot comment on whether these findings can be extended to densities and moisture content outside the range considered in this study, as it is well known that strength properties of timber depend on the moisture content, moisture fluctuations and density.

4.6. References

ASTM-D143. (2002). Standards test methods for small clear specimens of timber. Annual book of ASTM standards, section four: construction. Vol. 04.10 wood. West Conshohocken, USA.

Bobacz, D. (2002). In CNC-Technik gefertigte zimmermannsmäßige Verbindungsmittel - Untersuchung des Schwalbenschwanzzapfens (in German). Diploma thesis, Universität für Bodenkultur, Vienna, Austria.

Gustafsson, P.J. (1988). A Study of Strength of Notched Beams. Proceedings, CIB-W18, Parksville, Canada, 21-10-1.

Hochstrate, M. (2000). Untersuchungen zum Tragverhalten von CNC gefertigten Schwalben-schwanzverbindungen (in German). Diplom thesis, FH Hildesheim, Germany.

Kreuzinger, H., and Spengler, R. (1999). Zum Tragverhalten von maschinell abgebundenen Zapfenverbindungen aus Konstruktionsvollholz zwischen Haupt- und Nebenträger (in German). Technical report LKI 7313, Technische Universität, Munich, Germany.

Tannert, T. and Lam, F. (2006). Geometry parameters of Rounded Dovetail Connections. Proceedings, 9th World Conference on Timber Engineering, Portland, USA, 3-13-4.

Chapter 5: Effect of manufacturing parameters on the structural performance of Rounded Dovetail Connections[9]

5.1. Introduction

Until the mid-20th century, carpentry wood-to-wood connections were commonly used in construction with their design and manufacturing based on the experience of skilled wood workers. High labour costs, high degree of required workmanship, assembly difficulties, and inefficient use due to over dimensioning made these connections too expensive. Recent developments in wood processing machines have created the possibility of producing these connections cost effectively. The Rounded Dovetail Connection (RDC) and the Double Rounded Dovetail Connection (DRDC) are relatively new concepts adapted to be produced with a CNC-timber processor. A number of experimental studies on RDC provided valuable insight into the structural performance of this versatile connection (Kreuzinger and Spengler 1999; Hochstrate 2000; Bobacz 2002; Tannert and Lam 2006).

Connections are arguably the most important part in any structural timber system governing the serviceability and durability performance of structures (Snow et al. 2006). The structural performance of timber joints is affected by the manufacturing quality and the moisture content (MC) of the timber members amongst other factors such as wood species and the existence of defects in the wood.

[9] A version of this chapter has been prepared for publication. Anastas , H., Tannert, T., Barrett, J.D., and Lam, F. (2007). Effect of manufacturing parameters on the structural performance of Rounded Dovetail Connections.

Wood-to-wood connections rely on interlocking of their form to provide stiffness and strength; therefore it is essential to have accurately cut components. Wood shrinks and swells if exposed to moisture fluctuations below the fibre saturation point. This characteristic becomes important when the MC of the timber at the time of manufacturing differs significantly from the MC of the timber under service conditions; e.g. structures constructed with green timbers that dry while in service may experience the loosening of originally tight joinery over time. Moisture gradients have been shown to affect the capacity of curved glue-laminated beams. The capacity of beams in a moistening phase is almost halved compared to the mean value of seasoned specimens and beams subjected to climate change display larger variability in capacity than seasoned specimens (Jönsson 2005). Although timber structures are exposed to various climatic conditions, in most cases the strength and stiffness properties of connections are evaluated from results of test specimens conditioned to a standard condition (Nakajima 2000). The performance of the joints of these structures should be properly evaluated according to the conditions in which they are used.

Manufacturing tolerances can significantly impact the performance of connections. Therefore, reducing the variations in geometry and improving the quality of workmanship directly affects connection performance. Reducing the variability in the manufacturing process, CNC-processing technology provides repetitive, identical, very accurate and precise joint geometry. The individual set-up and the service condition of the processing machine and tooling, however, may affect the cut-quality and geometry, hence, the connection performance.

In previous studies at The University of British Columbia, it was proven that excellent tight fitting RDC can be produced, however, the issue of lack of fit resulting from drying of the timber after manufacturing was also encountered. No research on the influence of seasoning on

the structural performance of RDC under load has been done, neither has the effect of manufacturing parameters been studied previously although known to be of vital importance.

5.2. Objective

This work explores the influence of manufacturing parameters (MC fluctuations and tolerances) on the structural performance of RDC and DRDC under static shear loading.

5.3. Experimental design

Four climatic conditioning situations with practical relevance are examined. These are: DD - specimens dry at manufacturing and tested with low MC, DWD - specimens dry at manufacturing, subjected to high humidity, then dried and tested with low MC, WD - specimens subjected to high humidity, wet at manufacturing, then dried and tested with low MC, and WW - specimens wet at manufacturing and tested with high MC. The DD conditioning simulates the desired case of timber processed and used in dry condition. The DWD conditioning simulates a case where dry timber is cut, but then stored or transported in a wet climate, and dried again before being used in a building. The WD conditioning simulates the process of cutting timber with high MC that then dries inside the erected building. The WW conditioning occurs when green timber is processed, and loaded in a structure while it is still green.

The experimental layout for climatic conditions study is a two factor completely randomized design evaluated using analyses of variance (ANOVA). One factor is the conditioning with four levels (control and three variations) and the second factor is the dovetail configuration with two levels (single and double dovetail). A total of 50 specimens (consisting of

main beam and joist) were used in the tests, 10 for the control test series and five for each of the variations for both the single and double dovetail configuration.

Four additional tolerance situations are examined. These are: specimens with a 1 mm gap and a 2 mm gap were produced with a tenon smaller than the mortise by 1 mm and a 2 mm respectively on each side of the dovetail flange, and specimens produced using medium and high machine processing speed. These test series are compared to a control - specimens produced at low machine cutting speed and with tight fitting joint. The experimental layout for the tolerances study is a one factor completely randomized design comparing the four different conditions to the control. 20 specimens were used in the manufacturing tolerances tests. Five specimens each were manufactured with a 1-mm gap and a 2-mm gap, and at medium and high speed.

5.4. Material

Kiln-dried western hemlock (*Tsuga heterophylla*) was used in the study. The moisture content (MC) and the apparent density (based on specimen as tested weight and volume) of each specimen were determined before testing. Table 5-1 summarizes the material properties.

The RDC was applied to connect a joist to a main beam. The member width and height were chosen as 89 mm x 184 mm, respectively. Vertical shear loading mode was chosen with beam and joist lengths of 600 mm and 800 mm, respectively. To enable comparisons with previous studies, the dovetail geometry (Figure 5-1) was chosen as: width b_1 = 50 mm, depth t = 28 mm, dovetail angle a = 15°, flange angle k = 15° and dovetail height h_1 = 119 mm. For the DRDC, the height and width of the second dovetail were h_1 = 79 mm and b_2 = 57.5 mm, respectively. The Hundegger K2-5 5-axis beam processor was used to process all test specimens.

Figure 5-1: Geometric parameters of RDC (left) and DRDC (right)

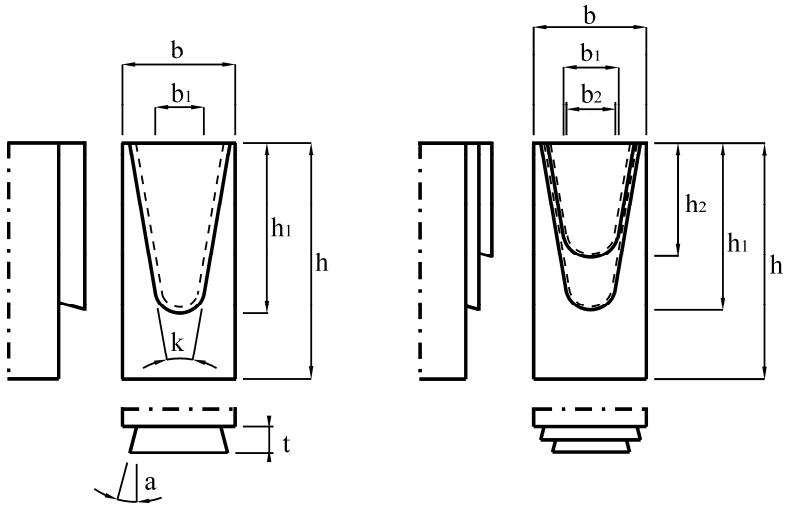

Table 5-1: Material properties for tests with varied manufacturing parameters

Test series	MC (%)				Density (kg/m^3)			
	Main beam		Joist		Main beam		Joist	
	Mean	StDev	Mean	StDev	Mean	StDev	Mean	StDev
Contr.-RDC	12.9	1.2	12.3	1.5	474	32	498	39
Contr.-DRDC	13.7	1.5	11.7	0.4	512	44	441	27
DWD-RDC	11.0	0.3	12.2	1.2	421	26	482	48
DWD-DRDC	11.3	0.5	12.2	0.6	479	14	526	58
WD-RDC	10.8	0.2	11.6	0.2	450	30	463	38
WD-DRDC	11.2	0.2	11.5	0.2	445	9	444	10
WW-RDC	23.4	3.3	21.8	1.2	539	57	497	58
WW-DRDC	22.7	2.1	21.9	1.5	572	48	504	47
S5-RDC	14.9	1.5	14.8	2.2	465	17	466	20
S9-RDC	15.3	1.5	14.5	1.6	481	30	456	19
G1-RDC	15.9	1.8	14.4	2.3	491	41	419	9
G2-RDC	14.3	1.9	13.5	0.5	521	27	444	18

5.5. Methods

Tests were performed similar to previous research on RDC so that the results can be compared. The test specimens were mounted on a test apparatus by supporting the main beam on two 100 mm x 100 mm x 10 mm steel plates, two other steel plates of 50 mm x 50 mm x 5 mm on the backside of the specimens prevented these from moving back (Figure 5-2). The main beam was not clamped, thus allowing minor rotation about its long axis, a situation that closely simulates the supporting condition in a real structure. The free end of the joist was simply supported on a 100 mm x 100 mm x 10 mm steel plate which rested on a damper with a spring stiffness of approximately 1 kN/mm, thus simulating an approximately 4 m long beam of the given section. The load was applied at a distance of 350 mm from the joint and distributed onto the joist with a steel plate with a diameter of 100 mm and 10 mm thickness.

Figure 5-2: Set up of shear tests; all dimensions in mm

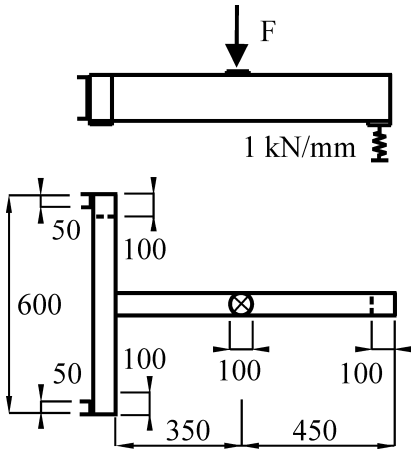

The applied load from the actuator, the force at the support of the free joist end and the vertical movement on both sides of the joint (as the relative displacements between main beam and joist) were recorded. The force transmitted by the connection was calculated as the

difference between the applied load and the load recorded at the free end of the joist. The vertical joint deflection was calculated as the average between the vertical movements of the two joint sides. The load regime was load controlled. One prototype specimen was used to estimate the capacity and set the rate of loading for the following tests to ensure that failure of the connection occurred after approximately six minutes, in accordance to EN-26891 (1991).

The maximum force applied (F_{ult}) represents the connection capacity. It is important to consider a deformation limit of the joint in order to prevent unacceptable non-structural damages of the surrounding structure. In this study, a 3 mm limit for the relative vertical deformation between main beam and joist was used and the load at 3 mm deformation ($F_{@3mm}$) was determined. For specimens that failed before deforming 3 mm, the peak force applied represents the load at 3 mm deformation.

5.6. Results

RDC control specimens show little initial connection slack due to alignment issues. The load increases linearly until reaching deformations between 2 mm and 3 mm. At that point a load is reached that leads to crack development. A load redistribution process initiates and stable crack development is observed. Further increases in load are associated with bigger increases in deformation until brittle failure occurs at capacity. RDC specimens show large variability in their capacity with 14 kN to 30 kN and fail after reaching deformations between 3 mm and 9 mm.

DRDC control specimens do not show any initial slack. The load-deformation curve is almost tri-linear. The load increases at the beginning of the actuator movement and linear behaviour occurs until reaching a deformation of approximately 1 mm. Then the curve flattens until reaching a deformation of approximately 4 mm. After this point the connection tends to

stiffen until reaching capacity. DRDC specimens show large variability in their capacity with values between 13 kN and 29 kN and fail after reaching deformations between 4 mm and 9 mm.

RDC specimens produced and tested under varying climatic conditions vary in their initial alignment behaviour. The load deformation response is linear and specimens exhibit large variability in capacity and maximum deformation. For DWD specimens the load increases right at the beginning and increases linearly until brittle failure. The load-deformation curve for WD is also almost linear. WW specimens show the highest initial alignment behaviour. DRDC specimens produced and tested under varying climatic conditions exhibit less variability in their alignment behaviour. Testing was halted for most specimens because they deformed so much that they touched the test apparatus. DWD show some initial alignment before the load increases slowly until reaching deformations between 5 mm and 10 mm, when it increases at a much higher rate. WD specimens exhibit less variability in capacity; the load initially increases at a low rate until reaching deformations of approximately 4 mm, and then at a much higher rate until failure. WW specimens do not show any initial alignment behaviour and their load-deformation curve is almost linear with the lowest stiffness of all specimens.

RDC produced at medium speed do not show any initial alignment behaviour; their load response is very similar to the control specimens. RDC produced at high speed show initial alignment behaviour. The load increases at a slow rate with large deformations until reaching a deformation between 1 mm and 4 mm, where it rises at higher rates until brittle failure occurs. RDC produced with a gap do not show initial alignment behaviour. Steep linear behaviour continues until reaching a deformation of approximately 2 mm and a load that leads to crack development. From that point on, stable crack development is observed and further increases in load associated with bigger increases in deformation until brittle failure occurs.

The load deformation curves for all specimens are shown in Figure 5-3. Table 5-2 gives a summary of the test result with the means and standard deviations of the tested variables.

Figure 5-3: Load deformation response of test specimens with varied manufacturing parameters

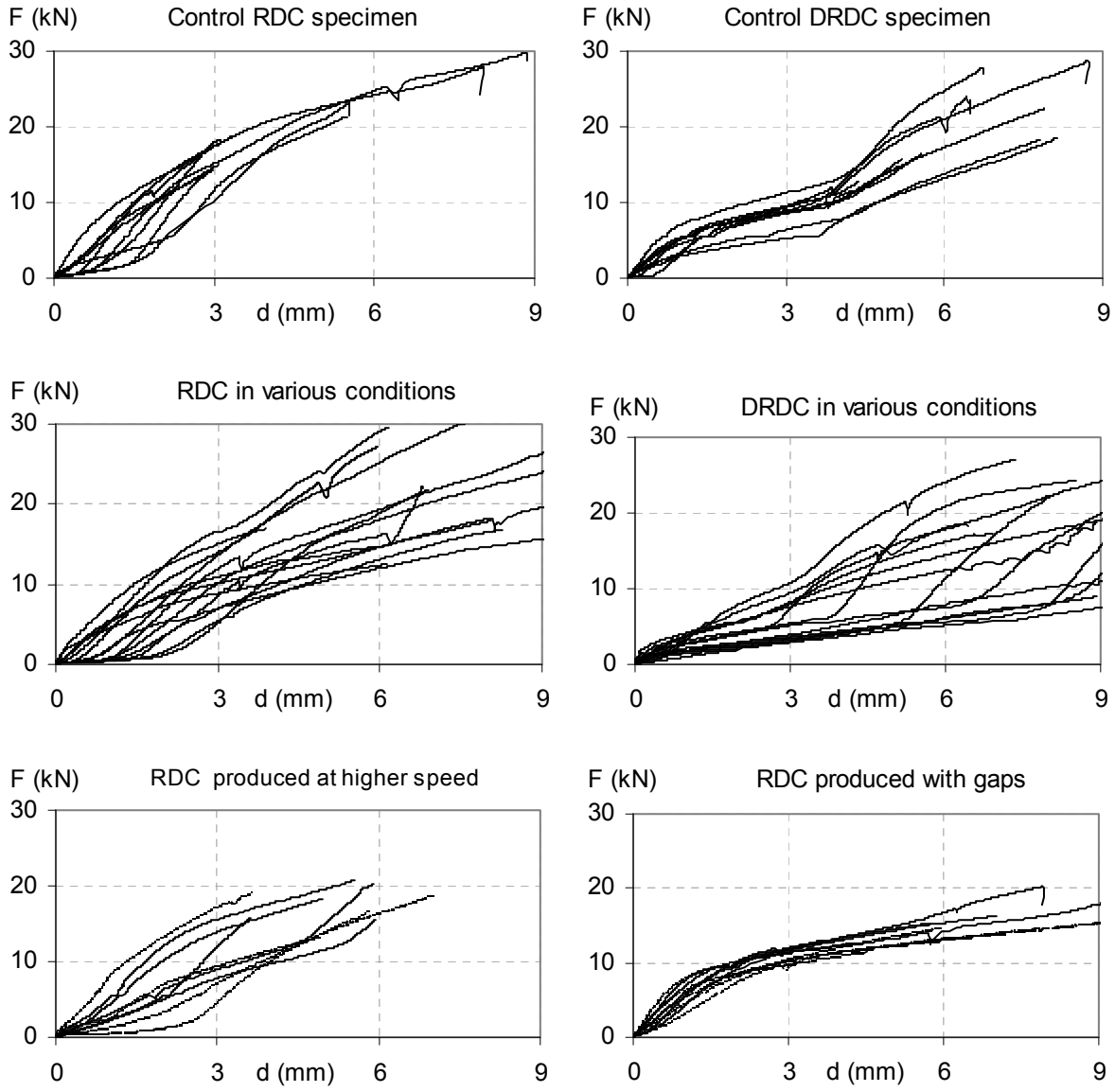

Table 5-2: Summary of shear test results with varied manufacturing parameters

Test series	F_{ult} (kN)		$F_{@3mm}$ (kN)		d_{max} (mm)	
	Mean	StDev	Mean	StDev	Mean	StDev
Contr.-RDC	19.9	5.6	14.9	2.7	4.6	2.3
Contr.-DRDC	20.0	5.5	8.6	1.7	6.6	1.5
DWD-RDC	27.4	5.1	10.8	4.4	8.7	3.1
DWD-DRDC	20.2	3.8	4.2	1.9	9.7	1.3
WD-RDC	18.4	7.1	11.9	1.9	6.2	2.7
WD-DRDC	22.8	3.2	5.3	1.4	10.0	1.3
WW-RDC	20.5	7.4	8.4	3.3	9.0	2.4
WW-DRDC	21.9	5.2	8.8	1.3	9.2	2.8
S5-RDC	18.1	2.5	11.6	3.3	5.2	1.0
S9-RDC	18.8	5.0	7.9	5.9	6.1	2.0
G1-RDC	20.3	9.5	11.7	0.2	8.2	5.0
G2-RDC	15.9	4.7	10.1	0.8	8.1	4.5

5.7. Analysis

The capacity (F_{ult}), the load at 3 mm deformation ($F_{@3mm}$), and the maximum deformation (d_{max}) of the connection under shear load were recorded and statistically evaluated using analysis of variance (ANOVA). ANOVA can be used for comparing means when there are more than two levels of a single factor and to determine whether observed differences in means are statistically significant. A p-value is calculated and compared to α, the significance level. If the p-value is smaller than α, then the null hypothesis of no differences between means is very unlikely, and is rejected. Table 5-3 gives a summary of the ANOVA comparing the different climatic conditionings and tolerances to the control.

Different climatic conditions have no statistically significant effect on the connection capacity and neither has the dovetail configuration. For the load at 3 mm deformation in the study of climatic conditions, it was determined that the interaction between conditioning and dovetail is statistically significant. Therefore, the factors cannot be interpreted separately. However, the specimens manufactured and tested in dry condition displayed a higher capacity than those exposed to varying climatic conditions and RDC specimens displayed a higher load at 3 mm deformation than DRDC for all the climatic conditions except for the wet-wet condition. Regarding the maximum deformation both dovetail type and conditioning have a statistically significant effect. DRDC reach larger deformations compared to RDC and the connections manufactured and tested in dry condition exhibit a lower deformation at failure compared to those exposed to the variable climatic conditions.

Tolerances do not affect RDC capacity; control specimens exhibited similar capacities like those produced at a higher speed and with a gap. The effect of tolerances on the load at 3 mm deformation is statistically significant. The control specimens exhibited, on average, 45% higher capacity than the other specimens. Finally, the effect of tolerances on the maximum deformation is not statistically significant, although the average maximum deformation of specimens produced with a gap is more than 50% higher than that of the control specimens.

Table 5-3: ANOVA results of shear tests with varied manufacturing parameters

Tested variable	Climate conditions			Tolerances
	p- Interaction	p- Conditioning	p- Dovetail	p
F_{ult} (kN)	0.134	0.350	0.819	0.736
$F_{@3mm}$ (kN)	0.005	<0.001	<0.001	0.006
d_{max} (mm)	0.292	<0.001	0.010	0.168

5.8. Discussion and conclusions

The presented work reduces the existing knowledge gap regarding the effect of manufacturing parameters on the structural performance of RDC. Changes of MC caused by varying climatic conditions have a significant effect on load at 3 mm deformation and maximum deformation. Specimens subjected to different climatic conditions exhibited a lower load at 3 mm deformation and showed larger deformations than those manufactured and tested in the dry condition. Joint tolerances do affect the structural performance of RDC. Specimens produced at low speed and with no gap have higher load at 3 mm deformation. Low cutting speed produces a clean cut and good fit joint, whereas high cutting speed causes vibration of the machine resulting in reduced connection accuracy.

Based on the results presented in this study, the authors recommend that RDC be manufactured using dry timber and ensure no significant changes in MC take place. It is also proposed that the joints be produced at low speed when using a CNC timber processor to ensure a good quality and good fit joint, resulting in a better structural performance. Given the scope of the presented work, the authors cannot comment on whether RDC are appropriate to resist seismic loads under reverse loading conditions or long-term loading. Additional work at UBC further studies this innovative connection to establish amongst other factors the possibility of reinforcements with self tapping screws. The authors recommend to further study applications of RDC to establish amongst other factors the process of creep during concurrent moisture changes.

5.9. References

Bobacz, D. (2002). In CNC-Technik gefertigte zimmermannsmäßige Verbindungsmittel - Untersuchung des Schwalbenschwanzzapfens (in German). Diploma thesis, Universität für Bodenkultur, Vienna, Austria.

EN-26891. (1991). Timber structures, Joints made with mechanical fasteners, General principles for the determination of strength and deformation characteristics. DIN Deutsches Institut für Normung e.V., Beuth Verlag GmbH, Berlin, Germany.

Hochstrate, M. (2000). Untersuchungen zum Tragverhalten von CNC gefertigten Schwalben-schwanzverbindungen (in German). Diplom thesis, FH Hildesheim, Germany.

Jönsson, J. (2005). Load carrying capacity of curved glulam beams reinforced with self-tapping screws. Holz als Roh- und Werkstoff, 63(5), 342-346.

Kreuzinger, H., and Spengler, R. (1999). Zum Tragverhalten von maschinell abgebundenen Zapfenverbindungen aus Konstruktionsvollholz zwischen Haupt- und Nebenträger (in German). Technical report LKI 7313, Technische Universität, Munich, Germany.

Nakajima, S. (2000). The effect of the moisture contents on the strength and stiffness properties of nailed joints and shear walls. Proceedings, 6th World Conference on Timber Engineering, Whistler, Canada, 1-1-3.

Snow, M., Zheng Chen, A. A., and Chui, Y. H. (2006). North American practices for connections in wood construction. Progress in Structural Engineering and Materials, 8(2), 39–48.

Tannert, T. and Lam, F. (2006). Geometry parameters of Rounded Dovetail Connections. Proceedings, 9th World Conference on Timber Engineering, Portland, USA, 3-13-4.

Chapter 6: Performance of Laminated Strand Lumber for Rounded Dovetail Connections [10]

6.1. Introduction

Until the middle of the 20th century, wood-to-wood joints were commonly used in construction with their design and manufacturing based on the experience of skilled carpenters. More recently, important developments in wood processing machines have created the possibility of producing more cost effective wood-to-wood connections (Bobacz 2002; Bamford 2003). The wooden dovetail is a centuries old connection that was developed as a simple yet effective means to join orthogonal members and has been extensively used throughout Europe and Asia. The Rounded Dovetail Connection (RDC) is a relatively new connection concept specifically adapted to be processed completely automated with a CNC-timber processor.

A number of experimental studies on the RDC provided valuable insight into the structural performance of this modern and versatile joint (Kreuzinger and Spengler 1999; Hochstrate 2000; Bobacz 2002). A new design, the Double Rounded Dovetail Connection (DRDC) was developed at The University of British Columbia (UBC) as part of a preliminary study on the structural performance of RDC. That research indicated that a less brittle failure mode may be achieved with DRDC since the load is transferred over the bearing areas of the two staggered dovetails, dispersing the stress concentrations. The complex load transfer mechanism of RDC and DRDC are governed by their geometric features (Figure 6-1).

---

[10] A version of this chapter has been published. Tannert, T., and Lam F. (2007). Performance of Laminated Strand Lumber for Rounded Dovetail Connections. Forest Products Journal. 57 (9) 63-67.

Figure 6-1: Geometric parameters of RDC (left) and DRDC (right)

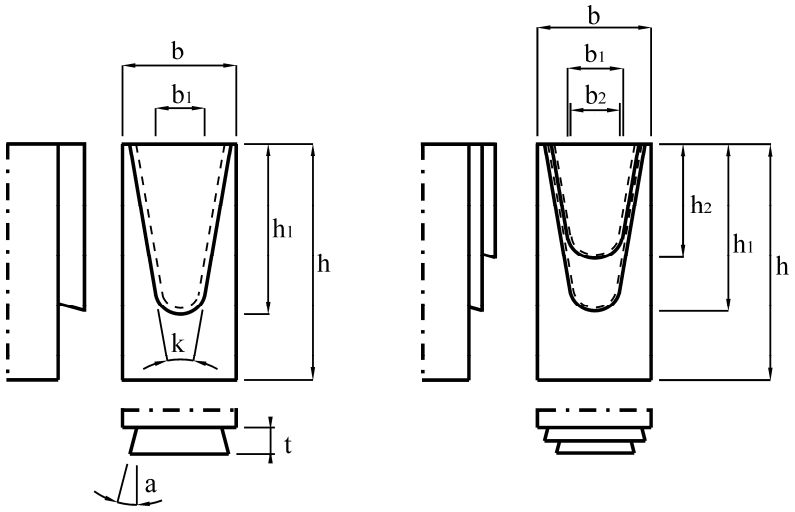

6.2. Timber joinery with Laminated Strand Lumber

High-grade structural composite lumber products in combination with CNC-technology present an opportunity for applying innovative connection methods in timber construction. TimberStrand® Laminated Strand Lumber (LSL) is highly uniform and dense, and compared to other wood products, LSL has a high shear strength to bending strength ratio and low variability in properties. Such characteristics can lead to improved connection efficiency. Some studies addressed this issue focusing on bolted connections (Moses 2000), timber rivets (Hampson 2003) and INDUO connectors (Steiniger 2003).

It was found that the performance of LSL in connections was superior to other common wood composite materials and enabled less severe requirements for spacing and end distances. Unfortunately, these favourable characteristics of LSL are neither fully understood nor applied. As a result, LSL is mostly used in residential construction as headers and beams products. In

such applications, designers rely on basic specifications on connection strength properties for common mechanical fasteners provided by the manufacturers.

More efficient connection methods and increased knowledge on timber joinery are needed to allow expanded general use of structural composite lumber products in timber construction. The performance of TimberStrand® LSL in beams with RDC under shear loading was examined in preliminary tests at UBC. The LSL specimens presented 50% higher connection strength compared to western hemlock (*Tsuga heterophylla*) and showed less brittle failure justifying further research.

6.3. Objective

The objectives of the presented study were to examine the structural performance of RDC and DRDC produced from TimberStrand® LSL in vertical shear tests and to compare the structural performance of RDC produced from LSL to that of western hemlock.

6.4. Material

The study used TrusJoist TimberStrand® LSL, E13 grade, a structural composite lumber manufactured from strands of wood from fast-growing, small-diameter species such as aspen (*Populus tremuloides*) or wood combinations, bonded with an isocyanate-based adhesive oriented mainly parallel to the longitudinal beam axis. TimberStrand® LSL members are available in thicknesses up to 140 mm, depths up to 1220 mm and lengths up to 14.63 m and present high and uniform density (NRC 2003). The Hundegger K2-5 5-axis beam processor was used to process all test specimens. It was observed that processing LSL increased tool wear. The results from the tests using LSL were compared to the results from tests that used kiln-dried

western hemlock. The moisture content (MC) and the apparent density (based on specimen as tested weight and volume) of each western hemlock specimen were determined. The average and standard deviation of MC and apparent density were 12.6% and 1.4%, respectively and 481 kg/m³ and 44 kg/m³, respectively.

Four series of test specimens were tested: 1) LSL-RDC: joints with single dovetail configuration produced from TimberStrand® LSL, 2) LSL-DRDC: joints with double dovetail configuration produced from TimberStrand® LSL, 3) Hemlock-RDC: joints with single dovetail configuration produced from western hemlock, and 4) Hemlock-DRDC: joints with double dovetail configuration produced from western hemlock. A total of 40 test specimens were produced: 20 from LSL and 20 from western hemlock, with 10 RDC and 10 DRDC specimens each. Two additional prototype specimens were used to calibrate the test apparatus and to estimate the connection capacity.

The joint was applied to connect a joist to a main beam. The member dimensions b and h of the specimens were chosen as 184 mm x 89 mm. Since it was of interest to study the behaviour of the connection and not bending strength of the beams, vertical shear loading mode was chosen with beam and joist lengths of 600 mm and 800 mm, respectively. To enable comparisons with previous studies, the dovetail geometry of the control geometry was chosen as: width b_1 = 50 mm, depth t = 28 mm, dovetail angle a = 15°, flange angle k = 15° and dovetail height h_1 = 119 mm. For the DRDC, the height and width of the second dovetail were h_2 = 79 mm and 57.5 mm, respectively.

6.5. Methods

Tests were performed similar to other research on RDC for the purpose of being able to compare results. The test specimens were mounted in a test apparatus by supporting the main beam on two 100 mm x 100 mm x 10 mm steel plates, two other steel plates of 50 mm x 50 mm x 5 mm on the backside of the specimens prevented these from moving back (Figure 6-2). The main beam was not clamped, thus allowing minor rotation about its long axis, a situation that closely simulates the supporting condition in a real structure. The free end of the joist was simply supported on a 100 mm x 100 mm x 10 mm steel plate which rested on a damper with a spring stiffness of approximately 1 kN/mm, thus simulating an approximately 4 m long beam of the given section. The load was applied at a distance of 350 mm from the joint and distributed onto the joist with a steel plate with a diameter of 100 mm and 10 mm thickness.

Figure 6-2: Set up of shear tests; all dimensions in mm

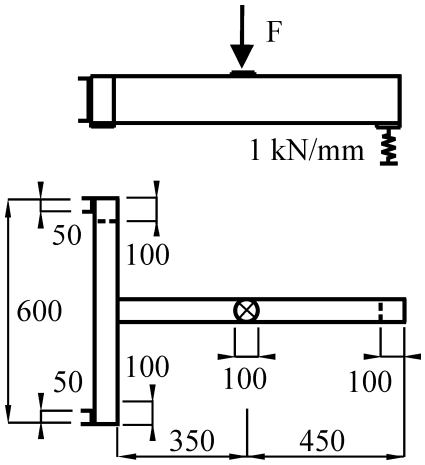

The applied load from the actuator, the load at the support of the free end of the joist, the vertical movement of the joint on both sides of the joint (as the relative displacements between main beam and joist), the horizontal movement of the joint, the deflection of the main

beam, as well as the deflection of the joist at the load application point were recorded with calibrated transducers. The force transmitted by the connection was calculated as the difference between the applied load and the load recorded at the free end of the joist. The vertical joint deflection was calculated as the average between the vertical movements of the two joint sides. The load regime was load controlled. Two prototype specimens were used to estimate the capacities for LSL and western hemlock specimens and set the load application speed for the following tests to ensure that failure of the connection occurred after approximately six minutes, in accordance to EN-26891 (1991). The load was applied until a reading was shown, all the transducer readings were set to zero, and then the load was increased until ultimate failure with a constant rate of loading.

The maximum force applied (F_{ult}) represents the connection capacity. It is important to consider a deformation limit of the joint in order to prevent unacceptable non-structural damages of the surrounding structure. In this study, a 3 mm limit for the relative vertical deformation between main beam and joist was used and the load at 3 mm deformation ($F_{@3mm}$) was determined. For specimens that failed before deforming 3 mm, the peak force applied represents the load at 3 mm deformation.

6.6. Results

RDC produced from LSL show initial slack due to alignment issues until reaching deformations between 1 mm and 3 mm. Then linear behaviour followed until reaching deformations of approx. 6 mm and loads reaching values of 20 kN to 30 kN. Further increases in load are associated with large increases in deformation. RDC specimens reached their capacity consistently at approx. 45 kN and failed after reaching deformations of 7 mm to 19 mm.

DRDC produced from LSL also show initial connection slack due to alignment. But in contrast to RDC, the linear part of the load deformation curves starts earlier at deformations between 0.5 mm and 1.5 mm and continues until reaching deformations of approx. 4 mm. At that point the load reaches similar values like RDC (25 kN - 35 kN) and further increases in load are associated with significantly larger increases in deformation. DRDC specimens reach their capacity at approx. 45 kN and failed after reaching deformations between 17 mm and 21 mm.

RDC specimens produced from western hemlock do not show much initial connection slack. The load is picked up at the beginning of the actuator movement and linear behaviour continues until reaching deformations between 2 mm and 3 mm. At that point a load is reached that leads to crack development with a drop in the load deformation curve in some test specimens. A load redistribution process initiates and stable crack development is observed. Further increases in load are associated with bigger increases in deformation until brittle failure occurs at capacity. RDC specimens show large variability in their capacity with 14 kN to 30 kN and fail after reaching deformations between 3 mm and 9 mm.

DRDC specimens produced from western hemlock do not show any initial slack due to alignment behaviour. The load-deformation curve is almost tri-linear. The load is picked up at the beginning and linear behaviour occurs until reaching a deformation of approx. 1 mm. Then the curve flattens until reaching a deformation of approx. 4 mm. After this point the connection tends to stiffen until reaching capacity. The DRDC specimens show large variability in their capacity with values between 13 kN and 29 kN and failed after reaching deformations between 4 mm and 9 mm. The results are summarised in Table 6-1. The load deformation curves were recorded and are shown for all specimens in Figure 6-3.

Figure 6-3: Load deformation response of test specimens from different materials

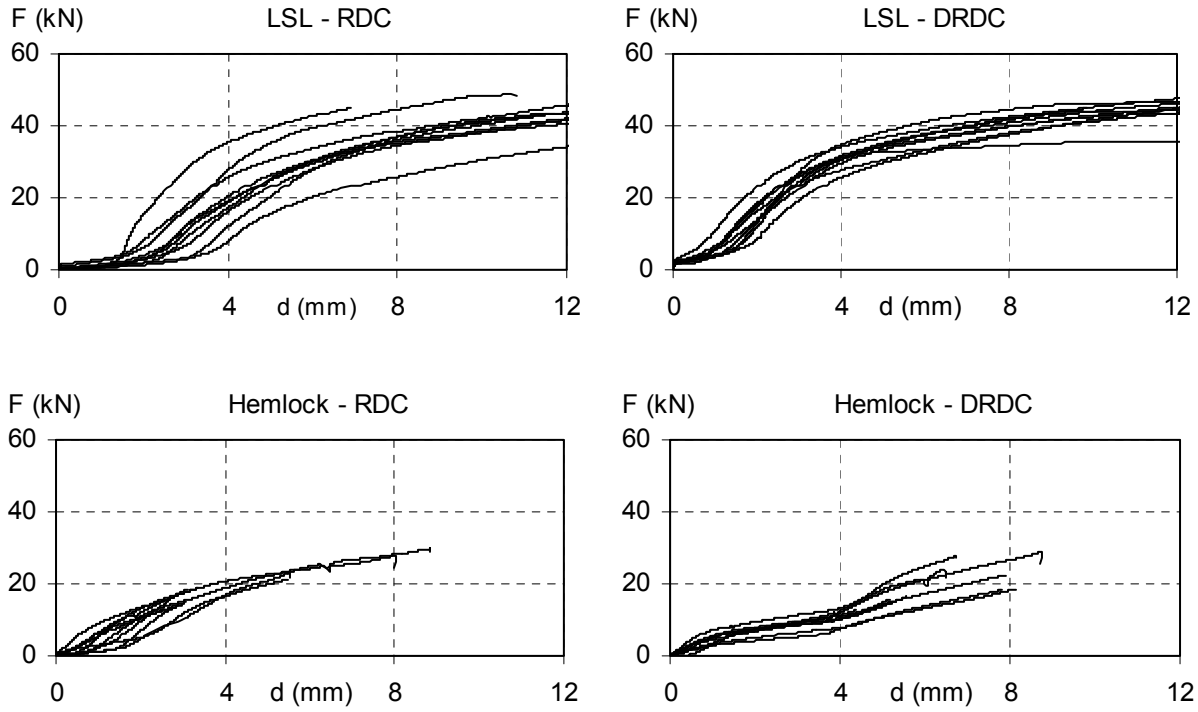

Table 6-1: Summary of shear test results with different materials

Test series	F_{ult} (kN)		$F_{@3mm}$ (kN)		d_{max} (mm)	
	Mean	StDev	Mean	StDev	Mean	StDev
Hemlock-RDC	19.9	5.6	14.9	2.7	4.6	2.3
Hemlock-DRDC	20.0	5.5	8.6	1.7	6.6	1.5
LSL-RDC	44.9	2.2	11.8	7.5	13.2	3.2
LSL-DRDC	46.8	3.2	24.7	3.1	16.7	3.7

6.7. Analysis

The capacity (F_{ult}) and the load at 3 mm deformation ($F_{@3mm}$) of the connection under shear load, as well as the maximum deformation (d_{max}) were recorded and statistically evaluated using analysis of variance (ANOVA). ANOVA can be used for comparing means when there are

more than two levels of a single factor and to determine whether observed differences in means are statistically significant. A p-value is calculated and compared to α, the significance level. If the p-value is smaller than α, then the null hypothesis of no differences between means is very unlikely, and is rejected. The experimental layout for the study was a two factor (material and dovetail configuration) completely randomized design. Table 6-2 gives the p-values from the ANOVA comparing LSL to western hemlock and RDC to DRDC. The comparison of average values, minima and maxima is illustrated in Figure 6-4.

Figure 6-4: Test results with different materials (bounds show extreme values)

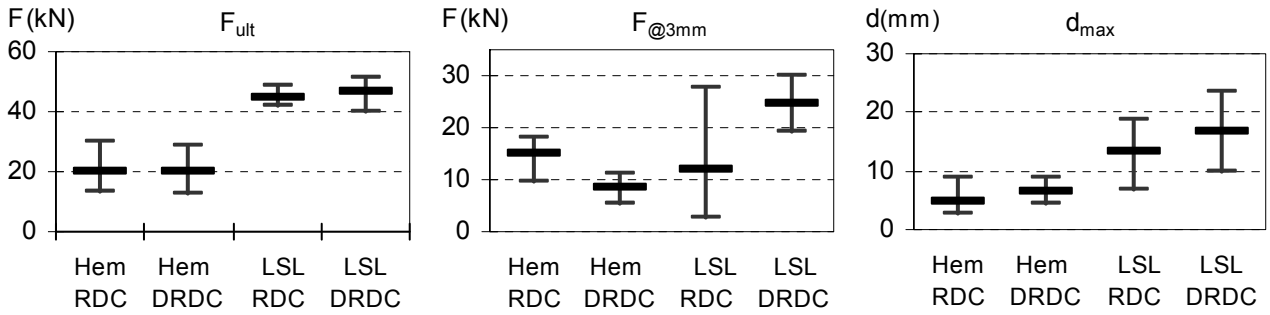

Using ANOVA, it was determined that the interaction between the factors material and dovetail geometry is not statistically significant at a level α=0.05 for the study of the capacity. LSL specimens have a significantly higher capacity than western hemlock specimens while there is no significant difference between RDC and DRDC for both materials. For the load at 3 mm deformation, the interaction between the factors material and dovetail geometry is statistically significant at a level α=0.05. Therefore, the factors cannot be interpreted separately. Multiple comparison tests (Bonferroni at a level α=0.05) showed that RDC are significantly weaker than DRDC for LSL specimens and significantly stronger for western hemlock specimens.

Furthermore, RDC for western hemlock are stronger than for LSL, while the opposite is true for DRDC. For the maximum deformations ANOVA determined that both factors are statistically significant: LSL specimens show significantly larger deformations than western hemlock specimens, independently from the dovetail configuration and the double dovetails show significantly larger maximum deformations for both materials.

Table 6-2: ANOVA results of shear test results with different materials

Tested variable	p- Interaction	p- Material	p- Dovetail
F_{ult} (kN)	0.516	<.0001	0.482
$F_{@3mm}$ (kN)	<.0001	<.0001	0.021
d_{max} (mm)	0.406	<.0001	0.004

6.8. Discussion

The study partly confirmed the findings from previous research at UBC of increased shear capacity and a more favourable failure mode using TimberStrand® LSL in beams with RDC tested under vertical shear loading. LSL specimens have higher capacity than western hemlock specimens for both single and double dovetail configuration. The load at 3 mm deformation of LSL specimens is only higher than that of western hemlock specimens for the DRDC configuration.

RDC produced from LSL show initial connection slip due to alignment issues resulting in very high variability in loads at 3 mm deformation and a lower average value. Unlike previous studies (Kreuzinger and Spengler 1999; Hochstrate 2000), the presented study did not apply any preload to close initial connection gaps, a testing procedure that may reflect more realistically the

condition in practice. In consequence, minor cutting inaccuracies led to the difference in initial alignment behaviour amongst the individual test specimens.

It was shown that DRDC are stronger than RDC for LSL specimens and weaker for western hemlock specimens. RDC produced from western hemlock do not show initial connection slack due to alignment. The load-deformation curve of DRDC produced from western hemlock is almost tri-linear. The middle part of the load-deformation curve with its low stiffness might be caused by connection inaccuracies with the second dovetail not completely participating in the load bearing.

LSL specimens show larger deformations than western hemlock specimens, independently from the dovetail configuration. This finding is explained by the different failure modes, in western hemlock specimens a crack developed and the specimens failed with brittle failure. LSL specimens showed a less brittle failure with the whole dovetail-end being sheared off (Figure 6-5).

Figure 6-5: Typical failure of RDC in LSL (left) and western hemlock (right)

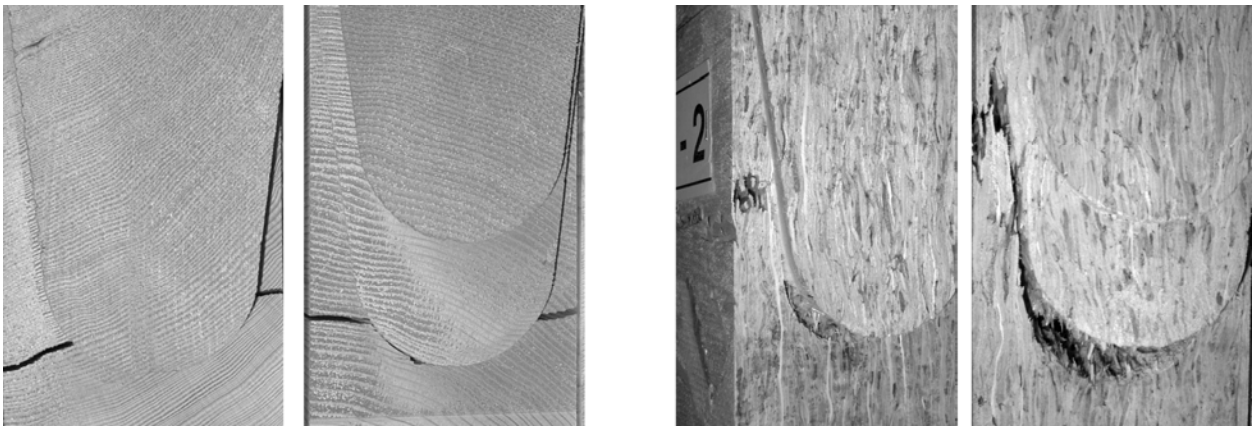

In contrast to the results of previous research at UBC, DRDC produced from western hemlock did not develop two cracks along the two planes with high tension perpendicular to the grain stresses. In that previous study, the main beam was clamped at the ends, in the presented study it was simply supported. Failure of single and double dovetail configurations in western hemlock was very similar and very brittle in both cases.

6.9. Conclusions

The presented work demonstrated that the versatile Rounded Dovetail Connection can be successfully applied in TimberStrand® LSL. Attention has to be directed to the larger deformations associated with that material. The work also demonstrated that the double dovetail configuration is a viable alternative for specimens produced from TimberStrand® LSL.

Given the scope of the presented work, the authors cannot comment on whether RDC are appropriate to resist seismic loads under reverse loading conditions or whether the results can be extended to significantly larger dimensions. The observed capacities and the loads at 3 mm deformation of western hemlock depend on the moisture content and moisture fluctuations of the timber. The reduction in cross section in timber members caused by RDC needs to be considered in the structural design process.

The authors recommend to further study applications of TimberStrand® LSL in timber connections to establish amongst other factors the influence of geometric and manufacturing parameters on its structural performance, including the initial alignment behaviour causing the variability in loads at 3 mm deformation and how to avoid it.

6.10. References

Bamford, S. (2003). The effects of advanced wood processing technologies on contemporary timber design. BSc graduating essay, The University of British Columbia, Vancouver, Canada.

Bobacz, D. (2002). In CNC-Technik gefertigte zimmermannsmäßige Verbindungsmittel - Untersuchung des Schwalbenschwanzzapfens (in German). Diploma thesis, Universität für Bodenkultur, Vienna, Austria.

EN-26891. (1991). Timber structures, Joints made with mechanical fasteners, General principles for the determination of strength and deformation characteristics. DIN Deutsches Institut für Normung e.V., Beuth Verlag GmbH, Berlin, Germany.

Hampson, J. A. (2003). Moment resistant connections with timber rivets in wood product substrates. MApplSc thesis, The University of British Columbia, Vancouver, Canada.

Hochstrate, M. (2000). Untersuchungen zum Tragverhalten von CNC gefertigten Schwalben-schwanzverbindungen (in German). Diplom thesis, FH Hildesheim, Germany.

Kreuzinger, H., and Spengler, R. (1999). Zum Tragverhalten von maschinell abgebundenen Zapfenverbindungen aus Konstruktionsvollholz zwischen Haupt- und Nebenträger (in German). Technical report LKI 7313, Technische Universität, Munich, Germany.

Chapter 7: Finite Element Model for Rounded Dovetail Connections [11]

7.1. Introduction

A number of experimental studies on Rounded Dovetail Connections (RDC) provided insight into their structural performance (Kreuzinger and Spengler 1999; Barthel et al. 1999; Blass and Saal 1999; Hochstrate 2000; Bobacz 2002; Dietsch 2005; Tannert and Lam 2006; Tannert et al. 2007). But the acceptance of RDC in the structural engineering community is affected by a lack of design data.

One approach for obtaining reliable data on the structural performance of RDC is by experimental testing. Due to the wide variability of material properties and different possibilities of connection designs, a large number of test repetitions are necessary, thus making this process very expensive. A more effective approach is to combine experiments with structural performance modeling using the Finite Element Method (FEM). Tests are needed for FEM model verification. The verified model can then be used to estimate the stress and strain distribution across the member while boundary conditions and material properties can be considered as variable input parameters and contributes to a better understanding of the load-displacement behaviour and failure modes of RDC. The structural performance of RDC can potentially be improved by considering its geometry as design parameters to reduce stress concentrations if detailed knowledge of the stress distribution within the connection is available.

[11] A version of this chapter has been prepared for publication. Tannert, T., and Lam, F. (2008). Finite Element Model for Rounded Dovetail Connections.

7.2. Objective

The objectives of this work are to define necessary physical parameters, develop an appropriate FEM model for RDC, simulate the structural performance of RDC, and validate the model by comparing numerical results with experimental observations.

7.3. Building the Finite Element Model

7.3.1. Elements, material properties and coordinate systems

The software ANSYS®, Version 10.0 was used. From the ANSYS® element catalogue, SOLID95 20-node elements were applied. These elements can accommodate complex geometries were deemed adequate to model the curved boundaries of RDC and provide higher accuracy while requiring more computation time than the lower order elements used in other studies (Dietsch 2005, Barthel et al. 1999, Bobacz 2002). The FEM model was built to closely resemble the in Chapter 4 described configuration of experimental tests of RDC.

Timber is a natural, anisotropic (cylindrically isotropic) and inhomogeneous material, but, in FEM models, it often is assumed to be homogeneous and defect free. For small specimens obtained relatively far from the pith, the influence of the growth ring curvature can be ignored so that properties are regarded as orthotropic. The properties used by SOLID95 elements for orthotropic material are the three elastic moduli (E_X, E_Y, E_Z), three Poisson's ratios (υ_{XY} , υ_{XZ}, υ_{YZ}) and three shear moduli (G_{XY}, G_{YZ}, G_{XZ}). Orthotropic elasticity is generally the most plausible material model for wood, but owing to its complexity it is applied only infrequently to 3D problems. For simplicity in modeling bigger specimens with similar height and width dimensions, the assumption of transverse isotropy with identical properties in the radial and tangential directions works well as long as linear elastic behaviour is applicable (Mihailescu

2001). The combined radial and tangential directions are referred to as perpendicular to grain ($\perp$) and the longitudinal direction is referred to as parallel to grain (II).

Kreuzinger and Spengler (1999) and Tannert and Lam (2006) showed that brittle failure modes initiate within the elastic range and dictate the capacity of RDC. In this work, transverse isotropy and linear-elastic properties were assumed as simplification of the real material and wood is considered homogenous and defect free, with constant moisture content, air temperature and wood temperature. The elastic properties were initially set to: $E_{II} = E_X = 10{,}000$ N/mm^2, $E_\perp = E_Y = E_Z = 300$ N/mm^2, $G_{XY} = G_{YZ} = 300$ N/mm^2, $G_{YZ} = 30$ N/mm^2, $\upsilon_{XY} = \upsilon_{XZ} = 0.012$, $\upsilon_{YZ} = 0.400$. The longitudinal modulus of elasticity was set to lower end of the scale of values reported by Barrett et al. (2001) and the other properties derived from property ratios reported by Green et al. (1999). Two local coordinate systems were defined, one for the joist and a second for the main beam, so that both members could either be assigned the same material properties, or alternatively be assigned different material properties for the individual beams.

7.3.2. Model geometry and mesh

Solid modelling, an approach in which the user describes the geometric boundaries of the objects and establishes controls over the size and shape of elements, was deemed efficient to model RDC. To reduce computation time, only one half of the beam configuration was modelled using symmetry. The FEM mesh was created using only brick elements. Weighting accuracy of results against computing time, the model was divided into different zones, depending on the stress gradients and the importance of the results in that particular area. The finest mesh (6 mm element length) was used along the bottom back line of the dovetail where the highest stresses occur. A coarser mesh was used for the remaining parts (Figure 7-1).

Figure 7-1: FEM mesh for main beam (left), contact (centre), and joist (right)

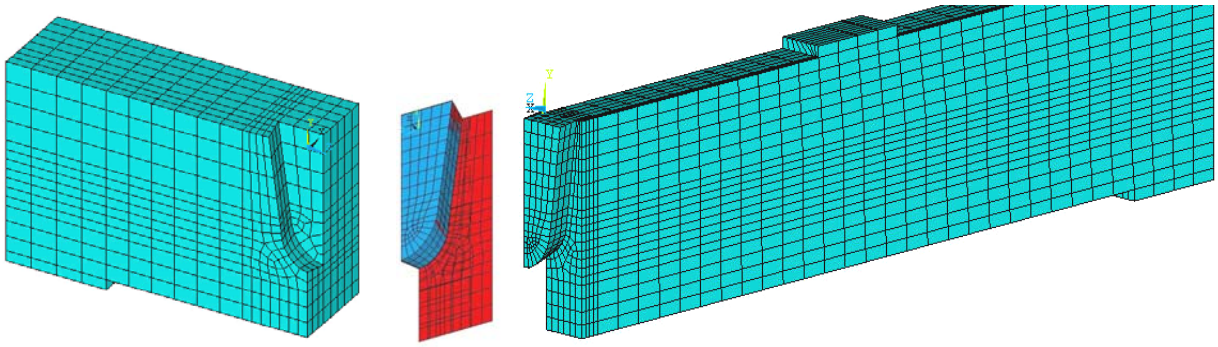

7.3.3. Contact modelling

Contact in FEM is defined as the process of two separate surfaces touching each other. In the common physical sense, contact surfaces do not interpenetrate; they transmit compressive normal forces and tangential friction forces, and are free to separate from each other. Contact is a changing-status-nonlinearity that includes changes of tangential stiffness and friction response. Both, changes in stiffness and frictional response, can cause severe convergence difficulties in numerical analyses and require an accurate load history, with small time steps. Commonly applied contact methods use a contact spring that is only active when the surfaces interpenetrate. Some finite amount of penetration is required to generate an interface contact force which is needed for equilibrium. However, most contacting bodies do not penetrate, and therefore, for best accuracy, the goal is to minimize the amount of modelled penetration (Ansys 2007).

TARGET170 and CONTACT174 surface-to-surface elements were used. These provide deformable surfaces and cover the underlying FEM mesh like a skin (Figure 7-1 centre). Contact stiffness (FKP), penetration tolerance (FTOL), friction coefficient (f), and initial connection gap (g) between the connecting members affect result accuracy and convergence behaviour and have to be specified. FKP and FTOL are unitless parameters that describe the relative stiffness of

contacting bodies and the allowable penetration in relation to the underlying element depth, respectively. Some trial and error studies were required to determine appropriate values. Based on these studies, FKP was set to 0.01, a value that allowed the solutions to converge using the default solver, and FTOL was set to 0.5, a value that allows penetration of the contacting surfaces, which reflects the actual behaviour of wood surfaces penetrating at irregularities.

Manufacturing tolerances significantly influence the performance of RDC. Initial gaps, caused by geometry differences of areas with no contact between the two connecting members, have to be considered, in order to model the initial alignment behaviour. Preliminary work suggested that good agreement between analytical and experimental load response curves can be achieved by modelling a gap between the connecting members of approximately 0.50 mm. The surface quality of the members plays an important role in the behaviour of RDC under load as it dictates the friction between them. The friction coefficient μ was taken as 0.3, similar to previous research (Bobacz 2000) and in the range of values reported by McKenzie and Karpovich (1968).

7.3.4. Significant stresses in RDC

To conduct a stress-based comparative study of the parameters that influence the structural performance of RDC and finally to develop a failure criterion for RDC, it is necessary to identify and evaluate significant stresses. Tension perpendicular to grain and shear parallel to grain stresses were shown to contribute to connection failure (Dietsch 2005). Figure 7-2 shows the cracked joist of a RDC and the stress distribution within the FE-model. The crack developed in the bottom of the tenon, at the tip of the rounded part. This location is clearly identified as a highly stressed zone in the stress plots from the FEM analysis. While this study is not sufficient to develop a failure criterion for RDC it was deemed sufficient for the parameter study.

Figure 7-2: Failed RDC (left) and stress in FEM model: tension perpendicular to grain (centre) and shear parallel to grain (right)

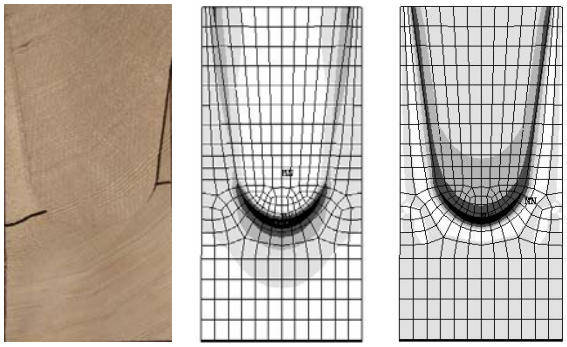

7.3.5. Defining parameters to model control test series

The mesh size had to be determined carefully, since maximum tension perpendicular to grain stress at singularities does not converge but increases with mesh refinement (Dietsch 2005). Stress singularities appear in the FEM model when the material is modelled as elastic while in reality it develops cracks that redistribute stress and reduce stress concentrations. The linear elastic model cannot accurately represent this behaviour. To enable a comparison of peak stresses for different models, an equal mesh density has to be chosen while balancing mesh refinement and computation time. Since no changes in stresses were observed for further refinements, for the remainder of the study the mesh at the dovetail areas was refined using a 6 mm element length to reach the mesh shown in Figure 7-1.

A series of simulations was carried out in a parameter study varying one model parameter at a time. Elastic material properties, contact properties, and geometry parameters were varied. For each variation, the values of the relative vertical joint deformation and the joist deflection versus the applied load were recorded. Based on these simulations, the parameters were set to: $E_{II} = E_X = 12{,}000$ N/mm^2, $E_{\perp} = E_Y = E_Z = 600$ N/mm^2, $G_{XY} = G_{YZ} = 400$ N/mm^2,

G_{YZ} = 40 N/mm^2, NU_{XY} = NU_{XZ} = 0.02, NU_{YZ} = 0.40. The longitudinal modulus of elasticity in accordance with values reported (Barrett et al 2001) and the other properties derived from property ratios reported (Green et al 1999). The friction coefficient μ was set to 0.25, the support stiffness 800 N/mm, the contact stiffness FKP = 0.02 and the penetration tolerance FTOL = 0.5.

The gap depth was varied from 0 mm to 1.00 mm in steps of 0.25 mm. The combination of relatively high contact stiffness and gap size made it necessary to use the unsymmetric solver option in ANSYS® which uses a full Newton-Raphson solution procedure and significantly increases computation time but decreases convergence difficulties. Joint displacement increased proportionally with gap size, while joist deformation is almost unchanged. Tension perpendicular to grain and shear parallel to grain tresses increase with gap size and excellent agreement can be achieved with modelling a 0.50 mm gap. The model reflects well the experimentally observed behaviour for both vertical joint displacement and joist deformation (Figure 7-3) proving that it is possible to accurately model the load deformation response of RDC. A detailed analysis of the parameter influence on maximum stresses in tension perpendicular to grain and shear parallel to grain, as well as joist deflection and relative vertical joint deformation is given in Appendix K.

Figure 7-3: Load deformation response: FEM model versus tests for control series

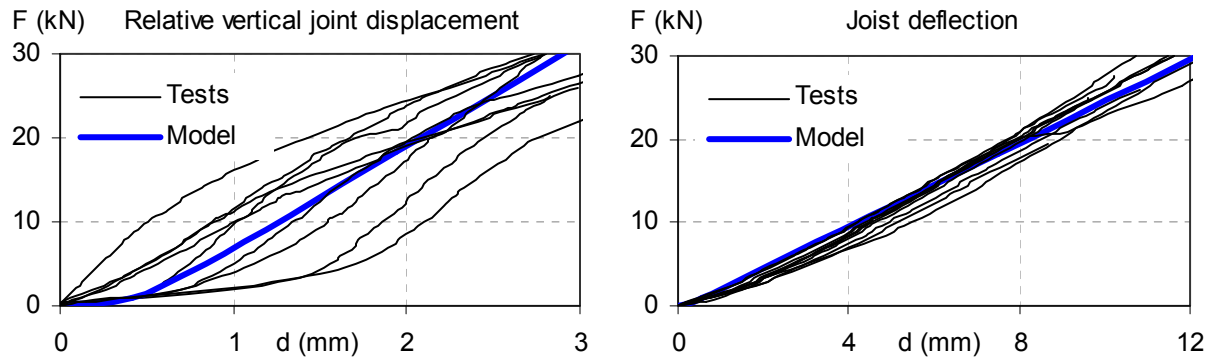

7.4. Model validation

The accuracy of the presented FEM model was validated by simulating the load displacement curves of test series carried out at UBC, and several tests done by other researchers (Bobacz 2002, Hochstrate 2000, Kreuzinger and Spengler 1999, Blass and Saal 1999). The elastic material and other model parameters for these simulations are listed in Appendix L.

7.4.1. Modelling all UBC test series

The different test series reported by Tannert and Lam (2006) were modelled, using their material properties and failure loads as model input. The differences between test series can be accounted for by adjusting the elastic parameters according to apparent density and moisture content and adjusting the gap depths and friction coefficient. This procedure allowed fitting the model load deformation response to the typical load deformation response of each test series (Figure 7-4).

Figure 7-4: Load deformation response: FEM model versus tests for different UBC test series

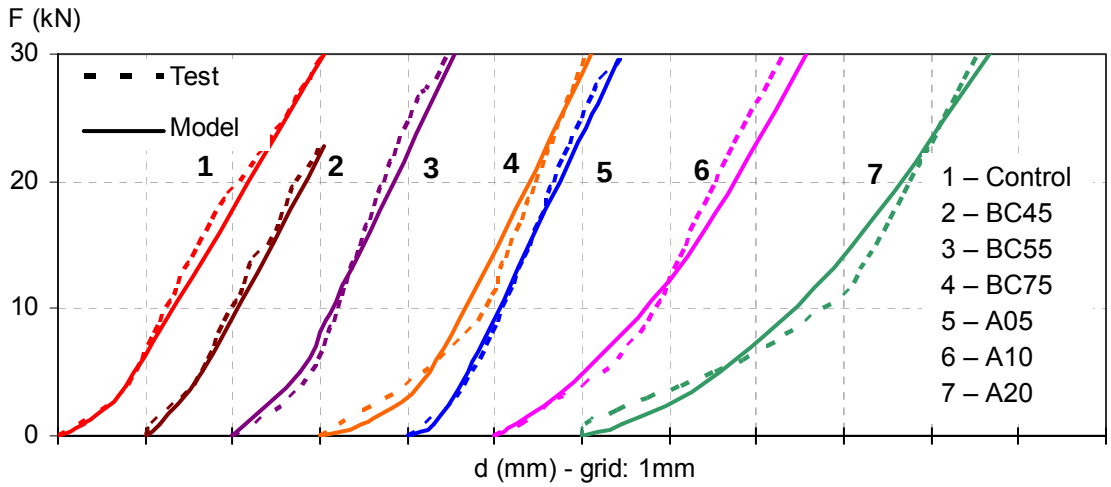

7.4.2. Modelling control series test specimens

The model was developed to fit the average test curve for the control test series. The load deformation curves of all individual test specimens were also modelled, using their material properties and failure loads as model input. The elastic parameters were adjusted according to the apparent density (using a regression according to UBC data) and moisture content (using data by Green et al. 1999) as recorded from the test specimens. The growth ring density, as number of rings per 50 mm, was considered as it influences density and therefore the elastic properties. The growth ring orientation, as angle with values between 0º for horizontal and 90º for vertical orientation, was represented by the angle between global FEM and local element co-ordinate systems. The radial and tangential elastic properties were used individually as input for the joist, and the material axes were rotated accordingly in the model. Varying the friction coefficient and the gap depths allowed fitting the model curves to the experimental load deformation response of each individual specimen (Figure 7-5).

Figure 7-5: Load deformation response: FEM model versus tests for individual test specimens

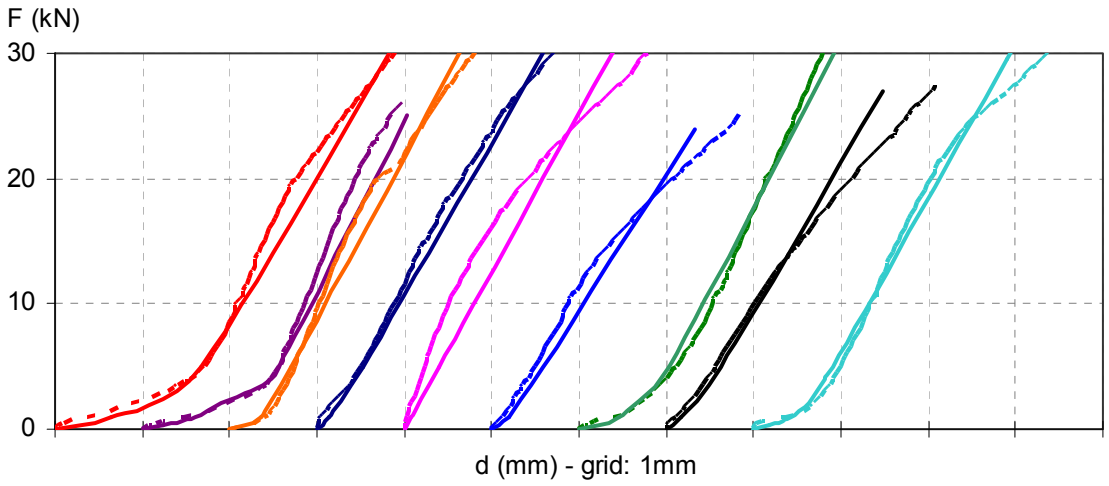

7.4.3. Modelling tests from other research

Previous tests at UBC (Tannert et al. 2007) used similar RDC geometry and a similar test up as in the previously modelled tests. The main beam was clamped at its ends preventing it from rotating along its long axis. A preload was applied to close any existing connection gaps and therefore no initial load slip behaviour was observed. Figure 7-6 a illustrates agreement between model and experiment for the vertical joint displacement (d) versus joint force (F).

Selected test from other institutes were modelled, varying the loads, support conditions, geometry and material parameters according to the respective tests. Assumptions had to be made regarding the material properties as not all parameters were available from the literature. Figure 7-6 b shows good agreement between model and experiment for the early parts of the load deformation response the curves for the F-D test series done by Hochstrate (2000). Figure 7-6 c and d show good agreement between model and experiment for tests done by Bobacz (2002). A preload was applied to force the RDC together and eliminate potentially existing gaps. The initial load increase without any displacement was not modelled which explains the initial deviation between the model curve and the experimental curve. Figure 7-6 e and f show reasonable agreement between model and experiment for tests done by Kreuzinger and Spengler (1999). Again, a preload was applied and the initial load increase without any displacement seen in the experimental curve was not modelled which explains the deviation between model and the experimental curve. Moving the model curve by 3 kN brings it close to the experimental curves. Finally, Figure 7-6 g and h show comparisons with tests done by Blass and Saal (1999). Good agreement between model and experiment for series I (tight fitting joints) was achieved while the experiment for series II (loose joints) cannot be modelled adequately due to a lack of information on the exact geometry parameters.

Figure 7-6: Load deformation response: FEM model versus tests for tests from other research

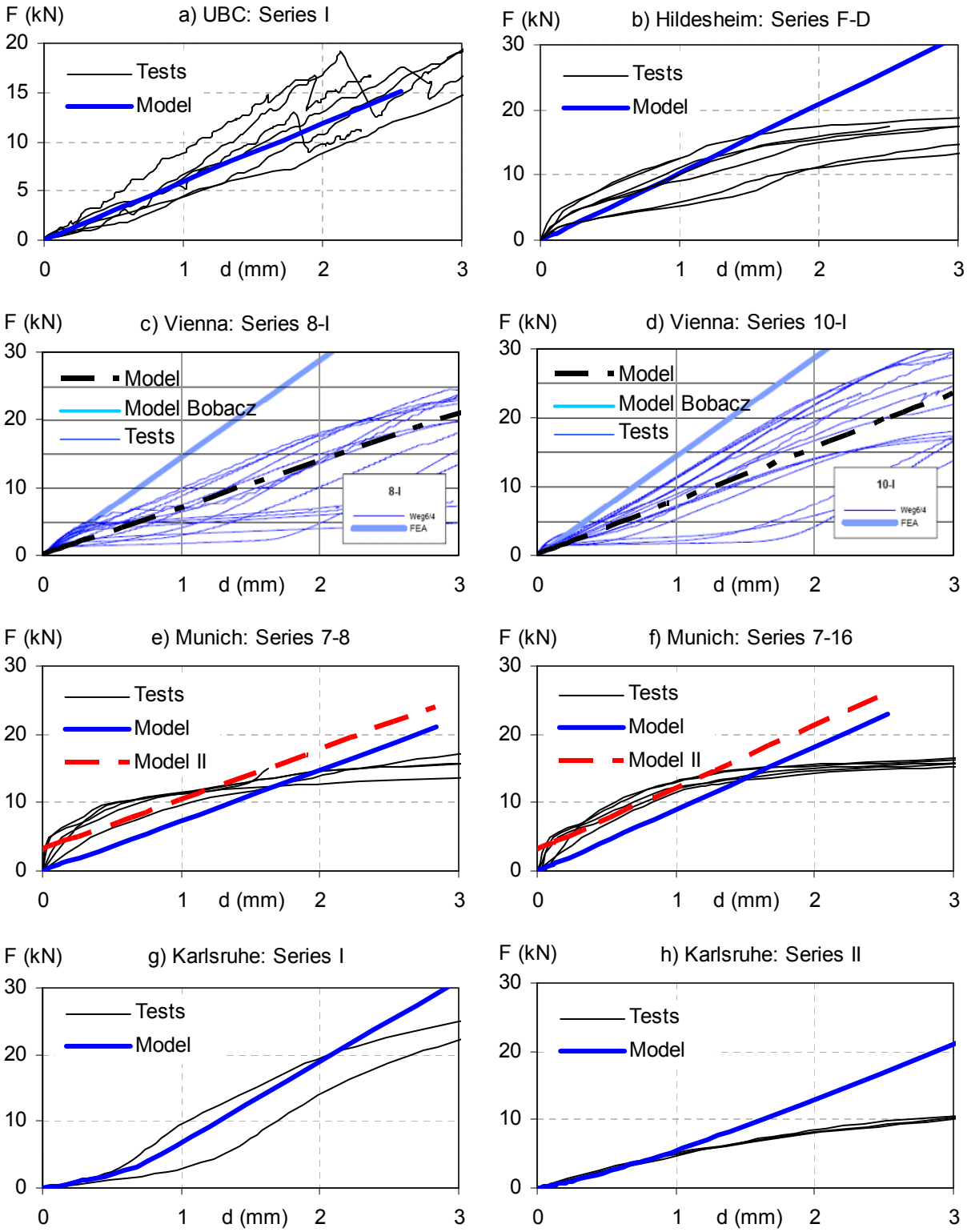

7.5. Discussion and conclusions

The presented FEM model for the analysis of the structural performance of RDC connecting two wooden members includes geometrical parameters, such as the dimensions of the members and the connection between them; and physical parameters, such as mechanical properties of the wood and the applied boundary conditions and external loads. The principal parameters influencing the structural performance of RDC are studied; these are: element type and density, contact parameters, material properties, and boundary conditions. Problems with the implementation of these parameters such as convergence and obtaining the solution are analysed and an appropriate model for RDC is presented.

In designing FEM models of RDC, the wood can be modelled with linear elastic and transverse isotropic material properties. Varying the model parameters over a realistic range yielded parameters that provided an excellent fit for the load deformation curves from UBC experimental test series. Incorporating grain angle, ring width, moisture content, density, and initial load-slip alignment behaviour allowed modeling the behaviour of individual test specimens. The model was validated with further RDC experiments. Given the limited information on some of these tests at least acceptable agreement between experimental and numerical load deformation curves was obtained. The comparisons between the developed model and the various test results show that the model is reliable in predicting load displacement behaviours and can therefore be used to study failure criteria and to predict failure loads. The model can be applied for modeling the load-deformation behaviour of different series and for probabilistic modeling using the variables as random input parameters.

7.6. References

Ansys. (2006). Release 10.0 Documentation for ANSYS. <http://www.ansys.com> (May, 2006).

Barrett, J. D., Lam, F. and Nakajima, S. (2001). Material strength properties for Canadian species used in Japanese post and beam construction. Proceedings, CIB-W18, Venice, Italy, 34-6-1.

Barthel, R., Jagfeld, M., and Gengnagel, C. (1999). Analytische Untersuchungen einer maschinell abgebundenen Zapfenverbindung aus Konstruktionsvollholz zwischen Haupt- und Nebenträger mit Hilfe der FE- Methode (in German). Report, Technical University Munich, Germany.

Blass, H. J., and Saal, H. (1999). Orientierende Tragfähigkeitsversuche an Haupt-Nebenträgeranschlüssen mit schwalbenschwanzähnlicher Zapfenverbinding sowie SFS-Holzschrauben (in German). Test report No. 996107, Universität Karlsruhe, Germany.

Bobacz, D. (2002). In CNC-Technik gefertigte zimmermannsmäßige Verbindungsmittel - Untersuchung des Schwalbenschwanzzapfens (in German). Diploma thesis, Universität für Bodenkultur, Vienna, Austria.

Dietsch, P. (2005). Development of a finite-element model for parameter studies of a dovetail connection. Diploma thesis, Technische Universität, Munich, Germany.

Green, D. W., Winandy, J. E., and Kretschmann, D. E. (1999). Mechanical properties of wood. In: Wood handbook - wood as an engineering material. Forest Products Laboratory, Madison, USA.

Hochstrate, M. (2000). Untersuchungen zum Tragverhalten von CNC gefertigten Schwalben-schwanzverbindungen (in German). Diplom thesis, FH Hildesheim, Germany.

Kreuzinger, H., and Spengler, R. (1999). Zum Tragverhalten von maschinell abgebundenen Zapfenverbindungen aus Konstruktionsvollholz zwischen Haupt- und Nebenträger (in German). Technical report LKI 7313, Technische Universität, Munich, Germany.

McKenzie, W. M., and Karpovich, H. (1968). The frictional behaviour of wood. Wood Science and Technology, 2(2), 139-152.

Mihailescu, T. (2001). An investigation of the performance of mortise and tenon joints using the finite element method. Journal of the Institute of Wood Science, 15(5).

Tannert, T. and Lam, F. (2006). Geometry parameters of Rounded Dovetail Connections. Proceedings, 9th World Conference on Timber Engineering, Portland, USA, 3-13-4.

Tannert, T., Prion, H., and Lam, F. (2007). Structural performance of RDC under different loading conditions. Canadian Journal of Civil Engineering, 34(12), 1600-1605.

Chapter 8: Size effect failure criterion for Rounded Dovetail Connections [12]

8.1. Introduction

Rounded Dovetail Connections (RDC) are a relatively new method for connecting structural members (Figure 8-1 left) with its load transfer mechanism governed by its geometric features (flange angle k, dovetail angle a, dovetail height h_1, dovetail width b_1, dovetail depth t, and member height and width h and b), see Figure 8-1 right. A number of experimental studies on RDC provided valuable insight into their structural performance (Kreuzinger and Spengler 1999; Blass and Saal 1999; Hochstrate 2000; Bobacz 2002; Tannert and Lam 2006; Tannert et al. 2007). Joist failure mode of RDC under shear loading was shown to be brittle and occur in the elastic range of the load deformation response and capacity does not increase proportionally with specimen size.

The acceptance of RDC in the structural engineering community is affected by a lack of design data. The most effective approach for obtaining data and understanding the structural performance of RDC is to combine experiments with Finite Element Method (FEM) modeling. Tests are needed to define material properties and for model verification. The verified model can estimate the distribution of internal forces, stresses and strains across the member while boundary conditions and material properties can be considered as variable input parameters.

[12] A version of this chapter has been prepared for publication. Tannert, T., and Lam F. (2008). Size effect failure criterion for Rounded Dovetail Connections.

Figure 8-1: RDC application (left) and geometric parameters (right)

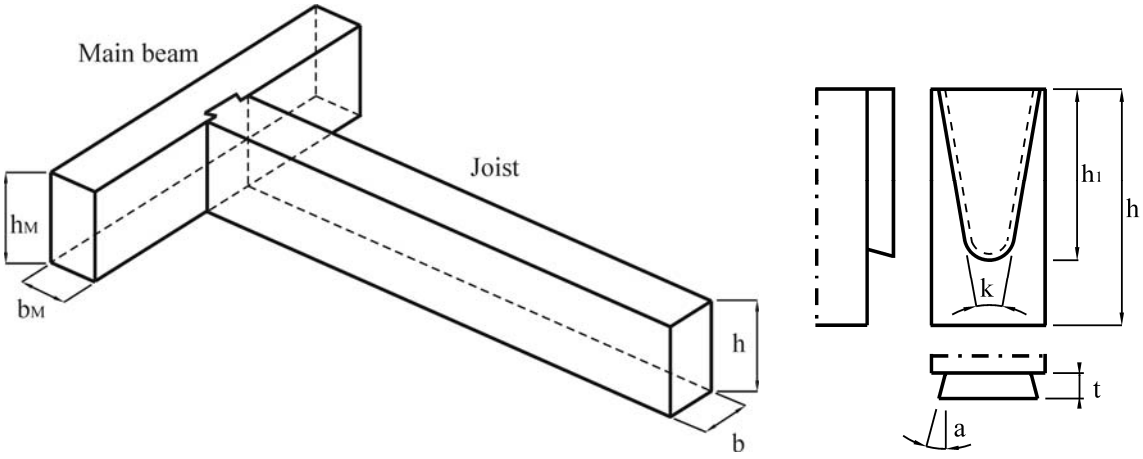

Although a verified FEM model contributes to a better understanding of internal stresses, load-displacement behaviour and failure modes of RDC, a failure criterion is necessary to estimate their capacity. In order to establish a failure criterion, a FEM model must consider geometric, physical, and mechanical parameters. Such a model was developed at The University of British Columbia (Tannert 2008). The model was calibrated against experimentally observed load deformation curves, validated with a range of tests, and shown to reliably predict load displacement behaviour. FEM studies showed that with detailed knowledge of the stress distribution within RDC, the structural performance can potentially be improved by considering the geometry as design parameters to reduce concentration of tension perpendicular to grain and shear parallel to grain stresses. Therefore the model can be extended to study failure criteria and to predict RDC capacity.

8.2. Objective

The objective of this work is to develop a failure criterion for RDC that takes into account the size effect for tension stress perpendicular to grain and shear stress parallel to grain.

8.3. Theoretical background

8.3.1. Failure criteria

Failure criteria are used to predict failure for a given a stress state. Depending on the material behaviour a certain state of stress will produce plastic deformation in a ductile material or fracture in a brittle material. For isotropic materials, failure criteria have been developed from the physical material behaviour; for wood available failure criteria are unifying empirical rules providing fits to experimental data. A number of criteria applicable to composite materials and wood have been developed; various summaries are given, one of the most recent by Kasal and Leichti (2005). A commonly applied failure criterion for wood was proposed by Norris (1962), see Equation 8-1:

$$\left(\frac{\sigma_X}{f_X}\right)^2 - \left(\frac{\sigma_X \sigma_Y}{f_X f_Y}\right) + \left(\frac{\sigma_Y}{f_Y}\right)^2 + \left(\frac{\tau_{XY}}{f_{XY}}\right)^2 = 1$$

$$\left(\frac{\sigma_Y}{f_Y}\right)^2 - \left(\frac{\sigma_Y \sigma_Z}{f_Y f_Z}\right) + \left(\frac{\sigma_Z}{f_Z}\right)^2 + \left(\frac{\tau_{YZ}}{f_{YZ}}\right)^2 = 1 \qquad \text{Equation 8-1}$$

$$\left(\frac{\sigma_Z}{f_Z}\right)^2 - \left(\frac{\sigma_Z \sigma_X}{f_Z f_X}\right) + \left(\frac{\sigma_X}{f_X}\right)^2 + \left(\frac{\tau_{ZX}}{f_{ZX}}\right)^2 = 1$$

where σ_X, σ_Y, σ_Z, τ_{XY}, τ_{XZ}, τ_{ZX} are the stresses in the X,Y,Z directions and XY, XZ, YZ planes, and f_X, f_Y, f_Z, f_{XY}, f_{XZ}, f_{ZX} are the corresponding material strength parameters, with f_X, f_Y, f_Z being different for tension and compression. Each of the equations represents an ellipsoid and any condition of stress is represented by a point in the space enclosed by these ellipsoids. As long as the point lies within the volume common to the ellipsoids, the material is deemed not to have failed.

Amongst others, Tsai and Wu (1971) proposed a tensor polynomial failure theory that can consider all possible stress interactions and creates a closed failure surface in the stress space. Tensor polynomial failure criteria like Tsai-Wu are based on empirical curve fitting considerations and not on physical reasoning. These criteria do not include material-specific failure mechanisms and the resulting strength-degradation in the post-critical range is therefore independent of type and direction of loading. In the Tsai-Wu criterion, failure under biaxial tensile stress depends on the values of the compressive failure stresses which is physically unacceptable (Hashin 1980).

Hashin argued that a general criterion for unidirectional fibre composites should distinguish among the various failure modes and proposed four separate criteria for transversely isotropic materials. The criterion for tensile matrix failure is shown in Equation 8-2:

$$\frac{\left(\sigma_Y^2 + \sigma_Z^2\right)}{\left(f_{T,\perp}\right)^2} + \frac{\left(\tau_{YZ}^2 - \sigma_Y \sigma_Z\right)}{\left(f_{S,\perp}\right)^2} + \frac{\left(\tau_{XY}^2 + \tau_{ZX}^2\right)}{\left(f_{S,II}\right)^2} = 1 \qquad \text{Equation 8-2}$$

where $f_{T,\perp}$ is the tension strength perpendicular to grain and $f_{S,\perp}$ and $f_{S,II}$ are the shear strengths perpendicular and parallel to grain, respectively.

Although there has been a significant volume of work in failure criteria development, a general and simple unified model is not available. Moreover, the existing criteria do not explain the well known observation of the size effect of the stressed volume in timber that fails in a brittle way when multiple stresses are present in the failure region.

8.3.2. Size effect – Weibull theory

The fact that strength decreases with an increase of stressed volume can be explained by the Weibull weakest link theory. Other explanations of the size effect are based on the concepts of fracture mechanics (Smith et al. 2003) and the hypothesis that the cylindrical orthotropic structure of wood causes stress-concentrations in large specimens (Pedersen et al. 2003).

Weibull (1939) recognised that a critical material flaw dictates failure strength and that the probability of encountering a strength-reducing flaw is increased when the stressed volume of the material is increased. Weibull theory predicts the influence of the size of the stressed volume and the stress distribution over this volume on the strength of materials with brittle fracture behaviour. The cumulative probability of failure F of a volume V subjected to a single non-uniformly distributed stress $\sigma = \sigma(x, y, z)$ is given by Equation 8-3:

$$F = 1 - \exp\left[-\frac{1}{V} * \int_V \left(\frac{\sigma - \sigma_0}{m} \right)^k dV \right] \qquad \text{Equation 8-3}$$

where σ_0 the strength threshold of the 3-parameter Weibull distribution, m and k are scale and shape parameters. Often, σ_0 is accepted to be 0 resulting in a 2-parameter distribution. The parameters can be estimated by fitting to experimental data using various procedures.

The common and straight forward Weibull theory approach has be en successfully applied to wood but it ignores the presence of more than one stress component which is important to be considered in more complex situations such as the capacity and strength of connections.

8.3.3. Incorporating size effect in failure criteria

Timber is commonly assumed to be a linear elastic, homogeneous, transversely isotropic and brittle material with deterministic properties in strength analysis for timber engineering in stress-based failure criteria. In situations where the failure is caused by fracture due to tension perpendicular to grain stress, predictions of models based on these assumptions can be misleading (Smith et al. 2003). Recognition of size effects and the stochastic nature of the material properties by use of Weibull theory are important when using conventional strength-based failure criteria. Ranta-Maunus (1996) integrated tension perpendicular to the grain stresses in order to incorporate the non-uniform stress state introduced by the transverse anisotropy. The effective (or damage relevant) Weibull stresses, are calculated according to Equation 8-4:

$$\sigma_{t,90}^{*} = \left(\frac{1}{V} \int_{V} \sigma_{t,90}^{k} dV \right)^{1/k} \qquad \text{Equation 8-4}$$

where the Weibull stress $\sigma_{t,90}^{*}$ is the value of constant stress that gives the same probability of failure as the actual stress distribution for the stressed volume V. The idea of damage relevant stresses is to weigh local stress peaks according to Weibull theory.

8.4. Proposed failure criterion

8.4.1. Relevant stresses and stressed volume in RDC

Experiments indicated that failure of RDC in the joist member (Figure 8-2) is caused by tension stress perpendicular to the grain and shear stress parallel to grain (Kreuzinger and Spengler 1999; Tannert and Lam 2006).

Figure 8-2: Typical failure of RDC in shear test

The FEM model was used to analyse the distribution of all stress components in the dovetail joist section (Figure 8-3). Timber is a cylindrically isotropic material, but in FEM models it often is assumed to be transverse isotropy with identical properties in the radial and tangential directions which are referred to as perpendicular to grain. Failure developed at the tip of the dovetail, a location that is clearly identified by the highest stresses.

Figure 8-3: Stress distribution in RDC for different stress components

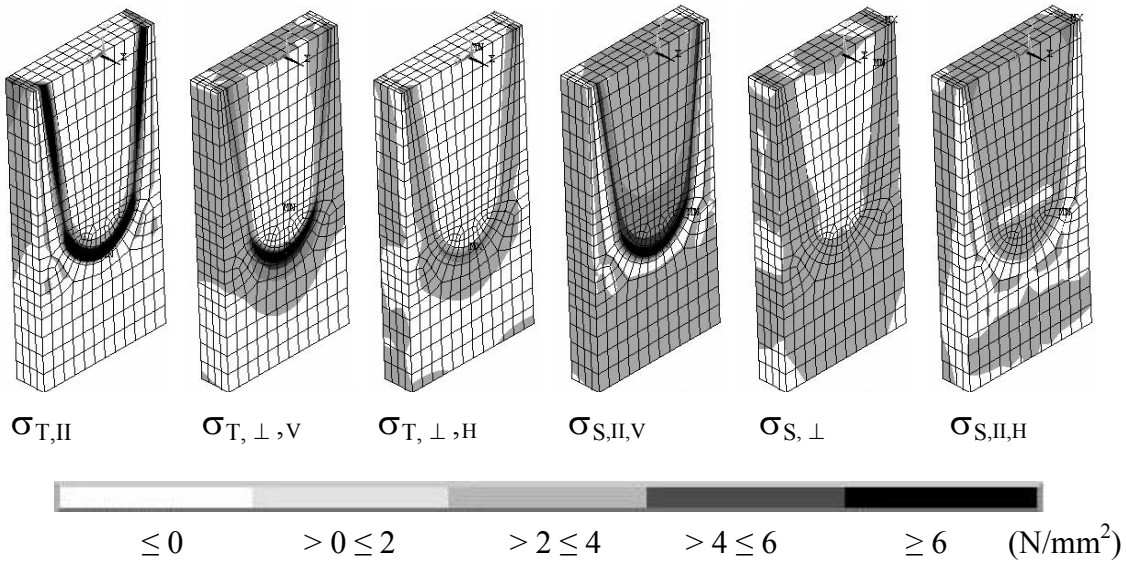

Tension parallel to grain stress ($\sigma_{T,II}$) is the highest in magnitude and distributed along the dovetail flange. The stress is caused by the force that is pulling the joist tenon out of the main beam mortise. It will be shown that it does not contribute significantly to RDC failure. The vertical tension perpendicular to grain stress ($\sigma_{T,\perp,V}$) is localized and substantial in magnitude with the peak located at the tip of the rounded dovetail part. The stress is caused by the main load bearing mechanism of the connection similar to a notched joint. The horizontal tension perpendicular to grain stress ($\sigma_{T,\perp,H}$) is smaller in magnitude and originates from the wedging forces of the joist tenon into the main beam mortise. This stress can increase when an initial load is applied to force the connecting parts of the RDC together in order to eliminate potentially existing gaps. Shear stress parallel to grain in the vertical plane ($\sigma_{S,II,V}$) is localized and substantial in magnitude with the peak at the same location as the peak of the stress in tension perpendicular to grain. Shear stresses parallel to grain in the horizontal plane ($\sigma_{S,II,H}$) and perpendicular to grain ($\sigma_{S,\perp}$) are not localized and low in magnitude.

8.4.2. Stress volume integral calculation

To calculate stress volume integrals for the tension perpendicular to grain and shear parallel to grain stresses, the stress field can be numerically integrated over the volume using a Gauss integration scheme (Foschi and Barrett 1976). The summation of stresses according to Equation 8-5 is shown to be sufficiently accurate for small volumes V_i:

$$\sigma_j^* = \left(\frac{1}{V_{ref}} \int_V \sigma_j^{kj} dV \right)^{1/kj} \approx \left(\frac{1}{V_{ref}} \sum \left(\sigma_j^{kj} * V_i \right) \right)^{1/kj} \qquad \text{Equation 8-5}$$

where V_{ref} is a reference volume, σ_j is the integrated stress and k_j is the shape parameter.

A study was conducted to evaluate which volume has to be considered for calculating the stress integrals. Three different approaches were considered: (I) the whole joist, (II) an extended connection area (length 50% of beam height), and (III) the dovetail tip. For test series reported by Tannert and Lam (2006), the stress volume integrals for tension perpendicular to grain and shear parallel to grain stresses were calculated using V_{ref} = 16,387 mm^3 (1 in^3) and for simplicity $k_{T,\perp} = k_{S,II} = 5.0$. For tension perpendicular to grain stress, there is a slight increase from Volume III to Volume II, but no further increase to Volume I. The stress is typically localized around the dovetail tip and integrating the stresses of the connection area covers all relevant stress. For shear parallel to grain stress, there is a significant increase from Volume III to Volume II, and a slight increase to Volume I. The shear stress is typically spread out throughout the beam; however, the stresses far away from the connection does not contribute to failure and can be ignored which significantly decreases computation time. It was decided to use the Volume with a length 50% of the beam height for calculating the stress volume integrals.

The mesh size had to be determined carefully, since the summation according to Equation 8-5 is only a valid approximation for the numerically "exact" Gaussian integration for high mesh refinement. The mesh was refined in 16 steps and the volume integrals for tension perpendicular and shear parallel to grain stresses was calculated varying the shape parameters k from 2 to 6. The volume integrals increase until reaching a certain mesh refinement. The increase is more severe for higher values of the shape parameter k, due to the nonlinearity of the equation. For tension stress, the volume integrals increase with higher k-values while for shear stress the opposite is true showing the difference between the localised tension perpendicular to grain versus the more distributed shear parallel to grain stress. It was decided that a mesh with element length of 5 mm at the dovetail tip is appropriate. For details see Appendix M and N.

8.4.3. Strength values

Values for strength thresholds entering any maximum stress criterion can be determined through tests on small clear wood specimens. 160 specimens each were tested for the brittle material properties (tension parallel and perpendicular to grain and for shear parallel to grain strength) according to ASTM-D143 (2002).

The mean values and (standard deviation) were: for tension perpendicular to grain strength $f_{T,\perp,ASTM}$ = 2.96 N/mm² (0.80 N/mm²), for shear parallel to grain strength $f_{S,II,ASTM}$ = 7.80 N/mm² (1.52 N/mm²), and for tension parallel to grain strength were $f_{T,II,ASTM}$ = 77.4 N/mm² (23.4 N/mm²). These values are in agreement with those reported by Barrett and Lau (1994). Tension parallel to grain strength was determined to test the hypothesis that tension parallel to grain stresses do not significantly contribute to failure of RDC.

The variability in strength properties is related to the shape parameter k (Barrett and Lau 1994) and can be approximated for typical coefficients of variation (CV) using Equation 8-6:

$$k = CV^{-1.085} \qquad \text{Equation 8-6}$$

Using the test results and Equation 8-5, the obtained shape parameters were $k_{T,\perp}$ = 4.15 for tension perpendicular, $k_{S,II}$ = 5.85 for shear parallel, and $k_{T,II}$ = 3.65 for tension parallel. The widely accepted values of the shape parameters of commercial softwood timber are for tension perpendicular to grain $k_{T,\perp}$ = 5.0 (Barrett 1974) and for shear parallel to grain strength $k_{S,II}$ = 5.5 (Foschi and Barrett 1976).

It is difficult to experimentally measure the unit volume strength f^* directly. Foschi and Barrett (1976) used 2D FEM analysis to relate $f_{S,II,ASTM}$ to $f^*_{S,II}$. Similar to this approach, FEM

models were analysed for the ASTM small clear specimen tests. The respective models were loaded with the forces that caused the average failure stresses for the tests. Using Equation 8-5 and the above shape factors, the unit volume strengths for the 50th percentiles were determined as: $f^{*}_{T,\perp}$ = 3.34 N/mm² for tension perpendicular to grain, $f^{*}_{T,II}$ = 72.7 N/mm² for tension parallel to grain, and $f^{*}_{S,II}$ = 7.55 N/mm² for shear parallel to grain.

8.4.4. Applicability of existing failure criteria

Various failure criteria were successfully applied to predict the location at which a fracture plane in wood might develop. It is important to recognise that simple strength based criteria may fail in regions with steep stress gradients, since they do not represent stress redistribution processes that occur in wood (Smith et al. 2003). Therefore the size effect concept should be incorporated to weight those regions of high stresses. Considering the problematic of incorporating size effect into complex failure criteria and the results from preliminary analyses, it was decided to study the Norris and Hashin criteria for their applicability for predicting the level of externally applied load at which fracture will occur in RDC.

These criteria are reformulated in such a way that only stresses that cause brittle failure modes are considered, see Equation 8-7. The influence of three brittle failure modes (tension perpendicular to grain in vertical and horizontal direction, tension parallel to grain and shear parallel to grain) are included to predict the level of externally applied load that leads to material failure. The proposed failure criteria combine the conventional failure criteria that predict failure due to stress combinations at a point with a size effect approach that uses stress integrals computed over a stressed volume.

IA) $$\left(\frac{\sigma_Y^*}{f_{T,\perp}}\right)^2 + \left(\frac{\sigma_X^*}{f_{T,II}}\right)^2 - \left(\frac{\sigma_Y^*\sigma_X^*}{(f_{T,\perp})^2}\right) + \left(\frac{\tau_{XY}^*}{f_{S,II}}\right)^2 = 1$$

IB) $$\left(\frac{\sigma_Y^*}{f_{T,\perp}}\right)^2 + \left(\frac{\sigma_Z^*}{f_{T,\perp}}\right)^2 - \left(\frac{\sigma_Y^*\sigma_Z^*}{(f_{T,\perp})^2}\right) = 1$$

Equation 8-7

IC) $$\left(\frac{\sigma_Z^*}{f_{T,\perp}}\right)^2 + \left(\frac{\sigma_X^*}{f_{T,II}}\right)^2 - \left(\frac{\sigma_X^*\sigma_Z^*}{(f_{T,\perp})^2}\right) + \left(\frac{\tau_{ZX}^*}{f_{S,II}}\right)^2 = 1$$

II) $$\frac{(\sigma_Y^{*2} + \sigma_Z^{*2})}{(f_{T,\perp})^2} + \frac{(\tau_{XY}^{*2} + \tau_{ZX}^{*2})}{(f_{S,II})^2} = 1$$

where σ^*_X, σ^*_Y, σ^*_Z and τ^*_{XY}, τ^*_{YZ}, τ^*_{ZX} are the stress volume integrals.

For the test series reported by Tannert and Lam (2006), stress volume integrals were computed with Equation 8-5 and used as input data for the criteria in Equation 8-7. The previously determined unit volume strengths were used as strength thresholds. For the modified Norris criterion (Equation 8-7 IA, IB and IC), failure in one of the three stress combinations is sufficient to cause failure of the connection. Criterion IA which includes vertical tension perpendicular to grain and radial shear parallel to grain stresses always governs, see Appendix O. The modified Hashin criterion (II) is even more conservative as it considers both tension perpendicular to grain stresses (vertical and horizontal) and both shear parallel to grain stresses (radial and tangential plane). It was decided that this criterion is appropriate to estimate the capacity of RDC.

In numerical simulations for all test series, the external loads were incrementally increased in order to calculate the connection forces that fulfill the proposed failure criterion. These simulations were carried out using the 50th percentile strength values determined for

stresses perpendicular to grain and shear parallel to grain. Table 8-1 shows the estimated 50th percentile values of RDC capacities (C_{II}) as well as the experimentally observed average capacities (F_{ult}) for the tests series. T-tests for the hypothesis H_0: F_{ult} is equal to C_{II}, are rejected for those cases were the p-value is smaller than $\alpha = 0.05$ (95% significance level). For these tests, a minimum coefficient of variation for all test series of 25% was assumed.

Table 8-1: Comparison between RDC capacity from tests and simulations

Test series	Tests F_{ult} (kN)	Criterion C_{II} (kN)	t-tests p
Contr.-RDC	19.9	14.1	**0.01**
BC45-RDC	22.8	18.4	0.14
BC55-RDC	25.9	16.1	0.12
BC75-RDC	12.5	11.4	0.47
A05-RDC	19.0	12.4	0.06
A10-RDC	24.5	13.3	**0.04**
A20-RDC	16.3	14.5	0.36
Contr.-DRDC	20.0	16.1	0.05
BC45-DRDC	29.7	21.5	0.06
BC55-DRDC	23.9	18.6	0.10
BC75-DRDC	12.6	12.0	0.67
AC05-DRDC	21.4	15.1	0.07
AC10-DRDC	25.0	15.4	**0.02**
AC20-DRDC	21.2	16.2	0.14

The criterion predicts strength of the tests series to be lower strength for all test series. The deviation between the predicted connection capacities and the experimentally observed maximum connection loads is explained by the fact, that in the experiments by Tannert and Lam (2006), the exact load at which the first crack developed was not recorded. The criterion predicts

first failure and not ultimate load which can be higher due to changed load transfer mechanism. Nevertheless, the hypothesis that the experimentally observed average connection capacity is equal to the values determined by the criteria is accepted for 11 of the 14 test series. In consequence, the criterion can be accepted to appropriately predict RDC capacity.

8.4.5. Validation of failure criterion by prediction of capacity of new test series

The failure criterion was further validated by predicting the 50th percentile values of capacity (C_{II}) of three previously not tested RDC test configurations, and then carry out experiments to determine the capacity (F_{ult}). In these tests, the RDC force causing unstable crack growth was measured and represents the capacity.

The specimen dimensions b, h and l, the dovetail geometric parameters b_1, h_1 and k are given in Table 8-2. Depth t and angle a were constant with 28 mm and 15°, respectively. The tests were carried out using a similar set up like previous tests (Tannert and Lam 2006). For test Series I, the free end of the joist was supported on a steel plate which rested on a damper with a stiffness of approximately 1 kN/mm. For test series II and III, the joists rested on a rigid support of 200 mm x 200 mm without damper. The load was applied at a distance of 450 mm from the joint and distributed onto the joist with 150 mm x 150 mm x 10 mm steel plate.

The tests series were modelled and the external loads were increased incrementally in order to calculate the connection forces that fulfill the criterion b. For Series I, the material came from the same batch as the material used in the previous tests, therefore the values for unit volume strength and shape factor were identical. Different material was used for Series II, and the unit volume strength and shape factor for tension perpendicular to grain were determined as $f_{T,\perp} = 2.80$ N/mm^2 and $k_T = 4.20$, respectively, based on 128 small specimen tests according to

ASTM-D143 (2002). T-tests were used to test hypothesis H_0: the experimentally observed average capacities (F_{ult}) are equal to the predicted 50th percentile values of RDC capacities (C_{II}). For all three series, H_0 is accepted (Table 8-2). An attempt to validate the criterion with other tests is shown in Appendix P.

Table 8-2: Validation of RDC failure criterion with test results

Test series	Specimen size			Dovetail geometry			RDC capacity		
	b (mm)	h (mm)	l (mm)	h_1 (mm)	b_1 (mm)	k (°)	C_{II} (kN)	F_{ult} (kN)	t-Test p
I	90	184	950	109	50	20	12.7	16.2	0.10
II	124	274	1,250	189	50	20	28.6	31.3	0.26
III	124	274	1,250	199	70	10	30.5	32.2	0.30

8.4.6. Applications for RDC failure criterion

A series of simulations was carried out varying the loading and support conditions. In the tests by Tannert and Lam (2006), the load was applied at a distance of 350 mm from the RDC, the free joist end was supported on a damper, and the main beam was free to rotate at its supports. In the variations, the load was applied at a distance of 150 mm from the connection and distributed over the lengths of the joist. For each of the three loading conditions, the support of the free joist end was modelled in two variations: using a spring support and using a rigid support. In one model, the rotation of the main beam was restricted. An increase in capacity is predicted when the load is applied further away from the connection. Capacity also increases when the joist is supported on a damper which simulated the ability to deflect under load; this increase is most severe for distributed loads and minimal when the load is applied close to the

connection. Fixing the main beam at its supports reduces RDC capacity. Detailed results of these simulations are shown Appendix Q.

The elastic material properties and geometry parameters were studied in another series of simulations. The longitudinal MOE was varied from 10,000 N/mm² to 14,000 N/mm² in steps of 1,000 N/mm covering the common range of values for western hemlock. Previous work at UBC showed that the friction coefficient has significant influence on the stresses in RDC and that accurate gap modelling is essential for achieving realistic load deformation curves. The friction coefficient was varied from 0.1 to 0.5 in steps of 0.1. Two different gap types were analysed: Type I with a width that continuously decreases from the bottom to the very top of the joint, and Type II that only exists below the rounded part of the dovetail tip. The depth of both gap types was varied from 0 mm to 2 mm in steps of 0.5 mm. Finally, using the models with a gap of 1 mm for both gap types, the friction coefficient was varied from 0.1 to 0.5 in steps of 0.1.

The results of the simulations showed that the longitudinal MOE does slightly influence RDC capacity with large increases in MOE (40%) leading to small increases in capacity (6%). The friction coefficient has significant impact on RDC capacity. Increasing the friction coefficient from 0.1 to 0.5 increases the capacity by 30%. Low friction values cause higher stress because most of the load is transferred on the bottom of the dovetail while with high friction the load is transferred more evenly over the height of the dovetail along the flanges. Increasing the depth of the gap leads to decreases in capacity. The effect of friction remains unchanged when combined with different gap widths, increased friction decreases RDC capacity. Detailed results from the study of model parameters are shown in Appendix R.

A final series of numerical simulations was carried out varying the member dimensions (l, b and h) and the dovetail geometry (k, h_1 and b_1). Loading and support conditions (distributed load along the joist, joist connected to main beams at both ends, and main beam free to rotate at its supports) were kept constant. The loads were increased incrementally to calculate the RDC capacities that fulfill the failure criterion C_{II}, and the ratios between capacities and the effective dovetail area (C_{II}/A_1) were computed, (Table 8-3). Two important conclusions can be drawn from this exercise: (I) the capacity increase for larger specimens is not proportional to the dovetail area - the incorporation of size effect into the failure criterion is effective, and (II) a dependency of capacity on the flange angle k is predicted, with wider angles increasing the capacity as local stress concentrations of tension perpendicular to grain stress are less severe.

Table 8-3: Predicted RDC capacity by connection geometry

Model	l [mm]	b [mm]	h [mm]	k [mm]	h_1 [mm]	b_1 [mm]	A_1 [mm^2]	C_{II} [kN]	C_{II}/A_1 [N/mm^2]
V11	3,300	89	184	10	129	58	7,927	19.0	2.40
V12	3,300	89	184	15	129	47	7,291	18.8	2.58
V21	4,400	89	286	5	200	60	12,902	22.7	1.76
V22	4,400	89	286	10	200	44	11,316	21.6	1.91
V32	4,400	140	241	10	169	105	17,651	28.1	1.59
V34	4,400	140	241	20	169	80	15,667	27.5	1.76
V42	5,400	140	341	10	239	91	24,118	34.4	1.43
V44	5,400	140	341	20	239	50	19,629	32.7	1.67
V52	5,400	191	291	10	204	153	30,003	34.7	1.16
V54	5,400	191	291	20	204	125	27,316	34.4	1.26
V62	6,500	191	394	10	276	139	39,976	41.9	1.05
V64	6,500	191	394	20	276	95	34,304	44.2	1.29

8.5. Discussion and conclusions

The objective of this work was to develop a failure criterion for Rounded Dovetail Connections that takes into account the size effect for timber. Joist failure of RDC under shear loading was shown to be typically brittle and occur in the elastic range of the load deformation response. Therefore the proposed failure criterion for RDC is based on stresses computed with a FEM model that uses linear elastic material parameters. In consequence, the criterion can only be applied to situations where brittle failure of the joist member dictates the connection capacity.

The proposed criterion recognizes size effects using Weibull theory by comparing volume integrals for stresses that cause brittle failure to strength thresholds of a unit volume and incorporating a size effect shape parameter. Shape parameters and strength thresholds are determined through tests on small clear wood specimens. A volume with a length of 50% of the beam height and a summation of stresses for small volume elements was shown to be sufficiently accurate. Tension perpendicular to grain and shear parallel to grain stresses are considered in the failure criterion. Under pure tension or pure shear stress, the criterion reduces to a simple Weibull type size effect. The consideration of the stress combination allows estimating the capacity of RDC. The criterion was validated by predicting the capacities of previously not tested RDC's.

The criterion predicts an increase in capacity when the load is applied further away from the connection, when the main beam is free to rotate along it long axis, and when the joist is not restrained from deflecting; this latter increase is highest for distributed loads and minimal when the load is applied close to the connection. The criterion can be applied to further study the influence of geometric parameters, manufacturing tolerances, and loading and support conditions on RDC capacity.

The criterion predicts an increase of capacity with wider dovetail flange angles which is explained by the reduction of tension perpendicular to grain stress concentrations and should be taken into consideration when designing the RDC geometry. The authors recommend carrying out reliability studies to account for the wide scatter of material properties and probabilistic modelling methods with inputs in parametric form to optimize the dovetail geometry depending on loading and support conditions and member dimensions.

The proposed failure criterion takes into account the size effect for timber and accounts for the reduction in capacity of large joints. Numerical simulations varying member dimensions and dovetail geometry, predict the capacity increase for larger specimens not to be proportional to the dovetail area. Further simulations indicated that tension perpendicular to grain strength and friction between the connected members dictate RDC capacity, therefore only timber without defects in the connection vicinity should be used to produce RDC. The criterion predicts an increase of capacity for tight fitting connections; in consequence RDC should be manufactured with tight fit that guarantee high friction between the connected timber members.

The immediate application of the failure criterion is the study of parameter influences on the capacity of Rounded Dovetail Connections. As part of future research, a reliability analysis of RDC is proposed recognizing that failures cannot be avoided, but that the expected number of failures can be minimized to be within a tolerated level. Such as study coupled with further experiments can lead to an equation that can be included in design codes. Ultimately, a thorough understanding of the brittle failure in complex connections such as RDC is crucial before reliable equations can be introduced in the design codes. More work is needed to achieve a general failure criterion that can also be applied to other carpentry wood-to-wood connections.

8.6. References

ASTM-D143. (2002). Standards test methods for small clear specimens of timber. Annual book of ASTM standards, section four: construction. Vol. 04.10 wood. West Conshohocken, USA.

Barrett, J. D. (1974). Effect of size on tension perpendicular-to-grain strength of Douglas-fir. Wood and Fiber, 6(2), 126-143.

Barrett, J. D., and Lau, W. (1994). Canadian lumber properties. Canadian Wood Council, Ottawa, Canada.

Blass, H. J., and Saal, H. (1999). Orientierende Tragfähigkeitsversuche an Haupt-Nebenträgeranschlüssen mit schwalbenschwanzähnlicher Zapfenverbinding sowie SFS-Holzschrauben (in German). Test report No. 996107, Universität Karlsruhe, Germany.

Bobacz, D. (2002). In CNC-Technik gefertigte zimmermannsmäßige Verbindungsmittel - Untersuchung des Schwalbenschwanzzapfens (in German). Diploma thesis, Universität für Bodenkultur, Vienna, Austria.

Foschi, R. O., and Barrett, J. D. (1976). Longitudinal shear strength of Douglas-fir. Canadian Journal of Civil Engineering, 3(2), 198-208.

Hashin, Z. (1980). Failure criteria for unidirectional fiber composites. Journal of Applied Mechanics, 47, 329-334.

Hochstrate, M. (2000). Untersuchungen zum Tragverhalten von CNC gefertigten Schwalben-schwanzverbindungen (in German). Diplom thesis, FH Hildesheim, Germany.

Kasal, B., and Leichti, R. J. (2005). State of the art in multi-axial phenomenological failure criteria for wood members. Progress in Structural Engineering and Materials, 7(1), 3-13.

Kreuzinger, H., and Spengler, R. (1999). Zum Tragverhalten von maschinell abgebundenen Zapfenverbindungen aus Konstruktionsvollholz zwischen Haupt- und Nebenträger (in German). Technical report LKI 7313, Technische Universität, Munich, Germany.

Norris, C. B. (1962). Strength of orthotropic materials subjected to combined stresses. Report No.1816, Forest Products Laboratory, Madison, USA.

Pedersen, M. U., Clorius, C. O., Damkilde, L., and Hoffmeyer, P. (2003). A simple size effect model for tension perpendicular to grain. Wood Science and Technology, 37(2), 125-140.

Ranta-Maunus, A. (1996). The influence of changing state of stress caused by mechano-sorptive creep on the duration of load effect. Proceedings, International COST 508 Wood Mechanics Conference, Stuttgart, Germany, 187-201.

Smith, I., Landis, E., and Gong, M. (2003). Fracture and fatigue in wood. Wiley & Sons, Chichester, England.

Tannert, T. (2008). Structural Performance of Rounded Dovetail Connections. PhD thesis. The Univesrity of British Columbia Vancouver, Canada.

Tannert, T. and Lam, F. (2006). Geometry parameters of Rounded Dovetail Connections. Proceedings, 9th World Conference on Timber Engineering, Portland, USA, 3-13-4.

Tannert, T., Prion, H., and Lam, F. (2007). Structural performance of RDC under different loading conditions. Canadian Journal of Civil Engineering, 34(12), 1600-1605.

Tsai, S. W., and Wu, E. M. (1971). A general theory of strength for anisotropic materials. Journal of Composite Materials, 5(1), 58-80.

Weibull, W. (1939). A statistical theory of strength of materials. Proceedings of the Royal Swedish Institute, Research No.151, Stockholm, Sweden.

Chapter 9: Design Guideline for Rounded Dovetail Connections [13]

9.1. Introduction

Rounded Dovetail Connections (RDC) are a relatively new method for connecting structural members. The use of RDC in timber construction has significantly increased in Europe, with the most common application being the connection of a joist to a beam or a beam to a girder (Figure 9-1 left). A number of experimental studies on RDC provided valuable insight into the structural performance of this versatile connection (Kreuzinger and Spengler 1999; Blass and Saal 1999; Hochstrate 2000; Bobacz 2002; Tannert and Lam 2006; Tannert et al. 2007). The load transfer mechanism of RDC is governed by its geometric features (Figure 9-1 right).

Figure 9-1: RDC application (left) and geometric parameters (right)

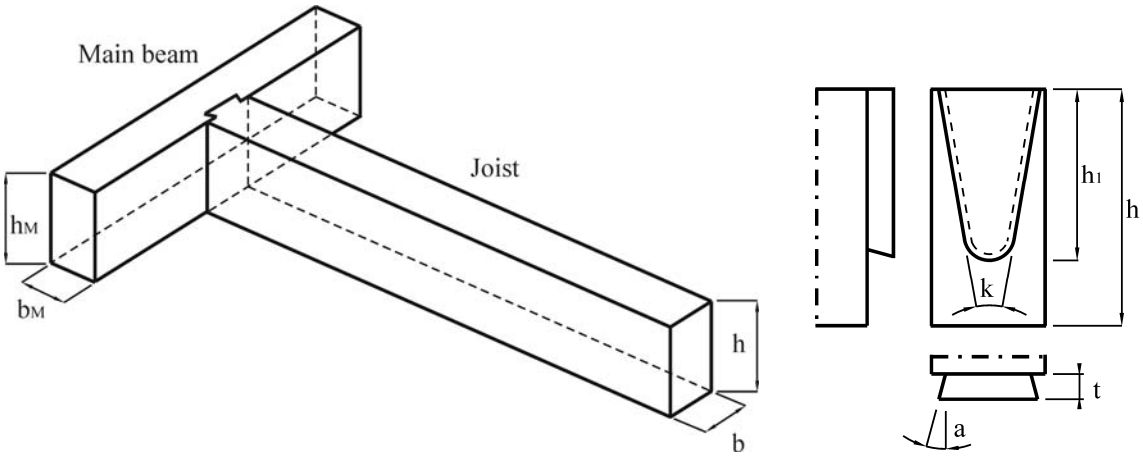

[13] A version of this chapter has been accepted for publication. Tannert, T., and Lam, F. (2008). Design Guideline for Rounded Dovetail Connections. Proceedings, ASCE conference on Structural Engineering, April 2008, Vancouver, Canada.

A revival of interest in timber frame buildings in the United States occurred during the 1970s and since that time, has led to growth in the timber framing industry to keep up with demand for timber frame structures (O'Connell and Smith 1999) and carpentry connections are being used in a growing number of timber buildings (Schmidt and Scholl 2000). But the acceptance of carpentry connections in the North American structural engineering and architectural community is affected by a lack of design values and provisions in building codes (Bamford 2003). Engineers and architects indicate that there is a diverse demand and need for guidance in designing connections in wood construction throughout North America, and existing design codes need to be expanded and updated to reflect the acceptance and use of modern wood connections (Snow et al. 2006). Nevertheless, the Rounded Dovetail Connection is increasingly being used, driving the demand and need for guidance in designing such connections in timber construction throughout North America.

9.2. Existing design recommendations for Rounded Dovetail Connections

9.2.1. Design equation for end notched beam supports

There are currently no design equations specifically for RDC in building codes. RDC are very similar to end notched beam supports - both structural details represent situations where brittle fracture via crack propagation is an issue. Design formulas for end-notched beam supports estimate the capacity by reduction of the allowable formal beam shear stress according to Equation 9-1:

$$\frac{1.5 * V}{(b * h_e)} = f_S * k_V \qquad \text{Equation 9-1}$$

where b is the beam width, h the beam height, h_e the notch height, f_S the shear strength of the wood and k_V a reduction factor which reflects the influence of the stress concentration due to the notch. Early design formulas for end-notched beams were not known to have any theoretical basis and the reduction factor k_V was equal to the ratio of h_e to h.

Gustafsson (1988) studied the strength of wooden beams with a rectangular end-notch on the tension side and concluded that notch failure always develops at the tip of a notch and that notch failure may be analysed theoretically by linear elastic fracture mechanics. The distance from the support to the notch tip was found to be of significant importance for notch strength and a closed-form equation based on fracture mechanics considerations was presented. This equation in modified form is now given in many design codes such as Eurocode 5 to calculate the capacity of end notched beam supports. However, analysis errors can be significant when the notch is very shallow or very short, for instance, in situations where very high glulam members are employed or RDC with their very short distance between notch and support.

9.2.2. Existing design guidelines for Rounded Dovetail Connections

Werner (2002) examined the load-deformation curves for RDC force versus relative vertical joint deformations under shear loading, he recommended limiting the joint deformation to 1.5 mm and he provided a design guideline for RDC. Since RDC can fail either by breaking of the joist or main beam, the two members are designed separately, see Equation 9-2:

$$F_{adm(Joist)} = \frac{2}{3} * A_1 * f_{S,adm}$$

Equation 9-2

$$F_{adm(Main\ beam)} = 0.09 * \left(h_M - h_1 + \frac{b_1}{2} \right) \quad (h_M, h_1, b_1 \text{ in mm, F in kN})$$

The design criterion for the main beam is an empirical formula developed by analyzing results from the different tests. It estimates the design load based on the expected location of the crack that develops on the mortise base before the main beams fails. The design criterion for the joist is based on the admissible shear stress $f_{S.adm}$, simply assuming the reduction factor k_V to be equal to 1, and the effective dovetail area A_1 according to Equation 9-3:

$$A_1 = \left[b_1 + \tan\frac{k}{2} * \left(h_1 - b_1/2 \right) \right] * \left(h_1 - b_1/2 \right) + \pi * b_1^2/8 \qquad \text{Equation 9-3}$$

According to Werner (2002), RDC stiffness C can be estimated with Equation 9-4:

$$C = 0.7 * \min\begin{cases} F_{adm(\text{Main beam})} \\ F_{adm(\text{Joist})} \end{cases} \quad (F \text{ in kN, C in kN/mm}) \qquad \text{Equation 9-4}$$

Although the Werner criterion is straight forward, it does not allow estimation of the capacity of RDC nor does it take into account the effect of member size on timber strength.

9.3. Objective

The objective of this work is to propose a design guideline for Rounded Dovetail Connections that takes into account size effect for timber strength in brittle failure.

9.4. Proposed design equation

The most effective approach for obtaining reliable data on the structural performance of RDC is to combine experiments with structural performance modeling using the Finite Element Method (FEM). Tests are needed to define physical material properties and for FEM model verification so that reliable statements can be made about the performance of RDC. The verified

FEM model can then be used to estimate the distribution of stresses and strains within the member as well as to study the load-displacement behaviour and failure modes of RDC.

9.4.1. Underlying failure criterion

Tannert and Lam (2006) studied the influence of geometric parameters on the structural performance of RDC under shear loading. Detailed information on material properties allowed the development and calibration of a FEM model to simulate the load deformation behaviour of RDC. The model was validated with a range of tests, and extended to study failure criteria for predicting RDC capacity. A failure criterion was proposed that takes into account size effects for the analysis of RDC. In this criterion, computed stress volume integrals are compared to stress thresholds, see Equation 9-5. The size effect in timber strength is incorporated by computing stress integrals for a failure relevant volume and experimentally determined shape parameters for the material strength distribution.

$$\frac{\left(\sigma_Y^{*2} + \sigma_Z^{*2}\right)}{\left(f^{*}_{T,\perp}\right)^2} + \frac{\left(\tau_{XY}^{*2} + \tau_{ZX}^{*2}\right)}{\left(f^{*}_{S,II}\right)^2} = 1 \qquad \text{Equation 9-5}$$

where σ^{*}_{X}, σ^{*}_{Z}, τ^{*}_{XY}, and τ^{*}_{ZX} are the stressed volume integrals of vertical and horizontal tension perpendicular to grain and shear parallel to grain stresses; $f^{*}_{T,\perp}$ and $f^{*}_{S,II}$ are the unit volume strength thresholds in tension perpendicular to grain and shear parallel to grain.

The criterion was successfully used to compare the predicted capacity of RDC with test results using timber dimensions and connection geometries which were not previously tested. Using the FEM model and the failure criterion, a series of simulations was carried out for various member dimensions (b and h) and the dovetail geometries (k, h_1 and b_1). Loading and support

conditions (distributed load along the joist, joist connected to main beams at both ends, and main beam free to rotate at its supports) were kept constant. For four different thresholds that cover the range of the 5th percentile strength of timber in tension perpendicular to the grain strength (1.4 N/mm^2, 1.6 N/mm^2, 1.8 N/mm^2, and 2.0 N/mm^2), the loads were increased incrementally to calculate the RDC capacities that fulfill the criterion (Table 9-1). These results can be used to develop an equation that predicts the 5th percentiles of RDC capacity.

Table 9-1: Predicted RDC capacity by connection geometry and strength threshold

Model	b [mm]	h [mm]	k [mm]	h_1 [mm]	b_1 [mm]	A_1 [mm^2]	$C_{II,f=1.4}$ [kN]	$C_{II,f=1.6}$ [kN]	$C_{II,f=1.8}$ [kN]	$C_{II,f=2.0}$ [kN]
V21	89	286	5	200	60	12,902	8.0	9.0	10.0	11.0
V22	89	286	10	200	44	11,316	8.0	9.0	10.0	11.0
V31	140	241	5	169	115	18,537	13.5	14.4	15.3	16.1
V32	140	241	10	169	105	17,651	13.4	14.2	15.0	15.8
V33	140	241	15	169	93	16,676	11.6	13.1	14.6	16.1
V34	140	241	20	169	80	15,667	12.1	13.6	15.1	16.6
V41	140	341	5	239	109	26,217	12.2	13.7	15.2	16.8
V42	140	341	10	239	91	24,118	12.0	13.5	14.9	16.4
V43	140	341	15	239	72	21,947	16.0	17.6	19.2	20.8
V44	140	341	20	239	50	19,629	19.4	20.9	22.3	23.8
V51	191	291	5	204	165	31,243	20.1	21.5	22.8	24.2
V52	191	291	10	204	153	30,003	19.6	20.9	22.1	23.4
V53	191	291	15	204	140	28,706	14.4	16.3	18.2	20.1
V54	191	291	20	204	125	27,316	14.7	16.6	18.6	20.5
V61	191	394	5	276	158	42,501	13.8	15.9	18.0	20.1
V62	191	394	10	276	139	39,976	13.8	15.8	17.8	19.8
V63	191	394	15	276	118	37,229	20.4	22.5	24.7	26.8
V64	191	394	20	276	95	34,304	21.0	23.1	25.2	27.4

9.4.2. Estimating RDC capacity

With the goal of determining the reduction factor k_V for a design formula according to Equation 9-1, a variety of possible regression models were run. Equation 9-6 provides a good fit with $R^2 = 0.72$ to the RDC capacities depending on the model parameters (f, b, h, k, h_1, b_1) listed in Table 9-1:

$$\frac{1.5 * V}{A_1} = f_S * \left(\frac{3{,}600\ \text{mm}^2}{A_1} \right)^{0.2} \qquad \text{Equation 9-6}$$

The proposed reduction factor takes into account the size effect of timber and reduces the capacity of the joist member of large RDC accordingly.

9.4.3. Comparison of predicted and experimental results

In order to validate the proposed design equation, the predictions from the equation are compared to the numerical results using the failure criterion according to Equation 9-5 and experimental results for UBC test series (Tannert and Lam 2006) and three additional test series for the 5th percentile values of the RDC capacities (Table 9-2). The 5th percentiles of the RDC capacities ($x_{5\%}$) were determined using Equation 9-7 (DIN-1052 2004):

$$x_{5\%} = x_{mean} * (1 - k * COV(x)) \qquad \text{Equation 9-7}$$

where x_{mean} is the test average, k is a coefficient that depends on the number of tests carried out and COV(x) is the coefficient of variation.

Stress volume integrals were computed and used as input data for the failure criterion in Equation 9-5. The 5th percentiles of unit volume strengths were determined through tests

according to ASTM-D143 (2002) as: $f^{*5}_{T,\perp}$ = 1.93 N/mm² and $f^{*5}_{S,II}$ = 5.01 N/mm², respectively for the material used by Tannert and Lam (2006) and $f^{*5}_{T,\perp}$ = 1.65 N/mm² for the material used in the additional tests. Good agreement was achieved between the experimental 5th percentiles of RDC capacity (COV(x) = 0.25 for all test series was assumed) and the predicted strength values. Part of the deviation between the predicted and experimental connection capacities can be explained by the fact the exact load at which the first crack developed was not recorded for the experiments reported by Tannert and Lam (2006). The criterion predicts first failure and not ultimate load which can be higher due to changes in the load transfer mechanism. The numerical model and in consequence the design equation cannot capture this increase in load. For design purposes the load at first failure is of primary interest. For the additional test series, the force applied (F_{ult}) that causes unstable crack growth represents the connection capacity.

Table 9-2: Comparison of RDC capacity from tests, simulations and design equation

Test series	Dovetail geometry				RDC capacity			$F_{@3mm}$
	h_1 (mm)	b_1 (mm)	k (°)	A_1 (mm^2)	$F_{ult,5th\%}$ (kN)	$C_{II,5th\%}$ (kN)	$C_{Equation}$ (kN)	(kN)
Contr.-RDC	123	50	15.0	7,146	10.3	8.5	7.9	14.9
BC45-RDC	143	50	15.0	8,715	9.5	10.9	9.2	15.1
BC55-RDC	133	50	15.0	7,917	10.8	9.6	8.6	17.4
BC75-RDC	103	50	15.0	5,683	5.2	6.8	6.6	12.5
A05-RDC	123	50	5.0	6,301	6.8	7.4	7.1	16.3
A10-RDC	123	50	10.0	6,722	10.2	8.0	7.5	15.0
A20-RDC	123	50	20.0	7,575	7.9	8.6	8.3	6.6
Shear-RDC	109	50	15.0	6,111	6.6	7.1	7.0	9.2
Series I	109	50	20.0	6,426	8.0	8.3	7.2	12.7
Series II	189	50	20.0	13,924	16.9	16.4	13.5	20.1
Series III	199	70	10.0	15,757	17.4	17.9	14.9	21.0

The geometric parameters and the proposed design equation were used to calculate the predicted 5th percentiles of RDC capacities. Equation 9-6 gives conservative results for all test series. It is important to consider a deformation limit in order to prevent unacceptable non-structural damage to the surrounding structure. The determination of such deformation limits is not regulated by testing standards or building codes. Tannert and Lam (2006) used a 3 mm limit for the relative vertical joint deformation to determine the load at 3 mm deformation ($F_{@3mm}$) of RDC under shear loading while Werner (2002) proposed a 1.5 mm deformation limit. The proposed design equation predicts 5th percentile capacities that are significantly lower than the experimentally observed loads at the chosen 3 mm deformation limit in all but one test series (RDC A20).

9.5. Design recommendations

The proposed design equation can be applied to estimate the capacity of the joist member of Rounded Dovetail Connections under shear loading. Since there are no data available on main beam failure from the UBC tests, the main beam members may be designed according to the equation provided by Werner (2002). The RDC connection stiffness cannot be estimated at this point because potential preloading and geometric parameters caused rather high variation in the initial alignment behaviour. Research to increase stiffness by reinforcing RDC with self tapping screws is being carried out at UBC and will provide more information on joint stiffness.

Depending on connection accuracy and fabrication techniques, very small loads are sufficient to cause significant initial alignment behaviour of RDC. Therefore joints should be tight fitting and manufactured using timber that has a moisture content close to the equilibrium moisture content that the timber will achieve in use.

In designing RDC, the reduced section of the main beam has to be accounted for and minimum distances need to be considered. Until further research provides more information, the general design rules recommended by Werner (2002): maintain minimum main beam width of t + 50 mm, maintain minimum main beam width of t + 100 mm for RDC on both sides of the beam, maintain minimum 600 mm distance between two joist connecting to one main beam, and maintain minimum 500 mm end distance between RDC and main beam end.

9.6. Conclusions

RDC are a viable connection concept that can be successfully applied in heavy timber construction in North America given appropriate design guidelines. The experimental and numerical research reported provides a database that has been used to develop a design equation that takes into account the known and experimentally observed size effect in timber. More work based on a reliability based performance criterion is needed to achieve a generally applicable design method that can be applied to different types of wood-to-wood connections.

9.7. References

Bamford, S. (2003). The effects of advanced wood processing technologies on contemporary timber design. BSc graduating essay, The University of British Columbia, Vancouver, Canada.

Bobacz, D. (2002). In CNC-Technik gefertigte zimmermannsmäßige Verbindungsmittel - Untersuchung des Schwalbenschwanzzapfens (in German). Diploma thesis, Universität für Bodenkultur, Vienna, Austria.

DIN-1052. (2004). Entwurf, Berechnung und Bemessung von Holzbauwerken - Allgemeine Bemessungsregeln und Bemessungsregeln für den Hochbau (In German). DIN Deutsches Institut für Normung e.V., Beuth Verlag GmbH, Berlin, Germany.

Gustafsson, P.J. (1988). A Study of Strength of Notched Beams. Proceedings, CIB-W18, Parksville, Canada, 21-10-1.

Hochstrate, M. (2000). Untersuchungen zum Tragverhalten von CNC gefertigten Schwalben-schwanzverbindungen (in German). Diplom thesis, FH Hildesheim, Germany.

Kreuzinger, H., and Spengler, R. (1999). Zum Tragverhalten von maschinell abgebundenen Zapfenverbindungen aus Konstruktionsvollholz zwischen Haupt- und Nebenträger (in German). Technical report LKI 7313, Technische Universität, Munich, Germany.

O'Connell, T., and Smith, P. (1999). The North American timber frame housing industry. Forest Products Journal, 49(1), 36-42.

Schmidt, R. J., and Scholl, G. F. (2000). Load Duration and Seasoning Effects on Mortise and Tenon Joints. Research report, USDA NRI/CGP Contract No. 97-35103-5053, University of Wyoming, Laramie, USA.

Snow, M., Zheng Chen, A. A., and Chui, Y. H. (2006). North American practices for connections in wood construction. Progress in Structural Engineering and Materials, 8(2), 39–48.

Tannert, T. and Lam, F. (2006). Geometry parameters of Rounded Dovetail Connections. Proceedings, 9th World Conference on Timber Engineering, Portland, USA, 3-13-4.

Tannert, T., Prion, H., and Lam, F. (2007). Structural performance of RDC under different loading conditions. Canadian Journal of Civil Engineering, 34(12), 1600-1605.

Werner, H. (2002). Queranschlüsse mit Schwalbenschwanz-Zapfenverbindungen, Vorschlag für die Bemessung (In German). Verband-High-Tech-Abbund im Zimmerhandwerk, Stuttgart, Germany.

Chapter 10: Self-tapping screws as reinforcement for Rounded Dovetail Connections [14]

10.1. Introduction

Rounded Dovetail Connections (RDC) are a relatively new method for connecting structural members (Figure 10-1 left). A number of experimental studies on the RDC provided valuable insight into their structural performance (Blass and Saal 1999; Kreuzinger and Spengler 1999; Hochstrate 2000; Bobacz 2002; Tannert and Lam 2006; Tannert et al. 2007). The load transfer mechanism in an RDC is influenced by its geometric features (Figure 10-1 right) which are flange angle (k), dovetail angle (a), dovetail height ($h_{1)}$, dovetail width (b_1), dovetail depth (t), and member height and width (h and b). RDC failure mode of the joist member under shear loading was typically brittle due to splitting of the beam similar to failure of an end notched beam support. Common methods for preventing splitting of timber members involve using reinforcements like glued-on wood panels, pressed-on metal plates, glass fibre reinforcements, glued-in steel rods or self tapping screws (Blass and Schmidt 2001). The design of RDC under shear load is governed by serviceability considerations. Depending on RDC geometry and manufacturing tolerances, the relative vertical deformation between joist and main beam member may reach values of 3 mm at loads as low as 30% of the connection capacity (Tannert and Lam 2006). One study (Blass and Saal 1999) explored the potential of improving the structural performance of RDC with reinforcements indicating possible increases of stiffness and capacity.

[14] A version of this chapter has been prepared for publication. Tannert, T., and Lam F. (2008). Self Tapping Screws as reinforcement for Rounded Dovetail Connections.

Figure 10-1: RDC application (left) and geometric parameters (right)

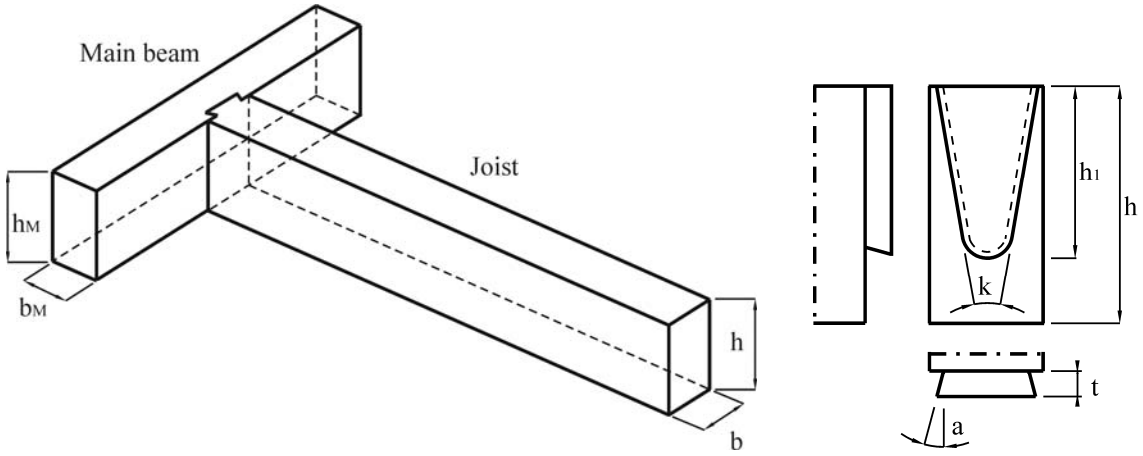

10.2. Reinforcements with self-tapping screws

The use of screws in heavy timber construction did not become popular until recently due to the limitations on the strength and available lengths of screws and code provisions that assumed that screws had no (or limited) withdrawal resistance. Modern self-tapping screws (Figure 10-2) with continuous threads have diameters up to 12 mm and lengths up to 600 mm, and they are hardened to produce a high yield moment, tensile and torsion strength. The cutting thread and surface coating are designed to avoid the need for pre-drilling thereby guaranteeing easy assembly. The continuous thread provides a mechanical connection along the embedded length, which makes them efficient for reinforcing timber prone to splitting. Self tapping screws with continuous threads present an alternative to the traditional reinforcement methods and provide new possibilities as reinforcements for numerous applications in timber structures.

Figure 10-2: Self tapping screw

Since the tensile and compressive strength of timber perpendicular to the grain is much lower than the respective strength values parallel to the grain, timber structures should be detailed minimizing stresses perpendicular to the grain (Blass and Bejtka 2004a). Examples of structural details where tension perpendicular to the grain stress occur are end notched beam supports, connections with load components perpendicular to the member axis as well as beams with holes. Beam supports are an example for a structural detail with compressive stresses perpendicular to the grain (Bejtka and Blass 2006) where self tapping screws provide an opportunity to increase capacity and stiffness.

Self-tapping screws increase the capacity of connections perpendicular to grain and produce a more ductile failure mode compared to non-reinforced members. To increase connection stiffness, screws can be placed at an angle to the interface between the connected members (Blass and Bejtka 2001). Self-tapping screws have also been shown to prevent curved glued laminated beams from splitting along the grain in tension perpendicular to grain (Jönsson 2005).

When RDC performance is governed by the joist member, capacity can be estimated similar to the capacity of end notched beam supports. For end notched beam supports reinforced with self-tapping screws, the load component perpendicular to the grain is entirely transmitted by tensile forces in the screws and the tension perpendicular to the grain strength of the timber is not

taken into account (Blass and Bejtka 2001). Consequently, screw withdrawal capacity ($R_{ax,k}$) and tensile strength ($R_{u,k}$) dictate the capacity (V_k) of a beam support according to Equation 10-1 (DIN-1052 2004):

$$V_k = \frac{n * \min(R_{ax,k}, R_{u,k})}{1.3 * \left[3 * (1 - h_e / h)^2 - 2 * (1 - h_e / h)^3\right]} \quad \text{Equation 10-1}$$

where h is the beam height, h_e is the beam height minus the notch height, and n is the number of screws.

Self-tapping screws can also be applied to connect joists to beams as only mean of connection. A simple truss-like model can be applied to estimate the capacity of such connections (Blass and Bejtka 2004b) using Equation 10-2 for cases with one angled screw and Equation 10-3 for connections with a pair of angled screws that cross each other:

$$V_{G/E,1,k} = \min(R_{ax,k}, R_{u,k}) * (\sin\gamma + \mu * \cos\gamma) \quad \text{Equation 10-2}$$

$$V_{G/E,2,k} = 2 * \min(R_{ax,k}, R_{u,k}) * (\sin\gamma) \quad \text{Equation 10-3}$$

where μ is the friction coefficient between the wood members. If no further information is available, μ can be assumed to be 0.25 (Blass and Bejtka 2004b).

The screw tensile strength depends on material and diameter. The withdrawal strength depends on density of the wood (ρ), the outer screw diameter (d), the minimum embedded length in the wood (l_{ef}), and the angle between the screw axis and the wood grain (γ). For angles γ between 45° and 90°, the characteristic strength $R_{ax,k}$ is a linear function of d and l_{ef} and a factor q which depends on screw type according to Equation 10-4 (DIN-1052 2004):

$$R_{ax,k} = \frac{q * \rho^2 * d * l_{ef}}{\sin^2 \gamma + \frac{4}{3} \cos^2 \gamma}$$ Equation 10-4

Screw tensile strength and withdrawal strength as well as the minimum edge and end distances and spacing between screws are regulated by product specific building code approvals.

10.3. Objective

Self-tapping screws increase the performance of structural members and details where stresses perpendicular to grain occur. The objective of this work is to use of self-tapping screws with continuous threads to improve the structural performance of RDC under vertical shear loading. Three different test series using specimens with different member sizes, joint geometry and loading conditions were evaluated by comparing the performance of non-reinforced specimens to the performance of specimens with three different reinforcement layouts.

10.4. Material

Three different series of specimens with RDC connecting a joist to a main beam were produced. The member dimensions b and h of the specimens were 90 mm x 184 mm for Series I and 124 mm x 274 mm for Series II and III, respectively. Beam and joist lengths were 500 mm and 950 mm for Series I and 500 mm and 1150 mm for Series II and III, respectively. The dovetail geometries were as follows: Series I: height h_1=109 mm, width b_1 = 50 mm, and flange angle k = 20°; Series II: h_1=189 mm, b_1 = 50 mm, k = 20°; and Series III: h_1=199 mm, b_1 = 70 mm, k = 10°. The depth t = 28 mm and angle a = 15 were constant for all test series.

Western hemlock (*Tsuga heterophylla*) was used for the study. The material for Series I was kiln-dried and then stored in dry inside climate, the material for Series II and III was air

dried. The moisture content (MC) and the apparent density (based on tested weight and volume) of each specimen were determined. Specimens for Series II and III were produced immediately before testing, while specimens of Series I were produced several month before testing. The average and standard deviation of MC and apparent density for Series I were 10.5% and 0.3%, respectively and 515 kg/m³ and 12 kg/m³, respectively. The average and standard deviation of MC and apparent density for Series II and III were 14.1% and 1.2%, respectively and 495 kg/m³ and 42 kg/m³, respectively.

Würth ASSY®-plus VG 8 mm screws with continuous threads were used to reinforce the specimens. The product specific building approval (Würth 2006) for these screws lists the tensile capacity ($R_{u,k}$) as 18.9 kN and a factor q = 0.00008 to calculate the withdrawal capacity of the screws at an angle of 90° between screw axis and grain direction (Figure 10-3 left), see Equation 10-5:

$$R_{ax,k} = 0.00008 * \rho^2 * 8 * l_{ef} \qquad \text{Equation 10-5}$$

The minimum spacing between rows of screws is $a_2 = 2.5*d$, minimum end and edge distances are $a_3 = 5*d$ and $a_4 = 4*d$, respectively. For inclined screws, the centre of gravity of the screw has to fulfill these spacing and distance requirements (Blass and Bejtka 2001 and 2004b).

The screws were installed in the timber without any pre-drilling using a pneumatic driver. The screw lengths were 280 mm for test Series I and 480 mm for Series II and III. Screws extending through the connected timbers were cut to avoid safety hazards during testing.

10.5. Experimental design

For Series I, two different reinforcement layouts were compared to non-reinforced control RDC specimens. The layouts were: (i) reinforcing the joist with one screw at a 90° angle between the screw axis and the wood grain of the joist, (ii) reinforcing both joist and main beam with one screw at a 55° angle between the screw axis and the wood grain of the joist member, similar to the configurations shown in Figure 10-3 (left and centre), but with only one screw. The experimental layout is a completely randomized design. The placement of the screws was selected to comply with minimum spacing, end and edge requirements.

For Series II and III, three different reinforcement layouts were compared to non-reinforced control specimens. These Series were reinforced with two screws and an additional layout was added: (iii) joist and main beam reinforced with screws at a 55° angle crossing each other, see Figure 10-3 (right). Pictures of reinforced specimens are shown in Appendix S. Series II and III are analyzed together as a randomized complete block design. In this type of experimental design the treatment levels (four levels: control and three reinforcement layouts) are assigned to blocks (which in the presented study are the test series) in a random manner. The test series are considered blocks because the changed specimen dimensions may influence RDC performance. This effect is not of primary interest, but by blocking the experiment, it is accounted for. A total of 52 specimens were produced and tested: eight non-reinforced specimens for Series I, 14 non-reinforced specimens for Series II and III each, and two reinforced specimens each for all reinforcement layouts.

Figure 10-3: Layouts of RDC reinforcements in series II and III

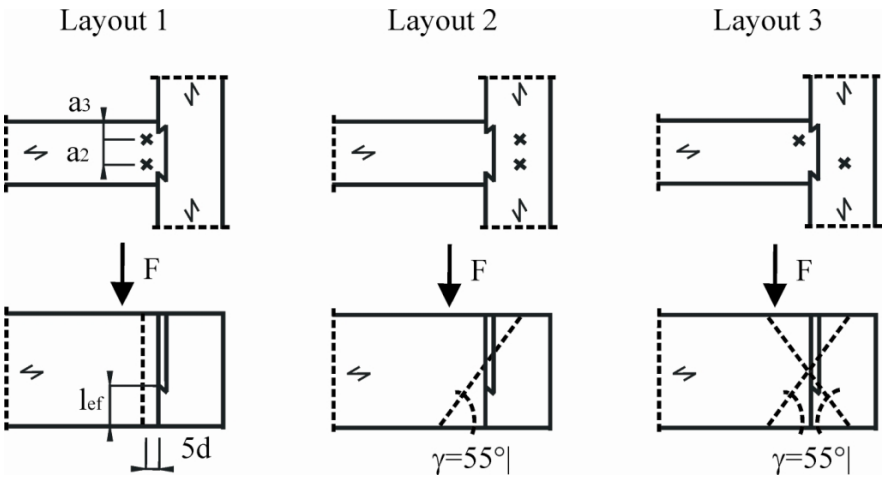

10.6. Test methods

Since the main objective was to study the connection behaviour rather than the bending strengths of the beams, a vertical shear loading mode was chosen. The test specimens were mounted in a test apparatus that supported the main beam on two 100 mm x 100 mm x 10 mm steel plates. Two timber blocks (100 mm x 100 mm) on the backside of the specimens prevented these from moving back (Figure 10-4). The main beam was allowed minor rotation about its long axis, a situation that simulates the support conditions in a real structure. For test Series I, the free end of the joist was simply supported on a 100 mm x 100 mm x 10 mm steel plate which rested on a spring with a stiffness of approximately 1 kN/mm. This test arrangement simulated the deflection of a longer (approximately 4 m) beam.

Since the expected loads for test Series II and III exceeded the capacity of the available spring, for these specimens the joist was supported on a rigid support without the spring. The load was applied at a distance of 450 mm from the joint and distributed onto the joist through a 150 mm x 150 mm x 10 mm steel plate. Because the end conditions for loaded members were

different between the test series, the presented results are comparative measures of the effects of altering reinforcement options for the chosen support configurations.

Figure 10-4: Set up for shear tests: Series I (left), Series II and III (right); all dimensions in mm

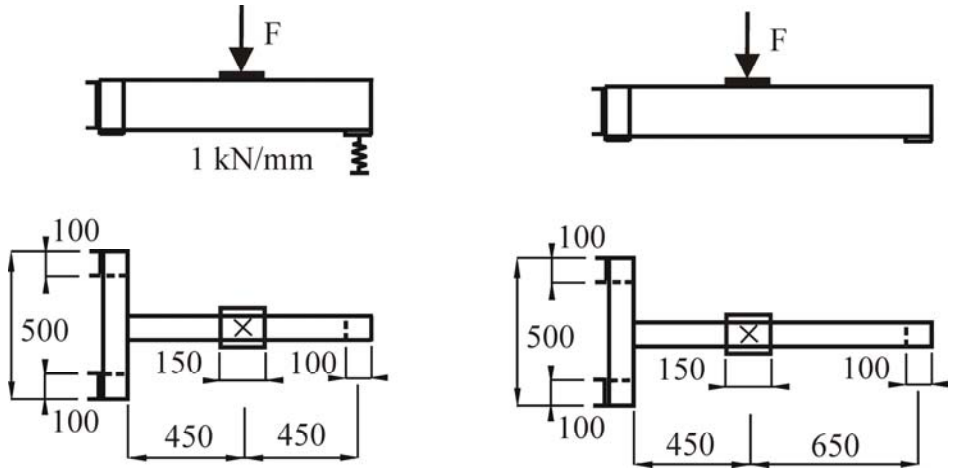

The applied load by the actuator, the relative vertical movement of the joint on both sides of the joint (as the relative displacements between main beam and joist), the deflection of the joist at the load application point, as well as the relative displacement between upper and lower edge of both sides of the joist close to the connection were recorded. The vertical joint displacement was calculated as the average of the two sides. The displacement between upper and lower edge of the joist indicated the load at which unstable crack growth initiated. A load of 2 kN was applied to close any pre-existing connection gaps, the load was reduced to zero, and then increased at a constant rate of loading to ensure that connection failure occurred after approximately six minutes, in accordance to EN-26891 (1991). After the initial test, the non-reinforced specimens with the least damage to the timber were reinforced with the screws and re-tested. The tension perpendicular to grain strength of the cracked timber is zero and only the withdrawal capacity of the screw determines the capacity for reinforced specimens.

10.7. Results

The force applied (F_{ult}) that causes unstable crack growth represents the connection capacity. Its 5th percentile can be used to determine the design load for the strength limit state. It is important to consider a deformation limit of the joint in order to prevent unacceptable non-structural damages of the surrounding structure and to determine a serviceability limit state. In this study, a 3 mm limit for the relative vertical deformation between main beam and joist was used and the load at 3 mm deformation ($F_{@3mm}$) was recorded. For specimens that failed before deforming 3 mm, the peak force applied represents the load at 3 mm deformation. The connection stiffness (k_S) was determined in accordance to EN-26891 (1991). F_{ult}, $F_{@3mm}$, k_S, as well as the deformation (d_{max}) at capacity were recorded for each specimen.

Non-reinforced RDC specimens do not show initial connection slack. In contrast to previous tests at The University of British Columbia (Tannert and Lam 2006) and similar to tests by Kreuzinger and Spengler (1999) and Bobacz (2002), an initial load was applied to press the RDC together, thereby eliminating potentially existing gaps. Variability of the load deformation response was high for Series I specimens and lower for specimens in Series II and III. The difference in variability is explained by the larger dovetail area of the latter series that make the specimens less sensitive to connection production inaccuracies. RDC capacity coincides with the maximum load applied for most specimens of Series I. Once a crack opened, crack growth became instable and the connection failed. Specimens of test Series II and II are much larger and in most specimens the load increased after splitting of the joist.

The reinforced specimens behaved differently, reinforcement led to an increase in capacity as now the screw withdrawal resistance dictates connection capacity. After reaching capacity, small increases in applied load in some test specimens were observed. The increase in capacity occurred for all reinforcement layouts. As expected, the reinforcements with screws at an angle (layouts 2 and 3) led to an increase of stiffness.

The test results are summarised in Table 10-1; the load deformation curves for all specimens are illustrated in Figure 10-5. All results of the individual test specimen are listed in Appendix T.

Table 10-1: Summary of shear test results on reinforced RDC

Test series	F_{ult} (kN)		$F_{@3mm}$ (kN)		k_S (kN/mm)		d_{max} (mm)	
	Mean	StDev	Mean	Mean	Mean	StDev	Mean	StDev
Series I - none	15.7	3.8	12.9	3.1	4.8	1.5	3.1	1.0
Series I - 90°	25.8	0.9	23.8	3.5	9.5	1.3	3.5	1.0
Series I - 55°	27.8	1.7	27.7	1.4	19.6	4.1	1.4	0.2
Series II - none	31.3	8.4	20.1	4.7	7.6	2.4	4.7	1.5
Series II - 90°	52.4	2.9	33.7	4.3	11.0	3.8	4.3	0.0
Series II - 55°	68.8	5.2	63.7	3.8	35.0	13.0	3.8	1.9
Series II - crossed	65.9	5.9	65.8	1.1	63.0	*	1.1	1.1
Series III - none	32.2	6.0	21.0	6.4	10.7	9.0	6.4	2.2
Series III – 90°	41.4	5.8	31.0	4.8	11.2	0.6	4.8	1.5
Series III – 55°	68.4	8.9	68.4	1.8	53.9	38.0	1.8	1.1
Series III - crossed	52.8	3.9	52.8	1.8	36.5	8.9	1.8	0.1

*only one results taken into consideration

Figure 10-5: Load deformation response of non-reinforced and reinforced specimens

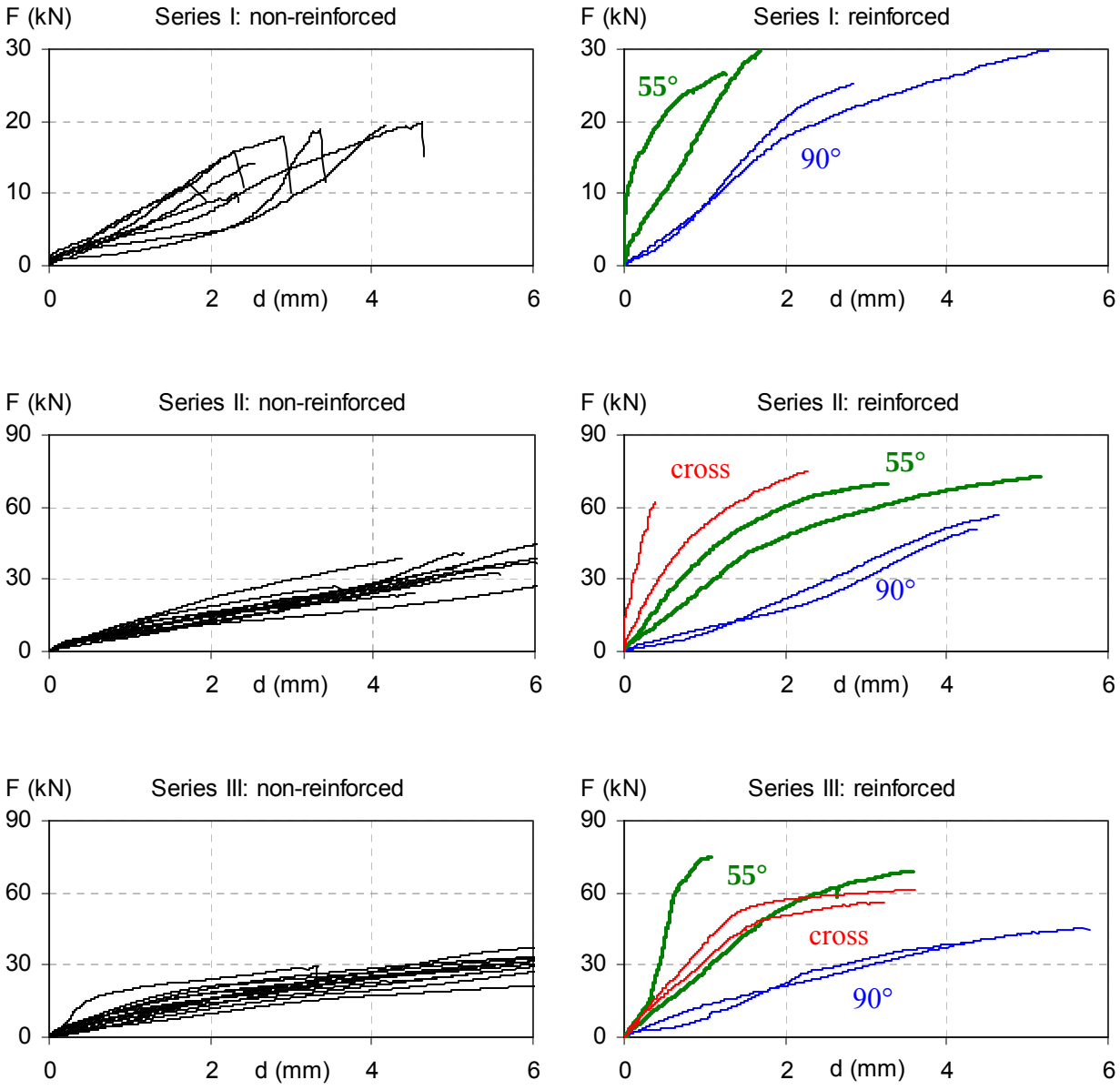

10.8. Analysis

The capacity (F_{ult}), the load at 3 mm deformation ($F_{@3mm}$), the connection stiffness (k_S), and the deformation (d_{max}) at capacity were statistically evaluated using analysis of variance (ANOVA). ANOVA can be used for comparing means when there are more than two levels of a single factor and to determine whether observed differences in means are statistically significant. A p-value is calculated and compared to α, the significance level. If the p-value is smaller than α, then the null hypothesis of no differences between means is very unlikely, and is rejected. Detailed explanations can be found in textbooks such as Montgomery and Runger (2003). Table 10-2 gives the p-values from the ANOVA that compared reinforced to non reinforced RDC.

Table 10-2: ANOVA results of shear tests on reinforced RDC

Tested variable	p-value Series I	p-value Series II and III
F_{ult}	0.002	0.012
$F_{@3mm}$	<0.001	0.005
k_S	<0.001	0.047
d_{max}	0.082	0.078

Reinforcement has a statistically significant effect ($\alpha = 0.05$) on connection capacity, the load at 3 mm deformation, and the connection stiffness but not on the deformation reached at capacity. Multiple comparison tests (Bonferroni at a level $\alpha = 0.05$) were used to determine which reinforcements layouts are statistically different. In Series I, both reinforcement layouts significantly increase capacity and load at 3 mm deformation but there was no significant difference between the two reinforcement layouts. Stiffness was increased with layout 2 using angled screws. In Series II and III, all three reinforcement layouts significantly increase capacity.

In addition, there is a significant difference increase of capacity for specimens when reinforced with screws at an angle of 55° compared to those reinforced with screws at an angle of 90°. The specimens with screws at an angle of 55° and crossed to each other significantly increase the load at 3 mm deformation and stiffness compared to non-reinforced specimens and those reinforced with screws at an angle of 90°. A similar finding was observed for the connection stiffness.

10.9. Discussion

Applying a preload of approximately 2 kN closes any connection gaps and thereby eliminates the connection slip due to alignment issues observed in a previous study (Tannert and Lam 2006) where minor cutting inaccuracies led to the differences in initial alignment behaviour among the individual test specimens. The testing procedure applied in this study is more representative of the conditions in practice where construction workers and the dead loads force the connection members together during construction.

For all tested specimen sizes, the initial fracture mode is always splitting of the joist member. RDC failure is initiated either when the tension perpendicular to grain strength or the withdrawal capacity of the screw is exceeded. Regardless of the reinforcement layout, connection capacity was increased compared to the non-reinforced specimens. The largest reinforcing effect was achieved when screws were oriented at an angle of 55°. In this case, the capacity was increased by 50% for Series I and more than 100% for Series II and III. The specimens in Series II and III exhibit high remaining load carrying capacity after initial RDC failure provided by the remaining withdrawal resistance of the screws. Since Series II and III

were reinforced with 2 longer screws, this resistance is higher than in Series I where one short screw was used.

Equation 10-1 was used to estimate the connection capacity of specimens reinforced with screws at an angle of 90°. Predicted capacities were significantly higher than those experimentally observed (Table 10-3). In contrast to notched beam supports, using the ratio of dovetail height to beam height (h_1/h) does not allow good agreement with test results. Substituting this ratio with a ratio of dovetail section area to member section area (A_1/A), Equation 10-1 yields conservative results where approximately 50% of the specimens had a capacity that was more than 2 times the calculated capacity.

Table 10-3: Comparison of experimentally observed capacity (F_{ult}) and estimated values (V_k) for RDC reinforced with screws at 90°

Test series	F_{ult} (kN)	h_1/h	A_1/A	$V_k=f(h_1/h)$	$V_k=f(A_1/A)$
Series I - 90°	25.8	0.59	0.31	23.7	11.1
Series II - 90°	52.4	0.69	0.27	84.3	23.6
Series III – 90°	41.4	0.73	0.29	91.9	21.2

Reinforcing the joist member with screws at an angle of 90° creates such high connection forces that the mortise support in the main beam is crushed (Figure 10-6 left). Ultimate failure still occurs when the screws reach their withdrawal capacity; however, producing dovetails with a height of 2/3 of the member height might cause main beam failure.

Equations 10-2 and 10-3 were used to estimate the connection capacity of specimens reinforced with screws at an angle of 55°. Experimentally observed capacities were up to a 100% higher than the estimated values (Table 10-4). Blass and Bejtka (2001 and 2004b) proposed that

single shear wood-to-wood connections with reinforcing screws placed under an angle to the interface between the members be designed based on a modified form of Johansen's yield theory. The load is transferred by a truss-like system where the screw is loaded in tension and the contact surface between the members is loaded in compression. Adopting this approach for RDC does not consider the interaction between direct load transfer of connected members and load transfer through shear and withdrawal capacity of the screw. The load carrying mechanism is changed; the screws are being sheared between the two connected timber members resulting in an increase of withdrawal resistance and a further increase of connection capacity of approximately 50%.

Table 10-4: Comparison of experimentally observed capacity (F_{ult}) and estimated values (V_k) for RDC reinforced with screws at 55°

Test series	F_{ult} (kN)	$V_{E,G,k}$ (kN)
Series I – 55°	27.8	9.7
Series II – 55°	68.8	43.5
Series II – crossed	65.9	37.0
Series II – 55°	68.4	38.1
Series III – crossed°	52.8	32.4

The current design equations cannot be easily modified to estimate the capacity of RDC reinforced with screws that penetrate both the joist and the main beam member. The development of a new mechanical model based on analytical considerations that take into account the very complex interactions among geometric parameters of RDC and screw placement within RDC could yield an appropriate design equation.

The reinforcement layout with screws at a 55° angle crossing each other where one screw reinforces the main beam mortise base was intended to increase the compression perpendicular to grain resistance at the mortise base. The structural performance however was not improved compared to reinforcement with the parallel screws at an angle of 55°.

Reinforcing only the joist with screws at an angle of 90° does not increase stiffness. The higher load at 3 mm deformation in Series I occurs because most specimens fail before reaching the deformation limit of 3 mm. Reinforcing both connected timber members with screws at an angle of 55° leads to a significant increase in stiffness, and a corresponding significant increase in load at 3 mm deformation. The relative vertical deformation between joist and main beam at failure is small (Figure 10-6 centre). The reinforcement layout with screws at a 55° angle crossing each other did not affect the failure mode (Figure 10-6 right) and did not improve structural performance when compared to the parallel screws at an angle of 55°.

Figure 10-6: Typical failure modes of reinforced RDC: 90° (left), 55° (centre), crossed (right)

10.10. Conclusions

This study demonstrates that the structural performance of Rounded Dovetail Connection can be improved significantly by using self-tapping screws with continuous threads to reinforce the connection. Reinforcing RDC with screws is a simple and economic method to increase the capacity and stiffness of connections where the timber is prone to splitting.

The capacity of RDC connections reinforcing only in the joist member can be estimated using a modified design equation given for reinforced notched beam supports as long as premature main beam failure is avoided. The load at 3 mm deformation and in consequence stiffness can be significantly improved by using self-tapping screws that reinforce both joist and main beam. Future work studying the contribution of the screws and the wood-to-wood connection in the load bearing process can optimize geometric design and reinforcement layout.

The study also showed that RDC capacity does not increase in proportion to dovetail area. Any failure criterion that estimates RDC capacity must consider size effects in tension perpendicular to grain strength. Furthermore, the experiments on non-reinforced specimens indicated that an increase in dovetail flange angle leads to increased shear capacity.

Given the scope of the presented work, the authors cannot comment on whether self-tapping screws with continuous threads improve the structural performance of RDC to resist seismic or long term loads. The authors recommend further studies of RDC reinforced with self-tapping screws subjected to reverse loading as occurs in seismic loading conditions. Additional research is also required to develop a design equation for predicting connection capacity when screws are placed at an angle to reinforce both joist and main beam.

10.11. References

Bejtka, I., and Blass, H. J. (2006). Self-tapping screws as reinforcements in beam supports. Proceedings, CIB-W18, Florence, Italy, 39-7-2.

Blass, H. J., and Bejtka, I. (2001). Screws with continuous threads in timber connections. Proceedings, RILEM Symposium on Joints in Timber Structures, Stuttgart, Germany, 193-201.

Blass, H. J., and Bejtka, I. (2004a). Reinforcements perpendicular to the grain using self-tapping screws. Proceedings, 8th World Conference on Timber Engineering, Lahti, Finland, Vol.I, 233-238.

Blass, H. J., and Bejtka, I. (2004b). Selbstbohrende Holzschrauben und ihre Anwendungsmöglichkeiten (in German). In: Holzbau Kalender 2004, Bruderverlag Karlsruhe. ISBN 3-87104-136-X.

Blass, H. J., and Saal, H. (1999). Orientierende Tragfähigkeitsversuche an Haupt-Nebenträgeranschlüssen mit schwalbenschwanzähnlicher Zapfenverbinding sowie SFS-Holzschrauben (in German). Test report No. 996107, Universität Karlsruhe, Germany.

Blass, H. J., and Schmidt, M. (2001). Self-tapping Screws as Reinforcement Perpendicular to the Grain in Timber Connections. Proceedings, RILEM Symposium on Joints in Timber Structures, Stuttgart, Germany, 163-172.

Bobacz, D. (2002). In CNC-Technik gefertigte zimmermannsmäßige Verbindungsmittel - Untersuchung des Schwalbenschwanzzapfens (in German). Diploma thesis, Universität für Bodenkultur, Vienna, Austria.

DIN-1052. (2004). Entwurf, Berechnung und Bemessung von Holzbauwerken - Allgemeine Bemessungsregeln und Bemessungsregeln für den Hochbau (In German). DIN Deutsches Institut für Normung e.V., Beuth Verlag GmbH, Berlin, Germany.

EN-26891. (1991). Timber structures, Joints made with mechanical fasteners, General principles for the determination of strength and deformation characteristics. DIN Deutsches Institut für Normung e.V., Beuth Verlag GmbH, Berlin, Germany.

Hochstrate, M. (2000). Untersuchungen zum Tragverhalten von CNC gefertigten Schwalben-schwanzverbindungen (in German). Diplom thesis, FH Hildesheim, Germany.

Jönsson, J. (2005). Load carrying capacity of curved glulam beams reinforced with self-tapping screws. Holz als Roh- und Werkstoff, 63(5), 342-346.

Kreuzinger, H., and Spengler, R. (1999). Zum Tragverhalten von maschinell abgebundenen Zapfenverbindungen aus Konstruktionsvollholz zwischen Haupt- und Nebenträger (in German). Technical report LKI 7313, Technische Universität, Munich, Germany.

Montgomery, D.C. and Runger, G.C. 2003. Applied Statistics and Probability for Engineers, Third edition. John Wiley & Sons Inc. ISBN 0-471-20454-4.

Tannert, T. and Lam, F. (2006). Geometry parameters of Rounded Dovetail Connections. Proceedings, 9th World Conference on Timber Engineering, Portland, USA, 3-13-4.

Tannert, T., Prion, H., and Lam, F. (2007). Structural performance of RDC under different loading conditions. Canadian Journal of Civil Engineering, 34(12), 1600-1605.

Würth. (2006). Würth ASSY VG plus Vollgewindeschrauben als Holzverbindungsmittel. Allgemeine baufsichtliche Zulassung Z-9.1-614. <http://www.wuert.de> (October, 2007).

Chapter 11: Discussion and conclusions

11.1. Summary of work

The objective of this research was to experimentally and numerically study the structural performance of Rounded Dovetail Connections (RDC) with the motivation to develop information to support the expansion of existing design codes to provide rationale design criteria for the acceptance and use of RDC in timber construction.

Different configurations of the wooden dovetail have been extensively used throughout Europe and Asia, with their fabrication primarily governed by practical considerations such as carpenters skills and available tools. Modern CNC timber processing machinery has changed these constraints to the extent that almost any desired geometry is now possible. One shape of interest was the Double Rounded Dovetail Connection (DRDC) that was developed at UBC. Preliminary tests on DRDC indicated that a less brittle failure mode and increased capacity may be achieved compared to the single RDC configuration.

Kiln dried western hemlock (*Tsuga heterophylla*) was primarily used as a material for the research. Naturally grown 90-year-old western hemlock stands represent much of the emerging timber supply in the British Columbia coastal forest and have traditionally been a prime export material for the Japanese post and beam construction market. Due to a decline of market share for traditional applications, new applications for western hemlock have to be found. The market for value-added building components in residential and non-residential wood construction in North America and Japan is a promising opportunity.

The structural performance of RDC was studied with an extensive experimental test programme covering different materials, different loading conditions and studying the influence of geometric and manufacturing parameters. Almost 200 specimens with RDC were tested, representing by far the largest test programme ever conducted on this type of connection.

The structural performance of RDC can be quantified by the connection capacity and load-deformation response. It is important to consider a limit for the relative vertical joint deformation in order to prevent unacceptable non-structural damage of the surrounding structure. Throughout the thesis, a 3 mm limit was used to determine the load at 3 mm deformation under shear loading. The relative vertical joint deformation reached at capacity was also recorded in order to give an understanding of the connection behaviour. Analysis of Variance was used to determine whether observed differences in means are statistically significant.

RDC are mainly used to transfer shear, but its geometry enables it to also resist other loading conditions. The structural performance of RDC under shear, tension, and bending along both the strong and the weak axis of the joist was evaluated. Under vertical shear RDC show linear elastic behaviour until they reach a load corresponding to crack development. It was demonstrated that RDC also have considerable tension and bending resistance. The RDC configuration provided higher tension capacity, while the performance was not significantly different from the DRDC configuration under other loading conditions.

Dovetail configurations with varying dovetail flange angle and dovetail height were tested under vertical static shear loading. Dovetail flange angle and dovetail height were shown to affect the structural performance of RDC.

The relation between the structural performance of RDC and material properties of the wood used for the connections was studied. A regression analysis was carried out considering moisture content and apparent density of joist and main beam, as well as growth ring density and growth ring orientation of the joist member as covariates and it was shown that it is impractical to determine a set of empirical equations to describe the relation between these factors and structural performance of RDC. Then the shear parallel to grain and tension perpendicular to grain strength of small clear specimens are related to RDC capacity. Results show that these small clear specimen strength values are not good predictor of RDC capacity.

Different climatic conditions and manufacturing tolerances were studied. It was found that RDC manufactured and tested with low and constant moisture content outperformed RDC evaluated under other climatic conditions. It was also determined that the joints produced at low speed and without a gap between the connecting members have better structural performance than those produced at higher speed and with a gap.

The performance of TimberStrand® Laminated Strand Lumber (LSL), a structural composite lumber product was studied. Test results showed that LSL specimens have higher capacity compared to western hemlock specimens. RDC load at 3 mm deformation in hemlock is higher than in LSL, while the opposite is true for DRDC. LSL specimens failed under larger deformations than hemlock, and DRDC failed under larger deformations for both materials.

Relying solely on experimental testing to obtain reliable data on the structural performance of RDC is very expensive. Due to the wide variability of material properties and the various possible connection designs, a large number of test repetitions are necessary to obtain reliable results.

A more effective approach is to combine experiments with structural performance modeling using the Finite Element Method (FEM). Tests are needed to define physical material properties and for model verification. The verified model can then be used to estimate the distribution of stresses and strains across the member while boundary conditions and material properties can be considered as variable input parameters. The verified FEM model helps to better understand the load-displacement behaviour and failure modes of RDC.

A FEM model for RDC was presented that includes geometrical parameters, such as the dimensions of the wooden members and the connection between them; physical parameters, such as mechanical properties of the wood and the applied boundary conditions and external loads; and internal parameters such as type and number of elements. The model was validated with experimental tests and good agreement was observed between the model and experimental load deformation curves. Therefore the model was suitable for developing a failure criterion for RDC.

For the development of engineering design rules, one of the most valuable benefits of experimental tests combined with FEM analysis is the insight gained about the complex 3-D distribution of stresses in the connection region. Comparing the magnitude of the stresses with the respective material strengths, the critical stress combination that impact RDC performance were found to be tension perpendicular to the grain stresses in vertical and horizontal direction and the longitudinal shear and the rolling shear stresses. It was thus decided to select these three stresses for the development of a stress based failure criterion for RDC.

A size effect failure criterion for the analysis of RDC was developed that compares computed stress volume integrals to stress thresholds. The size effect in timber strength is incorporated by computing stress integrals for a failure relevant volume and by using

experimentally determined shape parameters for the stress distributions. The failure criterion has immediate application for the design of RDC. It was used to estimate the capacity of untested RDC dimensions and connection geometries which were then validated experimentally.

Based on the failure criterion, a design equation of RDC was proposed. The guideline has immediate application for the design of RDC. It can be used to design RDC and predict their capacity. The proposed design guideline is suitable for a variety of applications in residential and non-residential timber structures and provides the engineering community with a new tool.

Finally, the use of self tapping screws as reinforcement to improve the structural performance of RDC under vertical shear loading was studied and it was demonstrated that self tapping screws significantly improve the structural performance of RDC.

11.2. Significance of work

The research is a major contribution to the knowledge of the structural performance of Rounded Dovetail Connections. The research is original because it combined a wide scope of experimental and numerical studies. The research provides information regarding a variety of factors, including the geometric and manufacturing parameters that affect the structural performance of RDC. The FEM model was successfully applied to study various parameters, including the effect of loading and support conditions on the capacity of RDC.

On of the major conclusions of the research is that the structural performance of RDC depends crucially on the load transfer between the connected members. Tight contact between these has to be guaranteed which implies that the timber should be processed at a moisture content that is similar to the equilibrium moisture content during use.

The three golden rules[15] of timber framing are valid for RDC and should always be followed: (I) The geometry of the joint should have mating surfaces that allow all structural loads to be transferred in bearing of one member against the other; (II) The wood removed to create the joint should not unduly weaken the member; and (III) The geometry of the joint should not be altered by shrinkage of the wood and bearing surfaces should remain in tight contact.

This research describes the structural performance of a rather complex connection using mathematics in engineering. The quotes by W.C. Foster[16] "A few engineers have advocated the use of mathematics in the design of trestles, but as wood is an article whose strength and properties vary rather widely with each piece, no dependency whatever can be placed on the results, and such practice is to be condemned." and A.R. Dykes[17] "Engineering is the art of modelling materials we do not wholly understand, into shapes we cannot precisely analyse, so as to withstand forces we cannot properly assess, in such a way that the public has no reason to suspect the extent of our ignorance." come to mind when evaluating such an endeavour.

While this work does not pretend to wholly understand the material used for RDC, it was successful in precisely analysing the shape of RDC and reduces the extent of ignorance regarding the shortcomings in the modelling and design approach. The work advocates the use of mathematics in the design of RDC, recognizing that wood is a material whose strength and properties vary rather widely with each piece, but accounts for this variation with proper statistical analysis and a strong base of experimental results.

---

[15] Brungraber, B. Timber Framer Guild.

[16] Dykes. A.R. British Institution of Structural Engineers.

[17] Foster, W.C. 1891. A Treatise on Wooden Trestle Bridges. Wiley.

11.3. Recommendations for future work

While the existing knowledge gap regarding the structural performance of RDC has been decreased, there is still work to be done to fully understand this complex connection. Most notably given the scope of the presented work, no comment on whether RDC are appropriate to resist seismic loads under reverse loading conditions or on the performance under long-term loading can be made. Future work should try to establish the performance under reverse and long-term loading and the process of creep during concurrent moisture changes.

The effect of beam pockets has to be considered and should be studied to make reliable statements on the effect RDC on the strength and stiffness of the main beam. Further experimental studies should also include joist to post connections and angled beam to rafter connections used in different structural applications. Geometric design of the connection depending on main beam and joist dimensions, and loading and support conditions can be further optimized by using the geometric parameters as input in a probabilistic design FEM model.

The FEM model developed in this work describes the brittle failure of the joist member. The model can be extended to include the nonlinear material behaviour under compression to better account for the mechanisms that have been reported in the literature for main beam failure. This approach would also allow optimizing main beam and joist design together. The presented model and failure criterion can be applied to model the structural performance and estimate the capacity of RDC under other loading conditions. The model and the failure criterion can also be applied to other carpentry type wood-to-wood connections.

The determination of unit volume strength values under combined stress conditions is a field for additional investigation. Brittle RDC failure is caused by a combination of tension

perpendicular to grain and shear parallel to grain stresses, but currently there is no standardised test specimen available for determining strength under such a combined stress state.

Alternatively to the chosen approach, a fracture mechanics approach can be chosen to analyse failure and capacity of RDC. Since linear elastic fracture mechanics analysis of wood only works well in situations where the stress intensity region adjacent to the notch is small compared to general dimensions of the member, it will have to be studied whether a non linear fracture mechanics approach works better.

The use of reinforcing in carpentry type wood-to-wood connections in the timber frame industry should be evaluated for different types of reinforcements to increase connection capacity and more importantly increase stiffness and decrease potentially existing connection alignment behaviour due to manufacturing tolerances or shrinkage caused by changes of moisture content. Regarding reinforcements with self tapping screws, the presented FEM model can be extended using a nonlinear spring to account for the screws.

RDC are a viable connection concept that given appropriate design guidelines can be successfully applied in timber construction. The experimental and numerical research provides a database that allows adjusting existing design recommendations taking into account the known and experimentally observed size effect in timber.

As part of future research, a reliability analysis of RDC is proposed recognizing that failures cannot be completely avoided, rather that designs can be obtained with a tolerable probability of failure, or risk that the design might not perform as intended. More work based on a reliability based performance analysis is needed to achieve a generally applicable method that can also be applied to different types of wood-to-wood connections.

Appendices

Appendix A: Discussion of failure criteria

Isotropic failure criteria

Isotropic failure criteria are not directly applicable to orthotropic materials, however, they provide a basis to improve understanding on material failure processes. Four groups of failure theories for isotropic material can be distinguished: I) maximum shear stress theory (Tresca) – yielding of ductile materials depends only on shear stress and stress states outside the failure surface lead to non-elastic behaviour; II) maximum distortional energy theory (von Mises) – failure occurs when the total strain energy at a point reaches a limit; III) maximum principal stress theory – failure of a material occurs when the maximum principal stress reaches a limit; and IV) maximum strain theory – failure of a material occurs when the normal strain at a point reaches a limit.

Classic composite failure criteria are based on the maximum distortional energy theory. In von Mises' theory, it is assumed that the strain energy caused by hydrostatic pressure does not contribute to the yielding of the material. However, this assumption is not valid for wood. In plane stress state, the von Mises invariant criterion can be written according to Equation A-1:

$$\left(\frac{\sigma_X}{f_X}\right)^2 - \left(\frac{\sigma_X \sigma_Y}{f_X f_Y}\right) + \left(\frac{\sigma_Y}{f_Y}\right)^2 + 3\left(\frac{\tau_{XY}}{f_{XY}}\right)^2 = 1 \qquad \text{Equation A-1}$$

where σ_X and σ_Y are the normal stresses in X and Y direction, τ_{XY} is the shear stress in the XY plane, f_X and f_Y are on-axis normal strengths (compression or tension) and f_{XY} is on-axis shear strength..

Linear and quadratic maximum stress failure criteria

A general maximum stress criterion for plane stress can be stated in following form:

$$\left(\frac{\sigma_X}{f_X}\right)^a + \left(\frac{\sigma_Y}{f_Y}\right)^b + \left(\frac{\tau_{XY}}{f_{XY}}\right)^c = 1 \qquad \text{Equation A-2}$$

Depending on the parameters a, b and c, various interaction criteria can be postulated. The simplest criterion for a biaxial stress state is linear with a = b = c = 1. For an off-axis stress state, rotated by an angle α to the on-axis system, stresses σ_X, σ_Y and τ_{XY} are replaced by transformed stresses σ_1, σ_2 and τ_{12} according to known transformations (Bodig and Jayne 1982). For uni-axial loading, the linear interaction criterion reads:

$$f_\alpha = \frac{f_X}{f_X/f_Y \sin^2\alpha + \cos^2\alpha + f_X/f_{XY} \cos\alpha \sin\alpha} \qquad \text{Equation A-3}$$

If the shear term is omitted, the denominator in Equation A-3 reduces to the Hankinson formula. Hankinson (1921) fitted experimental data of spruce under uni-axial compressive loading at a grain angle. The criterion is widely accepted and employed in design codes for off-axis loading of solid wood and glulam. For these materials omitting the shear term proved to be a reasonable approximation for off-axis tension strength (Aicher and Klöck 2001). The quadratic strength criterion (a = b = c = 2) results in an ellipsoidal strength envelope. While the extreme values of the linear criterion are always between angles of 0° and 90°, they may also be located at the boundaries of the angle range using the quadratic criterion, a fact that strongly increases flexibility for approximation of experimental data.

Norris failure criterion

Norris (1962) proposed a 3D failure criterion for wood using three expressions:

$$\left(\frac{\sigma_X}{f_X}\right)^2 - \left(\frac{\sigma_X \sigma_Y}{f_X f_Y}\right) + \left(\frac{\sigma_Y}{f_Y}\right)^2 + \left(\frac{\tau_{XY}}{f_{XY}}\right)^2 = 1$$

$$\left(\frac{\sigma_Y}{f_Y}\right)^2 - \left(\frac{\sigma_Y \sigma_Z}{f_Y f_Z}\right) + \left(\frac{\sigma_Z}{f_Z}\right)^2 + \left(\frac{\tau_{YZ}}{f_{YZ}}\right)^2 = 1 \qquad \text{Equation A-4}$$

$$\left(\frac{\sigma_Z}{f_Z}\right)^2 - \left(\frac{\sigma_Z \sigma_X}{f_Z f_X}\right) + \left(\frac{\sigma_X}{f_X}\right)^2 + \left(\frac{\tau_{ZX}}{f_{ZX}}\right)^2 = 1$$

where $\sigma_X, \sigma_Y, \sigma_Z, \tau_{XY}, \tau_{XZ}, \tau_{ZX}$ are the stresses in the X,Y,Z directions and XY, XZ, YZ planes, and $f_X, f_Y, f_Z, f_{XY}, f_{XZ}, f_{ZX}$ are the corresponding material strength parameters, with f_X, f_Y, f_Z being different for tension and compression. Each of the equations represents an ellipsoid and any condition of stress is represented by a point in the space enclosed by these ellipsoids. As long as the point lies within the volume common to the ellipsoids, the material will not fail.

Tsai-Azzi failure criterion

Tsai and Azzi (1965) discuss a general anisotropic theory of following form:

$$D_1(\sigma_Y - \sigma_Z)^2 + D_2(\sigma_Z - \sigma_X)^2 + D_3(\sigma_X - \sigma_Y)^2 + D_4\tau_{YZ}^2 + D_5\tau_{ZX}^2 + D_6\tau_{XY}^2 = 1$$

where

$D_1 = \tfrac{1}{2}\left[(f_Y)^{-2} + (f_Z)^{-2} - (f_X)^{-2}\right]$ $D_{2,3}$ by permutations of X, Y, Z Equation A-5

$D_4 = (f_{YZ})^{-2}$ $D_{5,6}$ by permutations of X, Y, Z

Hoffmann failure criterion

Hoffmann (1967) proposed a modified phenomenological fracture criterion for orthotropic brittle materials accounting for widely differing compressive and tensile strengths in various directions by adding linear stress terms:

$$C_1(\sigma_Y - \sigma_Z)^2 + C_2(\sigma_Z - \sigma_X)^2 + C_3(\sigma_X - \sigma_Y)^2$$

$$+ C_4\sigma_X + C_5\sigma_Y + C_6\sigma_Z + C_7\tau_{XY}^2 + C_8\tau_{YZ}^2 + C_9\tau_{ZX}^2 = 1$$

where

Equation A-6

$C_1 = \frac{1}{2}\left[(f_{T,Y}f_{C,Y})^{-1} + (f_{T,Z}f_{C,Z})^{-1} - (f_{T,X}f_{C,X})^{-1}\right]$ $C_{2,3}$ by permutations of X, Y, Z

$C_4 = (f_{T,X})^{-1} - (f_{C,X})^{-1}$ $C_{5,6}$ by permutations of X, Y, Z

$C_7 = (f_{YZ})^{-2}$ $C_{8,9}$ by permutations of X, Y, Z

where f_T and f_C are tension and compression strength, respectively.

Tsai-Wu failure criterion

Tsai and Wu (1971) developed a tensor polynomial failure theory that considers all possible interaction among stresses and creates a closed failure surface in the stress space. Although the polynomial expansion is proposed to be limited to linear and quadratic terms, the criterion includes a coupling term between normal strengths and allows mixed positive and negative signs. The failure criterion in index notation reads:

$$F_{ij}\,\sigma_i\,\sigma_j + F_i\,\sigma_i = 1$$ Equation A-7

where the F terms are strength parameters. For transverse isotropic materials in a 3D stress state, the criterion can be expanded in its quadratic form to:

$$F_1\sigma_1 + F_2\sigma_2 + F_2\sigma_3 + F_{11}\sigma_1^2 + F_{22}\sigma_2^2 + F_{22}\sigma_3^2 + F_{44}\sigma_4^2 + F_{55}\sigma_5^2 + F_{55}\sigma_6^2$$

$$+ F_{12}\sigma_1\sigma_2 + F_{12}\sigma_1\sigma_3 + F_{23}\sigma_2\sigma_3 = 1$$

Equation A-8

where

$$F_1 = \frac{1}{f_{II,t}} - \frac{1}{f_{II,c}} \quad F_2 = \frac{1}{f_{\perp,t}} - \frac{1}{f_{\perp,c}} \quad F_{11} = \frac{1}{f_{II,t} f_{II,c}} \quad F_{22} = \frac{1}{f_{\perp,t} f_{\perp,c}}$$

$$F_{44} = \frac{1}{f_{II}^2} \quad F_{55} = \frac{1}{f_{\perp}^2} \quad F_{12} \le \sqrt{F_{11}F_{22}} \quad F_{23} \cong F_{22} - \tfrac{1}{2}F_{44}$$

The criterion is invariant to coordinate transformation as proven by Bower and Koedam (1997) and is valid for any anisotropic material. The quadratic form is widely accepted, although some studies argue that removing higher-order terms reduces accuracy (Tennyson et al. 1978). Labossiere and Neale (1987) improved the experimental-theoretical correlation by modifying the method to calculate the strength parameters. Tsai and Wu (1971) assumed the interaction terms to be independent; therefore these cannot be expressed as a function of uni-axial strengths. The interactions can be defined in several ways (Wu 1972). In general, experiments at various stress combinations and levels varying over a range of grain angles are carried out. The fact that the failure results strongly depend on testing procedure complicates the study of the failure process. Liu (1984) determined the interaction term from the Hankinson formula. Williams et al. (2000) omitted all interaction terms, stating that such simplification yielded adequate results. Cowin (1979) determined the dependence of the strength in a direction inclined at angle to direction on the strength in principal axes and proved that it was possible to derive the Hankinson formula from the Tsai-Wu theory.

Ashkenazi failure criterion

Galicki and Czech (2005) discuss the failure criterion in tensor notation proposed by Ashkenazi and Ganov (1972):

$$\left(a_{ijkl}\,\sigma_{ij}\,\sigma_{kl}\right)^2 - \tfrac{1}{2}\left[\left(\sigma_{ii}\,\delta_{ij}\right)^2 + \sigma_{ij}\,\sigma_{ij}\right] = 0 \qquad \text{Equation A-9}$$

where a_{ijkl} are the components of the strength tensor, δ_{ij} is the Kronecker-delta, and the stress tensor components σ_{ij} can be determined by following equations:

$$a_{iiii} = \frac{1}{f_i},\quad \left(a_{ijij} + a_{ijji} + a_{jiij} + a_{jiji}\right) = \frac{1}{t_{ji}},$$
$$\left(a_{iijj} + a_{jjii}\right) = \frac{4}{f_{ij}^{45}} - \frac{1}{f_i} - \frac{1}{f_j} - \frac{1}{f_{ij}} = \frac{1}{f_i} + \frac{1}{f_j} - \frac{1}{t_{ij}^{45}} = \frac{\sqrt{3}}{r_{ij}} - \frac{1}{f_i} - \frac{1}{f_j}, \qquad \text{Equation A-10}$$

where f_i are the normal strength along the direction i, $f^{45}{}_{ij}$ are the 45° normal strength in the i-j plane, t_{ij} are the shear strength corresponding to the shear stresses acting in direction j in a plane whose normal is i, $t^{45}{}_{ij}$ are the shear strength corresponding to the shear stresses acting parallel with the i–j plane whose normal is the bisector of the angle between j and j, and r_{ij} are the strength values corresponding to the normal stresses of equal magnitude acting along the axis i and j. Szalai (1994) studied various strength theories applicable to wood and concluded that the Ashkenazi criterion represented the best fit to experimental data. The failure surface is of fourth degree which enables it to represent concave portions when viewed from the outside. The drawback of the criterion is that 24 engineering strength parameters are necessary. The Ashkenazi criterion is virtually unknown in the English literature and it is not used widely.

Hashin failure criterion

Hashin (1980) argued that a general criterion for unidirectional fibre composites should distinguish among the various different failure modes and model each mode separately. Equation A-11 shows the criteria for transversely isotropic material failure of: a) matrix tensile mode, b) tensile fibre mode, c) compressive fibre mode, and d) compressive matrix mode:

a) $$\frac{(\sigma_Y + \sigma_Z)^2}{(f_{T,\perp})^2} + \frac{(\tau_{YZ}^2 - \sigma_Y \sigma_Z)}{(f_{S,\perp})^2} + \frac{(\tau_{XY}^2 + \tau_{ZX}^2)}{(f_{S,II})^2} = 1$$

b) $$\frac{(\sigma_X)^2}{(f_{T,II})^2} + \frac{(\tau_{XY}^2 + \tau_{ZX}^2)}{(f_{S,II})^2} = 1 \quad \text{and} \quad \sigma_X = f_{T,II}$$

Equation A-11

c) $$\sigma_X = f_{C,II}$$

d) $$\left[\left(\frac{f_{T,\perp}}{2f_{S,\perp}}\right)^2 - 1\right]\frac{(\sigma_Y + \sigma_Z)}{(f_{T,\perp})} + \frac{(\sigma_Y + \sigma_Z)^2}{4(f_{S,\perp})^2} + \frac{(\tau_{YZ}^2 - \sigma_Y \sigma_Z)}{(f_{S,\perp})^2} + \frac{(\tau_{XY}^2 + \tau_{ZX}^2)}{(f_{S,II})^2} = 1$$

where X is the fibre direction, $f_{T,\perp}$, $f_{T,II}$, $f_{S,\perp}$ $f_{S,II}$ are the tension and shear strengths perpendicular and parallel to grain, respectively.

Tan-Cheng failure criterion

Tan (1990) proposed to predict off-axis tensile or compressive strength t_α at an angle α in the form of a Fourier sine series. Tan and Cheng (1993) developed a more general criterion for fibrous anisotropic materials. Since the strength of a lamina should depend on the lamina angle and be symmetric with respect to this angle, the strength of an off-axis lamina may be expressed as a cosine series. The criterion has the flexibility of any desired degree of accuracy. Hankinson's empirical formula for uni-axial loading can be derived by using the first two terms. One of the

main features of this criterion (similar to Tan's) is that it does not need the shear strength of a material, which is difficult to determine experimentally. The 3D failure criterion for orthotropic materials may be expressed in the following scalar form:

$$\left(\frac{\sigma_X}{X_\phi^i}\right)^2+\left(\frac{\sigma_Y}{Y_\theta^i}\right)^2+\left(\frac{\sigma_Z}{Z_\beta^i}\right)^2-\left(\sum_m\sum_n a_{mn}\cos n\varphi\cos m\theta\right)\left(\frac{\sigma_X}{X_\phi^i}\right)\left(\frac{\sigma_Y}{Y_\theta^i}\right)$$
$$-\left(\sum_m\sum_n b_{mn}\cos n\varphi\cos m\beta\right)\left(\frac{\sigma_X}{X_\phi^i}\right)\left(\frac{\sigma_Z}{Z_\beta^i}\right)=1 \qquad \text{Equation A-12}$$
$$-\left(\sum_m\sum_n c_{mn}\cos n\theta\cos m\beta\right)\left(\frac{\sigma_Y}{Y_\theta^i}\right)\left(\frac{\sigma_Z}{Z_\beta^i}\right)$$

where X, Y and Z are the material strength at angles to the material axis. The coefficients a, b, and c may be determined by the mechanical strength parameters. The indices m and n are even numbers and correspond to the uni-axial strength of the material under different angles. Tan and Cheng proposed m, n = 0, 2, 4 and using the strength values at angles of 0º, 90º and 30º or 45º. The upper index i stands for either + or – referring to the tensile or compression strength. Due to the complex nature of the criterion it has not been applied to 3D stress cases.

References for Appendix A

Aicher, S., and Klöck, W. (2001). Linear versus quadratic failure criteria for inplane loaded wood based panels. Otto-Graf Journal, 12, 187-200.

Askhenazi, E. K., and Ganov, E. V. (1972). Anizotropia konstrukcionnych materialov - Anisotropy of Structural Materials (in Russian). Machinostroenie.

Azzi, V. D., and Tsai, S. W. (1965). Anisotropic strength of composites. Journal of Experimental Mechanics, 5(9), 283-288.

Bodig, J., Jayne, B. (1982). Mechanics of wood and wood composites. Krieger Publishing Company, New York, USA.

Bower, M. V., and Koedam, D. H. (1997). Tensor polynomial failure criterion: coefficient limits based on convexity requirements. Journal of Reinforced Plastics and Composites, 16(5), 435-459.

Cowin, S. C. (1979). On the strength anisotropy of bone and wood. Journal of Applied Mechanics, 46(4), 832–838.

Galicki, J., and Czech, M. (2005). Tensile strength of softwood in LR orthotropy plane. Mechanics of Materials, 37(6), 677–686.

Hankinson, R. L. (1921). Investigation of crushing strength of spruce at varying angles of grain. Air service Information Circular, 3(259), US Air Service, Ohio, USA.

Hashin, Z. (1980). Failure criteria for unidirectional fiber composites. Journal of Applied Mechanics, 47, 329-334.

Hoffman, O. (1967). The brittle strength of orthotropic materials. Journal of Composite Materials, 1(2), 200-207.

Labossiere, P., and Neale K, W. (1987). On the determination of the strength parameters in the tensor polynomial failure criterion. Journal of Strain Analysis, 22(3), 155-161.

Liu, J. Y. (1984). Evaluation of the tensor polynomial strength theory for wood. Journal of Composite Materials, 18(3), 216-226.

Norris, C. B. (1962). Strength of orthotropic materials subjected to combined stresses. Report No.1816, Forest Products Laboratory, Madison, USA.

Szalai, J. (1994). Anisotropic elastic and strength theories of wood and wood-based composites (in Hungarian). Hildebrand Nyomda KFT, Sopron, Hungary.

Tan, S. C. (1990). A new approach of three-dimensional strength theory for anisotropic materials. International Journal of Fracture, 45(1), 35-50.

Tan, S. C., and Cheng, S. (1993). Failure criteria for fibrous anisotropic materials. Journal of Materials in Civil Engineering, 5(2), 198-211.

Tennyson, R. C., MacDonald, D., and Nanyaro, A. P. (1978). Evaluation of the tensor polynomial failure criterion for composite materials. Journal of Composite Materials, 12(1), 63-75.

Tsai, S. W., and Wu, E. M. (1971). A general theory of strength for anisotropic materials. Journal of Composite Materials, 5(1), 58-80.

Williams, J. M., Fridley, K. J., Cofer, W. F., and Falk, R. H. (2000). Failure modeling of sawn lumber with a fastener hole. Finite Elements in Analysis and Design, 36(1), 83-98.

Wu, E. M. (1972). Optimal experimental measurements of anisotropic failure tensors. Journal of Composite Materials, 6(4), 472-487.

Appendix B: Set ups for tests under different loading conditions

Figure A-1: Pictures of test set ups for: (a) shear tests, (b) tension tests, (c) bending along strong joist axis, and (d) bending along weak joist axis

(a) 

(b) 

(c) 

(d) 

Appendix C: Test results under different loading conditions

Table A-1: Material properties and test results for individual specimens of shear and tension tests

Specimen	Material properties				Test results		
	MC (%)		Density (kg/m^3)		F_{ult} (kN)	$F_{@3mm}$ (kN)	d_{max} (mm)
	Joist	Main	Joist	Main			
RDC - S - 0	11.7	11.7	586	408	20.6	7.9	7.7
RDC - S - 1	14.0	12.2	632	395	15.4	10.0	4.4
RDC - S - 2	13.7	12.4	599	408	15.7	10.4	4.0
RDC - S - 3	16.2	15.0	453	484	9.4	9.2	2.4
RDC - S - 4	16.0	16.2	444	487	7.2	6.5	2.3
RDC - S - 5	14.7	15.6	457	487	18.2	9.1	4.9
DRDC - S - 1	15.3	10.2	543	432	16.3	6.7	6.1
DRDC - S - 2	14.4	11.4	538	439	13.4	7.2	5.0
DRDC - S - 3	15.7	12.0	457	436	10.4	8.1	4.7
DRDC - S - 4	15.9	11.3	451	450	11.7	9.4	3.9
DRDC - S - 5	13.0	11.0	551	391	18.7	13.4	4.1
RDC - T - 0	14.9	14.9	500	494	8.6	3.8	4.8
RDC - T - 1	15.9	14.7	504	529	11.0	2.4	7.5
RDC - T - 2	17.0	15.1	492	529	11.6	5.7	5.5
RDC - T - 3	16.1	16.2	500	535	10.4	1.9	6.9
RDC - T - 4	14.3	15.7	462	546	10.4	4.8	4.4
RDC - T - 5	17.2	14.8	508	494	7.8	6.7	7.6
DRDC - T - 1	17.1	18.2	534	518	8.4	8.1	4.3
DRDC - T - 2	16.8	13.7	513	439	7.7	6.7	5.0
DRDC - T - 3	15.6	16.1	458	508	7.9	7.3	3.7
DRDC - T - 4	17.2	13.7	521	429	9.3	5.0	5.3
DRDC - T - 5	18.0	19.5	525	508	8.7	5.5	6.7

Table A-2: Material properties and test results for individual specimens of bending tests

Specimen	Material properties				Test results		
	MC (%)		Density (kg/m^3)		M_{ult} (kNm)	$M_{@1°}$ (kNm)	r_{max} (°)
	Joist	Main	Joist	Main			
RDC - H - 0	16.8	14.0	479	494	0.33	0.20	2.7
RDC - H - 1	14.5	13.5	475	491	0.78	0.37	6.0
RDC - H - 2	13.9	14.2	428	487	0.82	0.31	22.1
RDC - H - 3	15.5	13.5	487	477	0.32	0.26	19.2
RDC - H - 4	13.0	14.8	449	511	0.33	0.21	19.6
RDC - H - 5	16.3	16.0	471	491	0.43	0.22	18.3
DRDC - H - 1	12.9	16.0	441	518	0.50	0.19	12.8
DRDC - H - 2	15.6	15.2	508	511	0.18	0.12	11.2
DRDC - H - 3	15.2	15.5	538	518	0.44	0.36	14.9
DRDC - H - 4	13.4	16.6	534	511	0.16	0.10	17.5
DRDC - H - 5	15.3	15.2	471	525	0.39	0.28	18.6
RDC - V - 1	15.2	17.5	424	546	0.72	0.24	6.7
RDC - V - 2	16.2	15.7	475	546	0.60	0.49	5.8
RDC - V - 3	16.1	15.0	475	549	0.59	0.44	6.7
RDC - V - 4	16.0	14.7	475	539	0.69	0.39	7.5
RDC - V - 5	17.9	13.7	513	467	0.93	0.18	8.1
DRDC - V - 1	17.8	13.7	437	446	0.75	0.35	4.6
DRDC - V - 2	15.5	16.6	471	522	0.67	0.19	5.4
DRDC - V - 3	18.7	14.8	479	432	0.73	0.34	5.7
DRDC - V - 4	18.9	15.4	391	522	0.79	0.46	7.0
DRDC - V - 5	14.5	15.6	586	498	0.69	0.40	5.7

Appendix D: Set up for shear tests

Figure A-2: Pictures of test set up for shear tests

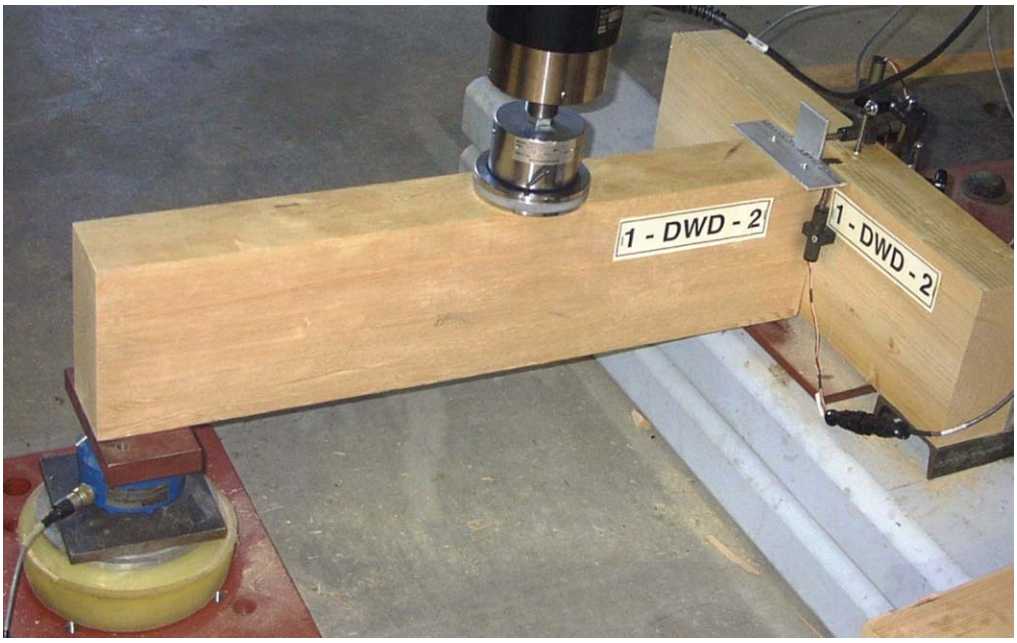

Appendix E: Specimens data and results for tests on geometry parameters

Table A-3: Material properties and test results for individual specimens

Specimen	Material properties						Test results			
	MC (%)		Density (kg/m^3)		Gr. Ring		F_{ult}	$F_{@3mm}$	d_{max}	k_S
					δ	w	(kN)	(kN)	(mm)	kN/mm
	Joist	Main	Joist	Main	(º)	No/50				
Contr.-RDC-1	11.4	12.8	463	453	80	38	23.2	20.8	5.5	5.28
Contr.-RDC-2	11.4	13.5	466	444	85	35	14.3	14.3	3.0	8.60
Contr.-RDC-3	11.8	14.3	463	453	80	34	28.0	22.5	8.0	4.34
Contr.-RDC-4	12.0	13.2	496	425	30	68	21.3	19.8	5.5	4.79
Contr.-RDC-5	11.0	13.6	540	449	75	39	18.8	18.8	3.4	5.79
Contr.-RDC-6	15.0	13.9	496	499	30	69	16.9	16.9	2.9	5.02
Contr.-RDC-7	11.0	13.5	483	499	40	58	13.6	13.6	2.8	4.51
Contr.-RDC-8	13.9	12.1	560	509	65	38	18.3	18.3	3.1	8.54
Contr.-RDC-9	14.2	11.4	553	513	75	37	14.9	14.9	3.1	4.77
Contr.-RDC-10	11.7	10.6	456	495	80	41	29.8	22.2	8.8	4.43
Contr.-DRDC-1	11.2	13.9	450	527	90	31	23.9	18.4	6.5	
Contr.-DRDC-2	11.8	16.3	470	564	80	48	27.9	19.6	6.7	
Contr.-DRDC-3	11.9	14.4	466	486	85	56	12.7	12.7	4.4	
Contr.-DRDC-4	12.0	11.0	453	578	85	65	28.7	17.5	8.7	
Contr.-DRDC-5	11.7	12.6	403	523	45	37	22.4	14.1	7.9	
Contr.-DRDC-6	11.9	15.4	400	532	40	38	18.3	10.9	7.8	
Contr.-DRDC-7	12.0	14.4	410	458	45	36	18.5	10.7	8.1	
Contr.-DRDC-8	11.8	13.8	440	449	20	33	15.6	14.8	5.2	
Contr.-DRDC-9	11.8	12.7	466	527	20	30	16.4	13.6	5.6	
Contr.-DRDC-10	10.9	12.7	456	472	15	32	15.2	14.2	5.3	
BC75-RDC-1	10.0	12.0	377	413	0	28	10.7	10.7	1.0	15.8
BC75-RDC-2	12.0	13.0	458	418	60	21	16.4	16.4	2.0	8.1
BC75-RDC-3	12.5	15.6	392	443	80	22	9.0	8.7	1.0	8.0
BC75-RDC-4	14.5	13.5	465	464	50	22	13.9	13.9	2.6	14.3

Table A-3 continued

Specimen	Material properties						Test results			
	MC (%)		Density (kg/m^3)		Gr. Ring δ	Gr. Ring w	F_{ult}	$F_{@3mm}$	d_{max}	k_S
	Joist	Main	Joist	Main	(º)	No/50	(kN)	(kN)	(mm)	kN/mm
BC75-RDC-5	13.0	12.0	406	362	70	23	12.4	12.4	2.2	6.4
BC75-DRDC-1	12.0	18.8	399	433	30	22	13.7	13.7	3.9	
BC75-DRDC-2	13.2	12.0	462	377	10	20	14.8	14.8	4.4	
BC75-DRDC-3	14.3	12.0	458	464	50	21	11.5	11.5	3.5	
BC75-DRDC-4	15.4	11.2	458	423	70	19	12.6	12.6	3.0	
BC75-DRDC-5	12.2	10.0	358	474	80	18	10.6	10.6	4.0	
BC55-RDC-1	9.5	8.0	406	527	70	49	14.4	14.4	1.7	8.4
BC55-RDC-2	12.3	15.2	583	458	90	79	37.6	33.9	7.0	12.9
BC55-RDC-3	12.5	14.6	576	462	85	68	40.0	36.4	6.6	12.4
BC55-RDC-4	12.6	14.5	490	536	80	41	18.6	18.6	2.9	6.7
BC55-RDC-5	13.0	12.5	483	467	85	38	19.1	19.1	3.6	8.6
BC55-DRDC-1	11.5	13.5	430	518	80	42	19.3	11.1	6.9	
BC55-DRDC-2	12.7	14.8	486	560	65	37	22.3	22.3	4.0	
BC55-DRDC-3	12.2	14.0	510	486	70	46	34.5	20.8	8.1	
BC55-DRDC-4	12.3	10.8	540	592	80	60	22.2	22.2	4.8	
BC55-DRDC-5	12.2	11.2	553	504	90	48	21.5	17.9	6.0	
BC45-RDC-1	12.0	12.2	533	527	70	47	19.8	19.8	3.8	6.7
BC45-RDC-2	13.4	14.7	526	444	60	50	21.0	21.0	3.5	11.4
BC45-RDC-3	11.5	15.4	473	453	80	44	27.8	22.3	7.5	6.6
BC45-RDC-4	12.9	15.6	553	541	70	81	18.2	18.2	1.9	13.8
BC45-RDC-5	13.0	14.4	563	481	85	75	27.5	27.4	3.7	11.9
BC45-DRDC-1	11.2	12.5	470	546	80	74	33.2	13.3	12.0	
BC45-DRDC-2	11.8	12.5	480	550	85	83	32.9	28.7	6.2	
BC45-DRDC-3	12.6	13.0	436	490	25	31	23.1	11.7	9.0	
BC45-DRDC-4	12.2	12.0	460	601	25	32	29.9	17.1	8.7	
BC45-DRDC-5	11.5	12.5	420	513	75	52	29.5	14.3	11.8	
A20-RDC-1	12.0	14.6	510	430	85	54	16.4	16.4	2.0	8.6
A20-RDC-2	11.4	14.0	520	583	70	45	15.2	15.2	1.8	8.5

Table A-3 continued

Specimen	Material properties						Test results			
	MC		Density		Gr. Ring		F_{ult}	$F_{@3mm}$	d_{max}	k_S
	(%)		(kg/m^3)		δ	width	(kN)	(kN)	(mm)	kN/mm
	Joist	Main	Joist	Main	(º)	No/50				
A20-RDC-3	11.7	14.8	533	601	75	42	16.4	16.4	2.4	9.8
A20-RDC-4	12.1	12.8	486	499	90	23	16.4	16.4	2.8	9.4
A20-RDC-5	11.8	12.1	480	606	85	21	17.4	17.4	2.7	8.3
A20-DRDC-1	11.6	12.0	486	449	85	26	14.6	14.6	3.7	
A20-DRDC-2	12.7	12.6	493	536	90	30	30.5	18.8	8.1	
A20-DRDC-3	12.4	13.5	573	536	60	35	22.6	22.6	4.8	
A20-DRDC-4	12.4	12.6	546	560	55	31	16.0	16.0	3.4	
A20-DRDC-5	12.1	11.4	510	541	85	57	22.0	22.0	4.5	
A10-RDC-1	12.0	15.6	536	462	90	41	31.4	22.2	12.8	5.8
A10-RDC-2	12.0	18.0	533	541	85	45	36.6	30.7	9.9	11.0
A10-RDC-3	12.5	15.0	520	592	5	39	19.5	19.5	4.7	5.6
A10-RDC-4	14.2	14.0	530	513	0	37	15.3	15.3	4.7	4.9
A10-RDC-5	12.2	15.4	540	643	75	38	19.6	19.6	2.3	12.7
A10-DRDC-1	13.8	14.2	543	555	75	49	24.7	21.5	5.9	
A10-DRDC-2	12.6	13.2	506	462	80	42	30.6	17.9	9.2	
A10-DRDC-3	13.4	15.0	513	541	75	34	29.8	27.1	5.4	
A10-DRDC-4	12.1	13.2	543	546	85	41	17.1	17.1	4.1	
A10-DRDC-5	12.8	12.5	536	555	65	43	22.7	22.7	5.0	
A05-RDC-1	12.8	14.4	433	430	50	33	17.3	17.3	4.2	3.5
A05-RDC-2	13.4	17.2	440	541	60	34	12.5	12.5	4.5	3.3
A05-RDC-3	16.3	13.6	460	592	55	62	21.3	19.2	6.7	4.9
A05-RDC-4	15.1	13.5	450	504	35	44	15.4	14.2	5.7	3.7
A05-RDC-5	12.4	16.2	583	647	75	31	28.3	18.7	6.5	8.6
A05-DRDC-1	12.8	12.4	580	523	80	34	27.3	18.7	10.0	
A05-DRDC-2	12.0	12.4	510	449	85	52	17.6	17.6	5.0	
A05-DRDC-3	14.0	14.0	510	532	75	59	26.5	17.6	7.2	
A05-DRDC-4	12.5	12.6	423	550	85	38	23.3	9.2	10.9	
A05-DRDC-5	14.3	11.2	416	546	90	37	12.6	12.6	4.5	

Table A-4: Summary of material properties for test series on geometric parameters

Series	MC (%)				Density (kg/m^3)				Ring Orientation δ (°)		Ring Width (No/50mm)	
	Joist		Main beam		Joist		Main beam					
	Mean	StDev	Mean	StDev	Mean	StDev	Mean	StDev	Mean	StDev	Mean	StDev
Contr.-RDC	12.3	1.5	12.9	1.2	498	39	474	32	64	22	46	14
Contr.-DRDC	11.7	0.4	13.7	1.5	441	27	512	44	53	30	41	12
BC75-RDC	12.4	1.6	13.2	1.5	420	40	420	38	52	31	23	3
BC75-DRDC	13.4	1.4	12.8	3.5	427	46	434	38	48	29	20	2
BC55-RDC	12.0	1.4	13.0	3.0	508	73	490	38	82	8	55	18
BC55-DRDC	12.2	0.4	12.9	1.8	504	49	532	43	77	10	47	9
BC45-RDC	12.6	0.8	14.5	1.4	530	35	489	43	73	10	59	17
BC45-DRDC	11.9	0.6	12.5	0.4	453	25	540	42	58	30	54	24
A20-RDC	11.8	0.3	13.7	1.2	506	22	544	77	81	8	37	14
A20-DRDC	12.2	0.4	12.4	0.8	522	37	524	43	75	16	36	12
A10-RDC	12.6	0.9	15.6	1.5	532	8	550	70	51	45	40	3
A10-DRDC	12.9	0.7	13.6	1.0	528	17	532	39	76	7	42	5
A05-RDC	14.0	1.6	15.0	1.6	473	62	543	83	55	15	41	13
A05-DRDC	13.1	1.0	12.5	1.0	488	68	520	41	83	6	44	11

Table A-5: Summary of test results for test series on geometric parameters

Series	F_{ult} (kN)		$F_{@3mm}$ (kN)		d_{max} (mm)		k_S (kN/mm)	
	Mean	StDev	Mean	StDev	Mean	StDev	Mean	StDev
Contr.-RDC	19.9	5.6	14.9	2.7	4.6	2.3	5.6	1.6
Contr.-DRDC	20.0	5.5	8.6	1.7	6.6	1.5		
BC75-RDC	12.5	2.9	12.5	2.9	1.8	0.7	10.5	4.2
BC75-DRDC	12.6	1.7	10.3	1.5	3.8	0.5		
BC55-RDC	25.9	11.9	19.6	5.3	4.4	2.3	9.8	2.7
BC55-DRDC	23.9	6.0	10.8	3.1	5.9	1.7		
BC45-RDC	22.8	4.5	15.1	5.9	4.1	2.0	10.1	3.2
BC45-DRDC	29.7	4.1	9.4	4.0	9.5	2.4		
A20-RDC	16.3	0.8	16.3	0.8	2.4	0.4	8.9	0.7
A20-DRDC	21.2	6.3	12.0	1.7	4.9	1.9		
A10-RDC	24.5	9.1	15.0	6.9	6.9	4.3	8.0	3.6
A10-DRDC	25.0	5.5	12.0	2.4	5.9	1.9		
A05-RDC	19.0	6.1	6.6	2.4	5.5	1.1	4.8	2.2
A05-DRDC	21.4	6.3	9.7	2.7	7.5	2.9		

Appendix F: Complete load deformation response for tests on geometry parameters

The load application regime according to EN-26891 (1991) can be used to demonstrate that RDC behaviour is linear elastic (Figure A-3). For the purpose of comparing the different test series, these unloading/reloading loops were not required.

Figure A-3: Load deformation response including unloading loops

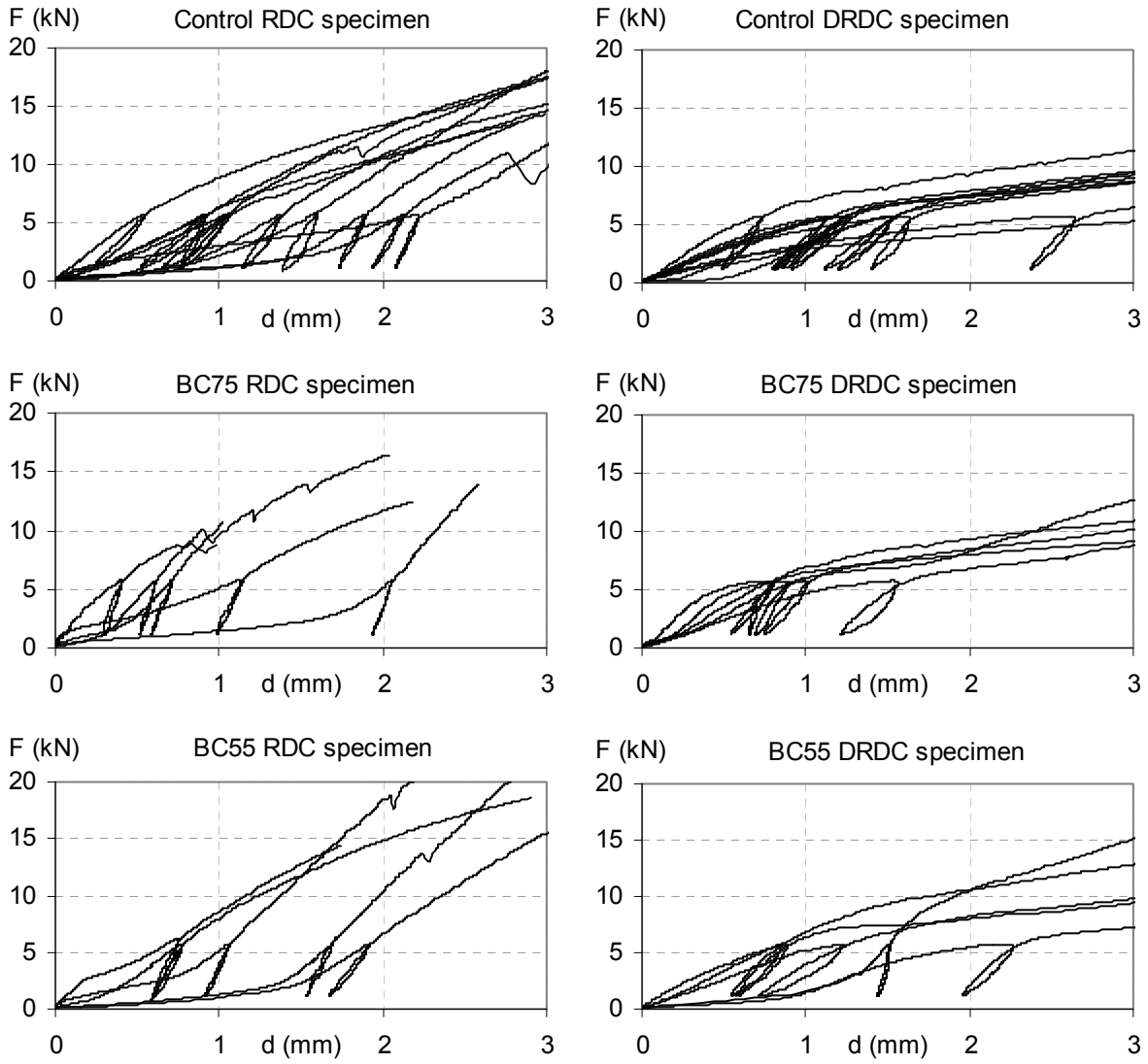

Figure A-3 continued

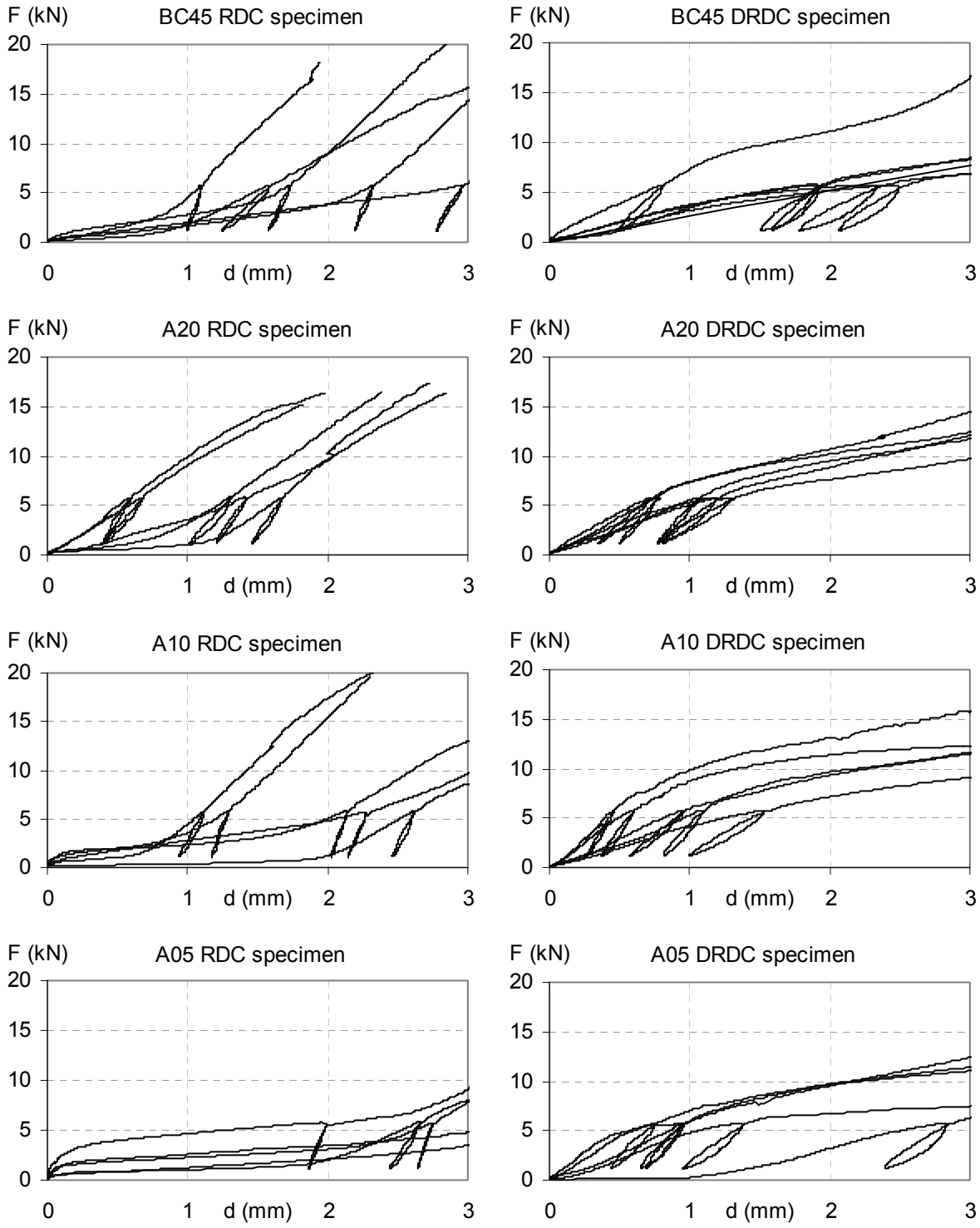

Appendix G: Multiple analysis of variance for results on geometry parameters

Multivariate analysis of variance (MANOVA) is advantageous in situations in which several dependent variables are studied simultaneously. In such cases, the studied variables are most often correlated and considering the univariate analyses separately does not take into account information contained in the data due to the correlation and might be misleading in terms of one factor having a significant effect while it does not or shadowing a significant effect that only becomes apparent when all dependent variables are studied simultaneously.

In a MANOVA for all specimens, the capacity, the load at 3 mm deformation, and the maximum deformation of the connection were statistically analysed. Table A-6 shows the partial correlation coefficients between these variables and the p-values from the MANOVA comparing the different test series. There is a strong correlation between the capacity and maximum deformation. The other response variables have very little correlation. The Wilks' Lambda test criteria for the hypothesis of no overall treatment effect gave an associated p-value <.0001; therefore the treatments differences are significantly different at a level α=0.05, which confirms the findings of the individual ANOVA's. Multiple comparison test results for the capacity show that BC45-DRDC specimens are significantly stronger than BC75-RDC and BC75-DRDC. Regarding the load at 3 mm deformation, BC55-RDC and BC45-RDC specimens are stronger than most DRDC test series. And finally BC45-DRDC specimens show larger deformation than most RDC test series (Figure A-4).

Table A-6: Partial correlation coefficients and p-values for MANOVA

	F_{ult}	$F_{@3mm}$	d_{max}
F_{ult}	1.00	0.38	0.81
$F_{@3mm}$		1.00	-0.01
d_{max}			1.00
p-value	<.001	<.001	<.001

Figure A-4: All test results with different geometric parameters (bounds show extreme values)

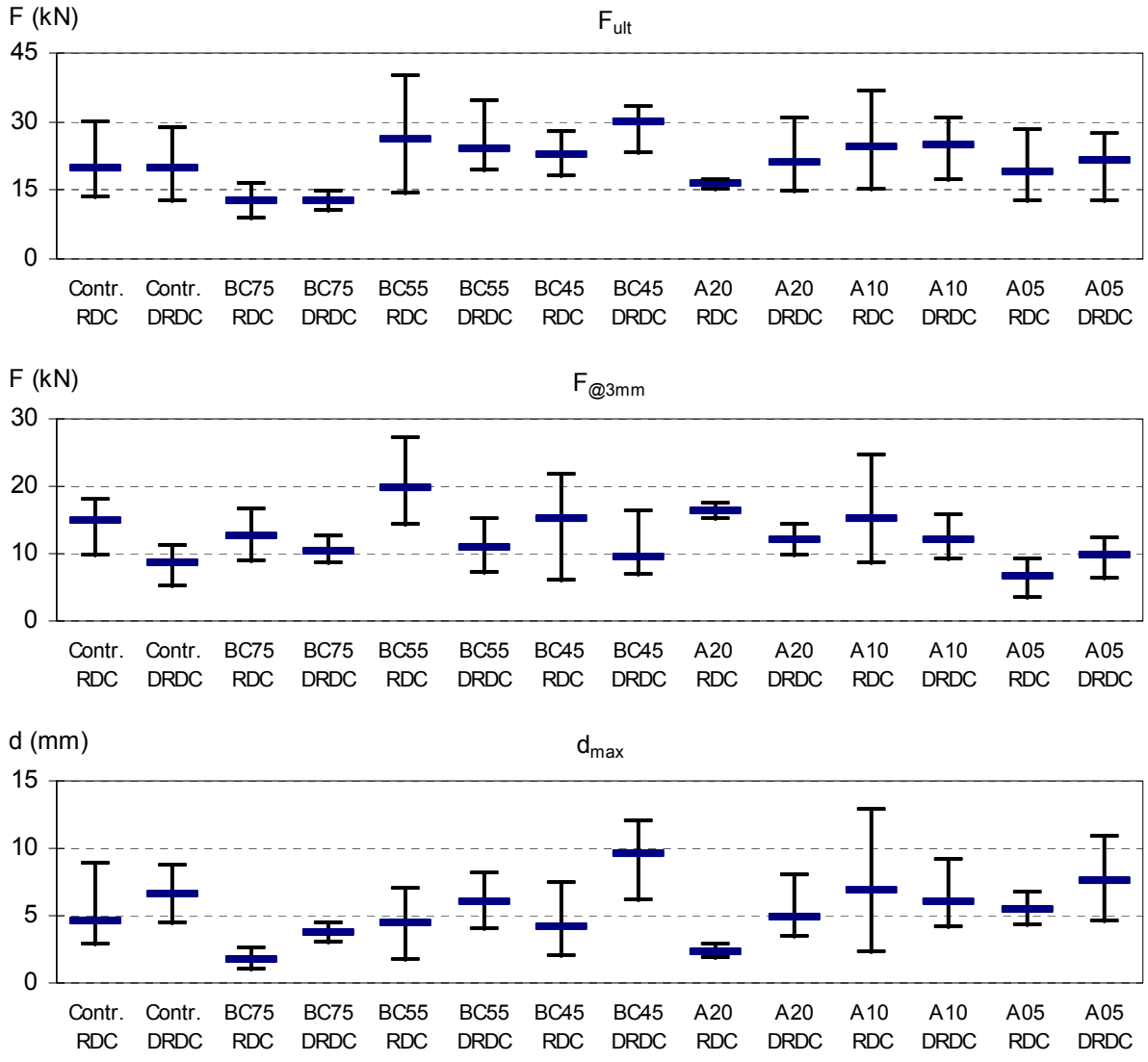

A second MANOVA only for RDC analysed the connection stiffness (k_S), in addition to F_{ult}, $F_{@3mm}$, and d_{max}. The stiffness was computed only for RDC specimens because of the different load deformation behaviour of DRDC that made it impractical to determine consistent parts of the load deformation curves for which to compute slopes. Given the characteristics of the load deformation curves, it was decided to compute the slopes values for the second linear part of the load displacement curves using the recordings of connection force and relative vertical joint displacement for loads between 3 kN and 16 kN. Table A-7 shows the partial correlation coefficients and the p-values from the MANOVA. There is strong correlation between the capacity and the maximum deformation. Load at 3 mm deformation and stiffness have moderate correlation while the other response variables have little correlation. The Wilks' Lambda test criteria for the hypothesis of no overall treatment effect gave an associated p-value <.0001; therefore the treatments differences are significantly different at a level α=0.05. Multiple comparison showed that BC55 specimens are stronger than BC75 specimens. A05 specimens have significantly lower load at 3 mm deformation than, BC55, A20, BC45, A10 and control specimens. A10 specimens showed larger d_{max} than A20 and BC75 specimens. BC75 specimens have higher and BC45 specimens have lower stiffness than A10 and control specimens.

Table A-7: Partial correlation coefficients and p-values for RDC MANOVA

	F_{ult}	$F_{@3mm}$	d_{max}	C
F_{ult}	1.00	0.38	0.81	0.27
$F_{@3mm}$		1.00	-0.01	0.48
d_{max}			1.00	-0.11
C				1.00
p-value	0.039	0.001	0.018	0.003

Appendix H: Recorded measurements for tests with varying geometric parameters

The averages for the test series of all recorded deformations can be used to calibrate a finite element model. Since the double dovetail configuration did not show relevant advantages, analyses were limited to the test series with single dovetail configuration. The average recordings of the individual test specimens of each test series are shown in the left side of Figure A-5. Given the specific characteristics of the load deformation curves being almost bi-linear, the slope values were computed for the second linear part of the load displacement curves. An initial slope for the first part of the load deformation curve where alignment behaviour was observed did not seem beneficial. For the vertical joist displacements, the recordings of connection force and average relative connection displacement for loads between 3 kN and 16 kN were used. For the other three recorded displacements, the same procedure was applied but the recorded values of applied loads between 6 kN and 30 kN were used as input. The obtained slopes are listed in Table A-8. The obtained regression curves are illustrated in the right side of Figure A-5.

Table A-8: Complete regression model for test series

Series	Vertical Joint Displacement	Horizontal Joint Displacement	Vertical Joist Deflection	Vertical Main Beam Deflection
Contr.-RDC	6.07	55.40	2.48	44.12
BC75-RDC	7.18	47.93	2.20	19.83
BC55-RDC	9.27	136.92	3.09	47.02
BC45-RDC	9.12	193.28	3.16	62.91
A20-RDC	8.72	85.37	3.04	77.60
A10-RDC	7.33	120.71	3.12	43.96
A05-RDC	4.88	181.31	2.45	63.32

Figure A-5: Load deformation response and regression curves for tests on RDC

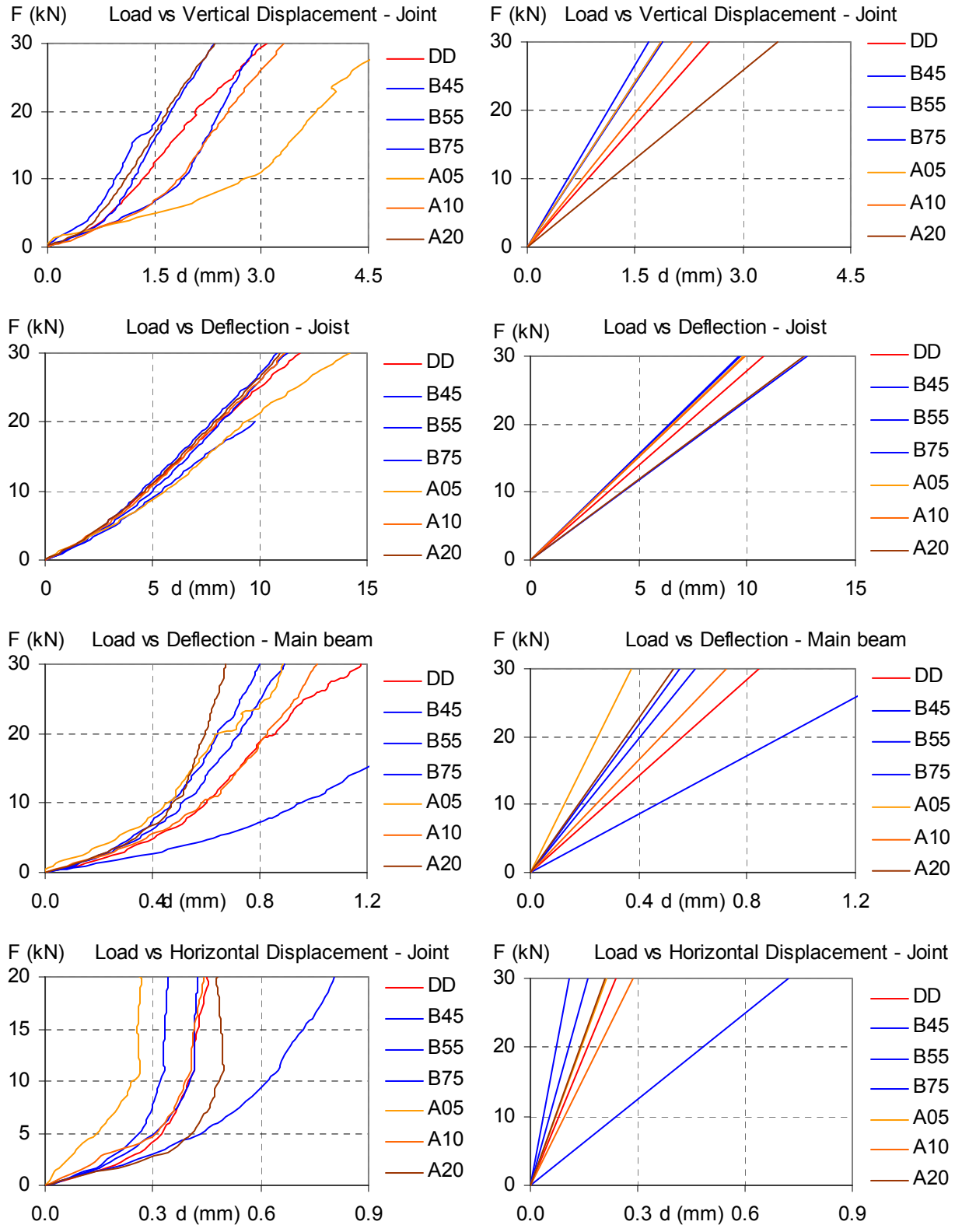

Appendix I: Relating material properties to structural performance of RDC

Figure A-6: Correlation of response variables with covariates

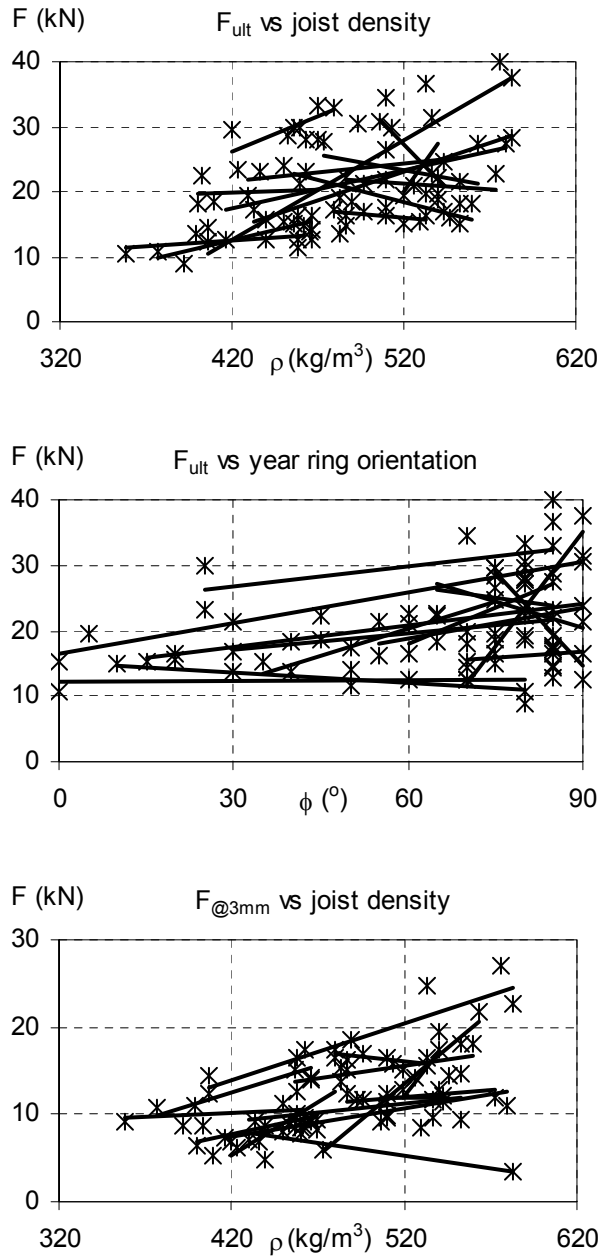

Appendix J: Specimens data and results for small specimen tests

Table A-9: Detailed data for small specimen tests

Specimen	Shear specimens				Tension specimens			
	Density (kg/m^3)		Strength (N/mm^2)		Density (kg/m^3)		Strength (N/mm^2)	
	Part a	Part b	Part a	Part b	Part a	Part b	Part a	Part b
Contr.-RDC-1	493.1	494.5	7.15	6.16	480.2	536.9	2.12	3.08
Contr.-RDC-2	493.0	491.3	6.94	7.04	485.4	485.4	2.77	2.74
Contr.-RDC-3	489.8	495.2	6.92	7.11	488.0	494.0	1.82	3.64
Contr.-RDC-4	513.3	504.9	8.69	7.89	512.1	516.5	4.82	2.52
Contr.-RDC-5	604.9	593.7	10.74	10.33	599.0	605.7	3.27	4.00
Contr.-RDC-6	506.0	505.5	8.26	8.84	508.6	502.1	2.78	3.41
Contr.-RDC-7	515.4	510.0	9.40	8.52	516.5	517.4	4.22	2.84
Contr.-RDC-8	607.6	611.8	10.34	10.36	610.1	611.6	4.11	5.47
Contr.-RDC-9	589.6	605.6	10.06	10.12	597.4	618.4	2.94	3.93
Contr.-RDC-10	476.5	509.1	6.78	6.80	512.4	481.4	2.22	3.02
Contr.-DRDC-1	448.6	454.4	6.38	6.28	337.6	434.1	3.50	1.66
Contr.-DRDC-2	501.4	501.4	6.87	6.74	496.5	494.9	3.07	2.25
Contr.-DRDC-3	497.2	492.0	7.59	6.69	490.0	493.1	2.04	2.79
Contr.-DRDC-4	489.5	484.3	6.86	7.18	486.2	485.4	2.97	1.49
Contr.-DRDC-5	445.6	413.3	6.13	5.95	437.3	470.6	3.07	3.23
Contr.-DRDC-6	400.7	389.6	5.30	5.06	394.2	400.5	2.42	2.41
Contr.-DRDC-7	395.1	483.7	5.86	7.65	417.7	408.9	2.43	2.25
Contr.-DRDC-8	484.5	528.7	7.98	8.16	596.2	476.8	3.62	2.18
Contr.-DRDC-9	466.2	469.2	8.90	7.65	470.9	465.2	3.18	3.25
Contr.-DRDC-10	504.5	474.8	8.20	8.01	498.2	462.9	2.82	2.15
BC75-RDC-1	389.5	354.5	5.13	5.42	370.2	359.1	2.55	1.40
BC75-RDC-2	479.6	470.4	7.50	8.00	493.7	495.7	2.26	2.94
BC75-RDC-3	387.4	373.1	5.77	5.28	397.8	391.1	1.97	2.22
BC75-RDC-4	473.0	518.2	8.05	7.72	519.0	489.3	2.13	2.65
BC75-RDC-5	370.1	404.2	4.99	6.06	395.4	402.7	1.58	1.36

Table A-9 continued

Specimen	Shear specimens				Tension specimens			
	Density (kg/m^3)		Strength (N/mm^2)		Density (kg/m^3)		Strength (N/mm^2)	
	Part a	Part b	Part a	Part b	Part a	Part b	Part a	Part b
BC75-DRDC-1	472.9	476.6	6.59	7.05	497.0	470.0	1.52	1.94
BC75-DRDC-2	351.0	354.2	4.70	4.47	363.3	357.3	2.46	1.17
BC75-DRDC-3	439.9	466.9	6.27	6.08	444.2	470.4	1.06	2.02
BC75-DRDC-4	431.4	451.0	6.15	6.01	433.9	456.1	2.66	n.a.
BC75-DRDC-5	347.4	355.5	5.41	4.74	359.0	350.1	1.11	1.25
BC55-RDC-1	474.3	450.3	7.35	6.43	442.5	451.9	2.30	2.12
BC55-RDC-2	606.2	621.5	8.68	7.90	613.9	609.4	4.37	2.81
BC55-RDC-3	612.5	606.3	10.16	7.23	612.7	613.4	3.87	4.28
BC55-RDC-4	529.6	527.1	6.48	8.28	527.8	565.6	3.01	3.27
BC55-RDC-5	517.6	516.8	6.76	7.11	528.0	504.7	3.01	3.13
BC55-DRDC-1	441.3	448.8	7.45	6.71	457.9	455.3	1.95	2.95
BC55-DRDC-2	534.7	559.4	7.91	8.01	535.7	543.3	3.09	2.88
BC55-DRDC-3	515.6	546.5	7.36	7.39	570.7	525.0	1.95	2.66
BC55-DRDC-4	582.6	593.7	8.95	9.93	588.5	480.2	4.26	5.06
BC55-DRDC-5	462.9	463.4	7.00	7.12	467.1	454.3	2.93	2.68
BC45-RDC-1	589.5	585.4	8.73	9.31	591.0	585.9	3.25	3.61
BC45-RDC-2	569.2	577.0	8.92	8.36	595.5	575.7	2.91	2.23
BC45-RDC-3	470.9	511.8	7.18	7.87	439.5	491.0	1.79	2.34
BC45-RDC-4	576.9	554.4	8.97	9.09	491.8	552.9	3.25	2.89
BC45-RDC-5	591.6	573.6	10.16	10.66	587.8	556.7	2.71	2.73
BC45-DRDC-1	486.0	483.2	7.73	7.53	481.3	485.7	2.58	3.03
BC45-DRDC-2	452.4	465.5	6.65	7.28	462.2	468.3	2.81	2.58
BC45-DRDC-3	469.5	432.6	7.28	5.50	437.4	454.2	1.97	1.81
BC45-DRDC-4	481.5	506.3	8.12	7.99	553.4	483.9	4.13	3.60
BC45-DRDC-5	538.9	586.0	7.95	8.97	586.8	598.1	2.82	2.72
A20-RDC-1	536.3	540.8	8.43	6.10	547.0	567.6	3.19	3.34
A20-RDC-2	575.0	561.5	8.92	8.73	566.1	486.7	2.86	3.13
A20-RDC-3	580.7	568.5	9.59	9.09	593.1	569.0	2.90	3.25

Table A-9 continued

Specimen	Shear specimens				Tension specimens			
	Density (kg/m^3)		Strength (N/mm^2)		Density (kg/m^3)		Strength (N/mm^2)	
	Part a	Part b	Part a	Part b	Part a	Part b	Part a	Part b
A20-RDC-4	490.0	528.2	8.05	8.49	505.2	507.5	2.64	2.74
A20-RDC-5	492.0	489.6	8.27	8.10	496.5	490.1	2.19	3.99
A20-DRDC-1	498.3	514.3	9.41	8.11	522.9	521.5	2.87	4.27
A20-DRDC-2	505.5	527.5	8.73	8.84	514.3	509.0	2.81	3.22
A20-DRDC-3	604.8	628.8	10.43	10.30	624.2	629.4	3.93	4.22
A20-DRDC-4	616.7	639.9	10.62	11.75	639.3	628.4	4.39	4.46
A20-DRDC-5	559.0	556.6	8.53	9.19	566.8	586.0	4.02	2.71
A10-RDC-1	456.8	451.9	6.55	8.86	606.4	593.6	3.24	2.82
A10-RDC-2	451.7	456.1	8.05	9.60	574.5	556.0	2.35	3.58
A10-RDC-3	460.4	462.9	9.07	8.02	576.5	553.0	3.48	3.41
A10-RDC-4	443.4	454.0	7.55	7.29	585.6	558.6	4.10	3.88
A10-RDC-5	646.9	642.1	8.42	6.10	593.3	559.5	3.57	2.84
A10-DRDC-1	640.4	673.4	10.52	9.63	596.8	572.3	3.80	4.15
A10-DRDC-2	483.6	530.8	9.32	8.55	553.7	563.8	3.51	3.59
A10-DRDC-3	500.7	526.3	9.38	8.03	558.1	539.9	4.03	4.69
A10-DRDC-4	448.4	461.5	9.53	5.73	584.2	542.0	2.58	2.83
A10-DRDC-5	451.4	446.9	8.16	8.39	538.0	525.9	2.56	3.23
A05-RDC-1	559.7	585.3	7.42	7.46	447.9	456.5	2.45	2.59
A05-RDC-2	544.3	577.7	6.40	6.47	456.9	450.3	2.50	2.49
A05-RDC-3	525.7	557.3	6.81	6.77	464.3	476.7	1.93	2.10
A05-RDC-4	545.8	571.2	6.89	6.50	449.3	471.4	2.19	2.40
A05-RDC-5	530.1	541.3	10.95	9.88	660.9	639.8	3.48	3.49
A05-DRDC-1	571.5	609.8	11.35	11.47	650.9	662.4	4.48	4.66
A05-DRDC-2	562.2	562.2	7.22	5.79	585.6	504.4	2.84	2.60
A05-DRDC-3	547.9	548.3	7.39	7.39	512.0	530.3	3.08	2.48
A05-DRDC-4	533.8	586.0	6.75	7.57	474.4	456.8	2.68	2.30
A05-DRDC-5	508.7	567.8	5.93	6.75	455.4	459.0	2.25	2.32

Appendix K: Parameter study for FEM model

The longitudinal MOE was varied from 9,000 N/mm² to 12,000 N/mm² in steps of 1,000 N/mm² therefore covering the common range of values determined for western hemlock (Barrett et al. 2001). There is clear correlation between the recorded deformations and the longitudinal MOE for both joint deformation and joist deflection. Deformation increases almost linearly with decreased MOE. The same phenomenon occurs for tension stress, although not as significant, while shear stress is almost identical for all values of longitudinal MOE. The transverse MOE was varied from 300 N/mm² to 600 N/mm² in steps of 100 N/mm². This corresponds to 3%, 4%, 5%, and 6% of the longitudinal MOE. There is an almost linear relation between the recorded deformations and the transverse MOE. The tension stress maximum remains unchanged but the shear stress maximum decreases significantly with increasing values of transverse MOE. The shear modulus (G) was varied from 300 N/mm² to 390 N/mm² in steps of 30 N/mm², corresponding to 3%, 3.3%, 3.6%, and 3.9% of the longitudinal MOE. There is a clear correlation between the recorded deformations and the shear modulus. The tensile stresses remain unchanged but the shear stresses increase significantly with increasing values of G. Poisson ratios were kept constant as a preliminary study had shown that no significant changes in stresses and deformations were observed when varying the ratio.

The damper stiffness (k) was varied from 700 N/m to 1,000 N/m in steps of 100 N/m. While stresses in the RDC remain almost unchanged, the joint deformation and joist deflection significantly decrease with higher k. Reasonable agreement with the experimentally recorded joist deflection was achieved when using a damper stiffness of 800 N/mm for the model. The stiffness of the real damper was measured experimentally and determined to be 920 N/mm. The deviation can be explained by the difference in load application. While in the stiffness test the

load was applied perfectly perpendicular to the damper and evenly distributed, it is applied concentrated on one edge by the beam due to bending deformation.

The friction coefficient (f) was varied from 0.2 to 0.5 in steps of 0.1. Lower values lead to higher stresses and larger deformations because most of the load is carried on the bottom of the dovetail. The penetration tolerance (PTOL) was varied from 0.5 to 0.2. There was no change in stresses or deformations observed suggesting that a value of 0.5 can be used. The contact stiffness FKP was varied from 0.01 to 0.04 in steps of 0.01. Higher values for contact stiffness caused more load to be transferred along the joint flanges and lower the tension perpendicular to grain stress maxima and joint deformation. There is no possibility to experimentally determine the contact stiffness inside a real joint; the general rule that higher values can lead to increased accuracy might not be accurate for wood surfaces as these penetrate each other in the real joint.

Effort was directed towards finding a contact stiffness that allows the model to converge while showing good agreement between modelled and experimentally observed load deformation curves. Using the ANSYS® default solver, the solution did not converge for contact stiffness higher than 0.03. Since convergence difficulties increase with initial gaps between the contact surfaces, another series was carried out with modelling no initial gap between the contact surfaces. As expected, the model converged with higher FKP values (up to 0.20). The trend of decreasing stress values and joint deformations remained but was less severe. Accurate gap modeling was essential for achieving realistic load deformation curves. Two different approaches were tried: Type I being a gap with a depth that continuously decreases from the bottom to the very top of the joint, and Type II being a gap that only exists below the rounded part of the dovetail (Figure A-7).

Figure A-7: Different gap types: Type I (left) and Type II (right)

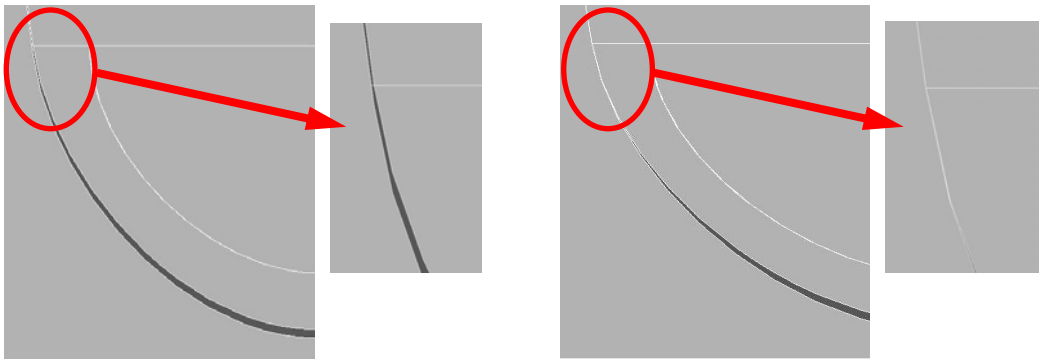

Gap Type I was varied from 0 mm to 0.75 mm in steps of 0.25 mm. The joint deformation and joist deflection increase linearly with increasing gap depth while stresses remain almost unchanged. No good agreement between analytical and experimental load deformation curves for the vertical joint deformation was achieved using gap Type I. Gap Type II was varied from 0 mm to 1.2 mm in steps of 0.3 mm and proved to be superior in achieving agreement between analytical and experimental load deformation curves for the vertical joint deformation. In contrast to gap Type I, stress peaks are significantly decreased with an increase in gap size. Figure A-8 shows the load deformation curves depending on type and depth of the gap.

Figure A-8: Influence of gap depth and type on relative vertical joint deformation

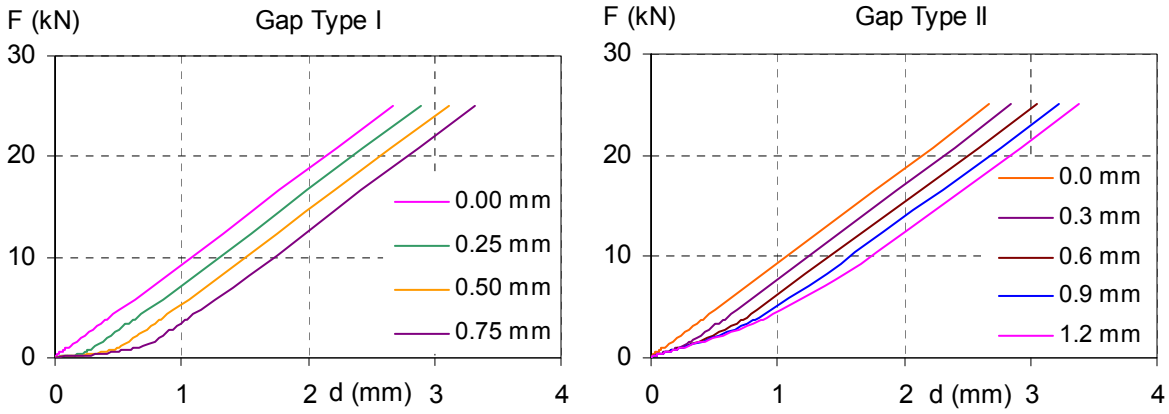

Table A-10: Parameter influence on deformations and stress maxima in RDC

Parameter	Joist deflection (mm)	Joint deformation (mm)	Max $\sigma_{T,\perp}$ (N/mm^2)	Max σ_{SII} (N/mm^2)
Control	11.06	3.32	3.28	2.97
E_L = 9,000 N/mm²	11.41	3.50	3.33	2.97
E_L = 11,000 N/mm²	10.76	3.18	3.22	2.96
E_L = 12,000 N/mm²	10.51	3.05	3.17	2.95
E_T = 400 N/mm²	10.80	3.20	3.26	2.74
E_T = 500 N/mm²	10.64	3.13	3.27	2.59
E_T = 600 N/mm²	10.52	3.07	3.27	2.48
G = 330 N/mm²	10.91	3.27	3.27	3.07
G = 360 N/mm²	10.78	3.21	3.26	3.15
G = 390 N/mm²	10.67	3.17	3.25	3.23
k = 700 N/mm	12.12	3.47	3.23	2.95
k = 900 N/mm	10.22	3.20	3.31	2.98
k = 1,000 N/mm	9.54	3.09	3.30	2.96
f = 0.2	11.13	3.46	3.56	3.23
f = 0.4	11.00	3.22	3.02	2.78
f = 0.5	10.96	3.14	2.81	2.76
FTOL = 0.40	10.99	3.20	3.21	2.97
FTOL = 0.30	10.99	3.20	3.21	2.97
FTOL = 0.20	10.99	3.20	3.21	2.97
FKP = 0.02 (with gap)	10.99	3.20	3.21	2.97
FKP = 0.03 (with gap)	10.92	3.07	3.07	2.94
FKP = 0.01 (no gap)	10.72	2.67	3.31	3.02
FKP = 0.03 (no gap)	10.59	2.42	3.18	3.04
FKP = 0.05 (no gap)	10.56	2.37	3.13	3.02
FKP = 0.10 (no gap)	10.53	2.31	2.95	2.93
FKP = 0.20 (no gap)	10.51	2.28	2.92	2.96
Gap depth Type I = 0.00mm	10.72	2.67	3.31	3.02
Gap depth Type I = 0.25mm	10.83	2.89	3.32	3.02
Gap depth Type I = 0.50mm	10.95	3.11	3.32	3.02
Gap depth Type II = 0.00mm	10.94	3.10	2.79	2.88
Gap depth Type II = 0.30mm	10.81	2.85	3.11	2.85
Gap depth Type II = 0.60mm	10.90	3.05	2.90	2.84
Gap depth Type II = 0.90mm	10.99	3.22	2.76	2.87
Gap depth Type II = 1.20mm	11.07	3.38	2.69	2.89

Figure A-9 illustrates the relative vertical joint displacement versus applied load for the models and the test average and shows that excellent agreement can be achieved with modelling a 0.50 mm gap.

Figure A-9: Load deformation response: FEM Model versus test results for control series

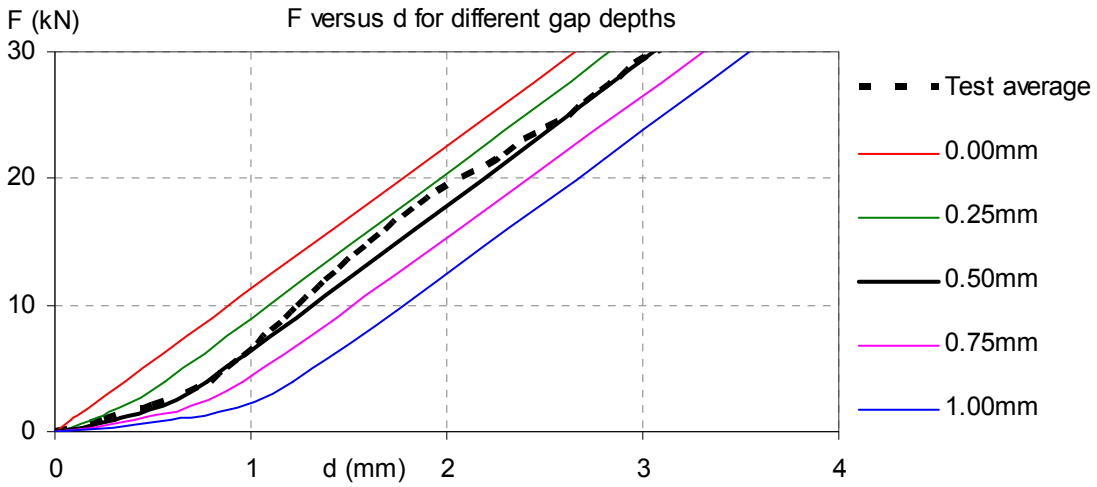

Appendix L: Parameters in FEM simulations

Table A-11: Material and model properties for individual test specimens of control series

Model	Density (kg/m^3)	MC (%)	ϕ (º)	W No/50	F_{ult} (kN)	E_L	E_R (N/mm^2)	E_T	gap (mm)	f
Specimen 1	463	11.4	80	38	23.2	12,000	720	360	1.75	0.35
Specimen 2	466	11.4	85	35	14.3	12,000	720	360	1.50	0.35
Specimen 3	463	11.8	80	34	28	12,300	738	369	0.40	0.50
Specimen 4	540	11.0	75	39	18.8	12,500	750	375	0.50	0.25
Specimen 5	496	15.0	30	69	16.9	12,000	720	360	0.00	0.35
Specimen 6	483	11.0	40	58	13.6	11,700	702	351	0.50	0.25
Specimen 7	560	13.9	65	38	18.3	13,500	810	405	0.80	0.50
Specimen 8	553	14.2	75	37	14.9	12,000	720	360	0.50	0.25
Specimen 9	456	11.7	80	41	29.8	12,000	720	360	0.60	0.30

Table A-12: Material and model properties for test series

Series	Density (kg/m^3)	MC (%)	F_{ult} (kN)	E_L	$E_{R,T}$ (N/mm^2)	gap (mm)	f
BC75-RDC	420	12.4	12.5	11,000	605	0.25	0.30
BC55-RDC	508	12.0	25.9	12,200	671	0.5	0.30
BC45-RDC	530	12.6	22.8	13,000	715	1.5	0.30
A05-RDC	506	11.8	16.3	11,500	632	3.0	0.25
A10-RDC	532	12.6	24.5	13,000	715	2.0	0.25
A20-RDC	473	14.0	19.0	12,800	704	0.4	0.35

Table A-13: Parameters for modelling tests from other research institutes

Model	E_L	$E_{R,T}$	$G_{XY,XZ}$	G_{YZ}	gap	f
	(N/mm^2)				(mm)	
UBC I	11,000	495	367	37	0.00	0.30
Bobacz 10-I	11,000	440	367	36	0.00	0.25
Bobacz 10-II	11,000	440	367	36	0.00	0.25
Kreuzinger 7-16	11,000	495	367	36	0.00	0.30
Kreuzinger 7-8	11,000	495	367	36	0.00	0.30
Blass tight	12,000	600	400	40	0.50	0.45
Blass loose	11,000	550	367	37	0.00	0.15
Hochstrate F-F	11,000	550	367	37	0.00	0.25
Hochstrate F-D	11,000	550	367	37	0.00	0.25

Appendix M: Comparing of different volume integrals

Three different approaches were considered: (I) the volume of the joist with approx. 9,000 elements, (II) an extended connection area (length 50% of beam height) with approx. 3,000 elements, and (III) the dovetail tip with approx. 200 elements (Figure A-10). For tests reported by Tannert and Lam (2006), the volume integrals for tension perpendicular to grain and shear parallel to grain stresses were calculated for the three different volumes, see Table A-14.

Figure A-10: Volumes considered for stress volume integration

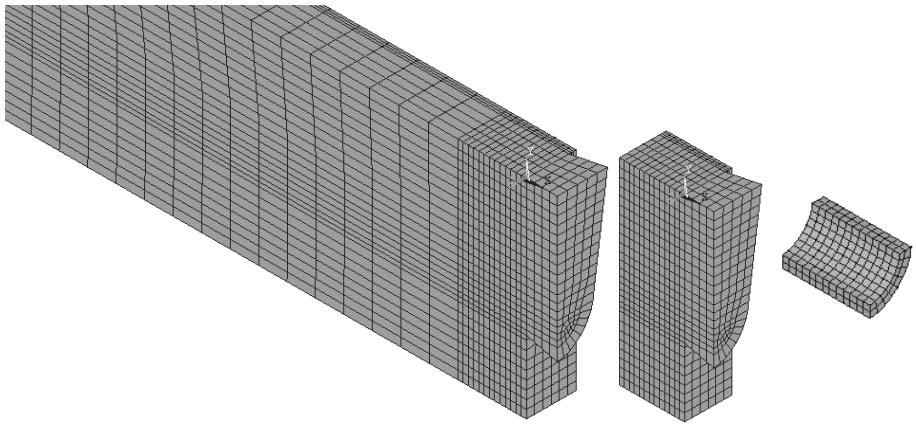

Table A-14: Stress integrals of different volumes for UBC test series

Model	Tension stress (N/mm^2)			Shear stress (N/mm^2)		
	Vol I	Vol II	Vol III	Vol I	Vol II	Vol III
Contr.-RDC	4.33	4.33	4.26	4.84	4.56	3.26
BC45-RDC	3.19	3.19	2.94	5.09	4.49	2.88
BC75-RDC	3.10	3.10	3.04	3.49	3.27	2.30
BC55-RDC	4.87	4.87	4.80	6.08	5.62	3.95
A05-RDC	6.01	6.01	5.97	6.14	6.06	4.71
A10-RDC	6.32	6.32	6.26	6.75	6.54	4.85
A20-RDC	3.19	3.19	3.07	3.79	3.48	2.41

Appendix N: Study of mesh size

The mesh was refined at the dovetail areas in 16 steps and the stress volume integrals for both tension perpendicular to grain and shear parallel to grain stresses was calculated varying the shape parameter k from 2 to 6. For both stresses the volume integrals increase until reaching a mesh sizes with 2,440 elements. The increase is more severe for higher values of the shape parameter k, due to the nonlinearity of the equation. For tension stress, the volume integrals increase with higher k-values while for shear stress the opposite is true. This again shows the difference between the localised tension perpendicular to grain stress versus the more distributed shear parallel to grain stress. It was decided that a mesh with 3,050 elements is appropriate.

Figure A-11: Dependence of stress volume integrals on mesh size for tension perpendicular to grain (left) and shear parallel to grain (right)

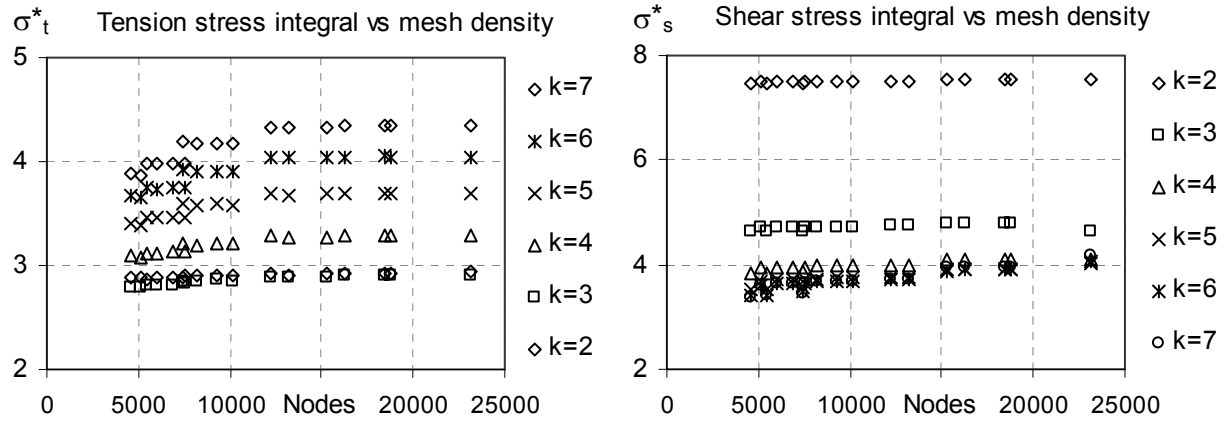

Appendix O: Volume integrals and failure criteria for FEM simulations

Table A-15: Estimated capacity for test series using different failure criteria

Test series	Failure criteria (kN)			
	IA	IB	IC	II
Contr.-RDC	14.8	17.9	54.0	13.8
BC45-RDC	19.4	25.0	68.0	18.0
BC55-RDC	16.9	21.0	60.7	15.8
BC75-RDC	11.8	14.1	45.9	11.1
A05-RDC	13.0	15.9	47.8	12.2
A10-RDC	13.9	17.0	50.6	13.1
A20-RDC	15.1	18.3	57.9	14.2
Contr.-DRDC	16.9	20.9	72.2	15.7
BC45-DRDC	22.7	29.6	87.1	21.0
BC55-DRDC	19.6	24.5	77.4	18.2
BC75-DRDC	12.8	15.0	51.7	12.0
A05-DRDC	15.9	19.4	63.5	14.7
A10-DRDC	16.3	20.2	68.0	15.0
A20-DRDC	17.0	20.9	75.3	15.8

Appendix P: Validation of proposed failure criterion

The proposed failure criterion was validated by modelling selected test series of other studies (Tannert et al. 2007; Bobacz 2002; Kreuzinger and Spengler 1999; Blass and Saal 1999; Hochstrate 2000) and incrementally increased the external loads in order to calculate the RDC forces that fulfill the criterion b (Table A-16). For this exercise, unit volume strengths and shape factors of 3.5 N/mm^2 and $k_T = 5$ for tension perpendicular to grain and 8.0 N/mm^2 and $k_T = 5.5$ for shear parallel to the grain were assumed as no detailed information is available. The criterion estimates capacity correctly for thirteen of fourteen series. Given the very limited information on specific test set up and material strength parameters, this result is very encouraging.

Table A-16: Estimated capacity versus experimental capacity for different test series

Test Series	F_{ult} (kN)	CII (kN)	t-Test p
UBC I	14.4	16.7	0.24
Bobacz 8-I	13.1	15.1	0.20
Bobacz 10-I	12.5	14.9	0.13
Bobacz 10-II	11.4	16.0	0.01
Bobacz 10-III	13.5	14.1	0.72
Kreuzinger 7-16	16.1	11.5	0.06
Kreuzinger 7-8	12.2	10.9	0.41
Blass tight	28.1	28.8	0.89
Blass loose	24.6	17.4	0.19
Hochstrate F-F	18.4	18.9	0.82
Hochstrate F-D	21.1	20.2	0.79
Hochstrate H-F	19.9	19.1	0.76
Hochstrate H-D	24.5	20.3	0.25
Hochstrate M-D	12.2	18.5	0.13

Appendix Q: Parameter study of different loading and support conditions

A series of simulations was carried out varying the loading and support conditions. In the tests by Tannert and Lam (2006), the load was applied at a distance of 350 mm from the RDC, the free joist end was supported on a damper with a stiffness of 1 kN/mm^{2,} and the main beam was free to rotate at its supports. In the simulations, the load was applied at a distance of 150 mm from the connection (C_150) and distributed over the lengths of the joist (C_550). For each loading condition the support of the free joist end was modelled in two variations: using a spring support and using a rigid support (D and R). In one model, the rotation of the main beam was restricted (C_350_F). For each simulation, the loads were increased incrementally until the computed stress integrals fulfilled the failure criterion. The corresponding RDC capacities for these loads were calculated (Table A-17). An increase in capacity was predicted when the load was applied further away from the connection. Capacity also increased when the joist was supported on a damper; this increase was most severe for distributed loads and minimal when the load was applied close to the connection. Fixing the main beam at its supports reduced RDC capacity.

Table A-17: Predicted RDC capacity by loading and support conditions

Model	loading	Support joist	Support beam	C_{II} (kN)
C_350_D	at 350 mm	damper	free to rotate	13.7
C_350_R	at 350 mm	rigid	free to rotate	13.1
C_350_F	at 350 mm	damper	fixed	12.9
C_150_D	at 150 mm	damper	free to rotate	12.1
C_150_R	at 150 mm	rigid	free to rotate	12.0
C_550_D	distributed	damper	free to rotate	13.5
C_550_R	distributed	rigid	free to rotate	12.3

Appendix R: Parameter study of elastic material properties and contact parameters

The elastic material properties and geometry parameters were studied in another series of simulations. The longitudinal MOE (E_{II}) was varied from 10,000 N/mm² to 14,000 N/mm² in steps of 1,000 N/mm covering the common range of values for western hemlock. Previous results at UBC show that the friction coefficient (f) has significant influence on the stresses in RDC and that accurate gap modelling is essential for achieving realistic load deformation curves.

The friction coefficient (f) was varied from 0.1 to 0.5 in steps of 0.1. Two different gap types were analysed: Type I with a width that continuously decreases from the bottom to the very top of the joint, and Type II that only exists below the rounded part of the dovetail. Both gap types were varied from 0 mm to 2 mm in steps of 0.5 mm. Finally, using the models with a gap of 1 mm for both gap types, the friction coefficient (f) was varied from 0.1 to 0.5 in steps of 0.1. For each simulation, the loads were increased incrementally until the computed stress integrals fulfill the failure criterion and the corresponding RDC capacities were calculated, as well as the ratios of these capacities to the capacity of the standard model, see Table A-18.

The longitudinal MOE had little influence RDC capacity. Large increases in MOE (from 10,000 N/mm² to 14,000 N/mm²) led to small increases in capacity (13.5 kN to 14.2 kN). The friction coefficient had a significant influence on RDC capacity. Increasing the friction significantly increased the capacity. Low friction values caused higher stress because most of the load was transferred on the bottom of the dovetail while with high friction the load was transferred more evenly over the height of the dovetail along the flanges. Both gap types influence the capacity, increasing the width of gap Type I led to small increases of stress, increasing the width of gap Type II led to significant increases of stress. The effect of friction

remained unchanged when combined with different gap widths, increased friction decreased RDC capacity. This effect of friction was slightly less severe when combined with gap Type I.

Table A-18: Simulated capacities for different parameter variations

Parameter variation	C_{II} (kN)	$C_{I,i} / C_{II,Standard}$
Standard	13.9	100%
MOE 10,000	13.5	97%
MOE 11,000	13.7	99%
MOE 13,000	14.0	101%
MOE 14,000	14.2	103%
f = 0.1	11.4	82%
f = 0.2	12.6	91%
f = 0.4	15.1	109%
f = 0.5	16.3	118%
GapT1 = 0.5 mm	14.1	102%
GapT1 = 1.0 mm	14.3	104%
GapT1 = 1.5 mm	14.5	105%
GapT1 = 2.0 mm	14.5	105%
GapT2 = 0.5 mm	14.0	101%
GapT2 = 1.0 mm	13.4	97%
GapT2 = 1.5 mm	12.1	88%
GapT2 = 2.0 mm	11.5	83%
GapT1 = 1.0 mm & f = 0.1	11.7	84%
GapT1 = 1.0 mm & f = 0.2	13.1	94%
GapT1 = 1.0 mm & f = 0.4	15.5	112%
GapT1 = 1.0 mm & f = 0.5	16.7	121%
GapT2 = 1.0 mm & f = 0.1	11.4	83%
GapT2 = 1.0 mm & f = 0.2	12.5	91%
GapT2 = 1.0 mm & f = 0.4	14.2	102%
GapT2 = 1.0 mm & f = 0.5	14.9	107%

Appendix S: Pictures of reinforced test specimens

Figure A-12: Reinforced test specimens: 90° (top), 55° (middle), cross (bottom)

Appendix T: Results for study of reinforcements

Table A-19: Results of individual specimens for test using reinforcements

Specimen	F_{ult} (kN)	$F_{@3mm}$ (kN)	$d_{@Fult}$ (mm)	F_{max} (kN)
Series I none - 01	17.9	17.9	3.0	
Series I none - 02	14.2	14.2	2.5	
Series I none - 03	15.7	15.7	2.4	
Series I none - 04	9.3	9.2	2.2	
Series I none - 05	19.3	14.8	4.4	
Series I none - 06	19.4	8.5	4.7	
Series I none - 07	11.4	9.1	1.9	
Series I none - 08	18.8	13.8	3.4	
Series I 90° - 01	26.5	22.5	4.2	
Series I 90° - 02	25.2	25.2	2.8	
Series I 45° - 01	26.6	26.5	1.3	
Series I 45° - 02	29.0	29.0	1.6	
Series II none - 01	38.5	29.9	4.3	50.7
Series II none - 02	40.7	17.9	5.0	47.8
Series II none - 03	47.0	20.4	8.2	48.3
Series II none - 04	30.1	20.2	4.7	50.6
Series II none - 05	29.4	20.3	4.1	48.3
Series II none - 06	28.5	14.3	6.2	42.7
Series II none - 07	36.3	19.2	5.8	50.3
Series II none - 08	34.3	21.7	4.9	35.0
Series II none - 09	32.7	17.9	5.5	32.7
Series II none - 10	23.1	18.8	4.2	31.9
Series II none - 11	37.4	20.9	5.2	45.6
Series II none - 12	19.2	19.1	2.1	27.0
Series II none - 13	23.2	22.2	3.3	49.7
Series II none - 14	18.0	18.0	2.7	36.6

Table A-19 continued

Specimen	F_{ult} (kN)	$F_{@3mm}$ (kN)	$d_{@Fult}$ (mm)	F_{max} (kN)
Series II 90° - 01	54.4	36.9	4.3	66.2
Series II 90° - 02	50.4	30.6	4.3	79.5
Series II 45° - 01	65.1	65.1	2.4	75.5
Series II 45° - 02	72.5	58.5	5.1	86.5
Series II cross - 01	61.7	61.6	0.4	61.7
Series II cross - 02	70.0	70.0	1.9	75.8
Series III none - 01	26.5	19.5	4.4	51.2
Series III none - 02	33.4	20.1	7.1	48.6
Series III none - 03	41.0	25.1	8.7	50.5
Series III none - 04	23.2	20.8	3.6	50.7
Series III none - 05	36.9	16.3	8.7	50.6
Series III none - 06	36.2	17.7	7.6	41.5
Series III none - 07	33.6	21.7	7.0	45.9
Series III none - 08	28.8	28.4	3.1	29.7
Series III none - 09	26.0	22.1	4.3	37.6
Series III none - 10	36.2	14.3	10.3	36.2
Series III none - 11	36.0	22.0	7.5	36.0
Series III none - 12	25.1	19.5	5.0	43.4
Series III none - 13	41.1	21.8	7.4	41.1
Series III none - 14	27.0	24.0	4.3	27.0
Series III 90° - 01	45.5	29.5	5.9	67.7
Series III 90° - 02	37.2	32.4	3.8	56.0
Series III 45° - 01	62.2	62.2	2.6	72.9
Series III 45° - 02	74.7	74.7	1.0	82.0
Series III cross - 01	50.0	50.0	1.8	56.2
Series III cross - 02	55.5	55.5	1.7	63.5

Filename: Thomas_Tannert_Thesis_Final.doc
Directory: C:\Documents and Settings\ttannert\My Documents
Template: C:\Documents and Settings\ttannert\Application Data\Microsoft\Templates\Normal.dot
Title: 1
Subject:
Author: ttannert
Keywords:
Comments:
Creation Date: 8/28/2007 4:45:00 PM
Change Number: 148
Last Saved On: 4/14/2008 9:53:00 AM
Last Saved By: ttannert
Total Editing Time: 3,856 Minutes
Last Printed On: 4/14/2008 9:56:00 AM
As of Last Complete Printing
Number of Pages: 255
Number of Words: 60,183 (approx.)
Number of Characters: 322,584 (approx.)